Session 3

Radiation protection of patients and staff in radiotherapy including brachytherapy

RADIOTHERAPY INDUCED CATARACT AMONG CHILDHOOD CANCER SURVIVORS; INCIDENCE AND PROTECTION

A. ABAZA
Email: aya_abaza@hotmail.com

G. EL- SHANSHOURY
Email: ghada.i.el-shanshoury@hotmail.com

H. EL- SHANSHOURY
Email: *hala.elshanshoury@yahoo.com*

Nuclear and Radiological Regulatory Authority,
Cairo, Egypt

Abstract

The increased number of cancer survivors has shifted attention to the possible risk of subsequent treatment-related morbidities, including cataracts. Recently, it is known that cataracts can be developed with lens doses exceeding a threshold of 5-8 Gy. The aim was to study retrospectively the role of radiation protection measurements in the incidence of radiotherapy induced cataract among childhood cancer survivors during the period of study (4 years) using statistical analysis. In follow-up clinic, 495 childhood cancer patients (leukemia, Lymphoma, soft tissue sarcoma and Wilms' tumor) were examined after 5years of starting treatment. The file of patients was revised for clinic-epidemiologic data. A questionnaire that included questions on cataracts, the surgical procedures related and the using of radiation protection measurements during radiotherapy was answered by the patients and their relatives. The Results indicate a strong association between ocular exposure to ionizing radiation and long-term risk of pre-senile cataract. It is possible to significantly reduce the risk of radiation cataract through the use of appropriate eye protection concluding that the increasing awareness among those at risk, better adoption and increased usage of protective measures, radiation cataract can become preventable despite lowering of dose limits.

Keywords: Cataract, Radiotherapy, Cancer survivors, Radiation Protection

1.   INTRODUCTION

The increased number of survivors has shifted attention to the possible long-term adverse effects of cancer treatments [1]. Long-term survivors are at risk for developing a broad spectrum of adverse outcomes, which may include early death, second neoplasms, and damage to the heart [15,26,28,14]. Additionally, neurosensory complications affecting the auditory, ocular such as cataracts, olfactory, or speech systems are commonly reported by childhood cancer survivors. Although some of these effects have a minor effect on the survivors' quality of life, others, such as blindness and cataract, may have various important consequences. [14,39,1] Fortunately, radiotherapy (RT) is a major element in the treatment and improved survival of childhood cancers [26], including cranial or craniospinal RT. It is nevertheless associated with an increased risk of adverse outcomes such as second cancers and sensory or psychosocial problems [28]. Since a child's visual system is immature and develops during the initial years of life, the consequences of future visual deprivation caused by cataracts and aphakia in children can be important and include anisometropia, aniseikonia and lack of accommodation [5]. Moreover, compared to adults, pediatric cataract surgery tends to be more complicated, requiring additional treatments to decrease the postoperative inflammation, secondary glaucoma, refractive instability of the developing eye and early and severe visual axis opacification. Most of the reported studies in pediatric cancer patients were limited by relatively small sample sizes and a lack of quantitative assessment of lens dose [13]. *Whelan et al.* [39] found an increased risk of cataract at doses greater than 2 Gy to the eye after evaluating the risk of developing late ocular complications in specific cancer treatments five or more years after diagnosis in the Childhood Cancer Survivor Study (CCSS). Other studies have suggested that cataracts are associated with doses below 2 Gy. Therefore, it is classified as stochastic rather than deterministic outcomes [9,27,18,8,]. A fair degree of consistency exists in the radiogenic risks for cataract in different groups exposed to radiation [16,29,42,9,27,23]. Since the 1950s, the prevailing view has been that only relatively high doses of at least several grays induce vision-impairing cataracts. However, the incidence of cataract induced by RT and cytotoxic chemotherapy (CT) among survivors of childhood cancer is often underestimated and underreported. Few   previous

studies [29,10,39] addressed the question of cataract after childhood RT for cancer. One retrospective study of retinoblastoma survivors [10] showed that eyes exposed to a therapeutic radiation dose of 5 Gy or more had a 6-fold increased risk for cataract extraction compared with eyes exposed to 2.5 Gy or less. Another study found that the dose of radiation to the eye was significantly associated with the risk for cataract [29,39]. On the other hand, *Whelan et al* [39] have also shown an increased risk for cataract in survivors who were treated with prednisone. Unfortunately, these studies have not provided findings on the risk for cataract for each of the main alkylating agents. To date, the possibility of interactions between exposure to specific groups of cytotoxic drugs and to ionizing radiation to the eyes also has not been considered [1].

The aim of the current work was to study retrospectively the role of radiation protection measurements in the incidence of RT induced cataract among childhood cancer survivors attending the follow up clinic in multi-cancer centers during the period of study (from January 2013 till January 2017).

2. MATERIAL AND METHODS

Full clinical examination was done to 495 patients 5 years after starting the treatment in 4 types of cancer survivors (158 leukemic patients, 183 Lymphoma, 89 soft tissue sarcoma and 65 Wilms' tumor) laying stress on eye examination. The file of patients was revised about all clinical data including the radiation dose, the other RT data including radiation protection measurement used and the occurrence of cataract or not. By doing a questionnaire that answered by the patients and their relatives we can catch the data that can be missed in the file. Patients received RT alone or in combination with CT and other modality treatments. Chemotherapy used are classified according to their known mechanisms of action in cells laying stress on corticosteroids which were prescribed for a median duration of 29 days per course in the form of dexamethasone with a median dose of 8 mg (dose range, 1 mg-40 mg).

2.1 Statistical analysis

The data are analyzed using some statistical tools. The analysis tools are confirmed in chi-square test (x^2-test), cumulative incidence (*CI*), relative risk (*RR*), odds ratio (*OR*) and their confidence intervals. The IBM SPSS for Windows (version 23.0) is used to fit cumulative incidence using Kaplan-Meier and cumulative hazard using Cox's proportional hazards regression model for cataract according to lens dose among five-year survivors. Attained age is used as the primary time scale. The Kaplan-Meier method for estimating survival functions and the Cox proportional hazards regression model for estimating the effects of covariates on the hazard of the occurrence of the event are commonly used statistical methods for the analysis of survival data. Estimating the incidence of an event as a function of follow-up time provides important information on the absolute risk of an event. In the absence of competing risks, the Kaplan-Meier estimate of the survival function is frequently used for estimating the survival function. One minus the Kaplan-Meier estimate of the survival function provides an estimate of the cumulative incidence of events over time. In the case study that follows, the incidence of cataract in patients is examined [3].

2.1.1 Cumulative incidence (*CI*) or incidence proportion is a measure of frequency, where it is a measure of disease frequency during a period of time [40]. *CI* is an estimate of risk. It is the proportion of individuals who experience the event in a defined time period [24]. *Event/Number during some time T = cumulative incidence*

2.1.2 *Relative risk (Risk Ratio) (RR)* is a measure of the risk of a certain event happening in one group compared to the risk of the same event happening in another group. In cancer research, risk ratios are used in prospective studies, such as cohort studies and clinical trials. A risk ratio of one means there is no difference between two groups in terms of their risk of cancer, based on whether or not they were exposed to a certain substance or factor, or how they responded to two treatments being compared. *RR* is the ratio of the risk or probability of an event occurring in group 1 (P_1) versus the probability of the event in group 2 (P_2). Then the relative risk is

$$RR = \frac{P_1}{P_2} \quad (35)$$

2.1.3 *The Confidence interval* (*CIs*) indicates the level of uncertainty is associated with the estimate of the intervention (the precision or accuracy of the estimate) [17]. Confidence intervals are used because a study recruits only a small sample of the overall population so by having an upper and lower confidence limit we can infer that the true population effect lies between these two points. Most studies report the 95% confidence interval (95%CIs). The 95% confidence interval of Relative Risk as follows [32].

95% CIs= exp(ln(RR)-1.96× SE[ln(RR)]) to exp(ln(RR)+1.96× SE[ln(RR)])
Where, SE is the Standard Error

2.1.4 *Odd ratio (OR)* is the "measure of association" for a case-control study. It is a measure of the relative magnitude of the odds of exposure among individuals who have the disease (cases) and the odds of exposure among individuals who do not have the disease (controls). It quantifies the relationship between an exposure and a disease or outcome in a case-control study [19]. i.e. to quantify how strongly the presence or absence of property A is associated with the presence or absence of property B in a given population [41]. The odds ratio is calculated using the number of case-patients who did or did not have exposure to a factor and the number of controls who did or did not have the exposure. The odds ratio gives information about how much higher the odds of exposure are among case-patients than among controls. It is also one of several statistics that have become increasingly important in clinical research and decision-making. It is particularly useful because as an effect-size statistic, it gives clear and direct information to clinicians about which treatment approach has the best odds of benefiting the patient. The odds ratio is a way of comparing whether the odds of a certain outcome is the same for two different groups [25]. The odds ratio (OR) is defined as [38]

$$OR = \frac{(exposed\ cases)(unexposed\ cases)}{(exposed - cases)(unexposed - case)}$$

Where N is the number of patients, The, 95% confidence interval [30].

$$95\%\ CIs = exp(ln(OR)-1.96 \times SE[ln(OR)]) \quad to \quad exp(ln(OR)+1.96 \times SE[ln(OR)])$$

3. RESULTS

The studied patients included 319 (64.4%) males and 176(35.6%) females, with a male to female ratio of 1.81:1. Their ages ranged from 5 to 25 years at the time of study. The follow-up time for all patients ranged from 60 to 80 months with median of 46 months. The characteristic of the studied 5-year survival patients was presented in table (1). At the time of follow up, most of the survivors were seen between the ages of 10-20 years, 26(5.3%) of them are diabetics, and 398(80.4%) received RT during the course of treatment. Among 5432 patients attending the follow up of cancer clinic, 99 patients have cataract which comprises 1.8% of the total number of patients and 20% of studied group. They also comprise 24.9% among the patients who received RT. The incidence of cataract was found to be highly statistically significant among the abnormal weight, diabetic patients, in those using corticosteroid, and those received combined radio-chemotherapy (R/CT) as compared to normal weight, non-diabetic patients, those who didn't use corticosteroid, and those who received RT alone (p-value = 0.0021, <0.0001, <0.001, and <0.0001 respectively). It is not statistically significant among the age groups at the time of follow up or gender (p value = 0.5865 and 0.4525 respectively). The incidence of cataract was significantly reduced among who received lower radiation dose and by using the radiation protection measurements (p-value = <0.001 and <0.0001 respectively) indicating the importance of using lower RT dose in treatment and using these measurements in preventing the occurrence of cataract. Cumulative incidence of cataract for gender has been found to be higher in male (21%) than in female (18.2%), the risk in male to develop cataract was increased by about 1.2 times (RR=1.2) as that in female. The patients who has cataract at age 5-<15 year (CI= 19.9%) regularly have risk ≈1, it suggests little or no difference in risk of who has cataract as age 15-25 year (CI =20.2%). The control of body mass index is normal weight; the cataract risk in underweight patients was decreased about 0.5 times when compared to control patients, as well as, overweight and obese patients have CIs values closer to that of control patients (RR≈1). The risk of cataract in diabetic patients (CI=88.5%) is 5.5 times higher than that in non-diabetics (CI=16.2%). The risk of the patients treated with RT was 0.44 times lower (CI=15%) than the patients treated with R/CT (CI=34%). For using of corticosteroids, the risk of those who have cataract is about 2 times higher than those who not. The lower risk for cataract was observed in patients who received a radiation dose of 22-35 Gy (RR=0.50) as compared to who received a radiation dose of >35-60 Gy. The risk with using radiation protection measurements (CI=13.6%) is about 0.14 times lower than that with not using it (CI=98.1%) indicating a strong decrease in risk of cataract after using these measurements (Table 1). Regarding the OR, there are no difference between the patients who have cataract and who didn't have in relation to gender, age, and overweight & obese patients (OR approximately equal 1). But, the association of diabetes with the prevalence of cataracts, was 39 times higher (OR= 39.5), and 3 times more with using corticosteroid (OR= 2.775). The cataract is less likely to occur in case of underweight (OR=0.403), using RT alone (OR= 0.344), and in using radiation doses 22-35 GY (OR=0.429). Additionally, OR is extremely low in cataract patients using radiation protection measurements (OR=0.003) meaning that there is a strong association between using protective measurements and the prevention of cataract (Table 1).

Table 1: The characteristic of the Childhood Cancer Survivors

Parameter	Leuke N=158	Lym N=183	STS N=89	Wilms N=65	Total N=495		Cataract N=99		P-value	CI (%)	RR (95% CIs)	OR (95% CIs)
	No	No	No	No	No	%	No	%				
Gender									0.4525		1.155 (0.791 - 1.687)	1.196 (0.749-1.911)
Male	96	142	49	32	319	64.4	67	67.7		21.00		
Female	62	41	40	33	176	35.6	32	32.3		18.18		
Age at follow up time									0.5865		0.984 (0.691 -1.4)	0.98 (0.629-1.525)
5-<10	3	6	6	4	19	3.8	6	6.1		31.58		
10-<15	75	80	55	43	253	51.1	48	48.5		18.97		
15-<20	59	65	19	15	158	32.0	33	33.3		20.89		
20-25	21	32	9	3	65	13.1	12	12.1		18.46		
Body mass index									0.0021		0.475 (0.311 - 0.726)	0.403 (0.242-0.67)
Underweight (<18.5 kg/m^2)	69	72	36	37	214	43.2	26	26.3		12.15		
Normal (18.5–<25 kg/m^2)	73	85	40	25	223	45.1	57	57.5		25.56	1.104 (0.64-1.91)	1.144 (0.535-2.445)
Overweight (25–<30 kg/m^2)	11	17	9	2	39	7.9	11	11.1		28.21	1.029 (0.47-2.26)	1.040 (0.359-3.016)
Obese (30–≤35 kg/m^2)	5	9	4	1	19	3.8	5	5.1		26.32		
Diabetes status									<0.0001		5.459 (4.259 - 6.997)	39.645 (11.612-135.357)
Yes	9	11	4	2	26	5.3	23	23.2		88.46		
No	149	172	85	63	469	94.7	76	76.8		16.2		
Treatment modalities									<0.0001		0.441 (0.296 - 0.655)	0.344 (0.209-0.565)
No RT	24	13	18	42	97	19.6	0	0		0		
RT alone	35	103	33	12	183	37.0	27	27.3		14.75		
R/CT	99	67	38	11	215	43.4	72	72.7		33.49		
Use of Corticosteroids									<0.001		2.343 (1.421 - 3.863)	2.773 (1.563-4.925)
Yes	158	183	0	0	341	68.9	83	83.8		24.34		
No	0	0	89	65	154	31.1	16	16.2		10.39		
Parameter	**Leuke N=134**	**Lym N=170**	**STS N=71**	**Wilms N=23**	**Total N=398**		**Cataract N=99**		**P-value**	**CI %**	**RR (95% CI)**	**OR (95% CI)**
	No	No	No	No	No	%	No	%				
Cataract									0.5952			
Yes	34	43	19	3	99	24.9						
No	100	127	52	20	299	75.1						
Total RT Dose									<0.001		0.525 (0.360 - 0.765)	0.429 (0.265-0.695)
22 – 35 Gy	52	89	34	10	185	46.5	31	31.3		16.76		
> 35 – 60 Gy	82	81	37	13	213	53.5	68	68.7		31.92		
Use of R. Prot. measurements									<0.0001		0.139 (0.106 - 0.182)	0.003 (0.0004-0.0225)
Yes	124	132	67	22	345	86.7	47	47.5		13.6		
No	20	25	5	3	53	13.3	52	52.5		98.1		

CI: Cumulative Incidence, *RR:* Relative Risk, *OR:* Odd Ratio, *RT:* Radiotherapy, *R/CT:* Radio-chemotherapy

Cumulative incidence of cataract across attained age of childhood cancer survivors according to radiation dose using Kaplan-Meier method is shown in Figure (1). The cumulative incidence of cataract increases with the

increase of age. The incidence of cataract among who received lower radiation dose (group A) is higher in younger age (below 15 years old) than those who received higher dose in older age (group B). After the age of 15 years the incidence of cataract is approached to each other at all doses. However, Figure (2) shows cumulative hazard proportion in the case of absence of protection measurements using Cox regression method. The risk of cataract increases with age among who missing the protection measurements and it is higher in who received higher radiation dose (>35-60 Gy)
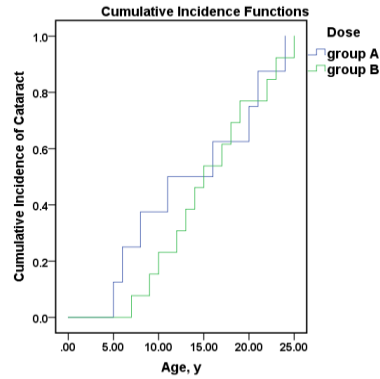
FIG.1: Cumulative incidence of Cataract Using Kaplan-Meier Method
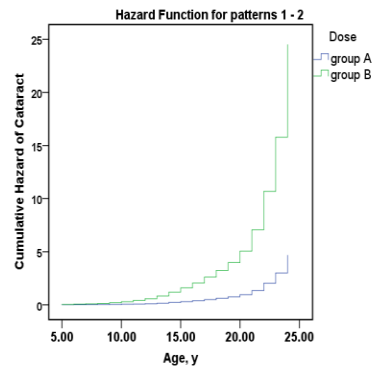
FIG. 2: Cumulative Hazard of Cataract Using Cox proportion Hazard Regression Method

Group A = doses 22-35 Gy, Group B = doses >35-60 Gy

4.   DISCUSSION

Induction of cataracts in humans has been viewed as a deterministic effect that had a dose threshold and for which the severity increased and the latency decreased as the radiation dose increased above that threshold [33]. The results of the current study provide risk estimates for the occurrence of cataract among pediatric cancer survivors with follow-up spanning more than 6 years. There is a strong association between ocular exposure to ionizing radiation and long-term risk of pre-senile cataract. The risk in male is slightly higher than that in female, but the incidence in age groups is the same and there is no significance between the groups. The difference in incidence is highly statistically significant among the abnormal weight, diabetic patients, in those using corticosteroid, and those received combined R/CT. The incidence was significantly reduced among who received lower radiation dose and through using appropriate protection measurement indicating that the use of radiation protection measurement carries a significant protection. Among the survivors who received radiation dose of 22 – 35 Gy and > 35 – 60 Gy, 31.1% & 68.7% reported developing a cataract within 5 years after initial cancer diagnosis respectively, accounting for 16.8% & 31.9% respectively of all cataract cases in this dose group. This demonstrates the relationship between latency and dose, and the need for long-term follow-up for assessing cataract risk after low-dose exposures. The relationship between RT and cataract formation has been described in many studies since the 1950s [20]. During childhood and adolescence, the number of both epithelial cells and fibers in the human lens increases by approximately 45–50% [31], raising the possibility of age-related sensitivity to radiation in cataract formation. This has been supported by studies among pediatric and adult cancer survivors, and particularly after single-dose total-body irradiation in bone marrow transplant recipients [11,36]. These studies have shown that cataract occurred in at least 20% of irradiated patients within several years after treatment. Among them, in at least three series of patients with unshielded eyes, the cumulative incidence reached 100% within 10 years of exposure [22]. In a previous study of infants who were exposed to a lenticular dose of 1 Gy for skin hemangiomas, an increase of one month in age at exposure was associated with lower risk for developing a posterior subcapsular opacity but higher risk for developing cortical opacity [16,8]. The current study did not show a clear dependency of age at RT on the risk for cataract. This, also, in accordance with *Alloin et al* [2] and *Allodji et al* [1] that pointed out that age at RT does not appear to affect the risk significantly. The cumulative incidence of cataract in the present study increases with the increase of age. The incidence of cataract among who received lower radiation dose is higher in younger age (below 15 years old) than those who received higher dose in older age. After the age of 15 years the incidence of cataract is approached to each other at all doses. However, Lack of information on type of opacity may therefore explain why we did not observe evidence of an effect of age at radiation exposure on cataract risk among children   and adolescents in this study [8]. In addition to the effects of RT, the chemotherapeutic agents, typically   used for the

management of childhood malignancies such as leukemia and lymphoma, were also associated with elevated risk of cataract independent of radiation exposure. Cataract formation can be a side effect of oxidative damage to cell membranes due to doxorubicin and cytosine arabinoside. Such damage has been demonstrated in rabbit eyes [6] as well as in small studies of pediatric cancer patient populations [22]. But, the magnitude of risk associated with exposure to CT generally was lower than that associated with RT [8]. However, Melphalan was significantly associated with the risk for cataract development, possibly due to the combined toxic effect of this CT agent with radiation exposure [37,1,34]. Contrary, *Sijssens et al* reported a significantly lower risk of cataract surgery over time in patients treated with methotrexate. On the other hand, Cataractogenesis is also a documented feature of corticosteroids in the current study. In several previous studies [21,7,12], the association between RT and risk of cataract was not affected by steroid use. Other recent study, the risk of cataracts was significantly associated with exposure to prednisone in a dose dependent fashion, especially, in a radiation dose of 30 Gy or greater to the posterior fossa or the temporal lobe [29,39]. *Allodji, et al* [1] reported that the analyses did not support modification of the risk for cataract by administration of glucocorticoids (n=15) or the presence of diabetes mellitus (n=56). This is in contrary with the present study. However, these observations are of potential value for caregivers treating children at high risk of therapy induced cataract [8].

On the other hand, current radiation protection guidelines are predicated on the assumption that cataractogenesis is a deterministic event and requires a threshold radiation dose before cataracts will develop [18]. A previous published study [39] revealed a significantly increased risk of cataract at doses greater than 2 Gy to the eye. But *Chodick et al* [8] found elevated risk of cataract from a dose of ≥0.5 Gy. This is supported by International Commission on Radiological Protection (ICRP) that reduced the putative human threshold values for radiation cataractogenesis to 0.5 Gy from previous values of 2–8 Gy [18]. Radiation protection standards recognize that it is not possible to eliminate all radiation exposure, but they do provide for a system of control to avoid unnecessary exposure and to keep doses in the low dose range. Doses below the thresholds for deterministic effects may cause cellular damage, but this does not necessarily lead to harm to the individual: the effects are probabilistic or 'stochastic' in nature [4]. For many cancer patients, radiation dose to the target tissue cannot be reduced because it would adversely affect curative efficacy. However, accurate radiation dose estimates and shielding design for the lens of the eye provide an opportunity to maintain the effectiveness of radiation treatments for young patients while reducing the risk of cataract [8].

5. CONCLUSION

The present study adds new information by providing risk estimates for the occurrence of late eye-related effects after a mean follow-up spanning more than 6 years from cancer diagnosis. It suggests that likelihood of cataract formation increases with increasing exposure to ionizing radiation with no apparent threshold level, a finding that challenges the National Council on Radiation Protection and International Commission on Radiological Protection assumptions that a radiation dose of at least 2 Gy is associated with increased cataract risk [9]. This risk can be significantly reduced despite lowering of dose limits through using appropriate eye protection, increasing awareness among those at risk, better adoption and increased usage of protective measures. Furthermore, future efforts should focus on methods to reduce cataracts in high-risk patients and to educate healthcare providers about the importance of screening this population for the development of cataracts.

6. REFERENCE

[1] Allodji, R.S., Diallo, I., El-Fayech, C., Kahlouche, A., Dumas, A., Schwartz, B., Oberlin, O., Benadjaoud, M.A., Labbé, M., Jackson, A., Bullet, J., Rubino, C., Haddy, N., De Vathaire, F., Association of Radiation Dose to the Eyes with the Risk for Cataract After Nonretinoblastoma Solid Cancers in Childhood, JAMA Ophthalmol (2016) 134(4):390-397.

[2] Alloin, A.L., Barlogis, V., Auquier, P., et al., Prevalence and risk factors of cataract after chemotherapy with or without central nervous system irradiation for childhood acute lymphoblastic leukaemia: an LEA study, Br J Haematol (2014) 164(1):94-100.

[3] Austin, P.C., Lee, D.S., Fine, J.P., Introduction to the Analysis of Survival Data in the Presence of Competing Risks, Circulation (2016) 133(6):601-609

[4] Australian Government, Australian Radiation Protection and Nuclear Safety Agency, SAFETY GUIDE, Radiation Protection in Nuclear Medicine, Radiation Protection Series Publication No. 14.2, This publication was approved by the Radiation Health Committee on 16 July 2008, and endorsed for publication by the Radiation Health & Safety Advisory Council on 8 August (2008).

[5] Baradaran-Rafii, A., Shirzadeh, E., Eslani, M., Akbari, M., Optical correction of aphakia in children, J Ophthalmic Vis Res (2014) 9:71–82.

[6] Bayer, A., Ereklioglu, C., Demirkaya, E., Altun, S., Karslioglu, Y., Sobaci, G., Doxorubicin-induced cataract formation in rats and the inhibitory effects of hazelnut, a natural antioxidant: a histopathological study, Med Sci Monit (2005) 11:BR300–4.

[7] Bray, L., Carey, P., Proctor, S., Evans, R., Hamilton, P., Ocular complications of bone marrow transplantation, Br J Ophthalmol (1991) 75:611–4.

[8] Chodick, G., Alice, J., Sigurdson, A.J., Kleinerman, R.A., Sklar, C.A., Leisenring, W., Mertens, A.C., Stovall, M., Smith, S.A., Weathers, R.E., Veiga, L.H.S., Leslie, L., Robisonh, L.L., Inskipa, P.D., The Risk of Cataract among Survivors of Childhood and Adolescent Cancer: A Report from the Childhood Cancer Survivor Study, Radiat Res (2016) 185, 366–374

[9] Chodick, G., Bekiroglu, N., Hauptmann, M., Alexander, B.H., Freedman, D.M., Doody, M.M., et al., Risk of cataract after exposure to low doses of ionizing radiation: a 20-year prospective cohort study among US radiologic technologists, Am J Epidemiol (2008) 168:620–31.

[10] Chodick, G., Kleinerman, R.A., Stovall, M., et al., Risk of cataract extraction among adult retinoblastoma survivors, Arch Ophthalmol. (2009)127(11): 1500-1504.

[11] Deeg, H.J., Flournoy, N., Sullivan, K.M., Sheehan, K., Buckner, C.D., Sanders, J.E., et al., Cataracts after total body irradiation and marrow transplantation: a sparing effect of dose fractionation, Int J Radiat Oncol Biol Phys (1984) 10:957–64.

[12] De Marco, R., Dassio, D., Vittone, P., A retrospective study of ocular side effects in children undergoing bone marrow transplantation, Eur J Ophthalmol (1996) 6:436–9.

[13] Friedman, D., Constine, L., Late effects of cancer treatment. In: Halperin, E., Constine, L., Trabell, N., editors. Pediatric radiation oncology. Philadelphia: Lippincott Williams and Wilkins, (2005).

[14] Geenen, M.M., Cardous-Ubbink, M.C., Kremer, L.C., et al., Medical assessment of adverse health outcomes in long-term survivors of childhood cancer, JAMA (2007) 297(24):2705-2715.

[15] Gudmundsdottir, T., Winther, J.F., de Fine Licht S., et al., ALiCCS Study Group. Cardiovascular disease in Adult Life after Childhood Cancer in Scandinavia: a population-based cohort study of 32,308 one-year survivors, Int J Cancer (2015) 137(5):1176-1186.

[16] Hall, P., Granath, F., Lundell, M., Olsson, K., Holm, L., Lenticular opacities in individuals exposed to ionizing radiation in infancy, Radiat Res (1999) 152:190–5.

[17] Hoffmann, T., Bennett, S., Del M, C., Evidence-Based Practice Across the Health Professions, 2nd Edition, eBook ISBN: 9780729582278, Paperback ISBN: 9780729541350, Churchill Livingstone Australia, Elsevier (2013)

[18] ICRP statement on tissue reactions / early and late effects of radiation in normal tissues and organs – threshold doses for tissue reactions in a radiation protection context. ICRP Publication 118. Ottawa, Canada: International Commission on Radiological Protection; 2012. (bit.ly/1LYN7Mr)

[19] Kaelin, M.A., Bayona, M., Case–Control Study, The Young Epidemiology Scholars Program (YES) is Supported by The Robert Wood Johnson Foundation and administered by the College Board, (2004).

[20] Kleiman, N., Radiation cataract, Ann ICRP (2012) 41:80–97.

[21] Lappi, M., Rajantie, J., Uusitalo, R., Irradiation cataract in children after bone marrow transplantation, Graefes Arch Clin Exp Ophthalmol (1990) 228:218–21.

[22] Leiper, A.D., Non-endocrine late complications of bone marrow transplantation in childhood: part II, Br J Haematol (2002) 118:23–43.

[23] Little, M.P., A review of non-cancer effects, especially circulatory and ocular diseases, Radiat Environ Biophys (2013) 52(4):435-449.

[24] Martin, J., Cumulative Incidence - Person-Time, CTSPedia, MaryB (2009) https://www.ctspedia.org/do/view/CTSPedia/StudyIncidenceCumul,

[25] McHugh, M.L. The odds ratio: calculation, usage, and interpretation, Biochemia Medica, (2009):19(2):120-6. http://dx.doi.org/10.11613/BM.2009.011

[26] Mertens, A.C., Liu, Q., Negliam J.P., et al. Cause-specific late mortality among 5-year survivors of childhood cancer: The Childhood Cancer Survivor Study, J Natl Cancer Inst. (2008) 100 (19):1368-1379.

[27] Neriishi, K., Nakashima, E., Akahoshi, M., Hida, A., Grant, E.J., Masunari, N., et al. Radiation dose and cataract surgery incidence in atomic bomb survivors, 1986–2005, Radiology (2012) 265(1):167-174.

[28] Oeffinger, K.C., Mertens, A.C., Sklar, C.A., Kawashima, T., Hudson, M.M., Meadows, A.T., et al., Childhood Cancer Survivor Study. Chronic health conditions in adult survivors of childhood cancer, N Engl J Med (2006) 355(15):1572-1582.

[29] Packer, R.J., Gurney, J.G., Punyko, J.A., et al. Long-term neurologic and neurosensory sequelae in adult survivors of a childhood brain tumor: Childhood Cancer Survivor Study, J Clin Oncol. (2003) 21(17):3255-3261.

[30] Pagano, M., Gauvreau, K. Principles of Biostatistics, Student Solutions Manual for Principles of Biostatistics, 2nd Edition. Belmont, CA: Brooks/Cole, (2000).

[31] Rosen, E., The lens. In: Yanoff, M., Duker, J., editors. Ophthalmology. St. Louis: Mosby (2004).

[32] Schechtman, E., Odds Ratio, Relative Risk, Absolute Risk Reduction, and the Number Needed to Treat—Which of These Should We Use? Value Health (2002) 5(5):431-6.

[33] Shore, R.E., Neriishib, K., Nakashimac, E., Epidemiological Studies of Cataract Risk at Low to Moderate Radiation Doses: (Not) Seeing is Believing, Radiat. Res (2010) 174(6b):889-894.

[34] Sijssens, K., Rothova, A., Van De Vijver, D., Stilma, J., De Boer, J., Risk factors for the development of cataract requiring surgery in uveitis associated with juvenile idiopathic arthritis, Am J Ophthalmol (2007) 144:574–9.

[35] Stare, J., Maucort-Boulch, D., Odds Ratio, Hazard Ratio and Relative Risk, Metodoloski zvezki. (2016) 13(1): 59-67

[36] Stava, C., Beck, M., Vassilopoulou-Sellin, R., Cataracts among cancer survivors, Am J Clin Oncol (2005) 28:603–8.

[37] Suesskind, D., Schrader, M., Foerster, M.H., Ernemann, U., Aisenbrey, S., Cataract formation: a possible complication of intra-arterial chemotherapy for retinoblastoma, Eur J Ophthalmol. (2014) 24(3):449-453.

[38] Szumilas, M., Explaining Odds Ratios, Journal of the Canadian Academy of Child and Adolescent Psychiatry (2010) 19(3): 227–229.

[39] Whelan, K., Stratton, K., Kawashima, T., Waterbor, J., Castleberry, R., Stovall, M., et al. Ocular late effects in childhood and adolescent cancer survivors: a report from the Childhood Cancer Survivor Study, Pediatr Blood Cancer (2010) 54(1):103-109.

[40] Wikipedia, Cumulative incidence, https://en.wikipedia.org/wiki/Cumulative_incidence (2017).

[41] Witmer, J.A., Statistics for Life Sciences, Third Edition, Study Guide, Just the Facts101 Textbook Key Facts, Prepared by Cram 101 Textbook Reviews, Content Technologies Inc. publications and Services, elSBN 9781490250762, E-2 5283. (2017).

[42] Worgul, B.V., Kundiyev, Y.I., Sergiyenko, N.M., et al. Cataracts among Chernobyl clean-up workers: implications regarding permissible eye exposures, Radiat Res. (2007) 167(2):233-243.

IAEA/WHO POSTAL DOSE QUALITY AUDITS
FOR RADIOTHERAPY: REASONS FOR ERRORS
IN CLINICAL DOSIMETRY

T. BOKULIC
Dosimetry and Medical Radiation Physics Section, IAEA
Email: t.bokulic@iaea.org

P. KAZANTSEV
Dosimetry and Medical Radiation Physics Section, IAEA
Email: p.kazantsev@iaea.org

B.HEALY
Dosimetry and Medical Radiation Physics Section, IAEA
Email: b.healy@iaea.org

J. IZEWSKA
Dosimetry and Medical Radiation Physics Section, IAEA
Email: j.izewska@iaea.org

Abstract

The IAEA together with WHO has been operating a postal auditing service to validate the calibration of radiotherapy beams in radiation oncology hospitals in developing Member States since 1969. This service provides an independent verification of the dose delivered by radiotherapy treatment machines using thermoluminescent dosimeters (TLDs).

Approximately 12300 radiotherapy beams, throughout the world, have been checked since the introduction of the service. Audit results show that in the early years of the service, only about 50% of the beams checked had correct calibration which means that the difference between the dose measured with TLD and the dose stated by the hospital was within 5%. This fraction has been constantly growing until now when the percentage of acceptable results is about 97%. Detailed analysis of the information provided by the audit participants in their data sheets was conducted and it has been shown that in the last five years (2012-2016), the most common reasons for dosimetry errors were calculation mistakes (27%) and set-up errors (18%). In about 44% of cases, data were not made available to provide a reliable explanation for the reasons of discrepancies in dosimetry.

1. INTRODUCTION

High quality and safe radiotherapy treatment with adequate outcome for the cancer patient can only be ensured when a high degree of accuracy and reproducibility in radiation dose delivery is in place. The calibration of the radiation beam is the first and fundamental step in the complex radiotherapy process. If the radiation beam is erroneously calibrated, radiotherapy treatment will be incorrectly delivered; too much dose may lead to severe side effects due to the unnecessary irradiation of the normal tissue surrounding tumour, while insufficient dose to the tumour does not ensure its adequate control. In the case of large deviations between the planned and the delivered doses, the consequences can be fatal. Larger dosimetric errors have a substantial impact on the radiotherapy outcome and persisting smaller errors, if unnoticed, may result in a sub-optimal treatment of large numbers of patients.

Dosimetry audits are an efficient tool to ensure consistency in radiotherapy. They may be organized as postal audits [1-4], using solid state dosimeters which are sent to the audited hospital for irradiation, or as on-site audits using ionization chambers and suitable phantoms [5-7]. The audits can cover different levels from reference dosimetry to advanced radiotherapy techniques.

This paper gives an overview of the results of the IAEA/WHO postal dose audit service and analyses reasons for hospital dosimetry errors and deviations registered in audits.

2. METHODS

The IAEA/WHO TLD postal dose audit service has been offered to IAEA Member States eligible to receive Technical Cooperation support from the IAEA and to WHO Member States on WHO's request.

In each dosimetry audit run, hospitals that applied for the audit, are supplied by the IAEA Dosimetry Laboratory (DOL) with dosimeters to be irradiated and a set of instructions, and data sheets to collect the relevant information. Dosimeters are irradiated in the radiotherapy beam, either with a high-energy photon beam produced by a Co-60 unit or by a linear accelerator, using hospital's treatment facilities. The standard IAEA dosimeter holder is used and irradiation is done in a water phantom in the reference conditions, 10 cm x 10 cm field size at 10 cm depth and in either fixed source to surface (SSD) or source to axis distance (SAD) set-up. Hospitals are requested to calculate the dose to the dosimeter following the clinical practice used for the patient dose calculations. Upon irradiation, the dosimeters are returned to the IAEA where they are evaluated by the DOL. If the difference between the participant's stated dose and the measured dose is less than 5%, the results are considered acceptable. For results outside the 5% acceptance limits, a follow-up procedure is initiated which aims at resolving the observed deviations. A second dosimeter set is sent to the hospital and interaction with hospital medical physicists is established in an attempt to identify the cause of the deviation. If necessary, local or international experts in medical radiation physics may be contacted to visit the hospital and assist in resolving the deviation.

For each dosimeter set, the detailed analysis of the information provided by the participants in their data sheets is done by IAEA. This involves reviewing the participant's calculation of the dose delivered to the IAEA dosimeter and analysing the details of ionization chamber dosimetry performed by the hospital. Any deviation between the dose reported by a participating hospital and that determined by the IAEA is investigated.

3.   RESULTS

In the period 1969-2016 of the IAEA/WHO dose audit service, 12292 checks using TLDs have been performed to verify the calibration of 5128 high energy photon beams in 2228 radiotherapy hospitals in 132 countries. Initially, only about 50% of the beams checked had the results within the acceptance limit of 5%. The results improved with time, in particular after the introduction of the systematic follow-up of poor results in 1996 by providing a second dosimeter for repeat irradiation.

The downtrend of poor audit results outside the 5% acceptance limits for the period 2000-2016 is depicted in Fig. 1. Deviations are distributed into two groups according to their magnitude: 5-10% and >10%. In 2000-2016, the percentage of deviations outside the 5% limits decreased from 22% to 3%. In the last five years, the percentage of deviations decreased from 9% in 2012 to 3% in 2016 including the decrease, from 4% to 1.5% and from 5% to 1.6% in the groups 5-10% and >10% deviations, respectively.
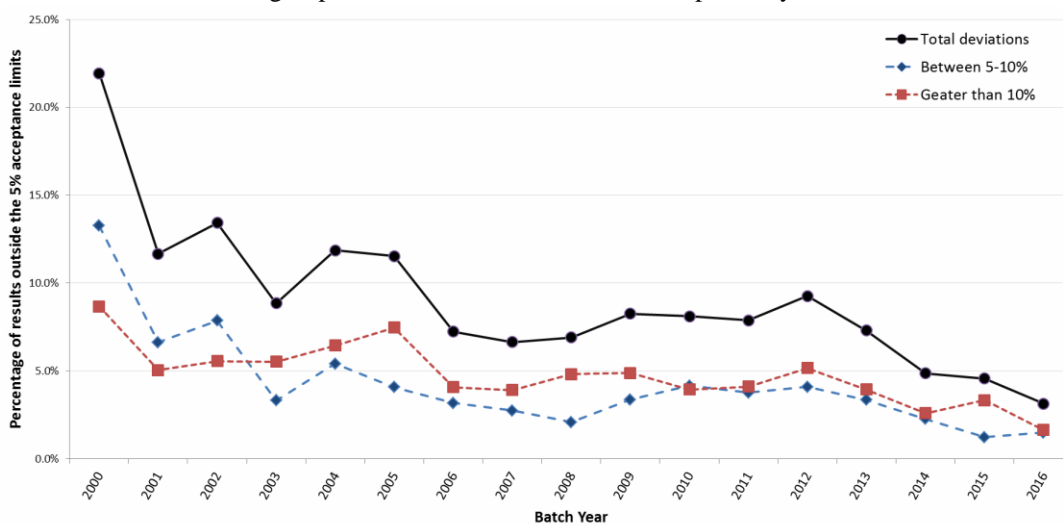
FIG 1. Percentage of hospital TLD results outside the acceptance limits recorded by the IAEA/WHO dose audit service in the period 2000-2016.

Overall, in the last five years, 3194 beams were checked and 188 deviations outside the acceptance limits have been detected. The frequency of occurrence of deviations outside the acceptance limits of 5% in the period 2012-2016 has been grouped according to the cause of deviation as shown in Fig. 2; 51 (27%) of these were attributed to calculation errors and 34 (18%) to set-up errors that accounted for discrepancies between the intended and the actual TLD irradiation geometry. Other errors 21 (11%) were related to issues with ionization chamber dosimetry and various dosimetry mistakes leading to discrepancies between the dose reported in the participant's data sheet and that determined by the DOL from TLD readings. Insufficient data were provided in 83 (44%) data sheets that did not allow for analysis of the cause of deviation.
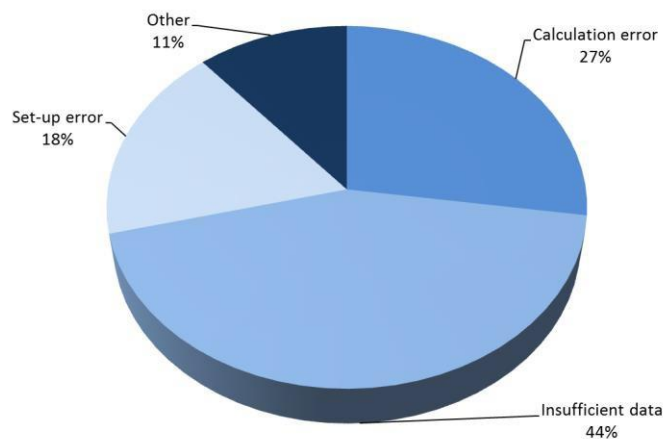
FIG 2. The percentage of occurrence of TLD results outside the acceptance limits of 5% recorded during 2012-2016 and grouped according to the cause of deviation.

4.   DISCUSSION

The IAEA/WHO TLD audit service has witnessed significant improvements in basic dosimetry practices in radiotherapy hospitals across the world. Data in Fig. 1 suggest that the percentage of hospital errors detected in dosimetry audits in 2000-2016 has decreased over seven-fold, i.e. from 22% to 3%. In the last five years, the percentage of deviations decreased three-fold, i.e. from 9% in 2012 to 3% in 2016. These improvements in radiotherapy dosimetry can be attributed to the overall progress in technology, better education of medical physicists and also to regular participation of hospitals in dosimetry audits. Unfortunately, 3% of the recent results remained uncorrected due to local issues and deficiencies that cannot be resolved remotely, such as the use of obsolete radiotherapy equipment, insufficient availability of clinically qualified medical physics staff or lack of modern dosimetry systems in some hospitals.

As can be seen from Fig. 2, typical causes of deviations identified in audits are calculation errors and set-up errors. The group with calculation errors contains mistakes in the determination of dose to TLD using inconsistent clinical dosimetry data. Such errors typically lead to magnitudes in deviations of up to 10%. As showed in Fig. 1, deviations of 5%-10% decreased from 4% in 2012 to 1.5% in 2016. Very large deviations occurred (20% or more) when participants irradiated dosimeters with the number of monitor units (MU) or time needed to deliver the dose to the depth of dose maximum and not to the depth where the dosimeters were located (10 cm). This is typically caused by misunderstanding of the steps required in the dose calculation. In most set-up errors, the confusion is typically made between the beam output (e.g. given for the SSD set-up) and the irradiation of the TLDs (SAD setup) or vice versa. These types of errors, depending on SSD/SAD value, have the magnitude in the range 10% to 18%. The percentage of large deviations >10% decreased from 5% in 2012 to 1.6% in 2016 (Fig. 1). Although calculation errors, set-up errors or their combination do not necessarily prove the deficiencies in the beam calibration, they give an indication of likelihood of human mistakes that may weaken the quality of clinical dosimetry in hospitals. Education and training of medical physicists in clinical dosimetry are of crucial importance in reducing the occurrence of these mistakes.

Other errors were mostly recorded due to the misunderstanding in the application of correction factors for ionization chamber dosimetry or incorrect chamber calibration, incorrect data reporting, insufficient attention by

the hospital staff during the TLD irradiation or misinterpretation of the irradiation instructions. It happens occasionally, that one TLD of the two provided to the hospital, is irradiated twice, resulting in double dose to one TLD and zero dose to the second one. In another case the participant reported power failure during TLD irradiation resulting in an unknown dose to TLD.

In about 44 % of poor results insufficient data were reported by hospitals to reliably determine the cause of the deviation. Frequently in this group, information related to the clinical beam output was incomplete or the dose determined locally from ionization chamber measurements was not reported. This suggests that properly qualified medical physicists were not available or these hospitals used external services for the beam calibration and therefore were not able to report the details of dose measurements. In some cases, even with a fully completed data sheet and after the communication with the participant it was not possible to determine the origin of the deviation.

In addition to the regular follow-up process triggered by the results outside the acceptance limits, about 20% of the participants with acceptable audit results were contacted to clarify additional information such as an inconsistency between their ionization chamber dosimetry with the TLD result or because the calibration of their ionization chambers expired.

5. CONCLUSION

Dosimetry audits by the IAEA/WHO help assure accurate basic radiation dosimetry, allow hospitals to demonstrate compliance with standards, and help to provide assurance that patients are receiving accurate doses. Audits address errors in dosimetry, help to resolve them and stimulate improvements in dosimetry practices.

The IAEA/WHO postal dose audit service has been successfully used for an independent verification of radiotherapy beam calibrations in low and middle income Member States for 48 years. Generally, it is observed that the fraction of audit results outside 5% acceptance limits decreases with time. It shows that participants gain access to better radiotherapy and dosimetry equipment, build capacity in radiotherapy medical physics and improve cancer patients management through more accurate radiotherapy dosimetry.

REFERENCES

[1] IZEWSKA, J., ANDREO, P., The IAEA/WHO TLD postal programme for radiotherapy hospitals, Radiother Oncol 34 (2000) 65-72.

[2] IZEWSKA J, ANDREO, P., VATNITSKY, S., SHORTT, K. The IAEA/WHO TLD postal dose quality audits for radiotherapy: a perspective of dosimetry practices at hospitals in developing countries. Radiother Oncol 69 (2003) 91–97.

[3] FERREIRA, I.H., DUTREIX, A., BRIDIER, A., CHAVAUDRA, J., SVENSSON, H. The ESTRO-Quality assurance network (EQUAL). Radiother Oncol 55 (2000) 273–84.

[4] IBBOTT, GS. QA in radiation therapy: the RPC perspective. J Phys Conf Ser 250 (2010) 1–7.

[5] THWAITES, D.I., WILLIAMS, J.R., AIRD, E.G., KLEVENHAGEN, S.C., WILLIAMS P.C. A dosimetric intercomparison of megavoltage photon beams in UK radiotherapy centres. Phys Med Biol 37 (1992) 445–61.

[6] GERSHKEVITSH E., PESZNYAK C., PETROVIC B., GREZDO J., CHELMINSKI K., DO CARMO L.M., IZEWSKA J., VAN DYK J. Dosimetric inter-institutional comparison in European radiotherapy centres: Results of IAEA supported treatment planning system audit, Acta Oncol, 53, (2014) 628-636.

[7] CLARK C., AIRD E., BOLTON S., MILES E., NISBET A., SNAITH J., THOMAS R., VENABLES K., THWAITES D., Radiotherapy dosimetry audit: three decades of improving standards and accuracy in UK clinical practice and trials, Br J Radiol. 88 (2015): 20150251.

THE ROLE OF SSDL IN ASSURING RADIATION PROTECTION OF PATIENTS IN RADIATION THERAPY

W. Bulski, K. Chelminski, P. Ulkowski, W. Slusarczyk-Kacprzyk
Secondary Standard Dosimetry Laboratory, The Maria Sklodowska-Curie Memorial Cancer Centre and Institute of Oncology,
Warsaw, Poland
Email: w.bulski@zfm.coi.pl

Abstract

The paper describes, as an example, the role of the Polish Secondary Standard Dosimetry Laboratory in assuring radiation protection of patients by means of providing calibration of ionization chambers, TLD postal dosimetry audits, MLC performance testing and the end-to-end audits for conformal or intensity modulated radiation therapy. The historical review of the methods and results are presented. The influence of SSDL in Warsaw on radiation protection of patients in Poland is discussed. The future plans and aims of the Polish SSDL are depicted. The IAEA/WHO, through its network of SSDLs around the world, disseminates standard methods of technical reports or pilot studies of newly developed methods for calibration or auditing. Suitable high quality equipment was provided by the IAEA, as well as special materials and technical support to the SSDL in Warsaw. The activity of the SSDL and services provided for Polish radiotherapy centres result in a reduction of discrepancies between planned doses and doses delivered to patients. The newly tested IAEA methods of end-to-end on site dosimetry audits allow for monitoring and improving quality of IMRT in Poland. The traceability of standards used for the calibration of therapy level dosimeters from Polish radiotherapy centers is assured by the IAEA dosimetry laboratory. The consistency of methods performed in the Polish SSDL with the PN/EN ISO:17025 norm is supervised by the Polish Center for Accreditation – a member of ILAC, both for calibration of dosimeters and for the testing of the dose determination in radiotherapy centers. The rapid technological development of radiotherapy requires particular attention devoted to techniques and institutions which provide services for assuring the radiation protection of patients treated in radiotherapy centres with standard methods, as well as with newly developed ones. The service provided by the SSDL in Warsaw is highly evaluated by the participants of the organized audits, and by customers of the calibration laboratory in Warsaw. The personnel of the SSDL takes part in workshops and conferences organized by the IAEA in order to maintain a high quality of service, which is provided to radiotherapy centers in Poland.

1. INTRODUCTION

The Polish Secondary Dosimetry Laboratory was created in 1966, on the basis of the Physics Laboratory of the Oncology Centre in Warsaw founded originally by Maria Sklodowska-Curie as the Radium Institute in the year 1932. Since its beginning the Physics Laboratory was devoted to developing methods for measurement of radiation delivered to patients treated in the home institute as well as for the control of radiation delivery in other hospitals. The equipment of the SSDL in Warsaw had been acquired with significant support from the IAEA. Since 1988, the laboratory in Warsaw is a member of the IAEA/WHO network of SSDLs, and provides calibration of therapy level dosimeters with cylindrical or plane-parallel ionization chambers in a Co60 beam, and with well chambers using a Ir192 source. Since 2014, the SDDL in Warsaw is an accredited calibration laboratory according to the PN/EN ISO17025 norm, and is annually audited by the Polish Centre for Accreditation – a member of the ILAC association. The accreditation according to the PN/EN ISO17025 norm was also obtained for postal TLD dosimetry audits, which are performed annually in all Polish radiotherapy centres. Due to the activity related to the dosimetry audits, the SSDL in Warsaw collects actual detailed data about the radiation machines, beams and radiation sources, used both for tele- or brachytherapy, in the whole country and keeps such database. Currently, the methods of auditing new and complex techniques, such as intensity modulated radiation therapy (IMRT) modality, are introduced and tested in collaboration with the IAEA. The tested audit methods were developed within the framework of the IAEA projects: CRP E2.40.16 "Development of Quality Audits for Radiotherapy Dosimetry for Complex Treatment Techniques" and CRP E2.40.18 "Development of Quality Audits for Advanced Technology (IMRT) in Radiotherapy Dose Delivery".

2. MATERIALS AND METHODS

2.1. Equipement

The SSDL in Warsaw is equipped with Theratron 780E Cobalt 60 (MDS Nordion) unit used exclusively as a beam source for calibration of therapy level dosimeters or for irradiation of the reference TLD samples. For calibration of the well chambers, the microSeletron (Nucletron) afterloader with Iridium 192 source is used. The reference level dosimeters: Keithley 6517 (USA) and Fluke 35040 (USA) with Farmer type cylindrical chambers, as well as the Supermax 90018 (SunNuclear, USA) electrometer with PTW 35004 (Germany) well chamber are used as the standards.

The FIMEL-PCL3 (France) automatic reader is used for readout of the MT-N type TLD (LiF:Mg,Ti) (TLD-Poland) samples, which are received after irradiations performed according to the postal dosimetry audits.

For complex and advanced methods of irradiation, specially designed phantoms and new detectors are used in dosimetry audits. The Gafchromic (Ashland, USA) EBT3 radiochromic films have been introduced. The films are digitized with an Epson 10000XL Perfection (Seiko, Japan) flat-bed scanner. The FilmQA (3Cognition, USA) and home-made three-colour film calibration software is used in the determination of dose distributions from films irradiated according to the on-site end-to-end dosimetry audits. The EBT2 films are sent to participants in postal audits of multileaf collimator performance of advanced radiotherapy units.

The IMRT thorax phantom – model 002LFC (CIRS, USA) was used for on-site audits of 3D conformal teleradiotherapy techniques performed according to the suggestions and method presented in the IAEA-TECDOC-1583 report [1].

For pilot studies of the dosimetry audits in advanced and IMRT techniques, the phantoms made within the IAEA projects CRP E2.40.16 and CRP E2.40.18 were used by the SSDL in Warsaw [2].

2.2. Calibration

In the SSDL in Warsaw, the calibrations are performed in a Cobalt 60 beam, in terms of the absorbed dose to water, according to the IAEA TRS-398 code of practice. The calibration factors of the user's dosimeters are determined with the replacement method using the standard. The laboratory calibrate all types of cylindrical ionization chambers, as well as the most popular plane-parallel types of chambers (Markus, Roos) used with therapy level electrometers. Virtually all of the dosimeters used in Polish hospitals are calibrated in the SSDL in Warsaw. Since the standards are regularly calibrated in laboratories which are participants of the Comité International des Poids et Mesures (CIPM) Mutual Recognition Arrangement (MRA) – mainly in the IAEA (Austria), PTB (Germany) or in GUM (Poland), the traceability to the primary dosimetry standard is assured.

2.3. Dosimetry audits

Since 1991 the SSDL carries out TLD postal dosimetry audits in all Polish radiotherapy centres. The said audits are performed on a yearly basis. Initially, the audits were carried out in reference conditions but since 2004, they were carried out mostly in non-reference conditions.

Over the last 6 years, several dosimetry audits methods, including the "end-to-end" type, were introduced and tested by the SSDL in Warsaw for quality evaluation of 3D conformal radiotherapy (3DCRT) or IMRT performance in Polish oncology centres.

The method for auditing the 3DCRT was based on the IAEA-TECDOC-1583 [1] report and was developed and tested within the framework of the CRP E2.40.13 project "Development of procedures for dosimetry calculation in radiotherapy". In the audit, 8 planned cases with a gradually increased complication of the beam arrangement were created for the CIRS IMRT thorax phantom.

The methods of the quality audit for photon beams in the presence of heterogeneities was tested using a polystyrene phantom with bone and lung tissue equivalent slabs designed by the IAEA in which the TLD detectors and a cylindrical ion chamber were placed. Using the same phantom, with specially designed inserts for films, the 2D profile quality audit for small photon MLC shaped field sizes was also tested [2].

Within the framework of the IAEA projects: CRP E2.40.16 "Development of Quality Audits for Radiotherapy Dosimetry for Complex Treatment Techniques" and CRP E2.40.18 "Development of Quality Audits for Advanced Technology (IMRT) in Radiotherapy Dose Delivery", a four step audit was tested [3].

In the first step, the quality audit for dose rate dependence of small fields shaped with MLC was performed in Polish radiotherapy centres. This type of audit does not require any measurements to be performed on the treatment machine, because the calculation results obtained from audited treatment planning systems (TPS) were compared with the published benchmark data from The Radiological Physics Center (RPC) in Huston, USA (currently IROC) [4–5].

In the second step, the performance of multileaf collimators (MLC) was verified for a selected treatment machine in each of the Polish teleradiotherapy departments. The Gafchromic EBT2 films were sent to the participants for irradiation with a so called "picket-fence" pattern formed with MLC. The films were evaluated with FilmQA Pro (Ashland, USA) software to detect any traces of geometrical inconsistency in MLC performance.

The Gafchromic EBT3 films were used in an end-to-end audit of the IMRT technique on the treatment units for which the MLC was tested in the former audit. The specially designed cubic polystyrene phantom with a planning target volume (PTV) and organ at risk (OAR) inserts was used in the audit. The TLD capsules and films were placed in the PTV and OAR, in order to record the dose distributions due to irradiation of the IMRT plan created on the basis of computer tomography (CT) of the phantom. A chosen single IMRT field from the treatment plan was also used for irradiation of the film. In the audit, the phantom followed the patient path in each audited radiotherapy centre including pretreatment verification of the planned dose distribution. The films and TLDs were evaluated in the SSDL in Warsaw and compared with results of TPS calculations in terms of dose difference or the gamma index passing rate.

3.   RESULTS

The results of the TLD postal dosimetry have improved considerably over the years. Therefore, the initial tolerance level of ± 5% was decreased to that of ± 3.5%, which is the tolerance level adopted by the IAEA only for SSDLs.

In the quality audit for photon beams in the presence of heterogeneities, 10 departments were examined, which was in that time 1/3 of its total number. The discrepancies between the TPS calculations and the TLD measurements were within a ± 5% range under the bone or lung heterogeneities, and did not exceed ±10% for the TLD placed off-axis in lung equivalent media.

All Polish radiotherapy centres took part in the quality audit for dose rate dependence of small fields shaped with MLC. For fields larger than 2×2 cm^2, the resulting calculations differed less than 4% from the benchmark data. For the 2×2 cm^2 large fields, the differences between the calculated and measured output factors often exceeded 5%, but were still below 10%.

Thirty three Polish radiotherapy centres took part in the audit of MLC performance. The discrepancies between the strip positions of the picket-fence pattern recorded on films and that which had been expected were in the range of ±1.2 mm. The leaf positioning biases were in the range of -0.5 mm to 0.5 mm.

Twelve centres (out of 35) equipped with MLC featured accelerators participated in the end-to-end audit of the IMRT. In the gamma index evaluation of single field dose distributions, the passing rate was higher than 98.5% (at 3 mm / 3% of the maximum dose) in all cases. For the multi-field dose distribution of IMRT plans, the gamma index passing rate was higher than 95% in 11 cases. Discrepancies between the doses measured with TLD and that calculated with TPS were of below 5% in 10 centres for the PTV and in 9 centres for the OAR, and are in accordance with the results obtained with radiochromic films.

4.   DISCUSSION AND CONCLUSIONS

The service provided by the SSDL in Warsaw is highly evaluated by the participants of the performed audits, and by the customers who calibrate their dosimeters there. The laboratory contributes in improving and assuring radiation protection of patients from either excessive exposure or from underdosage during courses of megavolt radiation therapy ranging from simple to the most advanced techniques, such as IMRT. The activity of SDDLs, supported by IAEA methodology and resources, helps in assuring radiation safety of patients.

ACKNOWLEDGEMENTS

REFERENCES

[1] IAEA TECDOC 1583, Commissioning of radiotherapy treatment planning systems: Testing for typical external beam treatment techniques, International Atomic Energy Agency, Vienna 2008.

[2] IZEWSKA, J., WESOLOWSKA, P., AZANGWE, G., FOLLOWILL, D. S., THWAITES, D. I., et. al., Testing the methodology for dosimetry audit of heterogeneity corrections and small MLC-shaped fields: Results of IAEA multi-center studies, Acta Oncol **55** 7 (2016) 909–916.

[3] TOMSEJ, M., FOLLOWILL, D., GEORG, D., IZEWSKA, J., KRY, S., TENHUNEN, M., et al., Development of external dosimetry audits for advanced technology in radiotherapy dose delivery: An IAEA coordinated research project. Phys. Med. **31** S2 (2015) e29.

[4] FOLLOWILL, D., KRY, S., QIN, L., LOWENSTEIN, J., MOLINEU, A., ALVAREZ, P., et al. The Radiological Physics Center's standard dataset for small field size output factors. J Appl Clin Med Phys **13** 5 (2012) 4757.

[5] Erratum: The Radiological Physics Center's standard dataset for small field size output factors. J Appl Clin Med Phys **15** 2 (2014) 356–357.

POST-OPERATIVE RADIATION PROTECTION OF PEOPLE IN RU-106 BRACHYTHERAPY OPHTHALMIC PLAQUE SURGERY.

SIMONE BUSONI
Health Physics Department, AOU Careggi (Firenze University Hospital)
Firenze, Italy
Email: busonis@aou-careggi.toscana.it

LUCA FEDELI
Physics and Astronomy Department, Firenze University
Firenze, Italy

FRANCESCO ROSSI
Health Physics Department, AOU Careggi (Firenze University Hospital)
Firenze, Italy

CESARE GORI
Radiation Protection Expert, Firenze University
Firenze, Italy

Abstract
Exposure measurements around patients with implanted Ru-106 brachytherapy ophthalmic plaque are reported, together with attenuation properties of selected shielding materials.
In order to evaluate the shielding properties of materials, a plaque was fixed on a water equivalent phantom radiation and attenuation were measured. All measurements were performed with calibrated survey meters.
Simulation of bremsstrahlung spectrum emitted by patient was performed and data were compared with measurements results.
Exposure levels measured at 1m distance in front of the eye are 0.05 uSv/h/MBq, at 10cm from patient head, and 0.4uSv/h/MBq (front), 0.25uSv/h/MBq (lateral, opposed to plaque), 0.2 uSv/h/MBq (back).
Average exposure levels, under conservative assumptions, for medical staff is 17 μSv/patient and less than 23 μSv/patient for carers and comforters. TVLs in lead and concrete are about 1.6 cm and 13 cm respectively.

1. INTRODUCTION

The use of $^{106}Ru/^{106}Rh$ (^{106}Ru in the following) plaque was introduced in 1964 for choroidal melanomas therapy. This radioisotope emits β radiation with an end-point energy of 3.5 MeV [1] and X-γ rays of energy between 0.5 and 1.6 MeV [2]. Radiation protection of surgeon is considered in [3].

Workers and public exposure, during the recovery period of the treated patient, is evaluated in the following. In particular attenuation properties of selected shielding materials and exposure levels around patient head and transport safety container were measured. The X-γ and Bremsstrahlung (BS) spectrum emitted by the eye and its attenuation was simulated and compared with experimental measurements.

2. METHODS

^{106}Ru plaques are spherically shaped, with the inner radius of curvature ranging from 12 mm to 14 mm, and their diameter varying between 11.6 mm and 25.4 mm; the active material is deposited on a 0.8 mm silver bulk and covered with 0.1 mm of silver,. Plaque nominal activity varies between 10 MBq and 50 MBq.

Exposure measurements were performed around the head of five patients, in multiple positions at 10 cm and 1 m distance from the skin. Dose rates around the transport container were also measured, at contact and at 1 m distance. The container is cylindrically shaped, the inner part made of aluminium (1 cm thick), the outer coating of stainless steel (1 cm thick).

Attenuation measurements were performed simulating the eye with a 25 mm diameter plastic sphere, filled with water and the plaque attached on it. The plaque had an activity of 35.15 MBq.

All measurements were performed with a calibrated ionization chamber (Victoreen 451, Fluke Corp.,WA,USA) and a portable spectrometer (IdentiFINDER-2, Flir Systems Inc.,OR,USA) equipped with a 35 mm diameter x 51 mm long NaI (Tl) detector.

Selected materials (gypsum, brick, concrete and lead) attenuation properties were measured in "narrow" beam mode following the procedure described in IEC 61331-1:2014 [7]. Decision threshold (DT) and detection limit (DL) were evaluated according to [8], using a truncated Gaussian distribution and considering the uncertainties propagation as described in [9] with 95% of confidence level (CL); only measurements above DL were considered. In Figure 1 the experimental setup used for attenuation measurements is outlined.

A custom code (developed with Mathematica 9.0, Wolfram Champaign, IL USA) was developed to perform numerical simulation of BS spectrum; beta energy spectrum of ^{106}Ru was taken from [1]. Photon BS spectrum was calculated for both eye (25 mm water thickness) considering the appropriate cross-section [4]; normalization of spectrum was performed using the radiation yield [5]. Exposure rates were estimated using the Flux-to-Dose-Rate conversion function [6]. Finally, attenuation of some selected materials (lead and concrete) was calculated.

Fig. 1. Experimental setup for attenuation measurement (not in scale): (1) plaque, (2) eye phantom, (3) Pb diaphragms, (4) attenuation layer, (5) detector.

3. RESULTS

In Table 1 the average exposure levels (±SD) measured around five patients are reported; values are normalized to unit activity (µSv/h/MBq). Five positions around the head, at 10 cm distance from the skin were considered, plus two positions at 1m. *Plaque side* refers to the side of the head closest to eye with implanted plaque, *Front* is in front of the eye with the plaque, *Contralateral* is opposed to *Plaque side*, *Nape* is opposed to *Front*, and *Top* is above the head.

TABLE 1.   OCCUPATIONAL EXPOSURE (Normalised exposure rates in µSv/h/MBq)

Distance from skin	Plaque side	Front	Contralateral	Nape	Top
10 cm	0.44±0.08	0.40±0.07	0.25±0.04	0.20±0.05	0.18±0.04
1 m	0.05±0.01	0.04±0.01	-	-	-

Exposure levels around the transport container are nearly constant for any given direction; average values are (1.6±0.3) µSv/h/MBq at contact and (0.013±0.002) µSv/h/MBq at 1 meter.

In Table 2, HVLs and TVLs for selected materials are reported.

TABLE 2.   MATERIALS ATTENUATION PROPERTIES

	Pb	Concrete	Red Brick	Gypsum
HVL (cm)	0.4	2.9	5.5	14
TVL (cm)	1.6	13	17	41

Figure 2 shows the exposure rate transmission for different attenuation layer thicknesses in lead and in concrete (I_0 is the exposure rate after attenuation of the eye). Experimental data are shown with measurement errors, obtained as described in [9]; blue solid line and red dashed line represent the simulated data for lead and concrete respectively. DT of I/I_0 is 0.09, consequently values below this threshold are not statistically different from the background at a CL of 95%. DL is 0.21, this implies that results below this value are statistically not significant at a CL of 95%.
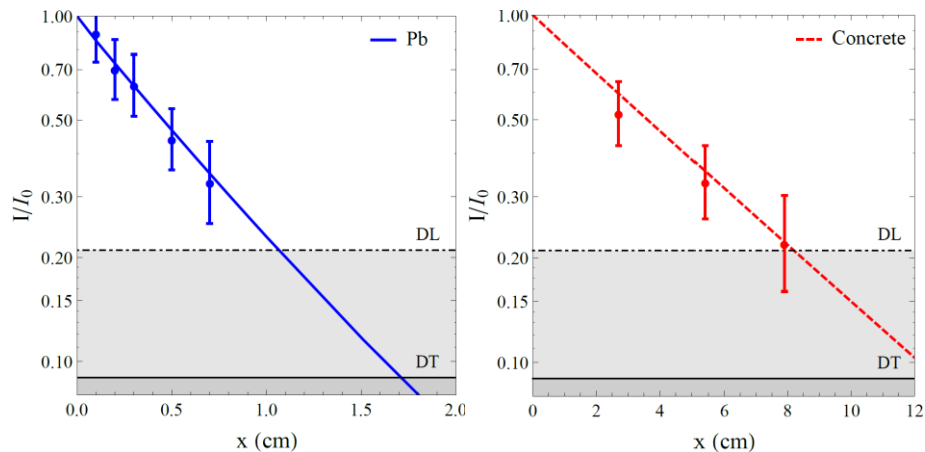
Fig. 2. Exposure rate transmission as a function of the attenuation layer thickness for lead and concrete. (measured and simulated data).

Figure 3 shows the simulated full spectrum of ^{106}Ru, including the X-γ and the BS radiation generated from the eye; blue solid line represents the spectrum outside the eye, red dashed line and green dotted-dashed line include the attenuation of the eye plus 2 mm of lead (Pb) and 10 cm of concrete respectively. Main contribution to total dose rate comes from X-γ rays, BS radiation contribution is around few percent.
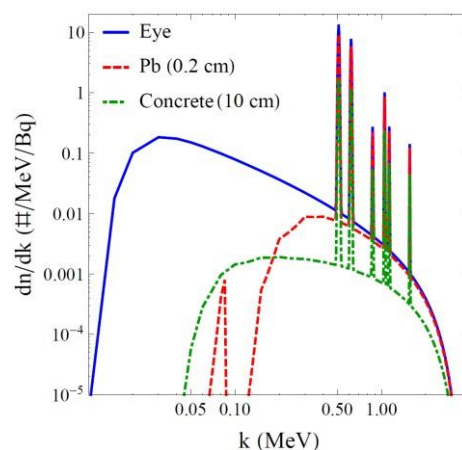
Fig. 3. ^{106}Ru full spectra, including the X-γ and the Bremsstrahlung radiation generated from the eye.

In Table 3 the dose rate in Hp(10), normalised to 1 MBq activity and at a reference distance of 1 m, is reported considering BS from eye. Effect of 2mm lead and 10 cm concrete shielding are considered The *Eye Front* column refers to the dose rate calculated with the attenuation of the eye alone; *Pb* and *Concrete* refer to the dose rates after the attenuation of the eye plus a shielding of 0.2 cm of lead and 10 cm of concrete respectively. First row shows dose rates from BS only, second row shows dose rates from X-γ, the last one represents total dose rate (sum of the previous two rows).

TABLE 3.   DOSE RATE in Hp(10) at 1 m+

Hp(10) at 1m (nSv/h/MBq)	Eye Front	Pb (0.2 cm)	Concrete (10 cm)
Bremsstrahlung	1.3	0.7	0.2
X-γ ray	26.2	19.2	3.9
Total	**27.5**	**19.9**	**4.1**

4. DISCUSSIONS

Measurements in proximity (10 cm) of the head of patient show a dose rate of the order of 0.44 µSv/h/MBq, which reduces to 0.04 µSv/h/MBq at 1 m. Main contribution to the radiation of [106]Ru, used as eye applicator, comes from X-γ ray, BS effect is quite small (around 5% of the total). Simulated data are in agreement with measurements for both lead and concrete shielding.

In the following scenarios, an activity of 25 MBq of the plaque is considered. A worker who assists a patient three times in a day, for 10 minutes for each operation, standing at 30 cm apart, and a recovery time of three days for each implant, receives a dose around 17 µSv/pt Considering an annual exposure limit of 1 mSv/y effective dose, a single worker is allowed to assist around 60 patients each year. In the same hypothesis, the dose for a worker who stands at 1.5 m for 8 hours in a day, considering 60 patients in a year, each recovered for three days, is around 0.65 mSv/y. For people of the public, considering a conservative total amount of 24 hours spent around the patient at 1 m, the exposure is about 23 µSv.

Dose rate at 1 m from transport container is about 3.3 µSv/h. Assuming a total transport time of half hour for each patient, and a total of 60 patients in a year, the total dose of a worker who transport the plaque is less than 100 µSv/y (considering a conservative distance from the plaque of 1 m during all transport time).

HVLs for lead and concrete are 0.4 cm (lead) and 2.9 cm (concrete), while TVLs are 1.6 cm (lead) and 13 cm (concrete).

5. CONCLUSIONS

Exposure measurements were performed around patient with [106]Ru implanted plaque, considering typical activity of the implanted plaques, and conservative recovery and assistance times, up to 60 patients may be treated in a year, without exceeding 1 mSv/y. For the same number of patients, even considering a 8 hours/day standing at 1.5m from the patient bed, the worker received dose is around 0.65 mSv/y.

Attenuation properties for selected materials were measured and agree with simulated results. Main contribution to the exposure comes from X-γ radiation, BS is almost negligible from radiation protection point of view.

In synthesis the use of [106]Ru plaque for ophthalmic treatments, considering a workload of about 60 patients/year does not require specific radiation protection shielding during hospitalization, both for medical staff and people from public.

REFERENCES

[1] E. Browne, R. B. Firestone, Table of Radioactive Isotopes; Wiley-Interscience (1986).

[2] Nucléide – Lara - Library for gamma and alpha emissions, http://www.nucleide.org/Laraweb.

[3] Thomas Laube, Dirk Fluhs, Cecilia Kessler, Norbert Bornfeld, Ophthalmology - Determination of Surgeon's Absorbed Dose in Iodine 125 and Ruthenium 106 Ophthalmic Plaque Surgery, 2000;107:366–369 (1999).

[4] H. W. Koch, J. W. Motz; Reviews of Modern Physics, Bremsstrahlung Cross-Section Formulas and Related Data; vol. 31 n. 4 (1959).

[5] J. H. Hubbell, S. M. Seltzer, X-Ray Mass Attenuation Coefficients, https://www.nist.gov/pml/x-ray-mass-attenuation-coefficients.

[6] Seog-Guen Kwon, Kyung-Eung Kim, Chung-Woo Ha, Philip S.Moon, Chong-Chul Yook, Journal of Korean Nuclear Society, Calculation of Neutron and Gamma-ray Flux-to-Dose-Rate Conversion Factors;, vol. 12, number 3, September 1980.

[7] International Electrotechnical Commission, Protective devices against diagnostic medical X-radiation - Part 1: Determination of attenuation properties of materials, IEC 61331-1:2014.

[8] Lloyd A. Currie, Analytical Chemistry; Limits for Qualitative Detection and Quantitative Determination, 40 (3), pp 586–593 (1968).

[9] BIPM, IEC, IFCC, ISO, IUPAC, IUPAP and OIML. Joint Committee for Guides in Metrology, Guide to the expression of uncertainty in measurement, (BIPM: Sèvres) (2008).

SHILDING DESIGN ASSESSMENT TO PROVIDE RADIATION PROTECTION AGAINST NEUTRON DOSE FOR 18 MV LINEAR ACCELERATOR IN RADIATION THERAPY UNIT

SUMEYRA CAN
Health Science University
Istanbul Bakirkoy Dr. Sadi Konuk Research and Training Hospital
Bakirkoy/Istanbul, Turkey
Email: sumeyracn@gmail.com

DIDEM KARACETIN
Health Science University
Istanbul Bakirkoy Dr. Sadi Konuk Research and Training Hospital
Bakirkoy/Istanbul, Turkey

Abstract

Undesirable neutron dose produced by medical linear accelerator operating above 10 MV causes the contamination of the therapeutic beam. These photo-neutron can create secondary gamma rays by consisting of inelastic and capture reactions. These interactions increase dose to the patient, medical staff and public. In this study, shielding design was evaluated for workers' safety against radiation damage caused by neutron dose while working with high x-ray energy (above 10 MV) in radiation therapy unit. NCRP Report No.151 was taken into account for shielding design calculation. To measure the H*(10) for leakage neutron, the neutron detector Thermo - Scientific RedEye N (DB-061 E) was used. Several measurement points were determined based on the maximum occupancy factors. Experimental measurement was obtained with different field sizes (3x3, 10x10, and 40x40) and different gantry angles (0º, 90º, 180, 270º). The annual H*(10) value for leakage neutron is maximum 1.34 mSv/year behind the door and 0.525 mSv/year at control room. It is %73.72 and %89.5 less than the threshold value respectively. As a result, the radiation therapy facilities is safe for medical staff. In addition, incorporating gantry angle and field size into analytical method will be beneficial for the worst case scenario.

Keywords: Radiation Protection, Radiotherapy, Neutron, Ambient Dose Equivalent H(10)*

1.   INTRODUCTION

Secondary neutron radiation can be produced by medical linear accelerator which has high x-ray energy (above 6 MV). This radiation emerges inside the materials of the accelerator head, patient and treatment room via photonuclear reactions. As a result of this photonuclear reactions, therapeutic beam contamination can be observed due to undesirable neutron dose while delivering the treatment [1,2,3,4]. This phenomenon gives rise to a crucial point for radiation safety of workers. Medical staff can be exposed to radiation during treatments outside treatment room due to the leakage neutron and photon radiation. Even though neutron interactions with the equipment is the radiation protection issue, data related to delivered neutron doses to medical staff during treatment duration outside the treatment room are limited [5,6]. For that reason, one of the most significant issue associated to radiation protection is the design and the facilities evaluation. NCRP Report No.151 provides the analytical methods for shielding calculation, the equivalent dose in the door, the properties of the radiation therapy unit (location, the room size, mazes, etc.) and neutron fluence in the maze entrance [7]. According to Kersey's method, the equivalent dose of neutron at the maze entrance is reduced by a factor 1/3 for the same total maze length via addition of a bend in the design of the maze [8,9,10]. However, Kersey's method is not sufficient to calculate neutron dose. Therefore, McGinley proposed a correction for Kersey's method by adding TVD. TVD is the distance that reduces the neutron dose by a factor 1/10 [7]. As a result, TVD and the H*(10) for leakage neutron is given:

$$TVD = 2.06\sqrt{S} \tag{1}$$

$$H_{n,D} = H_0 \times \left(\frac{S_0}{S_1}\right) \times \left(\frac{d_f^2}{d_1^2}\right) \times 10^{-d_2} \tag{2}$$

The aim of this study is to evaluate shielding design in terms of gantry angle and field size to provide radiation protection against neutron dose.

2. MATERIALS AND METHODS

2.1. Unit design and shielding calculation

Radiation Therapy Unit is located outside of the main hospital building as a different department. The building has two medical linear accelerators one CT Simulator. One of the medical linear accelerator room was shown in the Fig.1.
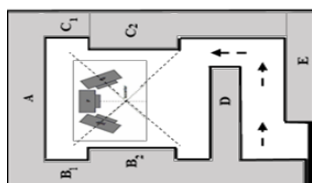
FIG.1. Design of Radiation Therapy Unit of Health Science University- Istanbul Bakirkoy Dr. Sadi Konuk Research and Training Hospital

Unit design and shielding calculation were done for medical linear accelerator operating 18 MV based on NCRP Report-151. The laboratory walls, which were built on an area of about 45 m^2 (except for maze), were named A, B$_1$, B$_2$, C$_1$, C$_2$, D, E on the plan. Based on NCRP and national regulations, 0.1 mSv/week or 5 mSv/year in dose equivalent were defined for controlled areas to reduce the effective equivalent dose from a linear accelerator to a point outside the room to an adequately low level. The thickness of the walls, base and ceiling were calculated based on the workload (W) of the linear accelerator treatment equipment. In addition, 26000 Sv per year was calculated by taking into account a total of 250 patients per week and a mean dose of 2 Gy per patient. SAD (Source to Axis Distance) =100 cm is used in calculations. Ordinary concrete (p=2035 g/cm^3) was used as shielding material. According to these parameters, the required wall thicknesses are given in Table 1.

TABLE 1.   SHIELDING THICKNESS

Walls	Shielding Thickness (cm)	Behind the Walls	Barrier Type	D (m)	U	T	P (mSv/year)
A	140	Garden	Secondary	5.5	1	1/20	1
B1	140	Linac-1	Secondary	6	1	1	5
B2	240	Linac-1	Primary	6.6	1	1	5
C1	140	Garden	Secondary	6.3	1	1/20	1
C2	240	Garden	Primary	6.7	1/4	1/20	1
D	125	Maze	Secondary	5.5	1	1	5
E	70/130	Control Room	Secondary	5.5+4.7	1	1	5
Ceiling-1	250	Ceiling	Primary	5.2	1/4	1/40	1
Ceiling-2	140	Ceiling	Secondary	5.1	1	1/40	1

2.2. Reduction of neutron dose equivalent and shielding efficiency

Patients and medical staff can receive additional dose because of neutrons produced by medical linear accelerators operating above 10 MV. Therefore, H*(10) for leakage neutrons should be taken into consideration. Elekta Synergy, which has 6-18 MV X-ray energy, was investigated for this study. Maximum energy of the medical linear accelerator and different angles of incidence of the accelerator head (0º, 90º, 180, 270º) and different field size (3x3, 10x10 and 40x40 cm^2) have considered to determine the maximum delivered dose to the medical staff. Each measurement was repeated 3 times to have accurate data and mean of these 3 measurements was recorded. In addition, regular treatment conditions of different treatment modalities (IMRT and Conformal Radiation Therapy - 2 Gy one fraction delivered at isocentre.) were used for realistic conditions. For activation measurements and testing purposes, maximum dose rate and 3000 MU were studied because higher MU value increases the amount of activation products created in the accelerator head.

For leakage radiation measurements while delivering the treatment, solid phantom with 10 cm thickness was placed on the couch at the isocentre to produce additional radiation dose scattered by the patient. SSD was 100 cm. H*(10) were measured based on the maximum occupancy factor (at the control room, against the door) to predict the effective dose due to external exposure and to determine the dose reduction to evaluate the shielding design. For that reason, Thermo - Scientific RedEye N (DB-061 E) was used to assess of the photon component. The effect of scattered low energy neutrons needs to be reduced (boron) and the response to high energy neutrons needs to be increased for neutron dose rate measurements. For that reason, the flex boron top cover plate was inserted. All measurements were compared with 5 mSv/year in dose equivalent were defined for controlled areas based on the national regulations.

3.   RESULTS

For different treatment modalities, the H*(10) was analyzed with the data obtained from different measurement points. 1-3 min after treatments, maximum dose rates was observed while delivering the conformal radiation therapy which includes 18 MV energy for some cases. In addition, IMRT is not efficient to produce neutron dose as expected. The H*(10) rates ranged in 0.3E-4 –1.5E-4 mSvh^{-1} (250-400 MU delivered for real treatments) at control room and behind the door respectively. The annual H*(10) value for leakage neutron is maximum 1.34 mSv/year behind the door and 0.525 mSv/year at control room. It is 73.72% and 89.5% less than the threshold value respectively. As a result, the radiation therapy facilities is safe for medical staff while delivering the treatment.

In addition to the real conditions, maximum dose rate and 3000 MU were studied for worst case scenario. It should be noted that measurements taken at these values are not the values used during normal treatment and it was used just for testing purposes. The ambient equivalent dose was investigated in terms of different angles and different field size to evaluate shielding design. Maximum H*(10) was shown in Table-2. When gantry angle is 270º and field size is 3x3, the maximum H*(10) for leakage neutron obtained during measurements and it is 6.5E-4 mSv/hour.

TABLE 2.   THE MAXIMUM H*(10) IN TERMS OF DIFFERENT ANGLES AND DIFFERENT FIELD SIZE

Field Size	Gantry Angle: 0º mSv/hour	Gantry Angle: 90º mSv/hour	Gantry Angle: 180º mSv/hour	Gantry Angle: 270º mSv/hour
3x3	6.4E-4	4.8E-4	5.5E-4	6.5E-4
10x10	5.7E-4	3.6E-4	5E-4	5.8E-4
40x40	4.9E-4	3.1E-4	4.7E-4	5.4E-4

The comparison H*(10) for leakage neutron with threshold value (5 mSv/year) in terms of gantry angle and field size was shown in Fig2. Additionally, the reduction of H*(10) for leakage neutron with field size was presented in Fig.3. Maximum leakage was observed when field size is 3x3 for all gantry angles. The annual H*(10) values for leakage neutrons is maximum 5.71 mSv/year behind the door and it is %14.2 more than the threshold value. The amount of activation products created in the accelerator head is %35 more when field size is 3x3 comparing the 40x40 field size. A strong correlation was observed between H*(10) reduction and increasing field size (R^2=0.99). As a result, the amount of activation products is proportional with small field size.

4.   CONCLUSION

The measurements of H*(10) for leakage neutron performed for three field size and four gantry angles represented in this study. Main concern of this study is to evaluate shielding design against undesirable neutron dose for radiation protection. This shielding design was done based on NRCP Report-151, however it was evaluated in terms of field size and gantry angle to determine whether the wall thickness is enough for radiation protection. It was proved that, the so-called facility is safe for medical staff. The annual H*(10) does not exceed the threshold value for regular treatment. Even though field size and gantry angle are not included in analytical method, this method provides effective shielding in radiation therapy unit.
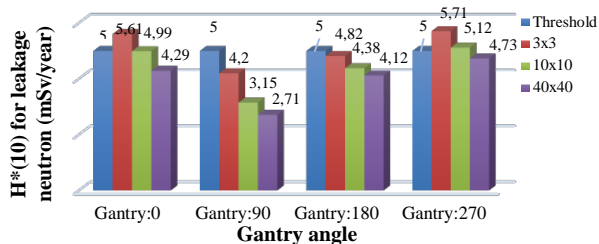
FIG.2. Comparison H*(10) for leakage neutron with threshold value in terms of gantry angle and field size
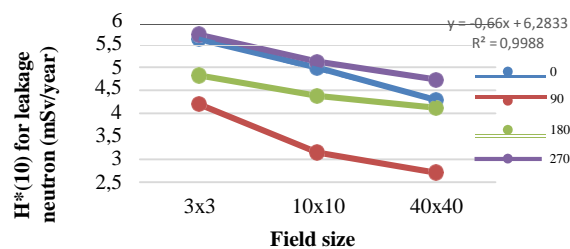
FIG.3. Reduction of H*(10) for leakage neutron with field size.

However, H*(10) for leakage neutron is more than threshold value when maximum dose rate and 3000 MU were applied for testing purposes. Therefore, incorporating gantry angle and field size into analytical method will be beneficial for the worst-case scenario. As a result, this represented study is useful to provide data about personal neutron dose as well as the assessment of wall thickness in terms of gantry angle and field size.

5.   FURDER INFORMATION

5.1.   **Author affiliation**

Sumeyra Can
Health Science University Istanbul Bakirkoy Dr. Sadi Konuk Research and Training Hospital
Istanbul, Turkey
sumeyracn@gmail.com

Didem Karacetin
Health Science University Istanbul Bakirkoy Dr. Sadi Konuk Research and Training Hospital
Istanbul, Turkey
didemkaracetin@gmail.com

REFERENCES

[1] DONADILLE, L., et al. Radiation protection of workers associated with secondary neutrons produced by medical linear accelerators. *Radiation Measurements*, 2008, 43.2: 939-943.

[2] RAMÍREZ, Pablo Víctor Cerón, et al. Neutron H*(10) estimation and measurements around 18MV linac. *Applied Radiation and Isotopes*, 2016, 117: 2-7.

[3] REBELLO, W. F., et al. Monte Carlo simulation of photoneutrons streaming inside radiotherapy treatment rooms as a function of gantry angles. *Progress in Nuclear Energy*, 2010, 52.3: 278-281.

[4] BARQUERO, R., et al. Neutron spectra and dosimetric features around an 18 MV linac accelerator. *Health physics*, 2005, 88.1: 48-58.

[5] HOWELL, Rebecca M., et al. Investigation of secondary neutron dose for 18MV dynamic MLC IMRT delivery. *Medical physics*, 2005, 32.3: 786-793.

[6] CHEN, C. C., et al. A detailed study on the neutron contamination for a 10MeV medical electron accelerator. *Nuclear Instruments and Methods in Physics Research Section A: Accelerators, Spectrometers, Detectors and Associated Equipment*, 2006, 562.2: 1033-1037.

[7] National Council on Radiation Protection and Measurements. NCRP Report No.151., Structural Shielding Design and Evaluation for Megavoltage X-ray Gamma Ray Radiotherapy. NCRP Press, Bethesda, MD (2005).

[8] HERNANDEZ-ADAME, Luis, et al. Design of a Treatment Room for an 18-MV Linac. *Nuclear Technology*, 2011, 175.1: 105-112.

[9] GHASSOUN, J.; SENHOU, N.; JEHOUANI, A. Neutron and photon doses in high energy radiotherapy facilities and evaluation of shielding performance by Monte Carlo method. *Annals of Nuclear Energy*, 2011, 38.10: 2163-2167.

[10] GHASSOUN, J.; SENHOU, N. The evaluation of neutron and gamma ray dose equivalent distributions in patients and the effectiveness of shield materials for high energy photons radiotherapy facilities. *Applied Radiation and Isotopes*, 2012, 70.4: 620-624.

RADIATION DETECTORS OF GREEN QUARTZ FOR DOSIMETRY

Edy E. Cuevas Arizaca
Instiute of Physics University of São Paulo
National University of San Agustin, Arequipa, Perú
Catholic University of Santa María, Arequipa, Perú
São Paulo, Brazil
Email: arizaca@if.usp.br

Shigueo Watanabe
Institute of Physics University of São Paulo
São Paulo, Brazil

Edemar Zanardo
Heart Institute University of São Paulo
São Paulo, Brazil

Nilo F. Cano
Federal University of São Paulo
São Paulo/Santos, Brazil

Abstract

Green quartz is very sensitive TL material for very low dose, this work present the first results on the response of green quartz pellets for radiation detection. Green quartz pellets were produced by sintering method, the pellets have a 6.0 mm diameter and 1.0 mm thick, sintering at 1200 ºC for 60 minutes. The pellets are irradiated with Co-60 γ-rays and the exhibit TL glow curve with peaks at 90, 120 and 220 ºC. The green quartz pellets showed a linear dose response curve for dose in the region of 0.1 to 1.0 Gy. The pellets was exposed to 6 MeV x-rays from linear accelerator used in radiotherapy the dose measured using ionization chamber compare favourbly with doses measured with green quartz pellets.

1. INTRODUCTION

Natural or synthetic silicate minerals are very sensitive materials concerning their Thermoluminescence (TL) properties, both for low and high dose radiation, Watanabe et al [1] have shown that two varieties of beryl are excellent detectors up to MGy radiation doses. There are other dosimetry systems such as those based on LiF or Al_2O_3 crystals, which are widely used [2] In the present work green quartz was studied. It responds to cGy doses as well as to hundreds of kGy doses.

Carvalho-Junior et al [3] and Rocha et al [4] investigated the dosimeters properties of quartz pellets manufactured by pressing of a homogeneous mixture of quartz and flocculated PTFE at room temperature.

As far as we know, no work has been studied on dosimeters properties of pellets produced only of green quartz by sinterization method for dose radiation. In the present work we have produced and investigated the behaviour of green quartz pellets subjected a dose radiation of x-ray and γ-radiation we present the first results.

2. MATERIALS AND METHODS

We have produced pellets by pressing green quartz powder. The Fig. 1 show picture of fragment. and then sintering at 1200 ºC for 60 minutes. Each pellet has a mass of about 50 mg and a diameter of 6.0 mm and 1.0 mm thickness. These pellets are show in Fig. 2. Grains with size smaller than 0.080 mm were used in x-ray diffraction analysis.

Fig. 1. Green quartz minerals.
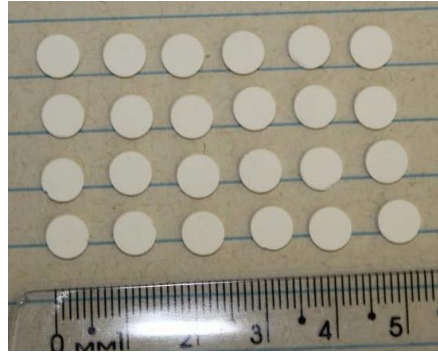
Fig. 2. Green quartz pellets.

The response of the pellets to low dose was evaluated in terms of their TL signal, using the reader system Harshaw, model 4500. The heating rate used in the TL measurements was 4 °C/s and temperature range of 50 to 400 °C.

The green quartz pellets were irradiated at the Radiation Technology Center, IPEN, using Co-60 source.

3.   RESULTS AND DISCUSSION

The powder x-ray diffraction pattern of green quartz is given in Fig. 3, indicating that all intense reflections match with the powder diffraction data of quartz which is reported in ICDD card n 01-78-2315.
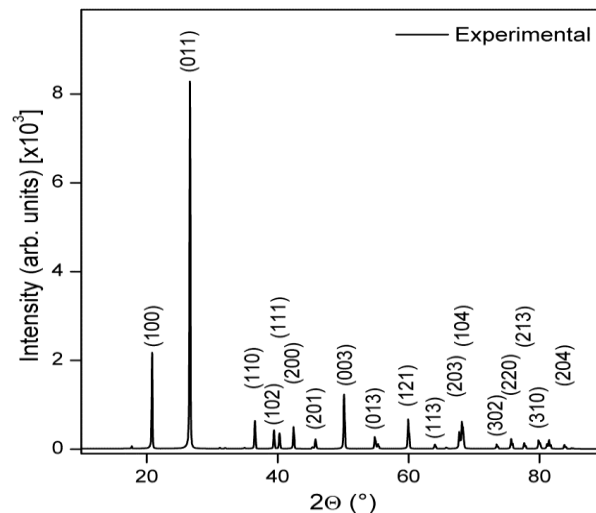
Fig. 3. X-ray diffraction of the quartz crystal.

The behavior of the TL glow curves of green quartz pellets as function of γ radiation for dose of 0.1 Gy up to 1.0 Gy is shown in Fig. 4. The glow curve of sample show an intense and dominant TL peak with maximum at 220 °C. The dose response of natural and synthetic materials for dosimetry applications is a very important properties, one ideal dosimeter has behaviour linear for all dose range. The pellets were irradiated with different γ-ray with doses between the range of 0.1 Gy and 1.0 Gy. Analyzing the dose response curves, observed in Fig. 5. It cam be observed that the TL response of green quartz pellets have behaviour linear due to the curve sin the range of 0.1 to 1.0 Gy.
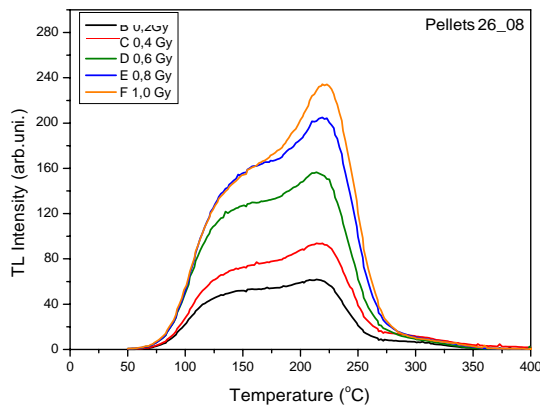
Fig. 4. TL glow curves of green quartz irradiated at different doses .
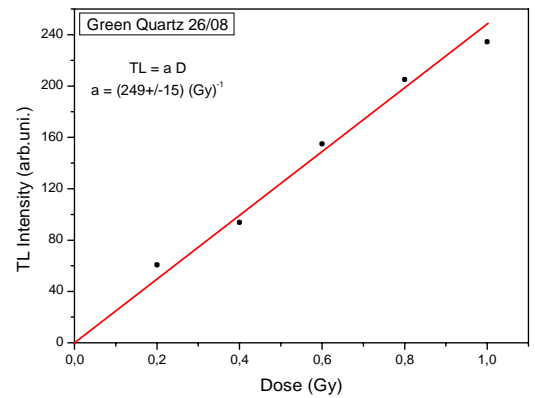
Fig. 5. TL intensity as function of γ dose.

Then exposed the pellets to 6 MeV x-ray from linear accelerator at a private hospital, usually is used in radiotherapy. A dose value of green quartz pellets was 1.027 ± 0.161 Gy and 0.971 ± 0.019 Gy by Hospital Ion chamber.

4. CONCLUSIONS

We produced chips of green quartz that are sensitive to ionizing radiation and are suitable for medical dosimetry applications. The calibration curve was obtained in the range 0.1 to 1 Gy using the peak at 220 ° C and evaluated in a linear accelerator X -ray with energy of 6 MeV. A dose value of 1.027 ± 0.161 Gy was measured while the dose measured by the ion chamber was 0.971 ± 0.019 Gy.

REFERENCES

[1] Watanabe, S., Cano, N.F., Carmo, L.S., Barbosa, R.F., Chubaci, J.F.D.,A., High and Very-high-dose dosimetry using silicate minerals. Radiation Measurements 72 (2015) 66-69.

[2] Matsushima, L.C., Veneziani, G.R., Campos, L.L., Study of optically stimulated luminescence of LiF:Mg, Ti for beta and gamma dosimetry. Radiation Measurements 56 (2013) 365-368.

[3] Carvalho-Junior, A.B., Barros, T.F., Guzzo, P.L., Khoury, H.J., Materials Research 15 (2012) 536-543.

[4] Rocha, F.G., Nascimento S.F., Santos, L.H.S., Nunes, M.G., Campos, V.P., Farias, T.M.B., Chubaci, J.F.D., Campos, L.L., Caracterização de pastilhas dosimétricas de quartzo verde para aplicação em dosimetria clínica. Revista Brasileira de Pesquisa e Desenvolvimiento 13 (2011) 31-34.

OUT-OF-FIELD RADIATION ORGAN DOSE MEASUREMENTS AND ASSOCIATED SECONDARY CANCER RISK ESTIMATION IN PATIENTS TREATED WITH BREAST CANCER IN LEBANON

Ibrahim DUHAINI, MS
Chief Medical Physicist & RSO at Rafik Hariri University Hospital
Beirut, Lebanon
Email: duhaini@yahoo.com

Nour HODROJ, MS
Medical Physicist Intern at Rafik Hariri University Hospital
Beirut, Lebanon
Email: nour.h8@hotmail.com

Saad AYOUBI, MD
Radiation Oncologist at Rafik Hariri University Hospital
Beirut, Lebanon
Email: saad.ayoubi@chn.com.lb

Sadek NEHMEH, PhD
Chief of PET and Nuclear Physics at Weill Cornell Medicine
New York, USA
Email: san2028@med.cornell.edu

Ahmad MAROUF, MD
Associate Prof., School of Medicine, Beirut Arab University
Beirut, Lebanon
Email: a.maarouf@bau.edu.lb

Mahmoud KOREK, PhD
Professor of Physics, Beirut Arab University
Beirut, Lebanon
Email: Mahmoud.korek@bau.edu.lb

ABSTRACT

Radiation is not selective to tumor cells but rather targets any cells that are in the process of replication when the therapy is applied, which accounts for the importance of the correct dose to ensure optimal efficiency with minimal side effects. The induction of cancers following radiotherapy (second cancers) has been known for many years, although the estimation of the probability of radiation carcinogenesis is not straight forward. The objective of this study was to measure the dose received by the skin surface of the treated breast as well as the dose to the lungs during breast radiotherapy, and to estimate secondary cancer risk and the probability of causation to the lungs. Measured and calculated surface skin dose were compared. Measured point doses of both lungs were compared to those calculated by TPS. Relative Risk (RR) and Probability of Causation (PC) of lungs were calculated from patient's mean doses to the organs using equations provided by BEIR V report. Results showed some difference between the measured and calculated doses. RR mean values showed 1.826 and 1.032 for ipsilateral and contralateral lungs respectively. In addition, PC mean values showed 43.22% and 3.099% for ipsilateral and contralateral lungs respectively. Dosimeter positioning and beam direction lead to discrepancies in measured doses. Breast cancer patients are at risk of developing second cancer of ipsilateral lung more than contralateral lung after radiotherapy treatment. Moreover, mastectomy patients have increased risk of cancer induction in ipsilateral lung with respect to breast conserving patients. In addition, increased relative risk is present at higher radiation doses; the higher the radiation dose, the higher the risk of second cancer induction. Finally, radiation is not the only cause of cancer, thus other risk factors should be considered when calculating relative risk.

1.   INTRODUCTION

The medical field had witnessed evolution in cancer therapy. Many new radiation therapy techniques had risen recently in the aim to increase tumour control and spare normal tissues. In addition, varieties of treatment planning systems are developed to adapt to the new techniques. Calculation of doses throughout the patient is currently performed in the planning stage of radiotherapy using computerized radiation therapy treatment planning systems (TPS). This is done in order to tailor particular radiotherapy regimens to each patient, aiming to improve patient outcomes.

Radiation can be described as a 'two edge sward' as it can cure cancer, but also could be the cause of cancer [1]. Improvements in cancer treatment have increased survival times and thus increased incidence of second cancers is expected [1]. Secondary tumors following radiotherapy may be observed around or well outside the margin of the planning target volume. The lungs are one of the affected organs after breast radiotherapy. It is believed that radiation to the lungs is considered carcinogenic.

2.   METHODS

First part of the study is to do dose measurements using RANDO phantom and GafChromic films as dosimeters during breast radiotherapy.

2.1.   Phantom and dosimeter:

Measurements were done at The National Center of Cancer and Research in Doha-Qatar. The RANDO Phantoms provide the detailed mapping of dose distribution that is essential for evaluating radiotherapy treatment plans. A male RANDO phantom with breast attachments was used. RANDO Phantoms are constructed with a natural human skeleton cast inside material that is radiologically equivalent to soft tissue. The RANDO lungs are molded to fit the contours of the natural human rib cage. The lower-density material in the RANDO lungs is designed to simulate human lungs in a median respiratory state. Dose measurements are obtained by using film or individual dosimeters. For dose mapping, RANDO Phantoms are sliced into 2.5cm sections. Hole grids are drilled through the phantom's soft tissue materials for the insertion of dosimeters.

GafChromic EBT3 dosimetry films were used for measurements. GAFChromic EBT-3 is designed for the measurement of absorbed doses of ionizing radiation. It is particularly suited for high-energy photons. The dynamic range of this film is designed for best performance in the dose range from 0.2 to 10 Gy, making it suitable for many applications in IMRT, VMAT and brachytherapy.

The films were calibrated prior to the experiment and a calibration curve was obtained. For dose measurements, $1x1\ cm^2$ films were labeled and attached within the phantom slabs at the following sites:
- Skin surface of the treated breast (left breast), superior, inferior, left, and right positions.
- At both lungs, ipsilateral and contralateral, at superior position at the lung slab. One film is positioned more medially with respect to the other

The irradiated films are read by the EPSON Expression 1000XL scanner after 48 hours of irradiation. The obtained readings were represented as percent of prescribed dose.

2.2.   Treatment planning and delivery

The phantom was CT simulated and the images were exported to the treatment planning system. Phantom planning was done using Eclipse planning system. The Eclipse™ treatment planning system is an integrated and comprehensive system supporting radiation treatment such as photon, FFF beams, protons, electrons, external beams, low-dose-rate brachytherapy and cobalt therapy. The rich functionality and efficiency of the Eclipse™ treatment planning system helps simplify modern radiation therapy planning for all standard treatment modalities, including 3D conformal, volumetric modulated arc therapy (VMAT), brachytherapy, electron and proton therapy. Eclipse allows clinicians to efficiently create and verify the best treatment plans for their patients. It uses the anisotropic analytical algorithm (AAA) which is a pencil beam superposition-convolution algorithm for dose calculations. It has shown good accuracy overall and a great ability to handle small fields in inhomogeneous media. The plan was 3D-CRT tangential beams of SAD technique with 50 Gy prescribed dose divided over 25 sessions for left breast treatment. Two   opposite

tangential beams were planned, where 6 and 15 MV energy was used in order to compensate for the large breast volume. In addition, 30° wedge was used in the field.

Treatment was delivered by the Varian medical system – RapidArc. It provides 6, 10, 15, and 18 MV photon energies. It is also provided with 120 dynamic MLCs.

The ipsilateral lung, contralateral lung, and the left breast were delineated and confirmed by the radiation oncologist and medical physicist. The surface skin dose of the left breast along with the point doses of the lungs were derived from the DVH and compared with the measured ones.

The second part of the experiment was done to estimate the relative risk of radiation induced second cancer of lungs following breast radiotherapy.

2.3. Patients

Twenty –one female patients that undertook radiotherapy for breast cancer at Rafik Hariri University Hospital-Lebanon were selected for the study. Their age ranges from 30 to 70 years with the average is 51 years. The patients underwent mastectomy or breast conserving surgery where 48% had mastectomy. In addition, both left sided and right sided breast cancer patients were included in the study where 43% are left sided.

2.4. CT Simulation

All patients had CT simulation with the same parameters. The scan field extended from the lower neck (6th cervical vertebra) to the mid abdomen. The slice thickness chosen was 5 mm. A breast board was used to fix the patient's position. The patient's affected arm is elevated and lead marks were attached to the patient's skin, one laterally, other at the middle, and third medially. These marks are then replaced with tattoos for position verification.

2.5. Treatment planning and delivery

Pinnacle[3] ADAC treatment planning system was used to construct treatment plan based on 3D-CRT SSD technique for patients. The Pinnacle[3] treatment planning system provides a comprehensive set of tools for setting up and evaluating treatment plans. The software includes options for simulation, photon, electron, stereotactic radiosurgery, proton, and brachytherapy treatment planning. For photon external beam treatment plans, Pinnacle[3] uses a 3D convolution superposition dose calculation algorithm. This model computes the dose from first principles and uses a limited set of measurements to fit the model to the measured data. Corrections are made in the model for patient surface irregularities, voxel-by-voxel CT density tissue inhomogeneities, phantom and head scatter, and beam-shaping devices such as bolus, wedges, blocks, multi-leaf collimators, and compensators.

The same plan was used for all patients. Two opposite tangential beams were created, one medial and the other lateral to the breast or chest wall. Each beam is of 50% weight; 30° motorized wedge was inserted to the beam field. The beam energy used is 6 and 15 MV. The prescribed dose was 50 Gy divided over 25 fractions each of 2 Gy.

At the treatment planning system, the Planned Target Volume (PTV), contralateral breast (CB), contralateral lung, ipsilateral lung, and heart were delineated for all patients according to the known

anatomy. The PTV and OAR contours were reviewed and confirmed by the radiation oncologist and a dosimetrist. The mean doses of ipsilateral and contralateral lungs were derived from the dose volume histogram (DVH).

After treatment planning, the dose was delivered by Elekta Precise linear accelerator. Elekta provides 6 and 15 MV photon beams along with 4, 6, 8, 12, and 15 MeV electron beams. It provides motorized wedges and 40 motor derived MLC system.

2.6. Estimation of second risk cancer

Relative risk of second lung cancer for both ipsilateral and contralateral lungs and Probability of causation were calculated using mean doses calculated from patient plans by the TPS. After obtaining mean dose of the lungs from DVHs, the effective dose was calculated according to the following equation:

Effective Dose

where E is the effective dose (Sv), W_R is the radiation weighted, and W_T is the tissue weighted factor. W_T and W_R values were provided by ICRP103 report, where 0.12 is the tissue weighted factor of the lung and 1 is value of W_R for photons [2].

The effective dose calculated was used to estimate the risk cancer using the equation 2 provided by BEIR V report where time after exposure was taken 25 years. PC was calculated from relative risk values obtained according to the following equations

$$—$$

$$\underline{\quad\quad}$$

3.   RESULTS

Surface skin dose for the left breast is, and point doses of the lungs are measured and compared with the calculated ones. The calculated and measured doses are presented as percent of prescribed dose are shown in table 1.

The calculated RR and PC values of the lungs -both ipsilateral and contralateral- and their average values are represented in table 2 along with the mean and effective doses of the lungs.

4.   DISCUSSIONS

4.7.   Phantom measurements

The measured doses were compared with those calculated by the TPS. The difference between the measured surface skin of the breast and the calculated one is not significant (<5%). Some differences are noted between the values of the lungs. This is mainly because of dosimeters positioning. The films were positioned parallel to the radiation beam, which leads to discrepancies in dose measurement. GafChromic films are known to have directional dependencies. A study was done to evaluate directional dependence in film dosimetry showed that when exposing film in a parallel orientation to the central axis of the beam; high readings of optical density can be measured [3]. Thus, over response when films are exposed parallel to the central axis of the beam is found. Moreover, studies showed that treatment planning systems has a limitation which is that radiation leakage through accelerator head is not always considered [4].

4.8.   Relative risk and probability of causation values

The relative risk of both contralateral and ipsilateral lung along with PC was calculated and shown in table 1. The mean of the relative risk of ipsilateral lung 1.826 is higher than that of the contralateral lung 1.032, where the t-test shows strong correlation and significant difference between the means RR value of ipsilateral and contralateral lung (r=0.762, p<0.05). This is because the ipsilateral lung is exposed to dose (732.504 cGy) higher than that of the contralateral lung (28.904 cGy) where the t-test shows strong correlation and significant difference between the means of the doses (r=0.761, p<0.05). The higher dose to the ipsilateral lung is associated with the inclusion of part of the lung into the irradiated field. This is shown in SEER study [5] where this risk was higher for the ipsilateral lung in comparison to the contralateral lung, relative risk 1.54 versus 1.81. This shows similar results to our study, except that our estimated RR to contralateral lung is lower than theirs, the reason may be because of the difference in planning techniques.

The relative risk of ipsilateral lung for mastectomy patients 1.937 is higher than that of ipsilateral lung for breast conserving patients 1.7084. Although the difference between means was not statistically significant (r=0.158, p>0.05), but this can be justified by the lower absorbed dose to ipsilateral lung for breast conserving patients due to the physical barrier of the remaining breast tissue [6].   The mean dose to ipsilateral lung of breast conserving patients is 628.28 cGy lower than that of mastectomy patients 831.39 cGy, but still not statistically significant (r=0.158,p>0.01).

The results show increasing values of RR as dose increase for both ipsilateral and contralateral lung as figure 1 and 2 respectively shows. The graphs represent linear relationship between dose and RR for both lungs which is confirmed by correlation tests (r=1, p<0.01). A similar study that made a systematic review of the epidemiological studies of the radiation dose-response relationship [7] showed the same results of increasing risks upon increase of lung dose. This was predicted because of the use of the linear model suggested by BEIR V report for estimation of second lung cancer.

The mean of probability of causation (PC) of contralateral lung (3.099%) is lower than that of ipsilateral lung (43.22%). This is obvious because the dose to the ipsilateral lung is higher than that of the contralateral lung, so that the relative risk.

Calculated PC of lungs showed strong correlation with dose with their doses; r=0.989, p<0.01 for ipsilateral lung and r=0.991, p<0.01 for contralateral lung. However the means of PC for both lungs are below 50%. This means that the dose from ionizing radiation contributes to less than 50% of risk of cancer induction. The reason behind this is that other factors that contribute to risk of cancer induction such as smoking are excluded in the study. BEIR V report states that other major risk factors besides radiation (smoking, exposures to solvents, medical radiation exposures, chemotherapy, etc.) should be known for more accuracy in calculation. A case controlled study from cancer the Connecticut Tumor Registry [8] showed an increased risk of 32.7 for second ipsilateral lung cancer for women who smoked and were treated with breast radiotherapy.

5. CONCLUSIONS

Dosimeter positioning and beam direction lead to discrepancies in measured doses. Breast cancer patients are at risk of developing second cancer of ipsilateral lung more than contralateral lung after radiotherapy treatment. Moreover, mastectomy patients have increased risk of cancer induction in ipsilateral lung with respect to breast conserving patients. In addition, increased relative risk is present at higher radiation doses; the higher the radiation dose, the higher the risk of second cancer induction. Finally, radiation is not the only cause of cancer, thus other risk factors should be considered when calculating relative risk.

6. TABLES

Table 1: Measured and Calculated Surface Skin Dose of Left Breast, and Point Doses of Ipsilateral and Contralateral Lung

| | Dose (% of prescribed dose) | | | | |
| | Left Breast[a] | Ipsilateral Lung | | Contralateral Lung | |
Position		Superior medial	Superior lateral	Superior medial	Superior lateral
Measured	85.5	7	105	4.5	6.5
Calculated	84	6.3	90	3.7	4.9

a: surface skin dose

Table 2: Mean dose, Effective dose, RR, and PC Values of Ipsilateral and Contralateral Lungs

| Patients | Ipsilateral Lung | | | | Contralateral Lung | | | |
	Mean dose (cGy)	Effective dose (Sv)	RR	PC (%)	Mean dose (cGy)	Effective dose (Sv)	RR	PC (%)
1	538.80	0.646	1.608	37.79	29.30	0.035	1.033	3.15
2	966.20	1.159	2.089	52.13	54.70	0.066	1.062	5.80
3	1178.10	1.414	2.328	57.05	33.10	0.040	1.037	3.59
4	310.80	0.372	1.350	25.90	22.90	0.027	1.026	2.15
5	429.80	0.515	1.485	32.64	14.70	0.018	1.017	1.62
6	382.00	0.458	1.431	30.10	18.10	0.022	1.020	1.99
7	1050.50	1.260	2.184	54.22	37.30	0.044	1.042	4.03
8	362.50	0.435	1.409	29.00	11.00	0.013	1.012	1.22
9	1276.60	1.531	2.439	59.00	40.70	0.048	1.046	4.37
10	768.30	0.921	1.866	46.41	33.80	0.041	1.038	3.67
11	1100.30	1.320	2.241	55.36	30.60	0.036	1.035	3.33
12	415.60	0.498	1.469	31.60	23.90	0.028	1.027	2.16
13	361.70	0.434	1.408	28.96	24.40	0.029	1.028	2.67
14	800.80	0.960	1.903	47.44	30.90	0.037	1.035	3.62
15	793.10	0.951	1.894	47.20	32.30	0.038	1.036	3.51
16	852.60	1.023	1.961	49.00	27.30	0.032	1.031	2.97
17	929.20	1.115	2.048	51.16	30.80	0.036	1.035	3.35
18	332.70	0.399	1.375	27.27	15.90	0.019	1.018	1.75
19	725.00	0.870	1.817	44.97	29.40	0.035	1.033	3.00
20	785.90	0.943	1.886	46.98	33.10	0.039	1.037	3.59
21	1022.10	1.226	2.152	53.54	32.80	0.039	1.037	3.55
Average	**732.5**	**0.878**	**1.826**	**43.22**	**28.90**	**0.034**	**1.032**	**3.099**

7. FIGURES
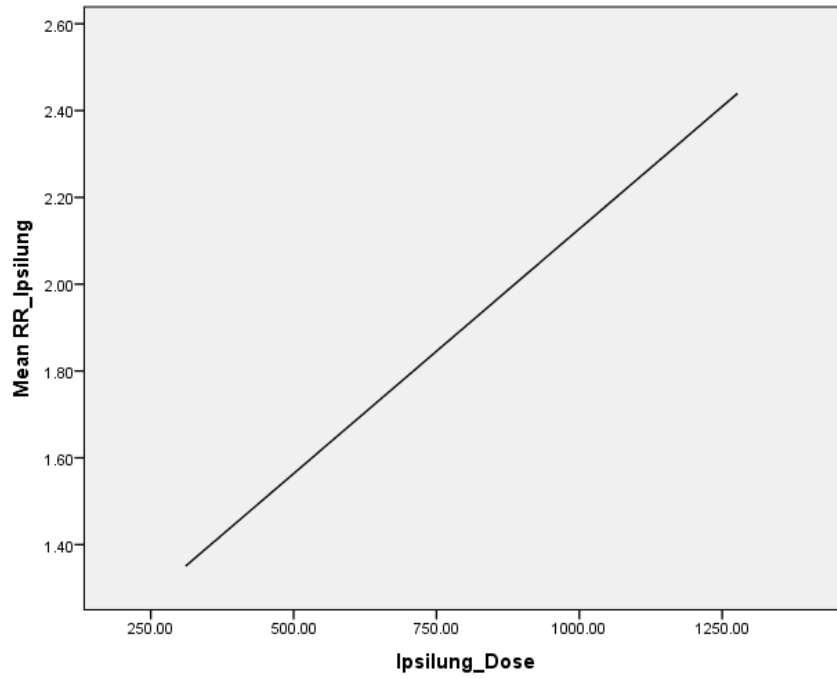
Figure 1: Variation of RR of Ipsilateral Lung as Function of Ipsilateral Lung Mean Dose.
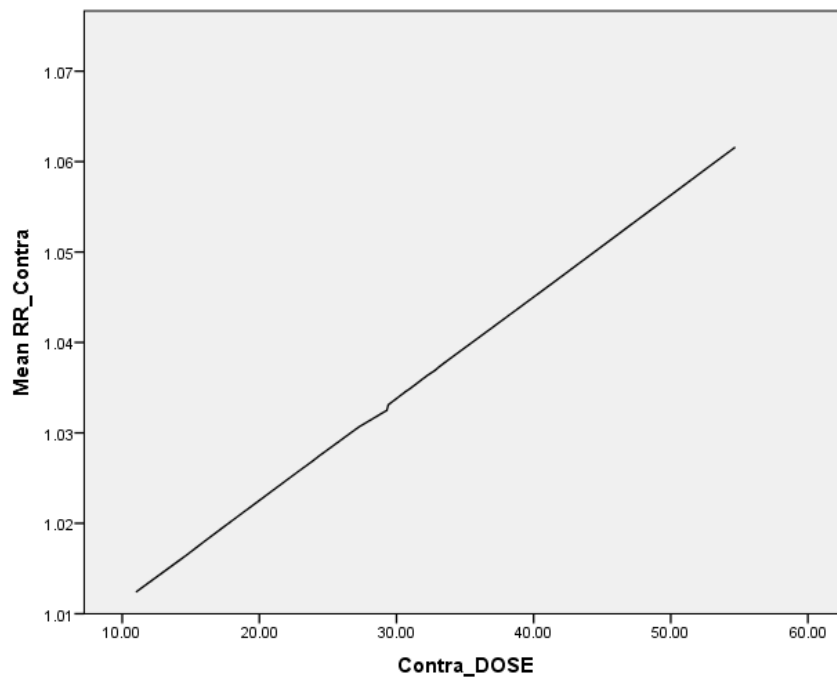
Figure 2: Variation of RR of Contralateral Lung as Function of Contralateral Lung Mean Dose.

8. REFERENCES

[1] J. Safora, R. O. Dag, D. Turi and M. Erik, "Contralateral breast doses following radiotherapy of the breast andregional lymph nodes:Measurements and treatment planning calculations," *The Gren Journal,* no. 82, pp. 332-336, 2007.

[2] ICRP publication 103, "The 2007 Recommendations of the Iinternational Commission on Radiological Protection," *Ann ICRP 2007,* pp. 1-322, 2007.

[3] S. Natalka, H. Peter, B. Martin, D. Alastair and M. Peter, "Directional dependence in film dosimetry: radiographic and radiochromic film," *Physics in Medicine and Biology,* vol. 46, 2001.

[4] M. Saveta, B. Jean-Marc, d. Francesco, H. Roger and O. Pawel, "out-of-fiels dose measurements in radiotherapy-An overview of activity of EURADOS Working Group 9: Radiation protection in medicine," *Elsevier,* pp. 270-275, 2014.

[5] A. Berrington de Gonzalez, R. Curtis, E. Gilbert, C. Berg, S. Smith, L. Stovall and E. Ron, "Second solid cancers after radiohterapy for breast cancer in SEER cancr registries," *Br J Cancer,* pp. 220-226, 2010.

[6] F. Vicini, V. Kini, P. Chen, E. Horwitz, F. Gustafson, P. Benitez, G. Edmundson, N. Goldstein, K. McCathry and A. Martinez, "Irradiation of the tumor bed alone after lumpectomy in selected patients with early-stage breasst cancer treated with breast conserving radiotherapy.," *J Surg Oncol,* pp. 33-40, 1999.

[7] B. Amy, G. Ethel, C. Rochelle, I. Peter, K. Ruth, M. Lindsay, R. Preetha and P. L. Mark, "Second solid cancers after radiotherapy: a systematic review of the epidemiological studies of the radiation dose-response relationship," *International Journal of Radiation Oncology Biology Physics,* vol. 86, no. 2, pp. 224-233, 2013.

[8] A. Neugut, T. Murray, J. Santos, H. Amols, M. Hayes, J. Flannery and E. Robinson, "Increased risk of lung cancer after breast radiotherapy in cegarrette smokers," *Cancer,* pp. 1615-1620, 2006.

ACKNOWLEDGEMENTS

EVALUATION OF PROSTATE CANCER TREATMENT PLANNING USING 3 DIMENSION CONFORMAL RADIOTHERAPY (3DCRT) AND VOLUMETRIC MODULATED ARC THERAPY (VMAT)

A.B.Farah
Sudan Atomic Energy Commission
Khartoum, Sudan
Email: atifabuf@hotmail.com

F.Ziglio
S.Chiara Hospital, Medical Physics department
Trento, Italy
Email: Francesco.Ziglio@apss.tn.it

D.Ravanelli
S.Chiara Hospital, Medical Physics department
Trento, Italy
Email: Daniele. Ravanelli@apss.tn.it

Abstract

This study was performed to evaluate the treatment planning of prostate cancer using three-dimension conformal (3DCRT) techniques with two different approaches (4 box fields, and 5 fields) and Volumetric Arc Therapy (VMAT) the real plan used for treatment. The evaluation was done using dosimetric parameters for Planning Target Volumes (PTVs) and organs at risk (OARs). In the prostate cancer the plan was done using 3DCRT with 4 fields, or 5 fields for treatment planning because both approaches give well coverage to the PTVs, while sparing the OARs. The VMAT technique gives good result for PTVs, rectum and femoral head, while for bladder it gives higher mean dose than 3DCRT, but all values are within the constraint.

1. INTRODUCTION

   The decision to use radiotherapy as a treatment modality must be based on adequate clinical work-up including confirmation of the histological diagnosis, staging, etc. In the radiotherapy process, different steps then have to be taken successively, Radiotherapy treatment can only produce good effects if it is delivered in an appropriate clinical context. Prostate cancer is now the commonest cancer in men, accounting for almost 25 per cent of all new male cancer diagnoses and is the second common cause of cancer related death in men [1]

   Computerized treatment planning systems TPS are used in external beam radiotherapy (EBRT) to generate beam shapes and dose distributions with the intent to maximize tumour control and minimize normal tissue complications. Patient anatomy and tumour targets can be represented as 3-D models. The entire process of treatment planning involves many steps and the medical physicist is responsible for the overall integrity of the computerized TPS to accurately and reliably produce dose distributions and associated calculations for EBRT, the planning itself is most commonly carried out by a dosimetrist, and the plan must be approved by a radiation oncologist and by a medical physicist before implementation in actual patient treatments, [2].

2. METHODS

   10 patients with localized prostate cancer were selected randomly, to plan and evaluate the prostate cancer and display the dosimetric parameters to the PTVs and OARs for 3DCRT technique with two different approaches, 4 box fields and 5 fields, and compare the data with planning from VMAT technique.

   The TPS used for 3DCRT plan is pinnacle3 from Phillips. The Pinnacle^3 treatment planning system provides a comprehensive set of tools for setting up and evaluating treatment plans. The convolution algorithm employed in the Pinnacle^3 planning system, Collapsed Cone Convolution algorithm (CCC) performs a full convolution superposition calculation. Rather than correcting measured dose distributions, the algorithm computes dose distributions from first principles and, therefore, can account for the effects of beam modifiers, the surface of the patient, and tissue heterogeneities on the dose distribution [3] & [4].

   The CT images were exported with all the structures from Monaco TPS to Pinnacle TPS, as present in fig 1, illustrated the delineation of structures of one of my case studies, the images and the isocenter position were Load into Pinnacle, the couch top was remove, the beams for both phases (0-64 Gy and 64-78 Gy) was defined, no wedge used, the density of bladder in patients with contrast medium was corrected, overriding the HU of the bladder to 1g/cm^3, the angles for all beams and the energy were defined, Automatic MLC aperture definition is (0.5 cm around the PTV as

seen in BEV, optimizing the collimator angle in order to better spare the OAR's), the dose grid (3mm) was defined, the calculation point using ROI was defined, the dose prescription and Beam weighting for two phases was defined, the dose using CCC was computed,
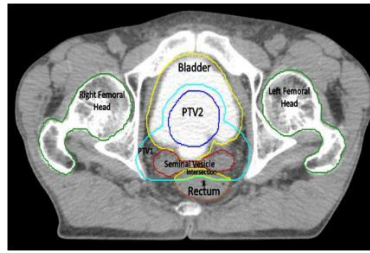
FIG.1 Delineation of structures: PTV1$_{(0-64Gy)}$,PTV2$_{(64-78Gy)}$,Seminal vesicle, and OAR (rectum, bladder, femoral heads(right and left), and the intersection between rectum and PTV1in transverse CT image .

For the first approach of 3DCRT 4 fields (anterior, posterior, and 2 laterals) with angles (0o, 180o, 90o, 270o) with different weights (30, 16, 27, 27) respectively and 15MV photon energy with two phases 0-64 Grays (32 fraction, 2 Grays/fraction), and 64-78 Grays (7 fraction, 2 Grays/fraction) sequential boost (SQB) was described.

In the second approach of 3DCRT 5 fields (anterior, 2 laterals, and 2 posterior oblique), the angles (0o,90o,120o, 240o, 270o), with different weight for each beam (20, 25, 15, 15, 25) respectively, and 15 MV photon energy, two phases 0-64 Grays (32 fraction, 2 Grays/fraction), and 64-78 Grays (7 fraction, 2 Grays/fraction) sequential boost was described this plan done with pinnacle3 TPS. Figure 2 illustrated the beams of both approaches on one of my case studies with 3DCRT for the first phase PTV$_{0-64Gy}$.

FIG.2 Beams in the two approaches of 3DCRT (4 fields, and 5 fields).

The intersection between the rectum and the PTV1$_{0-64Gy}$ was defined and the volume was recorded in terms of absolute volume (cm^3) and percentage of the total rectum volume (%), in order to test a possible correlation between this structures and the dosimetric parameters for the rectum.

The evaluation of the plans performed by display the isodose line, DVH, and from tabular DVH data I extracted the values of doses or volumes received specific dose for different structures, and I compared the data with QANTEC and local protocol used in Trento Hospital.

For the VMAT Technique the plan is carried out by one of the medical physicist in the department in Monaco TPS, the dosimetric quantities from DVH was extracted, the plan verification for VMAT technique performed by gamma analysis using octavious phantom, 2D array detector, and verisoft software.

The statistical analysis done using R software and non-parametric test (Wilcoxon) to check if the difference in dosimetric parameters between the techniques is statistically significant or not using P value (P< 0.05 is usually regarded as statistically significant and P> 0.05 regarded as non-significant).

3. RESULTS

All the dosimetric parameters were extracted from DVHs and the percentages were calculated using excel sheet for the structures: for the PTVs the percentage of the volume covered by the 95% of prescribed dose (V$_{95\%}$), for the Rectum the percentages of the volume covered by 50 Gy, 60 Gy, and 70 Gy (V$_{50Gy}$, V$_{60Gy}$, and V$_{70Gy}$), for the bladder the volume covered by 65 Gy, 70 Gy, and 80 Gy (V$_{65Gy}$, V$_{70Gy}$, V$_{80Gy}$, and mean dose), and for the Femoral heads The mean dose values were recorded for both femoral heads. The volume of intersection between rectum and PTV1$_{(0-64Gy)}$ is computed by the TPS in (cm^3), the values recorded and the percentages of the rectum intersection of rectum volume is calculated, Table 2 presented the values. The intersection of rectum with PTV1$_{(0-64Gy)}$ may affect on the rectum dose, where the intersection values are higher the dose to the rectum increase, and when the intersection has lower values the dose to the rectum is decrease an example is patient ID 9 has biggest values of intersection and rectum dose is higher.

4. Discussions

The evaluation of all the plans done through evaluate the coverage of PTVs, and compare the dose of the OAR with quantic constrain and local protocol used in Trento hospital.

4.1 PTVs Coverage

The coverage of the 95% of the prescribed dose to PTVs volume gives good result in both techniques (3DCRT and VMAT). Fig. 3 illustrated the dose distribution of 95% of prescribed dose with two techniques. We did not obtained 100% of coverage for all patients, because with some patients we need to make compromise between coverage of the PTV and sparing of the OARs. For the OAR (rectum, bladder, and femoral heads). The VMAT technique gives more conformal shape of coverage.
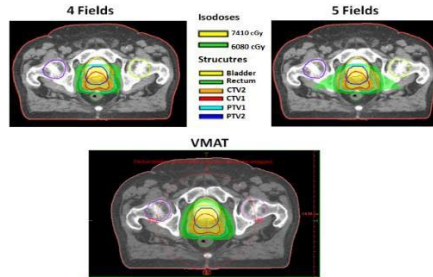
FIG. 3 Dose distribution of 95% of prescribed dose two techniques (3DCRT and VMAT)

4.2 Organ at Risk (OAR)

The dosimetric parameters extracted from DVHs to evaluate the plan for the structures: Rectum the percentages of the volume, covered by 50 Gy, 60 Gy, and 70 Gy (V_{50Gy}, V_{60Gy}, and V_{70Gy}), Bladder: the volume covered by 65 Gy, 70 Gy, and 80 Gy (V_{65Gy}, V_{70Gy}, Mean Dose), and mean dose, and Femoral heads: The mean dose values were recorded for both femoral heads(right and left).

4.2.1 Rectum

The histograms in fig (4) display the differences between two techniques the data for 3DCRT (4 fields and 5 fields) and VMAT the figure present the percentage of the rectum volume, covered by (50, 60, and 70) Gy. Patient ID 5 has obtained the highest value for the percentage of the rectum volumes (V_{50Gy}, V_{60Gy}, V_{70Gy}) probably because he has big seminal vesicles. In VMAT technique for the same patient the value decrease to the half because the movement of the gantry and MLC modulated the beam according to the shape of the target and decrease the irradiated volume of the rectum. The patient has ID 6 has almost similar values for (V_{50Gy}, V_{60Gy}) in 2 techniques.The lowest values for rectum with patient ID 10 because he has small seminal vesicles compared to patient ID 5 as illustrate in fig (4) , and the intersection between rectum and PTV1(0−64Gy) small intersection.
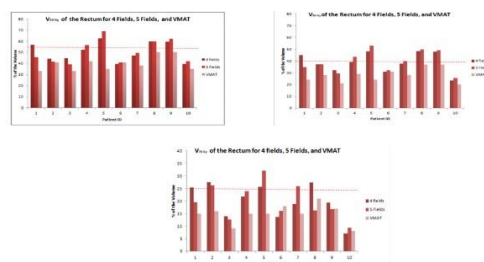
FIG. 4 V_{50Gy}, V_{60Gy}, and V_{70Gy} of the rectum 4 fields, 5 fields, and VMAT, The dashed Line illustrate the Dose constraint used in Trento Hospital.

4.2.2 Bladder

The histograms illustrated in fig (5) the comparison between techniques for the Bladder, the dosimetric parameters V_{65Gy}, V_{70Gy}, and mean dose , 3DCRT gives better result than VMAT, and 5 fields approach gives better result than 4 fields approach, in VMAT techniques three patients had obtain values greater than QUANTEC constraint for V_{65Gy}. For the mean dose all the values less than the constrain.
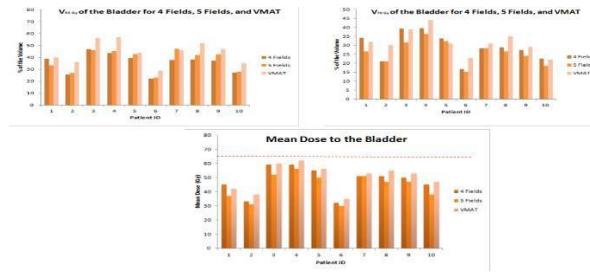
FIG. 5 $V_{65 Gy}$, $V_{70 Gy}$, and Mean Dose to the Bladder 4 fields, 5 fields, and VMAT, the Dashed line Illustrated the Dose Constraint used in Trento Hospital

4.2.3   Femoral Heads

For the femoral heads Figure (6) illustrated the mean dose for both (mean value) with 4 fields, 5 fields, and VMAT. The mean dose values were higher in 5 fields approach than 4 fields approach (except for patient ID 1 where the values were the same in both approach and VMAT give the half value of 3DCRT). and the better values with VMAT, Patient ID 5 has obtained higher values of dose than other patients. Patient ID 10 has obtained the lowest values in two technique.
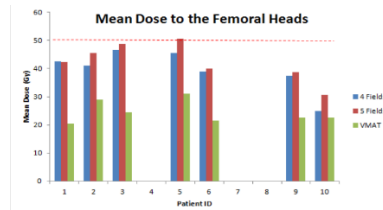
FIG. 6 Mean Dose to the Femoral Heads 4 fields, 5 fields, and VMAT, The dashed Line illustrate the Dose constraint used in Trento Hospital.

5.   conclusions

• For 3DCRT the 4 fields and 5 fields approaches can be used for prostate cancer treatment planning.

• The patients with big seminal vesicles has obtained higher dose to the rectum with 3DCRT because the volume of PTV is increased subsequently the volume of intersection with rectum increased also and the dose to the rectum become higher. This problem can be solved with modulation of VMAT RT technique because the isodoses can have concave shapes thanks to the intensity modulation. • An increase in the intersection between rectum and $PTV1_{(0-64)Gy}$ leads to an increase in the dose to the rectum.

• The factor that most influences the dose to the rectum is the posterior shape of the PTV1 (mainly due to seminal vesicles size).

• For the PTV1 and PTV2: all 3 methods (4F, 5F, and VMAT) fulfill the clinical requirements of target coverage.

• For the Rectum: VMAT technique allows dose reduction with respect to the 3DCRT plans for V_{50Gy} and V_{60Gy} and not for V_{70Gy}.

• For Bladder: all 3 methods fulfill the clinical requirements. 5 fields 3D-CRT technique allows dose reduction with respect to the other two plans regarding mean dose to the Bladder.

• For Femoral Heads: All 3 methods fulfill the clinical requirements, and VMAT technique allows dose reduction with respect to the 3DCRT plans regarding the mean dose to the femoral heads.

REFERENCES

[1] Ann Barrett Tom Roques Jane Dobbs, Stephen Morris. Practical Radiotherapy Planning. Hodder Arnold,and Hachette UK Company, UK, 4th. edition edition, 2009.

[2] International Atomic Energy Agency. Radiation Oncology Physics: A Handbook for Teachers and Students. IAEA, Austria, Vienna, 1th. edition edition, 2005.

[3] Philips Medical Systems. Pinnacle3 Physics, User Manual. Philips, Cleveland, USA, release 9 edition, 2009.

[4] Philips Medical Systems. Pinnacle3 Physics, Reference Guide. Philips, Cleveland, USA, release 9 edition, 2009.

PRODUCTION OF SYNTHETIC CRYSTAL OF CASIO₃ AND ITS APPLICATION IN LOW-DOSE DOSIMETRY RADIATION

Carlos D. Gonzales
Institute of Physics, University of São Paulo
São Paulo, Brazil
Email: clorenzo@if.usp.br

Shigueo Watanabe
Institute of Physics, University of São Paulo
São Paulo, Brazil

Roseli F. Gennari
Institute of Physics, University of São Paulo
São Paulo, Brazil

Cecilia M. Haddad
Radiotherapy Section, Hospital Sirio-Libanês
São Paulo, Brazil

Abstract

The use of different types of radiation is being increasingly widespread in various human activities such as intensive development radiation technologies, high nuclear energy, and nuclear medicine. The radiation, moreover, can be harmful to humans and dosimetry radiation becomes very important. There exist different systems in dosimetry radiation, based on thermoluminescent crystals being the most important one. Was produced synthetic polycrystals of calcium silicate $CaSiO_3$ by devitrification method, which in addition to the low cost and easy production it proved to be very sensitive as far as TL is concerned, in another word, it can be a useful radiation dosimeter. It has shown that 20 mg of $CaSiO_3$ can detect X-ray produced by 6 MeV electrons from a linear accelerator at a private Sirio-Libanés hospital in São Paulo, for its use in radiotherapy with a dose test of 1 Gy. In addition, 5.6 mg of $CaSiO_3$ in grains of $75 - 180$ μm size was exposed to 662 keV gamma rays from a Cs-137 source with a dose test of 10, 20 and 30 mGy, being sensitive at these doses. Therefore, there is a chance that it detects doses as low as few mGy such that it can be used in nuclear medicine or monitoring actual radiotherapy treatment.

1. INTRODUCTION

Different types of radiation are being increasingly widespread in nuclear medicine, in radiotherapy, etc., very low dose radiation is involved. Besides such usefulness of radiation, it can also induce some harm to the health of human involved with radiation. Hence the radiation dosimetry and establishing rules to protect against radiation become of most importance.

The dosimetry based in thermoluminescence (TL), the so-called TLD, started in late 1950's. LiF doped with Mg and Ti and later with Mg, Cu, P have been and still they are used as dosimetry materials [1]. Several other ionic crystals have been studied as dosimetry materials, among them Al2O₃: C and some others are also used extensively. At the Ionic Crystal Laboratory of the University of São Paulo, natural silicate minerals have been the object of investigation concerning their color, centers, Electron Paramagnetic Resonance (EPR) and TL properties, particularly under radiation. Many of these minerals have shown a high TL sensitivity, especially for high, sometimes, very high radiation doses. Some variety of quartz beryl, tourmaline, jadeite and other minerals can thus be used to monitor high-dose irradiation for food preservation, the color change of previous stone and other industrial applications, very often million Gy radiation are used. On the other hand for medical applications very low dose radiation are used. Organic materials are often used for dosimetry, however, only very few natural silicate minerals respond to such radiation, such as green quartz. In the present work, we produced synthetical silicate minerals to see its behavior under low and high dose irradiation.

2.   MATERIALS AND METHODS

To begin with, we aimed to produce a synthetic $CaSiO_3$. Starting with the stoichiometric balance of the components that were used. The chemistry equation used is: $CaO + SiO_2 \rightarrow CaSiO_3$, theoretical composition: $CaO = 48.3\%$ and $SiO_2 = 51.7\%$, but for to ensure the production of the Calcium metasilicate, we use: $CaO = 40.0\%$ and $SiO_2 = 50.0\%$ [2]. Thoroughly mixed in an alumina crucible this mixture is melted at 1550° C for two hours and then the temperature is lowered in a controlled manner by about 48 hours (devitrification method) [3]. Polycrystals of calcium were obtained and since the grain sizes are variable, they are sieved in such a way that grains of 0.080 to 0.180 mm size are retained for TL measurements.

These were carried out in Harshaw 4500 TL reader keeping 4° C/s heating rate. The irradiation was carried out in ^{60}Co γ-ray source at the Institute for Energy and Nuclear Researches (IPEN) in São Paulo, Brazil. Figure 1, (a) shows the Harshaw 4500 equipment and (b) calcium silicate polycrystalline obtained.

(a)   (b)

FIG.1. (a) Harshaw 4500 equipment, (b) synthetic CaSiO₃ polycrystalline.

3.   RESULTS AND DISCUSSIONS

Figure 2, shows glow curves for doses from 0.2 to 10 Gy using about 5.6 mg mass for each reading. One prominent peak around 120 and 260° C, are observed. Also, a shoulder can be seen around 320° C. Figure 3, shows TL response as a function of doses, the growth curve indicates the possibility to detect doses lower than 1.2 Gy. Actually, the TL response grows linearly up to about 1000 Gy and sub-linearly for doses above this value.

(a)   (b)
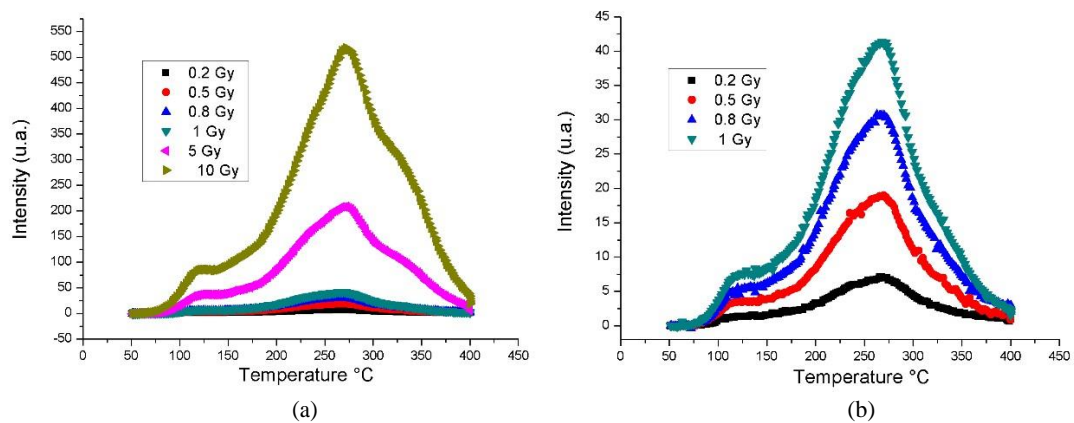
FIG. 2. TL glow curves of synthetic CaSiO₃ using a reading mass of 5.6 mg. (a) from 0.2 to 10 Gy, and (b) 0.2 to 1 Gy.
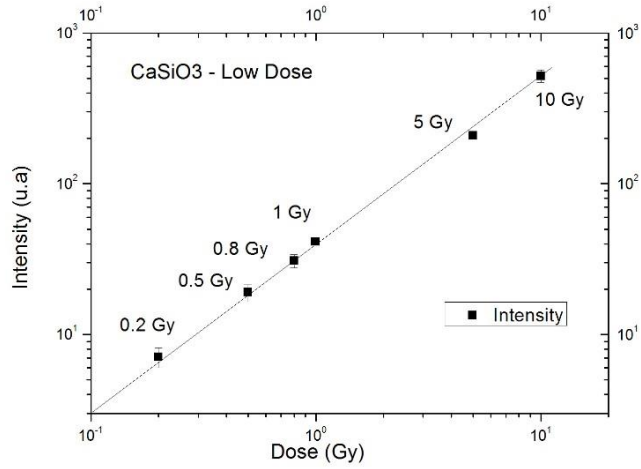
FIG. 3. TL response of synthetic CaSiO₃ as a function of doses.

Polycrystals of CaSiO₃ in grains of 75 -180 µm size, were exposed to 662 keV γ-ray from a Cs-137 source at IPEN. Figure 4, (a) shows the TL glow curves of CaSiO₃ irradiated with γ-ray doses of 10 mGy, 20 mGy and 30 mGy using a reading mass of ~5.6 mg, and (b) shows glow curves of CaSiO₃ irradiated with the same γ-ray doses using a reading mass of ~9.0 mg.
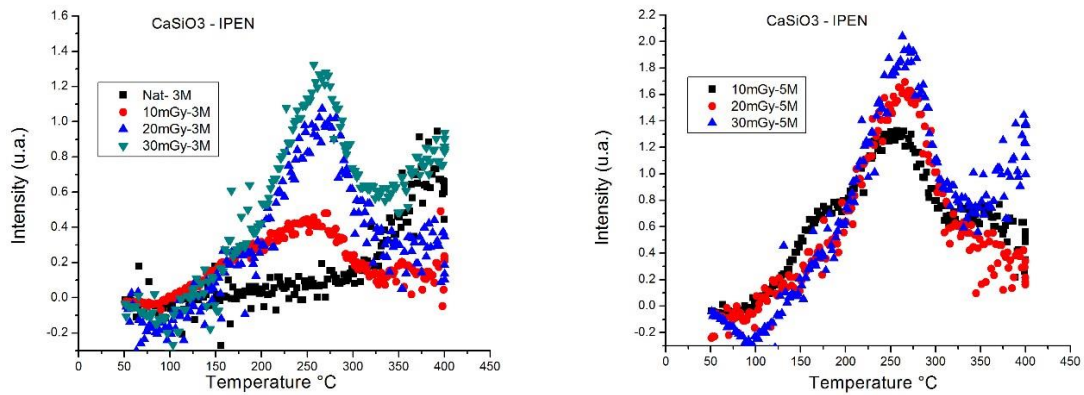
FIG. 4. Glow curves of synthetic CaSiO₃ irradiated with γ-ray doses of 10 mGy, 20 mGy and 30 mGy using a reading mass of 5.6 mg; (b) irradiated with the same doses using a reading mass of 9.0 mg.

Figure 5, shows TL as a function of doses around the prominent peak around 270° C, including the TL peaks of 10 mGy, 20 mGy, and 30 mGy. In all cases was used a reading mass of ~ 5.6 mg.

In addition, CaSiO₃ was exposed in grains to 6 MeV X-ray from a linear accelerator at a private Sirio-Libanés hospital in São Paulo, for its use in radiotherapy. The dose deposited of the equipment was 0.97136 ± 0.0194 Gy and calculated by Calcium Silicate Polycrystalline was 1.246 ± 0.046 Gy, obtaining a relative error of ~ 28 %. The mass used was 20 mg.
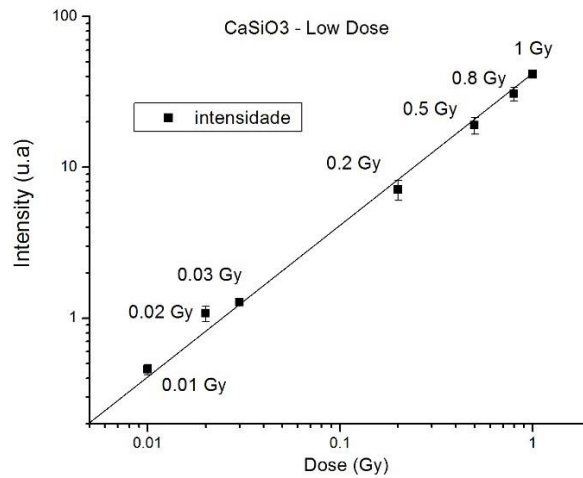
FIG.5: TL as a function of doses of synthetic CaSiO₃ around the prominent peak around 270° C including the TL peaks of 10 mGy, 20 mGy, and 30 mGy.

4. CONCLUSIONS

The behavior of the glow curve TL of the synthetic CaSiO3 at low dose makes it a strong candidate for use in medical applications. The next step will be the production of chips for a good handling to the synthetic silicate in future analysis.

ACKNOWLEDGEMENTS

REFERENCES

[1] Nakajima, T., Murayama, Y., Matsuzawa, T., Koyano A., Nuclear Instruments and Methods, Development of a new highly sensitive LiF thermoluminescence dosimeter and its applications, (1978) v. 155, p. 155-162.

[2] Hillert, M., Sundman, B., Wang, X., Metallurgical Transactions B, An assessment of the CaO-SiO2, (1990) v.21, n.2, p. 303-312.

[3] Cano M. N., Phd Thesis, Propriedades de termoluminescência, de ressonância paramagnética eletrônica e de centros de cor de diopsídio, Physics Institute of São Paulo University, São Paulo, Brazil, 2017.

SIMPLE AND INEXPENSIVE ELECTRON DENSITY PHANTOM TO CALIBRATE TREATMENT PLANNING SYSTEMS

Rezvan Ravanfar Haghighi

Medical imaging Research Centre, Shiraz University of Medical Sciences, Research Tower, Khalili Street, Shiraz 7193635899, Iran

S.Chatterjee

BGVS, Chemical Engineering Building (Old), Indian Institute of Science, Bangalore 560012, India

Vani VC

Department of Instrumentation and Applied Physics, Indian Institute of Science, Bangalore 560012. India

Reza Jalli

Medical imaging Research Centre, Shiraz University of Medical Sciences, Research Tower, Khalili Street, Shiraz 7193635899, Iran

Sefide Sefidbkht

Medical imaging Research Centre, Shiraz University of Medical Sciences, Research Tower, Khalili Street, Shiraz 7193635899, Iran

Ali Reza Shakibafard

Medical imaging Research Centre, Shiraz University of Medical Sciences, Research Tower, Khalili Street, Shiraz 7193635899, Iran

Abstract

Standard electron density phantom is commonly used to determine the dose distribution in patient's body by x-ray computed Tomography. We attempt to construct an inexpensive phantom and test its performance to calculate the electron density of different tissues. The phantom consists of, (1) outer body of phantom, filled with water, (2) test tube holders immersed in water, and (3) kickstand to fix the position of the phantom. Laboratory test tubes were filled with chemical compounds and inserted into the test tube holders. Chemical compounds were selected so that they are easy to handle, easily available, and have chemical properties close to those of different human organs. The Hounsfield Unit (HU) values of these chemicals at 110 kVp were used to calculate their electron densities. Solid rods with known electron densities were used to validate the findings of this study.

The electron density results showed that the error between the calculated and actual values for solid rods was less than 6%- being within the acceptable limits. This phantom gives satisfactory results with known samples and can be used with confidence as an electron density phantom.

Introduction

Ionizing radiations such as x-ray has a broad utility in medicine [1]. It can be used for the purpose of diagnosis in the range of 20-30 kVp in mammography [2], 40-140 kVp in conventional radiology [3] and Computed Tomography [4] (CT) and megavoltage energies to kill the cancerous cells and save the human patient's life, in radiotherapy [5]. On the other hand, x-ray can harm the normal tissues and produce stochastic and deterministic effects. Even very small amount of radiation dose can produce late effects such as infertility or cancer with its stochastic effect and higher doses (above a certain threshold) may produce deterministic effects [6, 7]. Therefore, one has to take care and balance between the usefulness and harm of x-ray beam, in its clinical utility. When the x-ray imaging justification is approved, one has to apply dose optimization methods to produce acceptable image quality with As Low As Reasonable

Achievable (ALARA) dose to the patient [8]. Also, radiotherapy treatment planning systems need to calculate dose distributions in patients in such a way that the maximum prescribed dose is delivered to the target or cancerous cells while the radiation dose to the normal tissues surrounding the target (tissues in the radiation field) has to be kept at the minimum level [9].

Between diagnostic imaging modalities, Computed Tomography is responsible for highest dose delivery to the patient (except interventional methods such as angiography) [10]. Different phantoms are used to test the performance of the CT systems through objective and quantitative evaluation of the image quality and radiation dose. The accuracy of Hounsfield Unit (HU) of water as a reference material, standard deviation or noise measurement, and the uniformity of the HU values of homogenous material like water have to be checked in a routine quality control tests. On the other hand, testing the ability of the CT machine to produce wide range of HU values, from air (-1000 HU) to bone (>1000 HU), or linearity of the CT machine is an essential quality control test in quantitative studies such as bone densitometry and DECT studies [11-13]. Although testing the linearity of CT machine has been emphasized in several literatures for decades, as far as we are aware, this point has vanished from the radar, in spite of its importance being pointed out in the past [14].

Computed tomography is used to find the relationship between HU values and electron density of different tissues. Treatment planning system in radiotherapy uses electron density to calculate dose distribution inside the human patients [9,15]. Spatial phantoms with different inserts mimic different human tissues and are used to calibrate treatment planning systems by CT machine.

Special phantoms are available in market in order to do different Quality Control tests for CT machine and for the purpose of electron density measurement. The price of these commercial phantoms are high and most of the medical centers are not able to provide them for CT and radiotherapy departments, especially in developing countries. The aim of this study is to design and construct an affordable phantom to do essential Quality Control (QC) tests for CT and can be used as electron density phantom to calculate dose distribution for treatment planning systems in radiotherapy.

Material and Method

Basic design

The design of the phantom is shown in figure 1. It essentially consists of two parts, (1) a permanent body of the phantom and (2) replaceable test tubes which are shown in Figs. 1 and 2 respectively. The body of the phantom is made of Perspex, is cylindrical in shape, being 20 cms in diameter and 17 cms in length. Test tube holders are also made of the same material. These test tube holders are arranged in two rows that are located at distances, 2.5 cms and 5 cms from the outer wall of the phantom. These test tube holders are placed at separation angle 90° for the inner row and 45° for the outer row. Each test tube holder is 10cms in length and has an inner diameter of 1.5 cms.
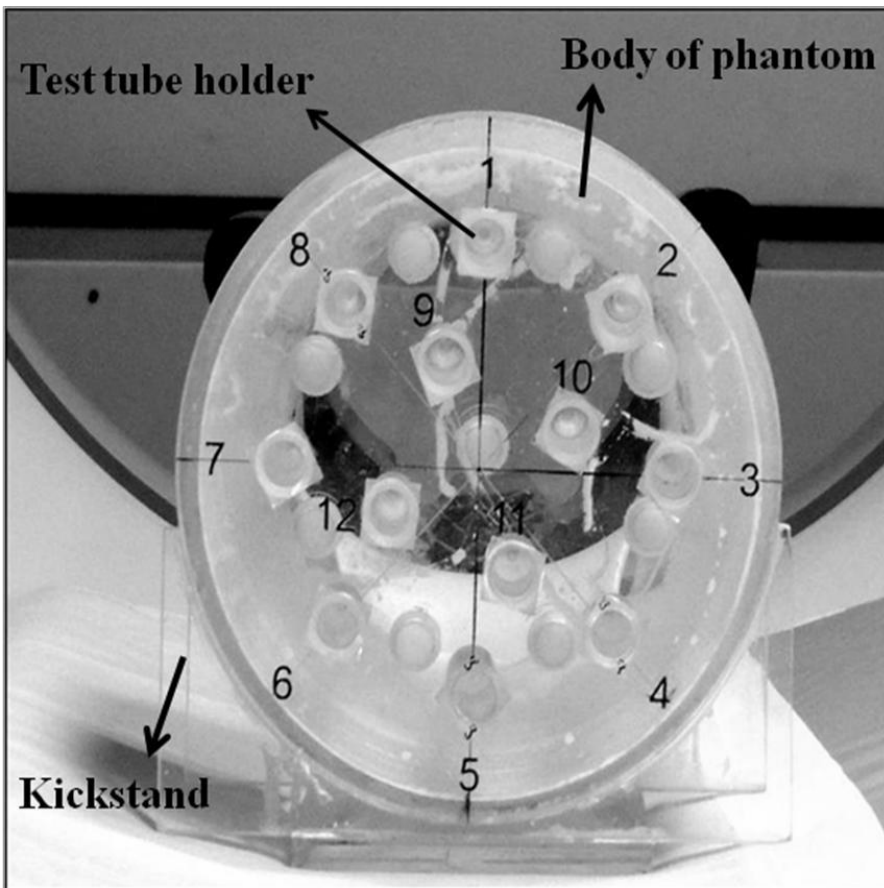
Fig.1. Different parts of the phantom consist of Kickstand to fix the phantom on top of the scanning table, body of the phantom which is filled with water and chemical compounds. There are 12 test tube holders, 8 and 4 test tube holders in the outer and inner layers respectively, to keep the test tubes.
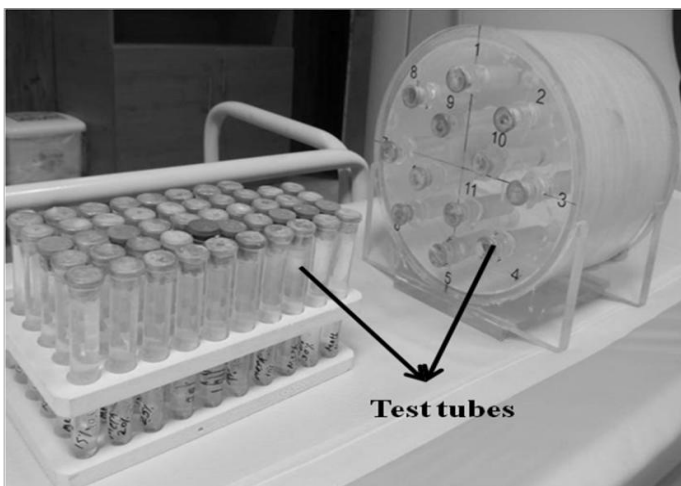
Fig.2. Ordinary laboratory test tubes are made of plastic with very low x-ray attenuation coefficient were filled with water and chemical solutions. These test tubes were inserted in the test tube holders inside the body of the phantom which is immersed in water

In this arrangement, we can take data simultaneously with 12 samples. The basic idea of having two separate rows of test tube holders at different depths inside the water is to check the beam hardening effect.

All the test tubes are made of plastic of low x-ray attenuation coefficient and their dimensions are roughly the same as

that of the test tube holders, in order that they fit well in these holders. During all the measurements, these sample holders are surrounded by water. The body of the phantom is held in the kick stand (Fig. 1), in its correct position, during the Quality Control (QC) tests and electron density measurement. During the construction stage and testing, the system was checked to be leak proof.

Sample preparation

For quality control tests, we used liquid samples. These were aqueous solutions of chemicals made in distilled water. We chose the chemicals in such a way that we could cover a wide range of values for the electron density (ρ_e) and effective atomic number (Z_{eff}). The chemicals were methanol, glycerol and potassium hydroxide. All the chemicals were of analytical grade and were procured from the Merck Chemicals. Aqueous solutions were made in 5,10,15,20,30,35,40 weight percentage, with weight measurements being done in a balance with 0.001 gm accuracy. After preparation these were kept in a fridge that was maintained at 4° C.

Above samples were used for calibration purposes. By using liquid samples we ensured that the samples were of uniform composition in all parts of the test samples, liquids solutions being more homogeneous than solids. With these liquid data, we could establish a calibration that could relate the HU values with the electron density (ρ_e) of the samples, where the electron density (ρ_e) was calculated from the known composition of the solution and by using Eq. (7) of reference [16]. For checking the reliability of the QC we next used solid rods of polymers like, polypropylene, Perspex, polyethylene, and paraffin wax (Fig. 3).
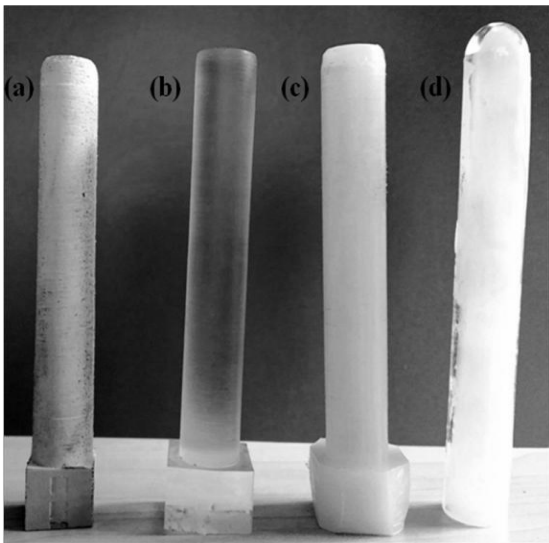
Fig.3. Solid rod test tubes made of (a) Polypropylene, (b) Perspex, (c) Polyethylene, and (d) paraffin wax.

These rods were 1.45 cms in diameter and 10 cms in length so that they fitted well in the test tube holders. From the measured HU values of these substances, we calculated their electron density, from which we estimated the density of the substances by using the formula,

$$\rho_e = \left(\frac{\rho}{m_p}\right) \times \left(\frac{Z}{M}\right) \qquad (1)$$

where ρ is the density of the substance, m_p= mass of the proton = *1.67 × 10^{-24} gm*, *Z*= total number of electrons in the molecule and *M*= molecular weight of the substance. We matched this calculated value of ρ, from Eq.(1) with that we found independently from the physical measurement of the density.

Scanning parameters for QC test

Siemens Emotion 16 slice CT scanner was used for all image acquisitions, by using *V= 80, 110, 130 kVp* as excitation voltages of the CT machine, with tube current (mAs) being equal to 135, while using 4.8 mm slice thickness and H31s convolution Kernel. This was uniformly followed in all cases, water, liquid solutions (Figs 4.a-c) and solid polymeric samples.
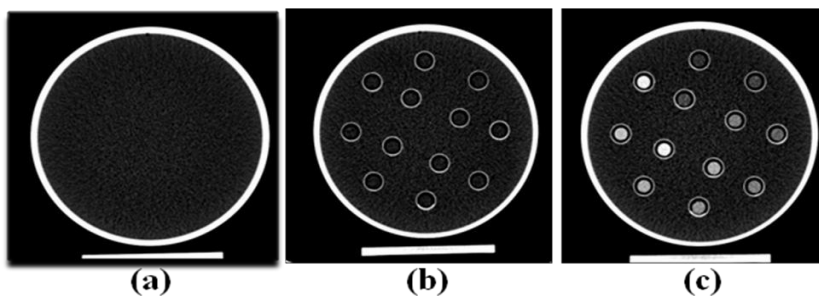
Fig.4. Axial slices of CT images of phantom containing; (a) water, (b) test tubes filled with water, (c) test tubes filled with different concentration of chemical compounds (here as an e.g outer test tubes filled with 5, 10, 15, 20, 25, 30, 35, 40% by weight and inner test tubes filled with 10, 20, 30, and 40% by weight of glycerol).

For linearity tests of CT machines, we tested each series of chemical compound separately. The sample with 5% weight by weight composition was placed at 12'o clock position of the outer row of test tube holders. In this outer row, other samples were of 10, 15, 20, 25, 30, 35, 40 % w/w composition. In the inner row we placed samples with 10, 20, 30, 40 % w/w (e.g. Fig 4.c).

We took the HU values in the water portion of the phantom (Fig. 4.a) to test the accuracy of the HU value, image noise and uniformity tests.
In every case (in chemical solutions), the region of interest (ROI) was kept sufficiently large (>30 pixels) in the middle part of each chemical solution inside the test tube (Fig. 4.c) and the HU_s value which was an average taken from three measurements, was recorded. It has to be noted that by the same method and the exact scan parameters HU value of water inside the corresponding test tubes (Fig. 4.b) were measured too. For all calculations we used the corrected HU_c value, given by,

$$HU_c = HU_s - HU_w \tag{2}$$

where HU_s, HU_w represent the HU values of the solution and of water. These data were used for standard QC tests and also for the test of linearity and electron density measurement.

Calibration for electron density

From the definition of HU values, we find, on defining *G(V)* as in Eq.(3.1) that

$$G(V) = 1 + \left\lceil \frac{HU(V)}{1000} \right\rceil \qquad (3.1)$$

$$G(V) = \frac{\hat{\mu}(V)}{\hat{\mu}_w(V)} \qquad (3.2)$$

where, $\hat{\mu}(V)$ and $\hat{\mu}_w(V)$ are respectively the average attenuation coefficients of the substance and of water, with the average being over all photon energies, in the source spectrum of the x-ray source for an applied voltage *V*, *V* being expressed in *kVp*.

It is known that in the range of x-rays that are used for CT, the main contribution to x-ray attenuation coefficient appears from the Compton scattering and photoelectron absorption. This allows us to write,

$$\hat{\mu}(V) = \rho_e \left[a(V) + b(V) Z_{eff}^x \right] \qquad (4)$$

where, the first term gives the contribution from the Compton effect and the second term gives the contribution from photoelectric absorption, with

$$a(V) = 66.62 \times 10^{-26} \hat{f}_{KN}(V) \text{ in } cm^2, b(V) = 54.75 \times 10^{-18} \hat{f}_{ph}(V) \text{ in } cm^2 \qquad (5)$$

with $\hat{f}_{KN}(V)$, $\hat{f}_{ph}(V)$ being the averages over the source spectrum, of the Klein Nishina coefficient and the photoelectric effect coefficient. We shall express ρ_e in units of 10^{23} per cm^3 so that the unit of $\hat{\mu}(V)$ is cm^{-1}. For low values of Z_{eff}^x, i.e. $a(V) >> b(V) Z_{eff}^x$, we can approximate Eq.(4) as,

$$\hat{\mu}(V) \approx a(V) \times \rho_e \qquad (6)$$

By scanning the HU values of different materials in different ranges of ρ_e and Z_{eff}^x we find the relation between these quantities and the observed HU values. This information are important inputs for radiation dose calculation, radiation therapy planning and radiation protection.

Results

Quality Control tests

The summary of results for the Quality Control tests are as follows.

HU value of water:

- At the centre of the axial slice (Fig. 4.a) the HU value of water was found to be -3.2, while the acceptable range of values is ± 4.0.

- The maximum of the deviation in HU values is within $\pm 0.6\%$ (acceptable value is within $\pm 25\%$ of the base value).

- Deviations in the HU values, measured at different points inside the axial slice (Fig. 4.a) are ± 2.0, everywhere while the acceptable value is ± 10.0.

Beam hardening tests:

- Figure 5 depicts the HU values of 10, 20, 30, 40 % w/w solutions of glycerol, in the two layers of test tube holders, taken at *V=110 kVp.* The differences of the HU values in the two layers are not significant, showing little beam hardening effect.
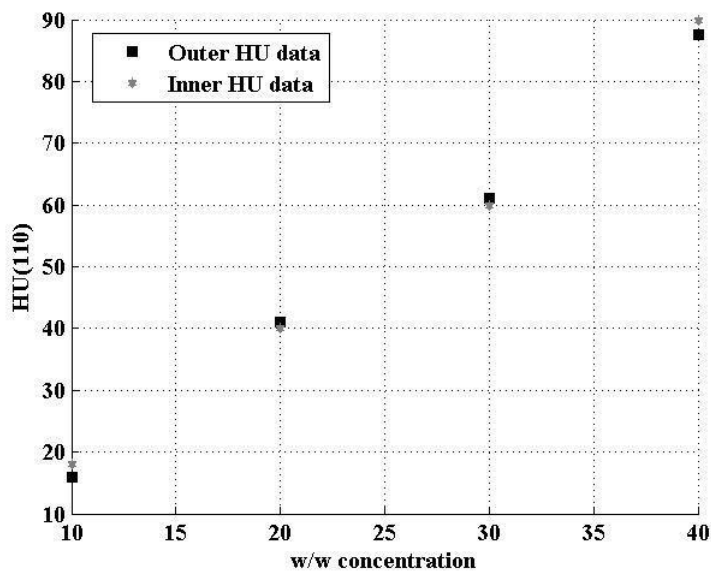
Fig.5. The HU values of different concentrations (10, 20, 30, 30, 40% w/w) of glycerol in the test tubes at the outer and inner layer of the phantom are very close to each other at 110 kVp and the error bars are too small in the present scale of the figure.

Linearity test
- In Figs. 6(a-c), we show the HU versus w% concentration plots.
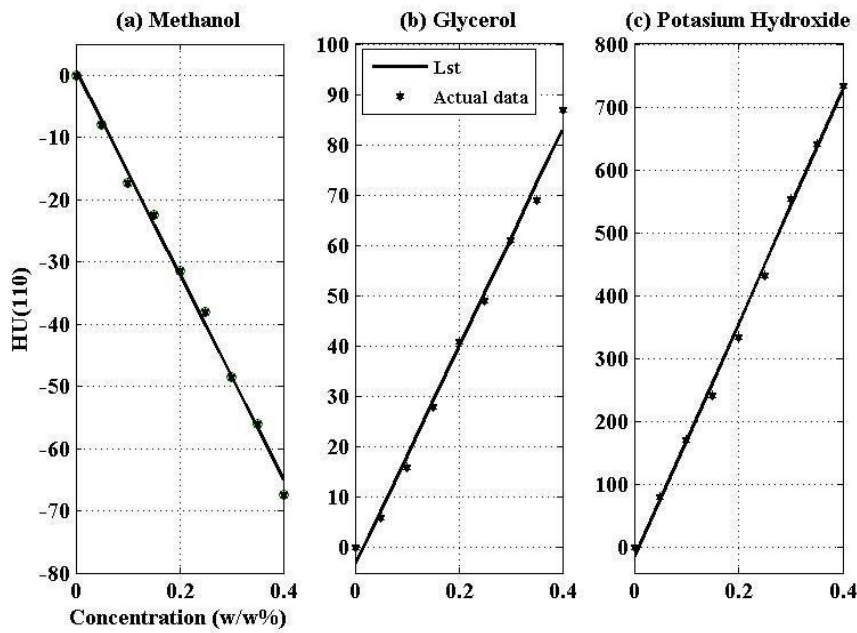
Fig.6. The slope of the fit between HU(110) and concentration (from 0 to 40% w/w) is (a) negative for methanol (b)) positive for glycerol and (c)) positive for potassium hydroxide.

- The HU values increase with w for glycerol and potassium hydroxide, i.e. with samples, whose physical density is greater than that of water. The HU values decrease with w for methanol, i.e. for a substance whose physical density is less than that of water. These are also the expected trends.

- The $G(V)$ versus ρ_e curves are seen to be linear for low Z_{eff} materials, as seen in Fig 7, and also for high Z_{eff} materials, as shown in Fig 8. The linearity is established in terms of the linear regressional fits in the two cases, which are seen to be satisfactory.
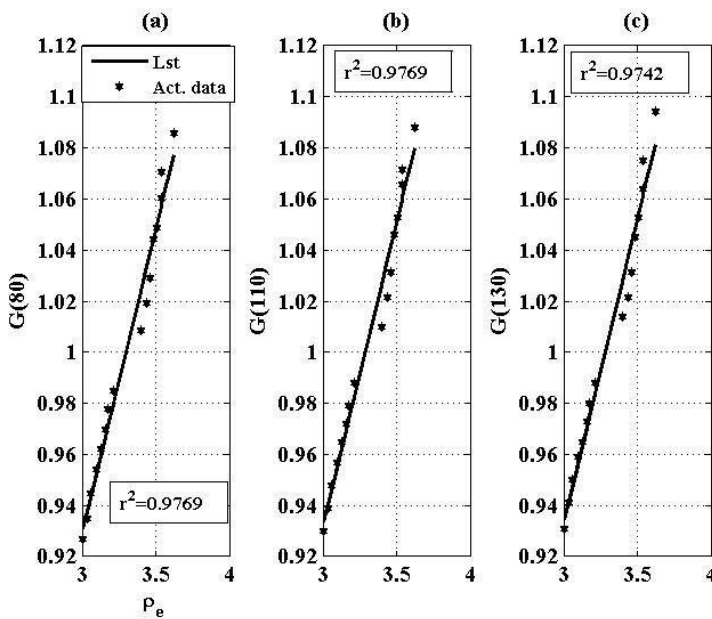
Fig.7. The least square fit between $G(V) = 1+ [HU(V)/1000]$ and ρ_e are made for 16 data points (5 to 40% w/w concentration) of methanol and glycerol at (a) 80 kVp with a=0.2377, b=0.2162, r^2=0.9769 (b)110 kVp with a=0.2373, b=0.2204, r^2=0.9769 (c) 130 kVp with a=0.2380, b=0.2191, r^2=0.9742.
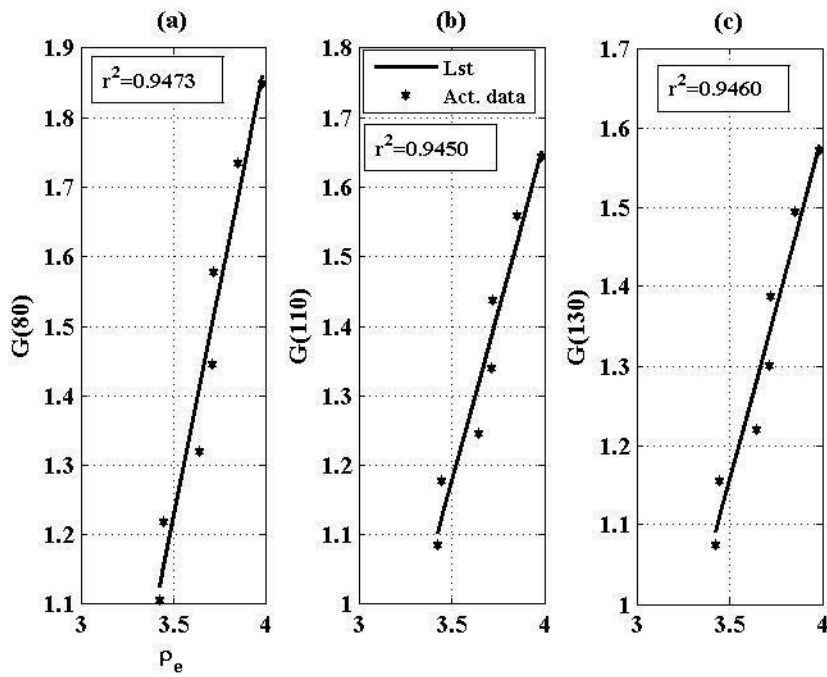
Fig.8. The least square fit between G(V) = 1+ [HU(V)/1000] and ρ_e are made for 7 data points (5 to 40% w/w concentration) of potassium hydroxide (KOH) at (a) 80 kVp with a=1.3167, b=3.3853, r²=0.9473 (b)110 kVp with a=0.9833, b=2.2664, r²=0.9450 (c) 130 kVp with a=0.8714, b=1.8946, r²=0.9460.

- A single linear G(V) versus ρ_e fit cannot be extended to cover the cases for all Z_{eff} values, as can be seen in the break in the two curves, which appears in Fig 9.
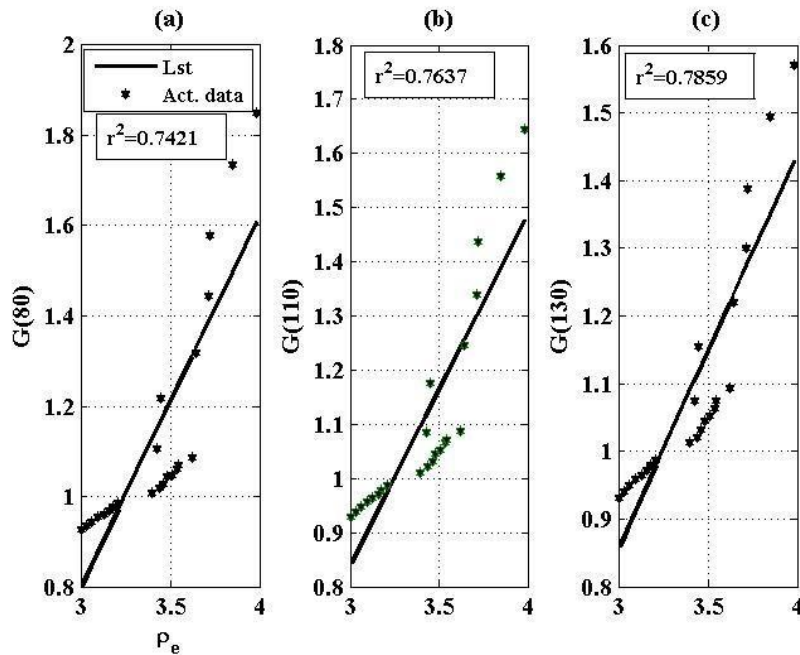
Fig.9. The least square fit between G(V) = 1+ [HU(V)/1000]and ρ_e for 23 data points (5 to 40% w/w concentration) of methanol, glycerol and potassium hydroxide at (a) 80 kVp with a=0.8231, b=1.6716 (b)110 kVp with a=0.6462,b=1.0980 (c) 130 kVp with a=0.5821, b=0.8903.

The break in the linear fits between G(V) and ρ_e is expected since at high Z_{eff} values, the photoelectric

absorption dominates, which varies as $[\rho_e Z_{eff}]^x$. Thus at high values of $[\rho_e Z_{eff}]$, the $G(V)$ versus $[\rho_e Z_{eff}]$ fit is expected to be linear. This is seen to be so, as given in Fig.10.
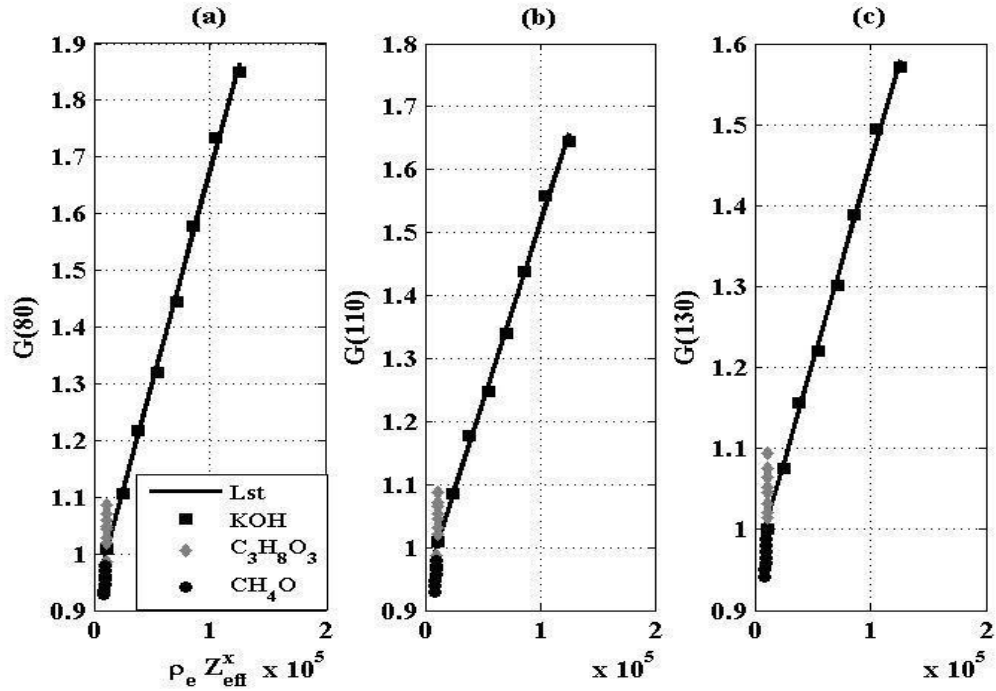
Fig.10. Least square fit of G(V) versus the photoelectric effect parameter "$\rho_e Z_{eff}^x$" for methanol, glycerol and potassium hydroxide at (a) 80 kVp with $r^2=0.9783$ while $a=7.5\times10^{-6}$ and $b=0.9246$, (b) 110 kVp with $r^2=0.9615$ while $a=5.673\times10^{-6}$ and $b=0.9464$, and (c) 130 kVp with $r^2=0.9558$ while $a=4.9550\times10^{-6}$ and $b=0.9587$.

Application as an electron density phantom.

- For substances with low Z_{eff}^x, we can use the approximation given in Eq.(6) and use the phantom as an electron density phantom, if the $G(V)$ versus ρ_e calibration be known. This calibration is given in Fig. 7.

- To check the accuracy of the above electron density calibration, we find the HU values of solid samples (those not used in calibration but whose ρ_e values are known independently) and determine the ρ_e values from the calibration and finally find their densities ρ by using Eq.(1). The comparison between the calculated values of ρ_e, as found from the HU data and those found by independent measurements are shown in Table 1. The two values match satisfactorily.

Table 1. Electron density ($\rho_{e\text{-}Cal} \times 10^{23}$) of Perspex, polyethylene, polypropylene, and paraffin wax, found by the use of calibration curve in Figure (5) and compared with the actual electron density ($\rho_{e\text{-}Act} \times 10^{23}$) of these substances.

Substance	Chemical formula	Z	M	Z/M	$\rho_{e\text{-}Act} \times 10^{23}$	$\rho_{e\text{-}Cal} \times 10^{23}$	% Error
Perspex	$(C_2O_2H_8)_n$	36	64	0.562	3.964	4.018	1
Polyethylene	$(C_2H_4)_n$	16	28	0.571	1.674	1.777	6
Polypropylene	$(C_3H_6)_n$	24	42	0.571	3.198	3.097	-3
Paraffin	(C_nH_{2n+2})	802	1402	0.572	2.723	2.687	-1

DISCUSSION

Importance of checking the linearity of CT machines

- Its *importance has been pointed out for long but the medical physics community has given little attention to it. As was pointed out by Kalender[14], "Nevertheless linearity has been demanded for CT systems, and it was already specified in the early days of CT (AAPM 1977). The practical problem was- and still is- that no adequate test tools were provided. The specification of a set of different plastics is inadequate, and the AAPM task group in its original specification acknowledged the "lack of rigor".* The μ-values for plastics such as polyethylene, Plexiglas and Teflon depend on the spectrum, detector characteristics etc. Therefore, they will show different behaviour for different scanners. Linearity can only be checked with object and phantom inserts in which only the density ρ is varied, but the composition and thereby the energy-dependent mass-attenuation coefficient μ/ρ is kept constant".

The method presented in the paper, gives a way to resolve the above problem and can be standardised.

Application in radiation dosimetry and radiation protection

- Experimentally determined values of *a(V)* and *b(V)* can give idea about the source spectrum of the x-ray source.
- By knowing *a(V)* one can calculate (a) the photon flux that is scattered from any organ to other organs (b) also the photon flux that comes out of the patient's body.
- By knowing *b(V)* one can calculate (a) the amount of tissues that are ionized by ejection of K-shell electrons (b) number of electrons that are released from the tissues, that can serve as secondary ionizing sources and can cause damage to the cells and tissues of the patient and also to others.

CONCLUSION

The paper gives details about the construction of a phantom that is capable of taking HU measurements with 12 samples at a single shot. The phantom is inexpensive and easily replicable, its costs may be about 1/5th of commercial phantoms. The paper gives a new method to test the linearity of CT machines, and suggests suitable sample preparations for this purpose. It is shown that this system can be standardised for use as an electron density phantom. Its usefulness for calculation of radiation dose and for radiation protection is pointed out.

ACKNOWLEDGEMENT

REFERENCES

[1] HARVEY, CJ, BLOMLEY, MJK, Principles and precautions of conventional radiography, Surgery **23** (2005) 158-161

[2] PISANO, ED, YAFFE, MJ, Digital Mammography, Radiology **234** (2005) 353-362

[3] RAHOMA, UA, CHUNDI, PK, Economic Evaluation of Conventional Radiography with Film and Computed Radiography: Applied at BMC, Advances in Computed Tomography **1** (2012) 23-29

[4] RAFF, GL, GALLAGHER, MJ, O'NEILL, WW, GOLDSTEIN, JA, Diagnostic Accuracy of Noninvasive Coronary Angiography Using 64-Slice Spiral Computed Tomography, Journal of the American College of Cardiology **46** (2005) 552-557

[5] ERBECO, RI, NGWA, W, MAKRIGIORGOS, GM, Localized dose enhancement to tumour blood vessel endothelial cells via megavoltage x-rays and targeted gold nanoparticles new potential for external beam radiotherapy Int. J. Radiation Oncology Biol. Phys. **81** (2011) 270–276

[6] LIN, EC, Radiation Risk From Medical Imaging, Mayo Clin Proc. **85** (2010) 1142-1146

[7] LITTLE, MP, WAKEFORD, R, TAWN, EJ, BOUFFLER, SD, DE GONZALEZ, AB, Risks Associated with Low Doses and Low Dose Rates of Ionizing Radiation: Why Linearity May Be (Almost) the Best We Can Do Radiology **251** (2009) 6-12

[8] KALRA, MK, NAZ, N, RIZZO, SMR, BLAKE,MA, Computed tomography radiation dose optimization: Scanning protocols and clinical applications of automatic exposure control Current Problem in Diagnostic Radiology **34** (2005) 171-181

[9] SCHNEIDERYX, U, PEDRONIZ, E, LOMAX, A, The calibration of CT Hounsfield units for radiotherapy treatment planning Phys. Med. Biol. **41** 1(996) 111–124.

[10] BINDMAN, RS, LIPSON, J, MARCUS, R, KIM, KP, MAHESH, M,GOULD, R, DE GONZA´LEZ, AB, MIGLIORETTI DL, Radiation dose associated with common Computed Tomography examinations and the associated lifetime attributable risk of cancer Arch Intern Med. **169** (2009) 2078-2086

[11] Euclid Seeram Computed Tomography, physical principles, clinical applications, and quality control 2001 second edition, W.B. Saunders Company, A Harcourt Health Sciences Company, New York, United States of America

[12] IAEA Hhuman Health Series No.19 Quality Assurance Program for Computed Tomography: Diagnostic and Therapy Applications 2012 International Atomic Energy Agency, Vienna International Centre, PO Box 100, 1400 Vienna, Austria

[13] LIN,JP, BECK, TJ, BORRAS, C, COHEN, G, JUCIUS, RA, KRIZ, RJ, NICKOLOFF, EL, ROTHENBERG, LN, STRAUSS, KJ,VILLAFANA, T, AAPM report No. 39 specification and acceptance testing of Computed Tomography scanners report of task group 2 diagnostic x-ray imaging committee ©1993 by the American Association of Physicists in Medicine 335 East 45th Street New York, NY 10017

[14] WILLI A. KALENDER Computed Tomography, Fundamentals, System Technology, Image Quality, Applications Publisher: Publics Corporate Publishing, Erlangen© 2005 by Publicis KommunikationsAgentur GmbH, GWA, Erlangen, printed in Germany

[15] KAROTKI, A, MAH, K, MEIJER, G, MELTSNER, M, Comparison of bulk electron density and voxel-based electron density treatment planning   j. applied clinical medical physics **12** (2011) 97-104.

[16]HAGHIGHI, RR, CHATTERJEE, S, VYAS, A, KUMAR, P, THULKAR, S, X-ray attenuation coefficient of mixtures: Inputs for dual-energy CT   Med. Phys. **38** (2011) 5270-5279.

Study of Gamma Ray and Fast Neutron Shielding Properties of some Concrete Materials

Nesreen Rageeb[1], Nadia Helal[1], Fayez Shahin[2] ,Mohamed Tarek[2],and Fadel Mohamed Ali[3]

[1]Radiation Safety Department, Egyptian nuclear& Radiological Regulatory Authority, Cairo, Egypt.
[2]Physics Department, Faculty of Science, Beni-Suef University, Egypt.
[3]Biophysics Department, Faculty of Science, Cairo University, Egypt.

Abstract:

Developing new cement based materials with excellent mechanical and attenuation properties is critically important for both medical and nuclear power industries. Concrete continues to be the primary choice material for the shielding of gamma and neutron radiation in facilities such as nuclear reactors, nuclear waste repositories, spent nuclear fuel pools, heavy particle radiotherapy rooms, particles accelerators, among others.

In this work shielding of gamma-rays and neutrons by concrete with different concentrationsof high density polyethylene (HDPE) mixed with different concentration of borax (BX)has been studied. Since most of the neutron shields at 8 MeV are more likely to penetrate,themacroscopic fast neutron removal cross-sections have been calculated and compared with the attenuation of gamma-rays with 8 MeV photon energy.The total mass attenuation coefficients, linear attenuation coefficients, half-value thicknesses and effective atomic numbers have been evaluated. The obtained results has been further validated usingXCOM (version 3.1). The measured and calculated valueswere comparedand a reasonable agreement has been observed.

In addition, neutron shielding has been treated in terms of macroscopic removal cross-section concept. The best values of polyethylene and density of concrete for maximum shielding against both neutrons and gamma-rays have been represented graphically. Also the transmission of both gamma rays and neutrons has been obtained as a function of thickness of concrete for all different concentrations.

1. Introduction

Developing of radiation shielding materials has been always an attractive area in the field of radiation applications in medical, agricultural, industrial, nuclear reactors and accelerator technologies, and future generation reactors.In the last few years, several studies have been devoted to develop a new type of concrete by changing the properties of different materials and cement. In construction of special critical buildings such as nuclear power plant and accelerator systems, the materials require a special care. Heavy elements such as lead are consideredto be anideal shielding material for ionizing radiation but the difficulties of their use as a shieldopen the way to develop new shielding materials. Construction of a new neutron shielding material attracts more attention due to their wide range of use in different applications[1]. For the construction of neutron shielding system; hydrogenous material is involved to moderate fast neutrons, boron compounds are mixed with the moderator capture thermal neutrons through the reaction$^{10}B_5$ (n, α)^{7}Li3 yielding 1.47 MeV α particles[2].Where the electron accelerators are widely applied in medicine with high energy over 8 MeV.Shielding is needed for the treatment rooms equipped with such

1

machines, to attenuate not only gamma rays but also neutron [3-4]. Computational investigations of neutron shielding and activation characteristics of borated concrete with polyethylene have been studied [??]. It was shown that the replacement of polyethylene in borated concrete greatly enhanced the shielding efficiency of the concrete, and total activity levels of the concrete were considerably decreased with this replacement [5]. Adding Borax ($Na_2B_4O_75H_2O$) has no significant effect on strengthen of concrete in the range up to 1% by wt, but it has significant effects on shielding efficiency in thick concrete shields (100 cm) as it reduces the capture gamma rays up to 80% better than un-borated concretes. Recently, increasing interest has been shown in the use of industrial plastic wastes for preparation of new composite materials. In respect of interest in radiation shielding materials there is associated demand for improved plastic composites that are also able to satisfy stringent requirements such as mechanical strength. Additionally, with polymeric materials providing good neutron attenuation, it has been suggested that these might also be made suitable as shields for gamma- and X- rays by adding a heavy mineral or metals [7]. Furthermore, mixing the principle differentmaterials in concrete by mineral additives at different percentages will change the attenuation parameters for gamma rays and neutrons such as linear attenuation coefficient (μ cm^{-1}), mass attenuation coefficients (μ/ρ cm^2 g^{-1}), effective atomic numbers (Z_{eff}), effective fast neutrons removal cross-section (Σ_R, cm^{-1}) and mass removal cross section (Σ_R / ρ, cm^2 g^{-1})of the concrete [8]. Most of the previous studies have been concerned with photon attenuation coefficients only [9-12] and treatment for neutron attenuation subjects is not given.For neutron attenuation calculations, the elastic and inelastic scattering reactions, and neutron-capture interaction process, are of great importance [13]. The effect of the sample can be described by an equivalent absorption cross-section called an effective removal cross section [14]. The removal cross-section is the probability that fast or fission energy neutron undergoes on first collision, which removes it from the group of penetrating, unclouded neutrons. The removal cross-section is considered to be constant approximately for neutron energies between 2 and 12 MeV [12]. The observed value of removal cross-section is in fact, roughly equal 2/3 of the total Σ_t (cm^{-1}), (scattering and capture) cross-section of the given material for neutrons having energies in the range of 6-8 MeV [4]. If concrete contains sufficient moderating material, the attenuation of neutrons will be determined by this removal process. The most effective shielding materials for mixed neutron and gamma-rays is obtained by mixed hydrogenous materials, heavy metal elements, and other neutron absorbers. Inelastic scattering by heavy elements and elastic scattering by hydrogen are quite effective to slow down fast and intermediate energy neutrons, and the absorbers can reduce secondary gamma-rays as well as thermal neutrons. Thus the evaluation process for the effectiveness of a shielding material must include, beside other parameters, its ability to attenuate gammas and neutrons.

2. Experimental and calculation methods
2.1. Materials and sample preparation

The sample which is presented in this work is a combination of different concentrationsof Polyethylene, Borax, Cement and Sand (PBCS) composites with different blending ratios.The sampleshave been prepared from High Density Polyethylene HDPE produced by: (SidiKerir Petrochemicals Co SAE (Sidpec)). Granular Borax produces by: (ETi MADEN iŞLETMELERI GENEL MÜDÜRLÜĞÜ made in TÜRKIYE), Ordinary Portland Cement (a National Cement company), sand

(ordinary sand) and tap water as additive material and from the percentage of the total weight of the shield. The percentage composition of the concerned composites is givenas a concentration of HDPY in the samples (6.25%, 12.5%, 18.75%, 25%, 31.25%, 37.5%, 43.75, wt .gm %), as shown in table 1.

Table 1: Percentage composition of HDPE and BX

Samples	Material (wt.%)	
	HDPE	BX
S_1	25	25
S_2	31.25	18.75
S_3	37.5	12.5
S_4	43.75	6.25
S_5	18.75	31.25
S_6	12.5	37.5
S_7	6.25	43.75

Firstly, the sand was well washed with tap water several times to dissolve water soluble salts then dried before mixing. Then HDPY,BX, cement and sand were blended with each other (on dry) in a variable speed mechanical mixer for a period of 5 min. The, water was added during the mixing for further 5 min to ensure that, a good homogeneous mixing has been achieved. The distributed homogeneous mixture was poured into a mould with 20 x 20 x 1.5 cm of dimension. The specimens were lifted to dry in the sun for 7 days. (The strength of the sample is week because it will be used as filler).

2.2. Fast neutron and gamma ray measurements

Neutron and total gamma ray spectrahave been measuredfor all samples with the above mentioned dimensions.

The total mass attenuation coefficients of γ-ray (µ/q)

In this section we summaries some theoretical relations used in the present work. If a material of thickness x is placed in the path of a beam of gamma radiations, the intensity of the beam will be attenuatedaccording to the Beer–Lambert's law [1]:

$$I(x) = I_o e^{n11} \qquad (1)$$

Where I_o is the initial photon intensity, $I(x)$ refer to those photons

that penetrate a distance x in an absorber and µ (cm^{-1}) is the linear attenuation coefficient of the material.The following relations represent half-value thickness (cm) in which the intensity of primary photon beam reduced by $\frac{i}{i}$:

$$HVT = \frac{\square\square\square}{1} \quad (2)$$

If we take the logarithm of both sides of using eq. (3), we obtain the mass attenuation coefficient for the target material:

$$\mu / \square = \frac{i}{\square} \ln\left(\frac{n_o}{n}\right) \qquad (3)$$

The mass attenuation coefficient (μ/ρ) for any chemicalcompound or mixture of elements is given by [12]:

$$\mu/\rho = \frac{1}{\sum_i (\mu/\rho)_i} \qquad (4)$$

Where ρ_i and $(\mu/\rho)_i$ are the partial density (the density as it appearsin the mixture) and the mass attenuation coefficient of the ith constituent, respectively and $w_i$is the weight fraction. A coefficient more accurately characterizing a given material is the density-independent mass attenuation coefficient μ/ρ ($cm^2 g^{-1}$).

2.2. The effective removal cross-sections for fast neutrons (RR)

Prompt neutrons from fission are produced at all energies up to 17 MeV. The attenuation process consists primarily of collisions in which either large energy degradation is accomplished or the neutron is widely deflected so that its total escape path is significantly increased. Following degradation, many successive collisions take place in a relatively short further excursion before the neutrons are absorbed at low energy. Because in general cross-sections decrease with increasing energy, the neutrons produced at higher energy have the best chance of penetration. Balancing this is the original distribution in which the lower energies predominate. For most shields the neutron produced at 8 MeV are most likely to penetrate [10]. A simplified calculation of attenuation is made on the basis of the neutrons at about 8 MeV. Some allowance is necessary for the neutrons that have collided but still escape, a factor usually called the buildup factor. This is taken account of by a compensating factor obtained by counting all neutrons as if they were in the high energy group. This simplifies the calculation, is reasonably accurate, and is conservative for shields that contain reasonable quantities of moderating, especially hydrogen, material. Examplesof such materials are water-bearing concrete, barites concrete [??].

2. Experiment set up

2.2. Neutron irradiation facility

The neutron source, namely, [241]Am -Be, were used in this experiment. This source was manufactured by Amersham Co., UK. The [241]Am -Be source is kept in a stainless steel pressurized vessel of 3 cm diameter and 7 cm height, with activity 5 Ci. The source was suspended by a wire to have free motion through a PVC tube of 5.5 cm x 140 cm side and 120 cm height. The source was calibrated, in its position, by secondary standard neutron monitor. The neutron monitor is of type NM2 manufactured in UK by Nuclear Enterprises Ltd. In the present study, the neutron monitor was used to detect the neutron emitted from the source by using two techniques for counting system.

2.3. Gamma - irradiation facility

TheCo-60 facility, used in this study, is gammatron S 65/S 80 made by Siemens of Germany. It was used for therapy purposes at the national Cancer institute (NCI) in

Egypt before donating it to National Institute for Standards (NIS) to be used in the therapy level calibrations. The source have mechanical motion was adjusted in all direction and checked with the field size, iso-center, Source-Surface-Distance (SSD) and angle of radiation to reduce the uncertainty value.

3. Results and Discussion

3.1. Thermal neutron and gamma attenuation

Figures 1and2 show the neutron dose rateand gamma rays for concrete shielding mixed with different concentration of high density polyethylene HDPE(high concentration of polyethylene 25%, 31.25%, 37.50%and 43.75%) and borax as a function of the thickness(from 1cm to 15cm).
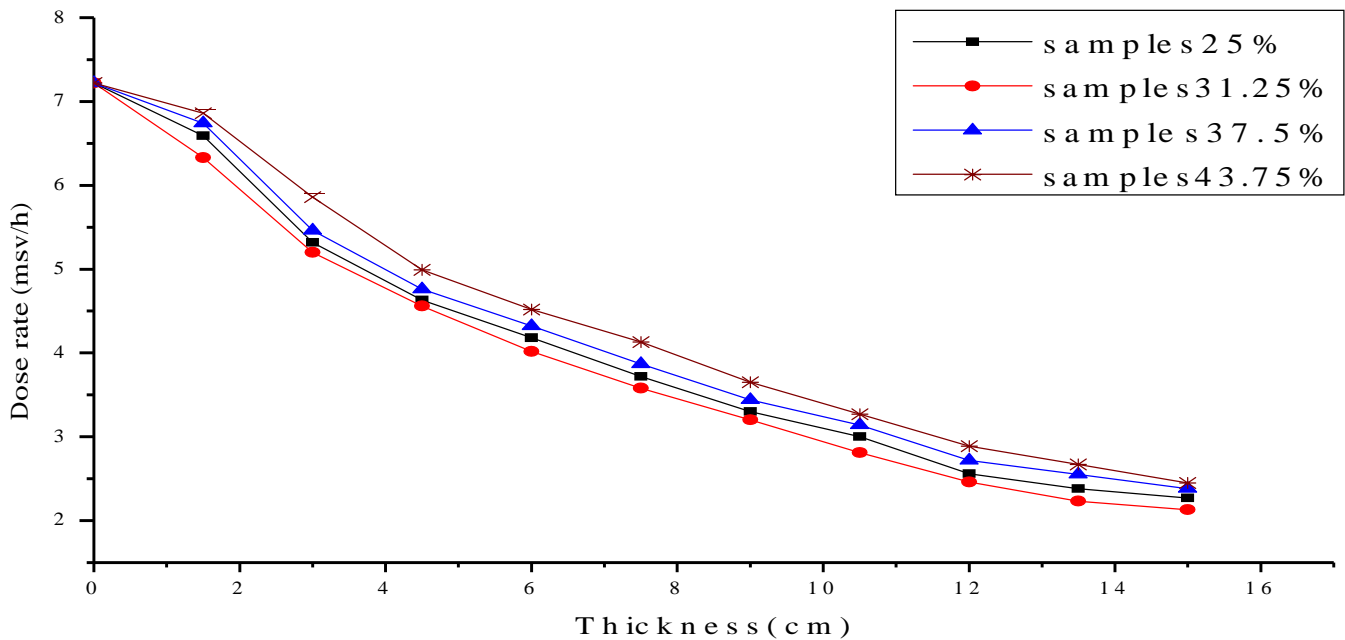
Fig.1.Attenuation neutron curve for samples with concentrations
(25%,31.25%,37.5%, 43.75%)
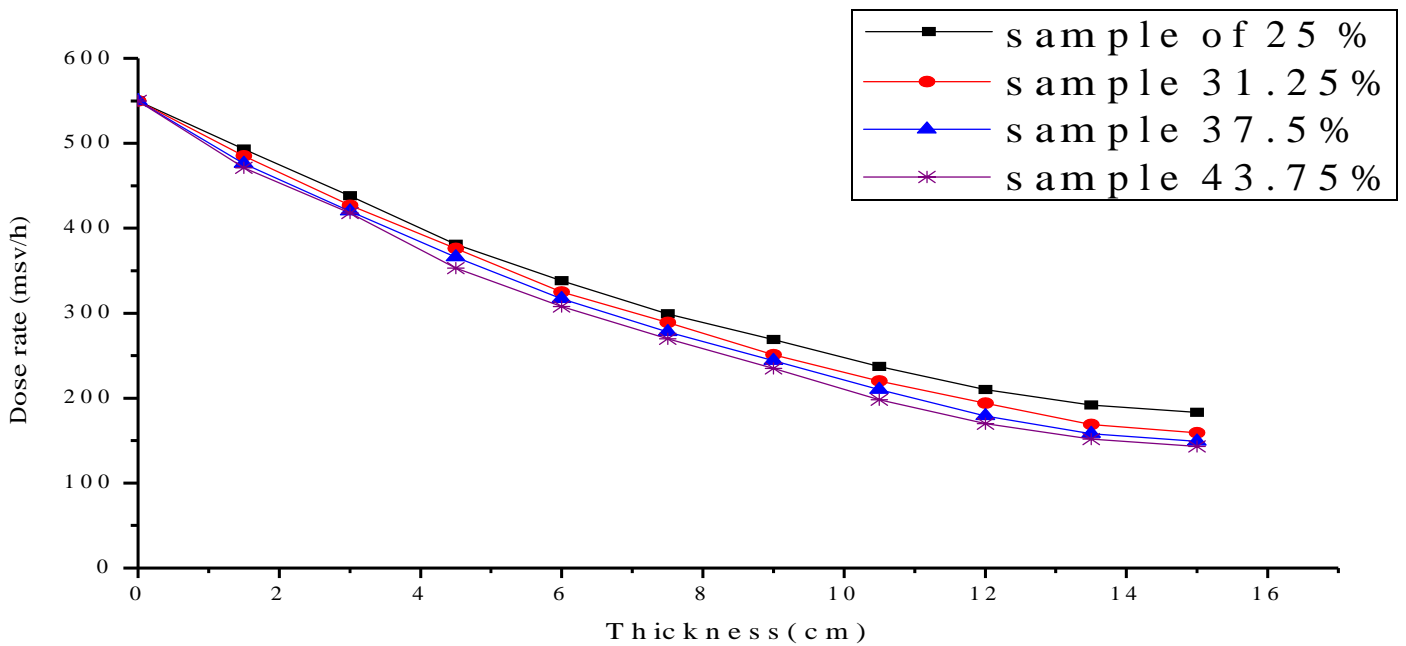
Fig.2. Attenuation gamma curve for samples with concentration (25%, 31.25%, 37.5%, 43.75%)
of high concentration of polyethylene.

Figures 3 and 4 show the neutron and gamma rays respectively for samples of
differentconcentration of high density polyethylene HDPE (low
concentration 25%, 18.75%, 12.50% and 6.25%) mixed with borax as a
fraction of thickness.
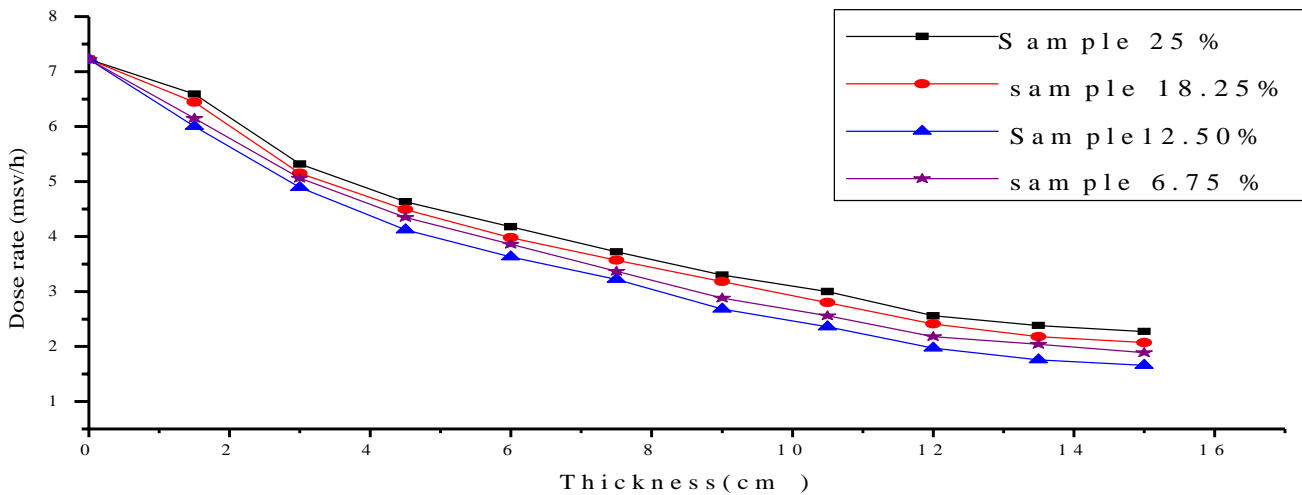
Fig (3) :Attenuation neutron curve for samples (25%, 18.75%,12.5%, 6.25%,50% Borax)
with law concentration of polyethylene
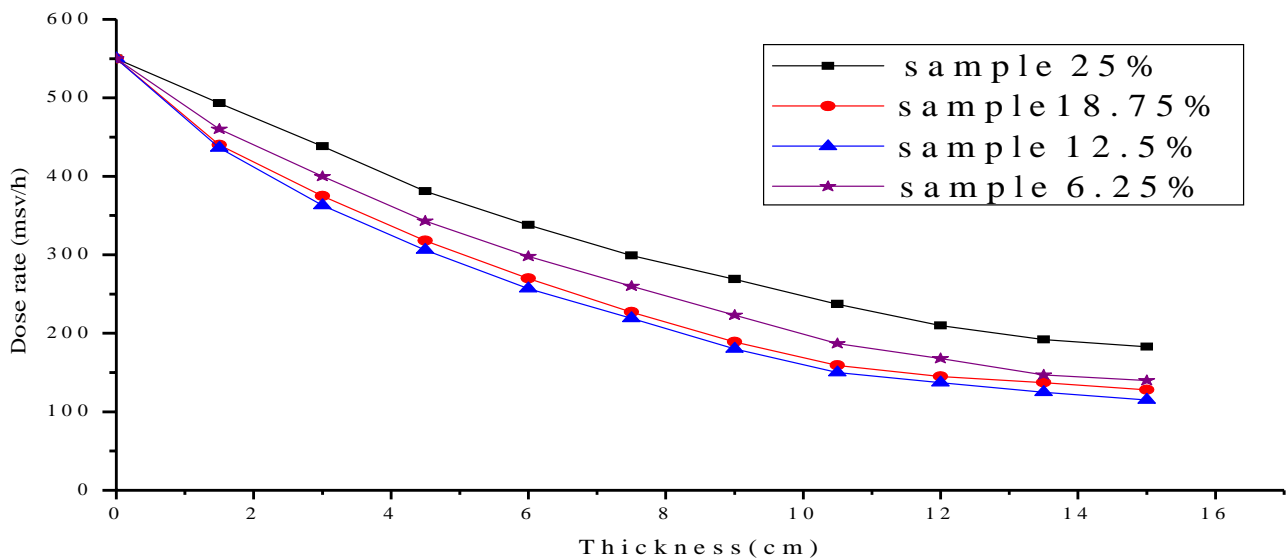
Fig(4): Attenuation gamma curve for samples (25%, 18.75%,12.5%,6.25%,50% Borax)
of low concentration of polyethylene

Figures 5 and 6 illustrated the relation between $Ln\ I/I_o$ and thickness to calculate the linear attenuation coefficient of the material(μ) that's given from relation $I(x) = I_o e^{n11}$ and also calculate the HVL ($X_{1/2}$) from the slope of the curves (for neutron and gamma rays respectively),that is for samples of concentrations (25%, 31.25%, 37.50% and 43.75%) respectively.
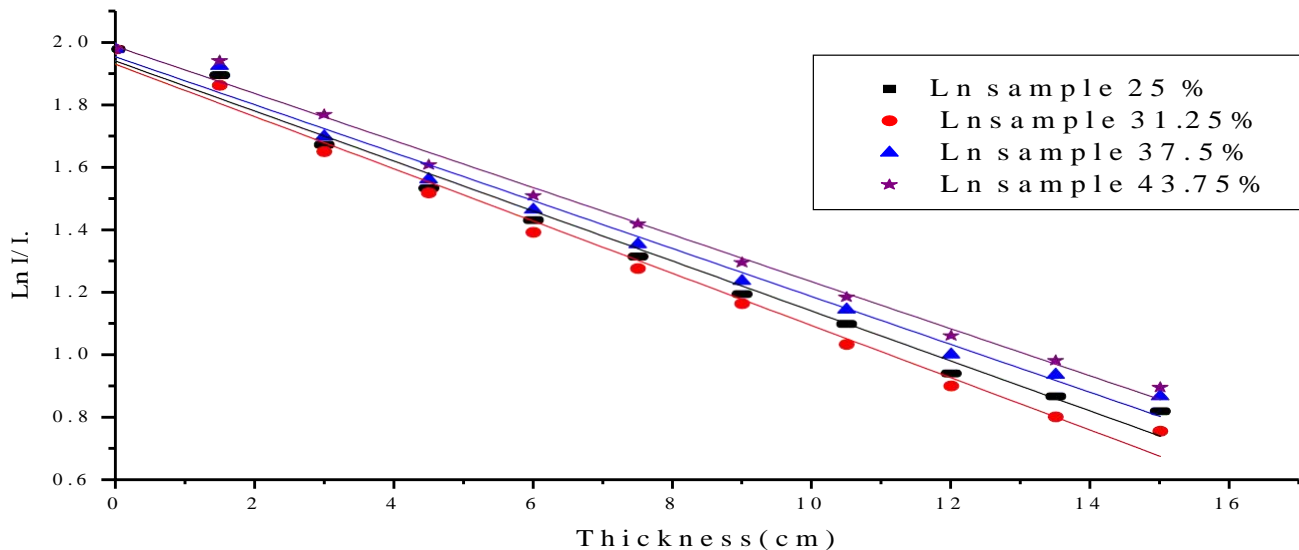
Fig(5): linear attenuation coefficient (μ) for neutron for samples of concentration
(25%, 31.25%, 37.5%, and 43.75%).
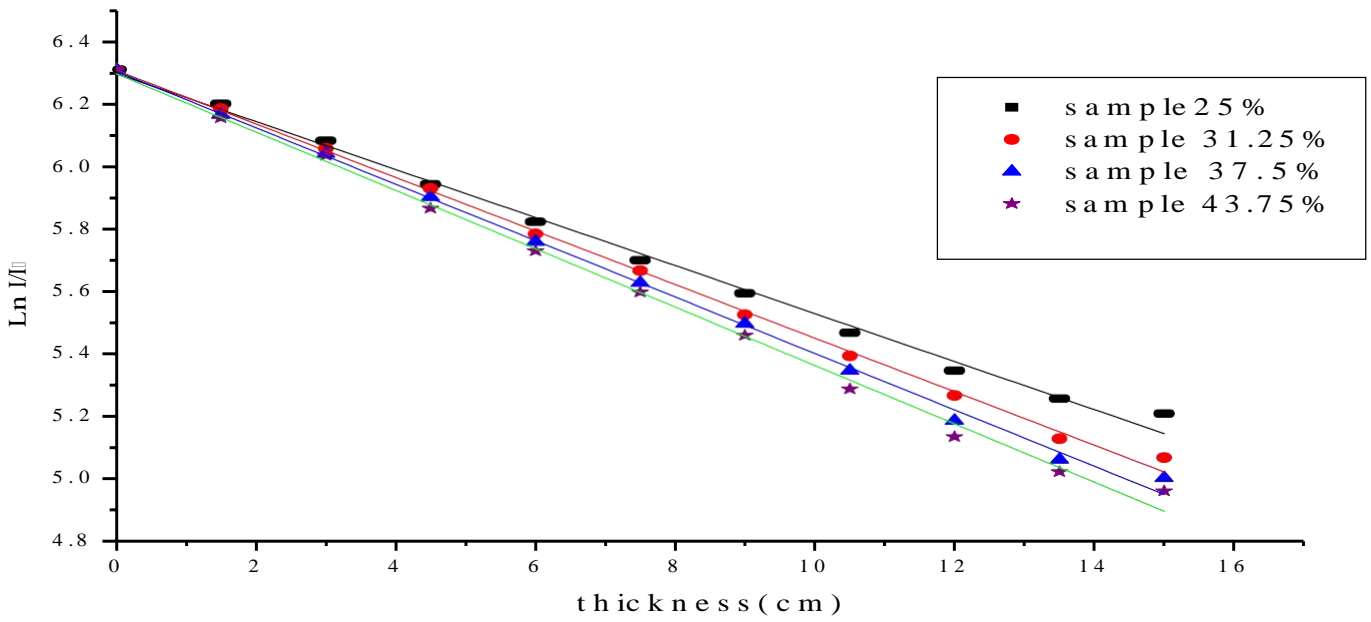
Fig (6): linear attenuation coefficient (μ) for gamma rays for samples of concentration
(25%, 31.25%, 37.5%, 43.75%).

Figures 7 and 8 show the relation between Ln I/I$_o$ and thickness for samples of
concentrations (25%, 18.75%, 12.50% and 6.25%). The values of the linear
attenuation coefficient of the material (μ) and HVL are inserted in table (1) &
(2) for neutron and gamma rays.
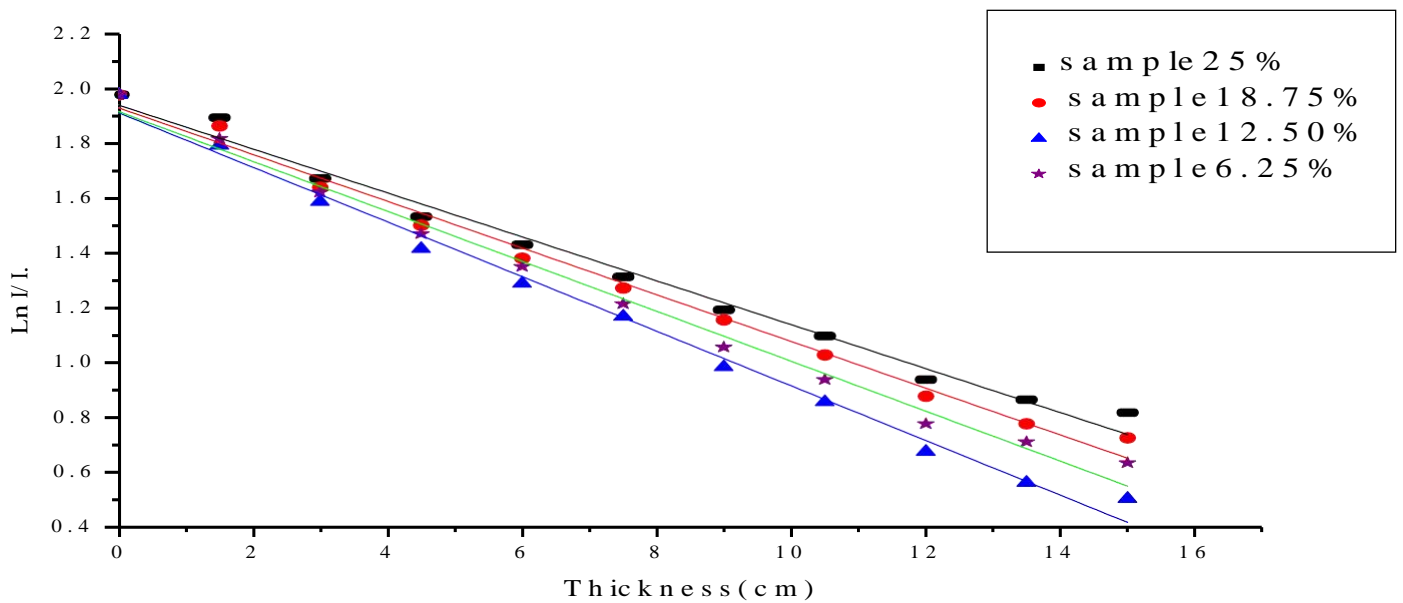
Fig (7): linear attenuation coefficient (μ) for samples (25%, 18.75%,12.5%, 6.25%,50% Borax)
with law concentration of polyethylene
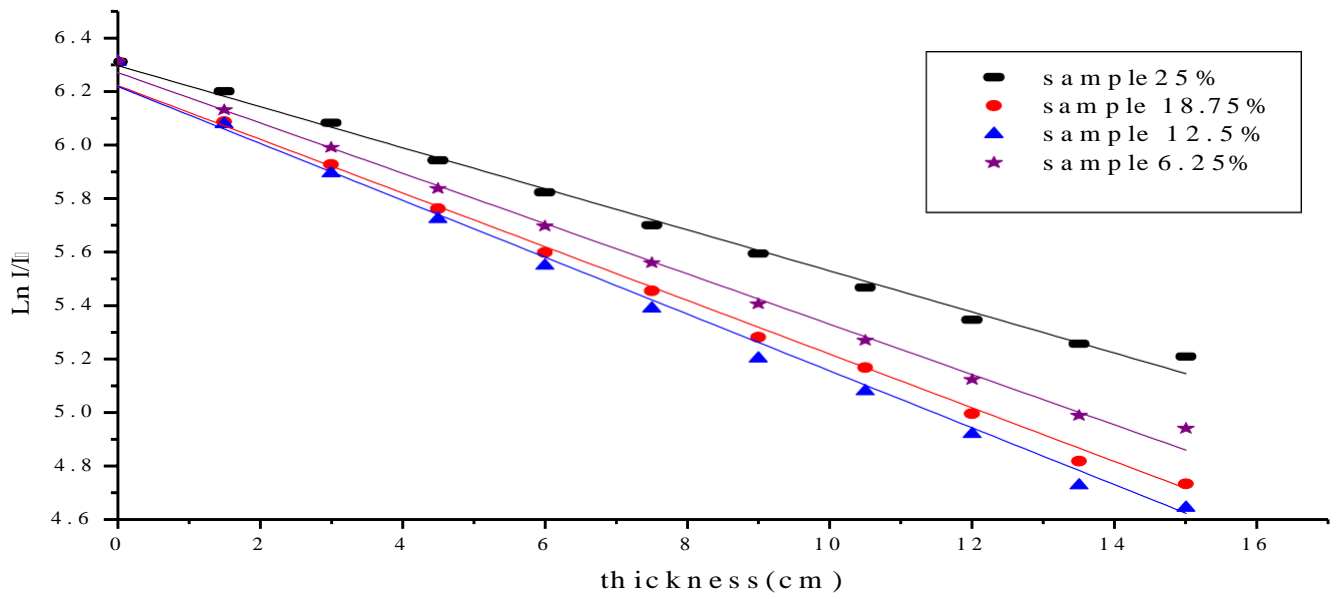
Fig (8): linear attenuation coefficient (μ) for gamma rays for samples (25%, 18.75%, 12.5%, 6.25%, 50%Borax) of low concentration of polyethylene

Figures 9 and 10 show theFitting exponential curve for figures 1 and 2 for neutron and gamma attenuation by shields for samples with concentration (25%, 31.25% ,73.5% , 43.75%).
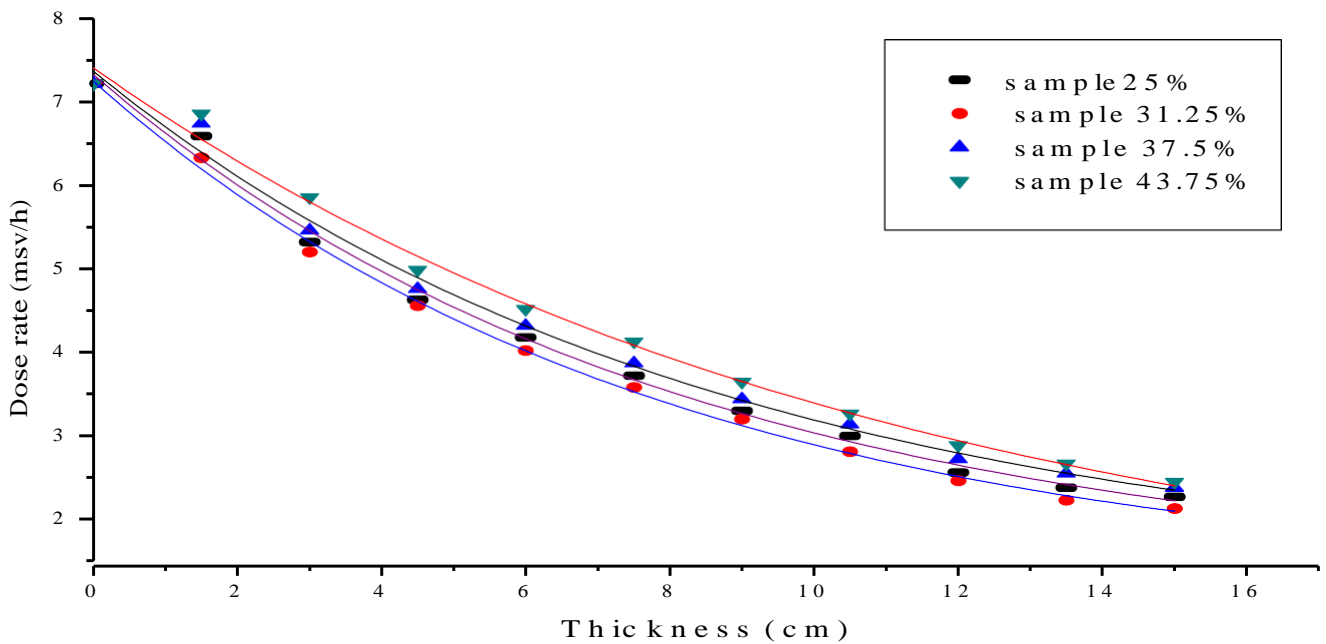
Fig (9) : Fitting exponential curve for neutron attenuation by shields with high for samples with concentration (25% ,31.25% ,73.5% , and 43.75%)
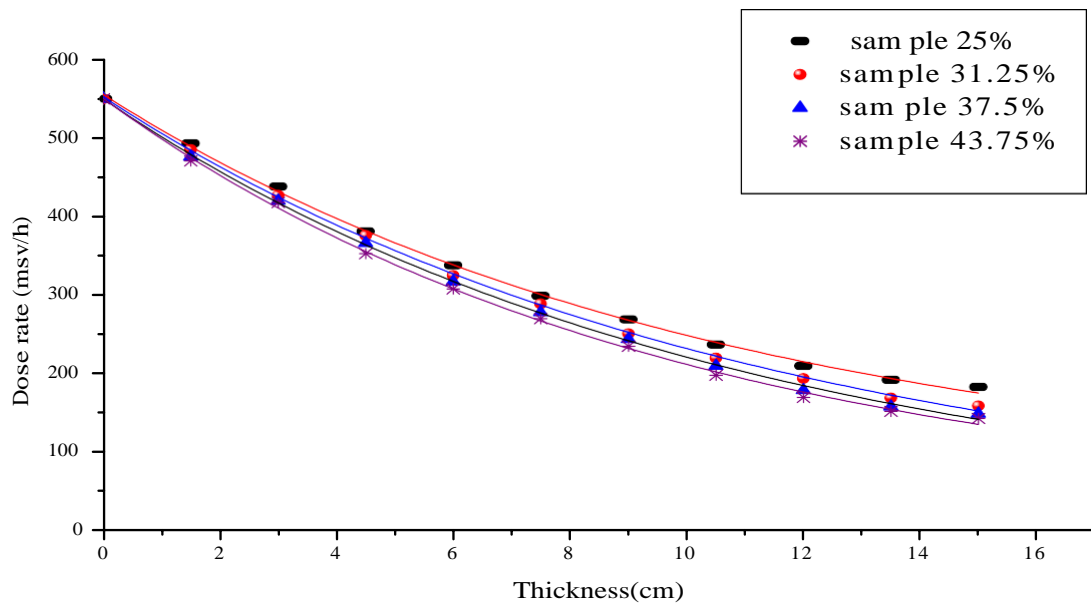
Fig (10): Fitting exponential curve for gamma attenuation by shields for samples of concentration (25%, 31.25%, 37.5%, and 43.75%).
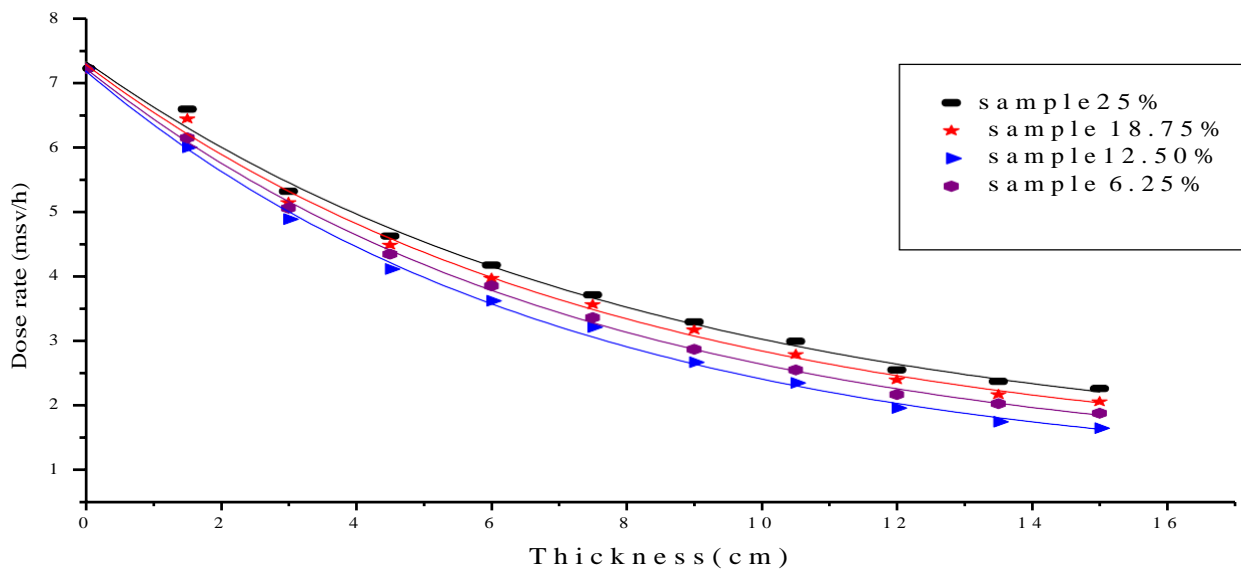
Fig (11): Fitting exponential curve for neutron attenuation by shields by law concentration of polyethylene (25%, 18.75%,12.5%,6.25%, and 50%Borax)
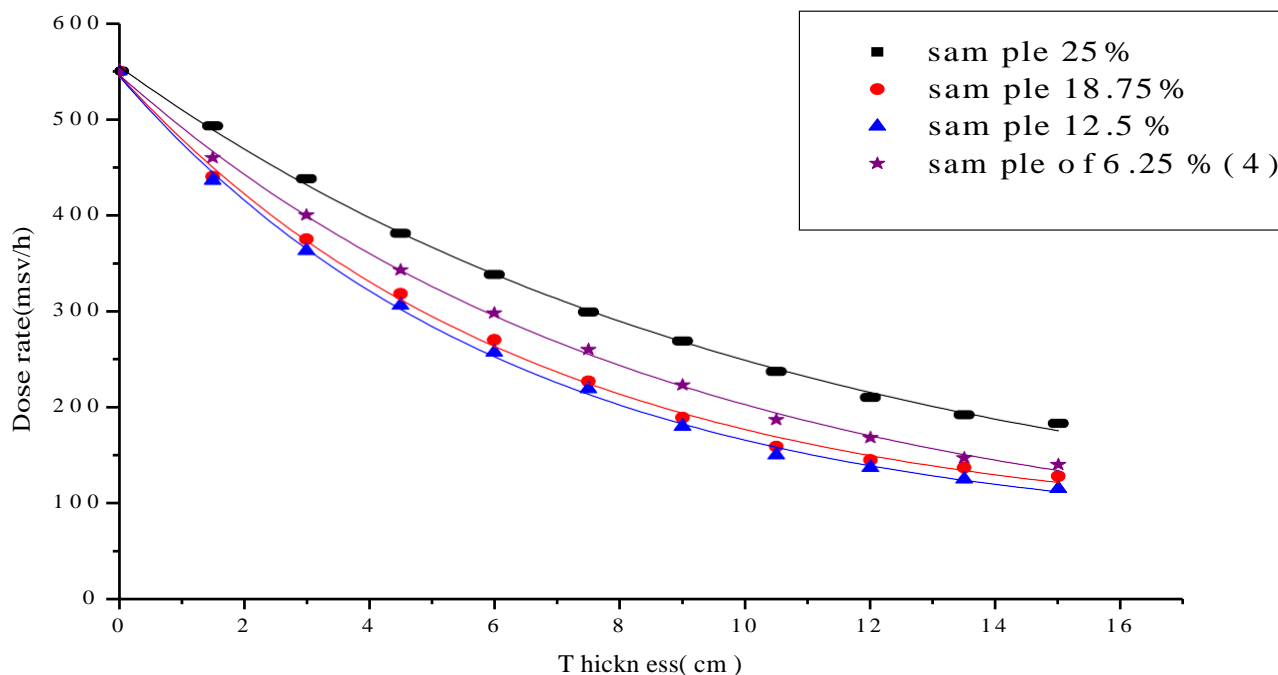
Fig (12): Fitting exponential curve for gamma attenuation by shields with law concentration of polyethylene (25%, 18.75%, 12.5%, and 6.25%)

Table (1):
The values of linear attenuation coefficient (μ) of shielding for neutron and gamma rays.

Samples	Linear attenuation coefficient $\mu(cm^{-1})$ for neutron	Linear attenuation coefficient $\mu(cm^{-1})$ for gamma
Sample 25%	0.07993 + E0.003	0.0767+ E0.00178
Sample 31.25 %	0.08352 + E0.0028	0.0856 + E0.00124
Sample 37.50 %	0.07664 +E0.0029	0.0901 +E0.00147
Sample 43.75%	0.07525 + E0.002	0.0932 + E0.00186
Sample 18.75 %	0.08501 + E0.00279	0.1003 + E0.00469
Sample 12.50 %	0.0994 +E0.00292	0.10623 +E0.00431
Sample 6.25 %	0.09088 + E0.0296	0.08577 + E0.00383

Table (2): The values of half value layer of shielding for neutron and gamma rays.

Samples	Half value layer HVL (x½) for neutron	Half value layer (x½) for gamma
Sample 25%	8.6701	9.9255
Sample 31.25 %	8.2974	8.4802
Sample 37.50 %	9.0423	9.4055
Sample 43.75%	9.2093	10.6681
Sample 18.75 %	8.1519	6.9093
Sample 12.50 %	6.9718	6.5236
Sample 6.25 %	7.6254	8.0797

Table (3): Fitting exponential for neutron and gamma attenuation curve

Samples	Fitting constant (t)for neutron $y = A1*exp(-x/t1) + y0$	Fitting constant (t)for gamma $y = A1*exp(-x/t1) + y0$
Sample 25%	8.12216+E0.87912	10.0599+E0.695
Sample 31.25 %	7.85265 + E0.49766	11.0974 + E0.521
Sample 37.50 %	8.63335 + E 1.12386	10.681+ E 0.542
Sample 43.75%	11 + E1.70502	9.810 + E0.588
Sample 18.75 %	7.77774 + E0.73082	6.58577 + E0.38166
Sample 12.50 %	7.0737 + E0.41684	6.32111 + E0.41684
Sample 6.25 %	7.40628 + E0.36385	8.542 + E0.4264

	Materials				
HDPE	Borax	Cement	H$_2$o	Sand	
Macroscopic cross section Σ_s(Scattering) cm^{-1}	3.275	1.636	132.696	3.953	
Macroscopic cross section Σ_a(absorption) cm^{-1}	0.027	10.886	14.039	0.0223	
Average logarithmic energy Decrementξ	1.358	3.064	0.542	1.32	
Slowing-Down power Sdp	3.727	5.013	71.85	3.0721	
Moderating Ratio mr	138.037	0.221	5.118	137.76	

1- Macroscopic cross section(Σ): it's interpreted as the rate of interactions per unit volume per unit neutron flux, given from;

$$\Sigma = N_o \sigma$$

Where N_o is the number of nuclei per cm^3 and σ is cross section per nucleus.

2- Average Logarithmic Energy Decrement(ξ) : it's the average change in Log E(energy) between two successive collision, given from this relation ;

$$\xi = \frac{\square}{\square\ \square/\square}$$

Where A is the atomic mass number.

3- Slow-down (Sdp):

$$Sdp = \xi\ \Sigma_s = \xi\ N_o\ \sigma_s$$

4- Moderating ratio (mr):

$$mr = \frac{\square\square\square}{\square\square}$$

Σ_s is the scattering cross section
Σ_a is the absorptioncross section

Volume fraction of material that used for the shielding:

Sample	Volume fraction of Polyethylene	Volume fraction of Borax	Volume fraction of Cement	Volume fraction of Sand
25 %	0.36	0.20	0.24	0.20
31.25%	0.43	0.14	0.23	0.19
37.5%	0.50	0.09	0.22	0.19
43.75%	0.56	0.04	0.22	0.18
18.75	0.28	0.24	0.25	0.21
12.5%	0.20	0.32	0.26	0.22
6.25%	0.10	0.39	0.28	0.23

V: is the volume fraction.

Conclusion

From measured and calculated results for different concentrations of composites, it can be concluded that:

(1) The flux intensity of the neutron and gamma rays decreases with increasing the thickness of the composites for all samples with different concentrations.

(2) The composites (S_6) were found to be the most effective attenuator for fast neutron and gamma rays; it attenuates 80 % of radiation. Also a 6.9 cm thick of the composite (HDPY, BX, cement and sand of concentration 12.5%, 37.5%, 25% and 25% respectively) reduced the dose equivalent rate of radiation to its half value.

(3) From the theoretical calculation of macroscopic cross section, Slowing-down power and moderating ratio showed a satisfactory agreement between the measured and calculated values.

References

1- Dyson Norman, "Radiation Physics with Applications in Medicine and Biology (Ellis Horwood series in physics & its applications)", Published by Ellis HorwoodLtd , Publisher(1993).

2- Moss, R. L.;   Stecher-Rasmussen, F.;   Rassow, J.;   Morrissey, J.; Voorbraak, W.; Verbakel, W.; Appelman, K.; Daquino, G. G.; Muzi, L.; Wittig, A.; Bourhis-Martin, E.; Sauerwein, W., "Procedural and practical applications of radiation measurements for BNCT at the HFR Petten", Nuclear Instruments and Methods in Physics Research Section B, Volume 213, (2004) p. 633-636.

3- A. Edward Profio. "Radiation Shielding and Dosimetry", John Wiley & Sons, Inc., New York (1979).547.

4- S. Glasstone and A. Sesonske, "Nuclear Reactor Engineering", third ed. CBS Publishers &Distributors,Shahdara, Delhi, India, (1986).

5- S.J. Park , J.G. Jang , H.K. Lee, "Computational investigation of the neutron shielding and activation characteristics of borated concrete with polyethylene aggregate"Journal of Nuclear Materials 452(s 1–3) (2014) 205–211.

6- M.H. Kharita, S. Yousef, M. AlNassar, " Review on the addition of boron compounds to radiation shielding concrete" Progress in Nuclear Energy, Volume 53, Issue 2, (2011) 207–211.

7- Katz, H.S., Milewski, J.V., "Handbook of Filler for Plastics", Van Nostrand Reinhold, New York, (1987).

8- S. E. Liverhant, "Elementary introduction to nuclear reactor physics", (1960).

9- Kurudirek, M., Buyukyıldız, M. and O. zdemir, Y. Effective atomic number study of various alloys for total photon interaction in the energy region of 1 keV–100 GeV. Nucl. Instrum. Methods Phys. Res. A 613 (2010) 251–256.

10- Akkurt, I., Akyıldırım, H., Mavi, B., Kilincarslan, S., Basyigit, C., Photon attenuation coefficients of concrete includes barite in different rate. Ann. Nucl. Energy 37, (2010) 910–914.

11- Damla D., Cevik U., Kobya A.I., Celik A., Celik N., Van Grieken R., Radiation dose estimation and mass attenuation coefficients of cement samples used in Turkey, Journal of Hazardous Materials 176, (2010) 644-649.

12- Ibrahim Turkmen , YukselOzdemir, Murat Kurudirek, FarukDemir, OnderSimsek, RamazanDemirbog, "Calculation of radiation attenuation coefficients in Portland cements mixed with silica fume, blast furnace slag and natural zeolite", Annals of Nuclear Energy 35(10): (2008) 1937-1943.

13- M. F. Kaplan, "Concrete radiation shielding: nuclear physics, concrete properties, design and construction" Longman Scientific & Technical, (1989) Technology & Engineering.

14- E.P. Blizard and L.S. Abbott, "Reactor Handbook", vol. III, Part B, Shielding. Interscience, New York (1962).

دراسة تأثير أشعة جاما والنيوترونات السريعة على بعض المواد الخرسانية المستخدمة كدروع واقية

علي محمد لضان – محمد طاقر – زيان شاهين – نادية هلال – نسرين اراغب

ملخص البحث

من سلسلة من الدراسات العملية النظرية لنوع جديد من الدروع الواقية من المصادر المشعة في هذه الدراسة, تم تبنين خامات محلية والتي يمكن استخدامها كمادة ضد أشعة جاما والنيوترونات السريعة في المجالات المختلفة. وتم عمل سبع خلطات بنسب مختلفة من الزيبارين والخواص وأشعة جاما والنيوترونات. وذلك بسبب خواصها الأيزينيان عال من الكتلة من مخازن الملوان والاسمنت الرمل. وركيزات مختلفة للعناصر الخاصة بصورة متجانسة مع كمية مناسبة من الإيماء حتى كون على شكل عجينة ثم يوضع تحت ظل لفجن تكرات وقطر (20 1.5*20 سم) وهي أقراص مربعة بمساحة (20 سم على لمعدل العادية الجوية الظروف ظل تحت, ثم الخلطات هذه الخاصة ثم اردنا معاملات لكل خطن, سواء 24 ساعة. وتم عمل الاختبارات الخاصة بهذه الخلطات, ثم اردنا معاملات لكل خطن, سواء 24 ساعة. 60 وذلك خلال الاجماع من مصدر كوبالت النيوترونات السريعة من مصدر امريسيوم وبريليوم 241 الضافة إلى ألفا. وبنسبة تازكرنا المخلنة. مخلنة السمك ذات تأثير وبتركيزات مختلفة تم اجراء العملية اردنا بنظرية للأشعة, حيث أن المخلنة تازكرنا مخلنة ذات السمك بنسبة الكثافة النيوترونين بالنسبة لأشعة جاما معاملات الكتلين, وسمك كمخلنة الخيط, وسمك الخاص الامعال للأشعة جاما بالنسبة الكثافة النيوترونين بالحساب معاملات الخلطة المكونة من. وبهمرة القزرائر الدراسة العملية بالنظرية إلى الوصول إن إلى 6.5 سم من الخلطة المكونة. التشيل. وكذلك معامل
د ئ بالنسبة % 25 , 25% , 37.5% , 12.5% تركيز عند لمرلون والاسمنت والبرواكس و الإيبين و الأبوالي النيوترونات لعرض أعلى درع هو التركيز ان ذاك هذا أبدأ تلك. وعند أقيمة للأشعاع إلى الكثائية الكمية الجرعة لمعدل خفضت تضمن أشعة جاما.

ASSESSMENT OF ACUTE REACTIONS AS RADIATION PROTECTION TOOL FOR PATIENTS TREATED WITH RADIOTHERAPY

GOURAV KUMAR JAIN

Department of Radiological Physics, SMS Medical College & Hospital

Jaipur, India

Email: gourav108@gmail.com

ARUN CHOUGULE

Department of Radiological Physics, SMS Medical College & Hospital

Jaipur, India

Abstract

The acute reactions are significant problem for cancer patients treated with radiotherapy. The objective of present study is to assess the acute skin and mucositis reactions in head and necksquamous cell carcinoma (HNSCC) patients. Acute reactions were studied in 50 advanced HNSCC patients undergoing external beam radiotherapy. All the patients received concurrent chemotherapy with conventional fractionated radical radiotherapy. The acute reactions were studied using a grade score system prepared with the analysis of RTOG, WHO, NCI CTC(v2.0) and MASCC/ ISOO toxicity evaluation guidelines. The patient age participated in study ranged from 20 to 75 years. In the present study skin toxicity starts to appear above the cumulative dose of 12 Gy (6 fractions). At the completion of the treatment ninety five percent of patients developed grade II skin toxicity. However, grade I mucositis toxicity observed in all the patients having less than 15 fractions of radiotherapy. Thereafter grade II mucositis was seen in ninety percent of the patients. Acute toxicities are significant problem in

HNC patients treated with radiotherapy. These toxicities affect quality of life. However, the acute toxicities analysis with delivered dose can be used to ensure patient radiation protection in radiotherapy.

1. INTRODUCTION

Carcinoma of Head and Neck accounts for around 30% of all cancers in male in India. External Beam Radiotherapy with chemotherapy has long been an important modality for the treatment of head and neck squamous cell carcinoma (HNSCC) and achieves high rates of local tumor control.[1] The main objective of present study is to assess the acute skin and mucosal reactions in advanced HNC patients treated with concurrent chemotherapy and radiotherapy.

2. MATIRIALS & METHODS

The acute skin and mucosal reactions were observed in 50 advanced HNSCC patients randomly selected in study having inoperable tumors. The study design was a prospective, single blinded study. All the patients received concurrent chemotherapy with conventional fractionated radical radiotherapy. The acute reactions were observed using a grade score system prepared with the analysis of Radiation Therapy Oncology Group (RTOG)[2], World Health Organisation (WHO)[3], National Cancer Institute (NCI) Common Toxicity Criteria (CTC) Version 2.0 (CTC, v2.0)[4] and the Multinational Association of Supportive Care in Cancer and the International Society of Oral Oncology (MASCC/ISOO)[5-7] toxicity evaluation guidelines. The acute reactions were categorized into 5 broad grades. The scoring grades were identified as grade 0, grade 1, grade 2, grade 3 and grade 4. The patients participated in the study were observed after each 5 fractions during radiotherapy.

3. RESULTS & DISSCUSSION

Eighty eight percent male patients were present in study age ranging from 20 to 75 years with an average age of 52 years in which 95% of men had history of either smoking or tobacco consumption or both for at least one year in their lifetime. The remaining 12% were women in which 16% had either this history. The equivalent field size (EFS) for radiotherapy treatment ranged from 9.0 to 15.5 cm^2 with average EFS 12.8 cm^2. None of the patients reported skin toxicity at cumulative dose less than 12 Gy (6 fractions). The worse skin toxicity seen in ninety five percent of patients was grade II dermatitis. The grade I mucositis was observed in all the patients receiving less than 15 fractions of conventional radiotherapy. Thereafter grade II mucositis was seen in ninety

percent of the patients. Very few of the patients in the study had experienced grade III or IV reaction. The findings of the present study suggested that there is a strong correlation between acute toxicities with delivered dose to patient. The acute reactions were observed as the qualitative indicator of the radiation protection to patient during head and neck radiotherapy treatment.

4. CONCLUSIONS

Acute mucosal and skin toxicity is a significant problem in HNSCC patients treated with radiotherapy with concurrent chemotherapy and it increases with increase in cumulative dose. Both these toxicities cause various symptoms that affect quality of life. They often become a barrier to successful delivery of complete treatment within a scheduled time. The assessment of acute reactions can be used to ensure patient radiation protection in radiotherapy.

REFERENCES

[1] SRIVASTAVA, V.K., Consensus Document for the Management of Buccal Mucosa Cancer, Indian Council of Medical Research, New Delhi, 2014.

[2] RTOG/EORTC Late Radiation Morbidity Scoring Schema (2017)

https://www.rtog.org/ResearchAssociates/AdverseEventReporting/RTOGEORTCLateRadiationMorbidityScoringSchema.aspx
[3] World Health Organization. Handbook for reporting results of cancer treatment. World Health Organization, Geneva, Switzerland, 1979, 15–22.

[4] Common Toxicity Criteria Manual, Common Toxicity Criteria, Version 2.0 (CTC, v2.0), National Cancer Institute (NCI), 1999.

[5] Clinical Guidelines Implementation Toolkit. European Oncology Nursing Society, 2005.

[6] Sonis, S.T., Elting, L.S., Keefe, D., et al. Perspectives on cancer therapy-induced mucosal injury: pathogenesis, measurement, epidemiology, and consequences for patients, Cancer 100 (Suppl) (2004) 1995–2025.

[7] Rubenstein, E.B., Peterson, D.E., Schubert, M., et al. Clinical practice guidelines for the prevention and treatment of cancer therapy-induced oral and gastrointestinal mucositis, Cancer 100 (9 Suppl) (2004) 2026–2046.

MEGAVOLTAGE COMPUTED TOMOGRAPHY (MVCT) DOSE ASSESSMENT AT DIFFERENT DEPTH

Sibel Karaca
TC Sağlık Bakanlığı,Erzurum
Bölge Eğitim ve Araştırma
Hastanesi
Erzurum, Turkey
Email: sibeltuzlaci@gmail.com

Hamit Başaran
TC Sağlık Bakanlığı,Erzurum
Bölge Eğitim ve Araştırma
Hastanesi
Erzurum, Turkey

Abstract

The aim of the study is to evaluate the point doses measured by different parameters at various depths with MVCT in the TomoTherapy Hi- Art (HT) treatment unit. HT is works in two modes: visual modes and therapy modes. The user can choose the scan length and image pitch value. The system has fine, normal and course pitch values. When the same volume is scanned during gentry rotation, the scan times of fine, normal, and course modes are different from each other. Cheese Phantom is used to evaluate the point doses. The measured values ranged from 0.64 to 2.67 cGy with an average dose of 1.40 cGy. The lowest MVCT dose is found when scanned 7 slices with a depth of 20 cm, 51 seconds; the highest MVCT dose is found when scanned 17 slice with a depth of 15 cm, 101 seconds. While when at course mode, high depth and low slices show that the dose values drop. The imaging in the IGRT method can be used before every therapy and can be used more than once if necessary. This is why while conducting the method, it is important that the best mode should be used in order to prevent patients from using unnecessary doses.

INTRODUCTION

In recent years, many radiotherapy devices also have image-guided radiotherapy (IGRT) [1,2]. Tomotherapy Hi-Art (Accuray Inc., Sunnyvale, CA) (HT) is an image-guided, intensity modulated radiation therapy (IG-IMRT) system that can obtain a megavoltage computed tomography (MVCT) scan prior to each treatment to minimize daily setup variations [3]. The HT system uses megavoltage computed tomography (MVCT) images for positioning [4]. MVCT is a sensitive imaging tool that allows anatomical details to be seen [5]. Daily MVCT datasets are registered to the treatment planning kilovoltage CT (kVCT) dataset using automated and/or manual image-fusion tools [3] The aim of the study is to evaluate the point doses measured by different parameters at various depths with MVCT in the TomoTherapy Hi - Art (HT) treatment unit.

Method

HT is a top-level therapy device with IGRT. The machine works in two modes: visual mode and therapy mode. In the imaging mode, the 6 MV therapy beam is set to 3.5 MV with a lower acceleration potential. During MVCT, the system turns all MLCs on. Scheduling in viewing mode. It is aimed to register MVCT images taken daily with kVCT images. Tomotherapy MVCT presents two parameters to the user in imaging mode. The first is the scan length selection parameter. The desired volume can be scanned in this way. The increase in the scan size also means that the scan time increases. Another parameter is to select the image pitch value. Another parameter is to select the image pitch value. This value means the length of the nominal slice thickness. The system offers 3 different pitch values. These are called Fine (2mm), Normal (4mm) and Coarse (6mm). When the same volume is scanned during gentry rotation, fine, normal, and course modes are different from each other during the scan.

In the study, point measurements were made at various depths using the Exradin A1SL ion chamber (Standard Imaging, Middleton, WI) connected to TomoElectrometer with Tomotherapy 'cheese' phantom (Gammex RMI, Middleton, WI). The cheese is a cylinder of 15 cm in radius and 15 cm in length, with a linear series of holes that extends on one face of the phantom for ionization chamber measurements. 0.057 cm3 Exradin A1SL ion chambers used in measurements. Different thickness boluses have been used for different depth measurements The values read from the electrometer are recorded as pico cloumb (PC). The values calculated according to the required fixed values, the pressure and the temperature of the environment are indicated on the table 1. And fugure 1. in terms of centi Gray (cGy).

Results
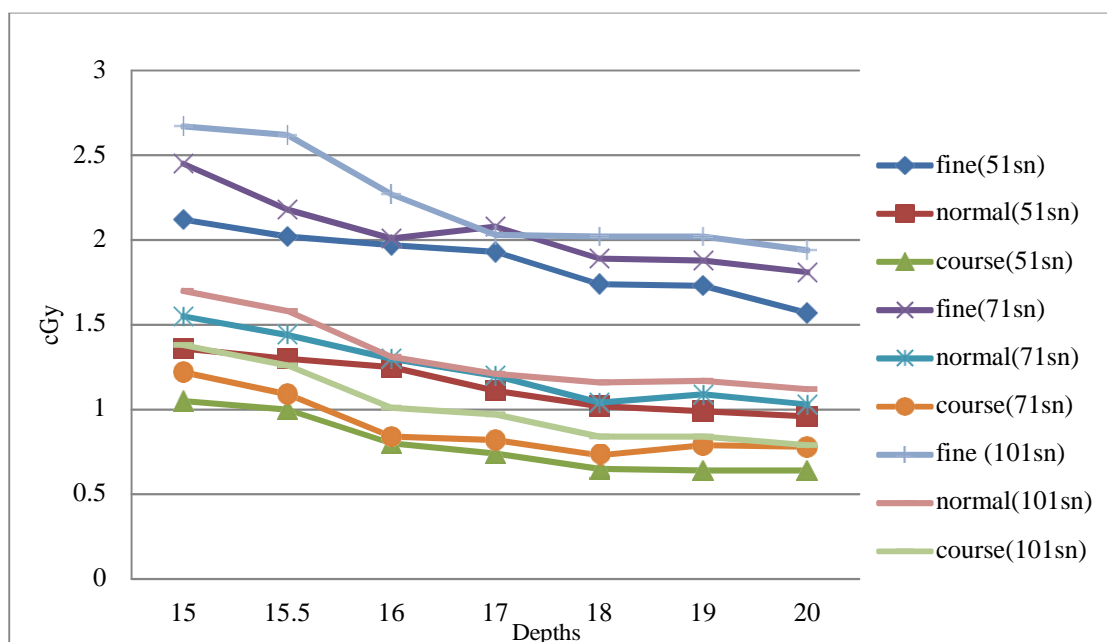
FIG 1. Chart showing measurement results at different depths and in different modes

Table 1. MVCT dose values obtained at different depths using Cheese Phantom

Depth (cm)	Scan Mode	Scan Time (sn)	Number of slices to be scanned	Scan length (cm)	Measured Value pC	Calculate value cGy
15	Fine	51	7	1,4	30,90	2,12
	Fine	71	11	2,2	35,71	2,45
	Fine	101	17	3,4	38,95	2,67
	Normal	51	7	2.8	19,95	1,36
	Normal	71	11	4,4	22,59	1,55
	Normal	101	17	6,8	24,91	1,70
	Course	51	7	4,2	15,39	1,00
	Course	71	11	6,6	17,77	1,22
	Course	101	17	10,2	20,12	1,38
15,5	Fine	51	7	1,4	29,40	2,02
	Fine	71	11	2,2	31,80	2,18
	Fine	101	17	3,4	38,30	2,62
	Normal	51	7	2.8	19,06	1,30
	Normal	71	11	4,4	21,05	1,44
	Normal	101	17	6,8	23,09	1,58
	Course	51	7	4,2	14,65	1,00
	Course	71	11	6,6	15,86	1,09
	Course	101	17	10,2	18,43	1,26
16	Fine	51	7	1,4	28,73	1,97
	Fine	71	11	2,2	30,63	2,01
	Fine	101	17	3,4	33,25	2,27
	Normal	51	7	2.8	18,21	1,25
	Normal	71	11	4,4	19,02	1,30
	Normal	101	17	6,8	19,15	1,31
	Course	51	7	4,2	11,73	0,80
	Course	71	11	6,6	12,26	0,84
	Course	101	17	10,2	14,76	1,01
17	Fine	51	7	1,4	28,16	1,93
	Fine	71	11	2,2	30,35	2,08
	Fine	101	17	3,4	29,61	2,03
	Normal	51	7	2.8	16,23	1,11
	Normal	71	11	4,4	17,50	1,20
	Normal	101	17	6,8	17,56	1,21
	Course	51	7	4,2	10,83	0,74
	Course	71	11	6,6	12,08	0,82
	Course	101	17	10,2	14,17	0,97
18	Fine	51	7	1,4	25,59	1,74
	Fine	71	11	2,2	27,66	1,89
	Fine	101	17	3,4	29,61	2,02
	Normal	51	7	2.8	13,94	1,02
	Normal	71	11	4,4	15,23	1,04
	Normal	101	17	6,8	17,02	1,16
	Course	51	7	4,2	9,59	0,65
	Course	71	11	6,6	10,64	0,73
	Course	101	17	10,2	12,33	0,84
19	Fine	51	7	1,4	25,39	1,73
	Fine	71	11	2,2	27,52	1,88
	Fine	101	17	3,4	29,56	2,02
	Normal	51	7	2.8	14,58	0,99
	Normal	71	11	4,4	15,93	1,09
	Normal	101	17	6,8	17,05	1,17
	Course	51	7	4,2	9,47	0,64
	Course	71	11	6,6	11,66	0,79
	Course	101	17	10,2	12,35	0,84
20	Fine	51	7	1,4	22,96	1,57
	Fine	71	11	2,2	26,36	1,81
	Fine	101	17	3,4	28,32	1,94
	Normal	51	7	2.8	13,97	0,96
	Normal	71	11	4,4	15,06	1,03
	Normal	101	17	6,8	16,42	1,12
	Course	51	7	4,2	9,46	0,64
	Course	71	11	6,6	11,36	0,78
	Course	101	17	10,2	11,43	0,79

The measured values ranged from 0.64 to 2.67 cGy with an average dose of 1.40 cGy. The lowest MVCT dose is found when scanned 7 slices with a depth of 20cm, 51 seconds with a result of 0.64 cGy. The highest MVCT dose is found when scanned 17 slice with a depth of 15 cm, 101 seconds with a result of 2.67 cGy.

Discussions and Conclusions

Solid water phantom (or cheese phantom) with multiple ionization chambers is commonly used in HT dose measurement [6]. In this study, Cheese phantom was used for MVCT dose measurements. The patient's dose is measured as is 1.5-3.0 cGy / image in MVCT. The dose to the patient is 1.5-3.0 cGy/image [7]. In this study, measurements were between 0.64 and 2.67 cGy using different parameters.

The dose taken during the MVCT image is much higher than the kVCT. The research conducts that once the doses are analysed, it can see that the measured values are highest when in fine mode with low depth and high slice. While when at course mode, high depth and low slices show that the dose values drop. The imaging in the IGRT method can be used before every therapy and can be used more than once if necessary. This is why while conducting the method, it is important that the best mode should be used in order to prevent patients from using unnecessary doses.

REFERENCES

[1] Yadav P, Tolakanahalli R, Rong Y, Paliwal BR.The effect and stability of MVCT images on adaptive TomoTherapy. J Appl Clin Med Phys. 2;11(4):3229. (2010)

[2] L. Meeks,Joseph F. Harmon Jr.et al. Performance characterization of megavoltage computed tomography imaging on a helical tomotherapy unit. Med Phys, 32:, (8), 2673–2681. (2005)

[3] Goddu S Murty, Mutic Sasa, et al. Enhanced efficiency in helical tomotherapy quality assurance using a custom-designed water- equivalent phantom. Med. Biol. 54 ,5663–5674. (2009)

[4] Crop F, Bernard A, Reynaert N. Improving dose calculations on tomotherapy MVCT images Journal of Applied Clinical Medical Physics. 13(6) 241–253 (2012)

[5] Yartsev S, Kron T, Van Dyk J. Tomotherapy as a tool in image-guided radiation therapy (IGRT): current clinical experience and outcomes Biomed Imaging Interv J 3(1):e17 .(2007)

[6] J. BalogClinical helical tomotherapy commissioning dosimetry, Med. Phys. 30(12) 3097,(2003)

[7] Amanda Jean Sprague Dyess. Patient dose verification for image-guided radiation therapy using a deformable registration tool Master of Science Medical Physics Unit McGill University Montreal,(2012)

Trends in radiation protection of patients in modern radiotherapy

Katia Sergieva[1], Petya Kostova[2], Victor Zlatkov[3]
[1]Queen Giovanna University Hospital, Sofia, Bulgaria
[2]University Oncology Hospital, Sofia, Bulgaria
[3]University Obstetrics and Gynecology Hospital "Maichin Dom", Sofia, Bulgaria

E-mail address: sergievakm@abv.bg

Abstract.

Modern radiotherapy reached a very high degree of complexity and sophistication in the recent years and expected to represent an added value for the cancer patients in terms of clinical outcomes and radiation protection. New equipment in imaging and radiotherapy has been successfully put in our clinical practice and radiation therapy has improved considerably. The significant change has been achieved in treatment of patients with gynecological cancer in terms of clinical outcome and improved radiation protection. In Bulgaria cervical cancer is still a medical and social problem. The treatment of cervical cancer is complex and requires a multidisciplinary approach. In our hospital the patients for cervical cancer are treated with two 360° coplanar 6MV VMAT arcs, following manufacturer instructions. The treatment technique has offered precise dose confirmation to this very complicated in geometrical terms target volume. In this way the radiation dose distributions are shaped to the target with a steep fall in the dose to the neighboring normal tissues. The newest technologies undoubtedly lead to constant trends in the enhancing of the basic principles of radiation protection - justification and optimization, allowing us to treat more cancer patients efficiently, effectively and safely.

1. Introduction

Five years after the Bonn Conference is the time to present the progress in our daily clinical practice triggered by the joint statement of IAEA and WHO entitled: "**Bonn Call for Action to improve radiation protection in medicine in the next decade".** It identifies the main action which should be considered to be essential for the strengthen of radiation protection since the increasing use of ionizing radiation and to improve the balance between the benefits and risks for the human health.

The purpose is to present the authors' perspective on strengthened manufacturers' contribution leading to enhancement of basic principles of radiation protection: justification and optimization in modern radiotherapy, since it is the technologically and computer based medical specialty and our achieved change in clinical practice for radiation therapy (RT) of patients with gynecological cancer.

Radiation protection in medicine has unique aspects and is an essential element of medical practice. [1] Radiotherapy has been driven by constant technological advances since the discovery of X-rays in 1895. Advanced radiotherapy technologies have been continuously improved and refined with the principal aim of improving treatment outcome by means of dose distributions which conform more strictly to clinical target volumes. A highly conformal dose distribution allows for dose escalation in the target volume without increasing the radiation dose to neighboring normal tissues, and for a reduction in radiation dose to normal tissues without decreasing the dose to the target. [2] Modern radiotherapy reached a very high degree of complexity and sophistication in the recent years and expected to represent an added value for the cancer patients in terms of clinical outcomes and improved radiation protection.

2. Material and methods

Modern radiotherapy is a very complex process of treatment planning and treatment delivery. Steps in the process include patient identification, preparation of a treatment directive, patient positioning and immobilization for planning and treatment, volume delineation from patient images, treatment planning and review, and treatment delivery. [3] It based on different technologies in imaging, in dose delivering, in dose measurements and in treatment assessment. The cutting-edge technologies are in the base of observed enhance trends in improved radiation protection of cancer patients receiving modern radiotherapy. The following achievements are supported the effective and safety management of cancer patients.

In imaging: High quality imaging has a huge contribution in cancer screening and radiotherapy. Technology improvements in current generation computer tomography systems (CT) are realized in reducing the dose, improved image quality and speed of investigation. The latest iterative reconstruction software in combination with the latest scanner detector technology allowing to perform CT with doses of less than 1 mSv. In the last 12 months, several CT vendors have introduced new systems with the latest in dose reduction hardware and software. [4] Several manufacturers released software updates to integrate of positron emission/computed tomography (PET/CT) images into radiation therapy planning. PET/MRI Scanners align the features of MR imaging — such as soft tissue contrast, diffusion-weighted imaging and dynamic contrast-enhanced imaging with the PET provided quantitative physiologic and metabolic data. Currently, radiation oncology is an application gained major value from double

modality synergetic images for more precisely delineation of location of tumors and therefore to individualize treatment for each cancer patient.

In Treatment Planning Systems (TPSs): TPSs are at the heart of modern radiotherapy and the key to improved patient outcomes and safety. Technological advances in TPS provides: Significant speed enhancements (calculation speeds up to four times faster than in previous versions); Increasing Automation – giving capabilities such as auto-segmentation, dose optimization and auto planning help healthcare professionals to focus on the critical aspects of care; Robust optimization based on 4-D computed tomography (CT) images. Unlimited patient data storage (Knowledge-sharing Platforms) helps clinicians to share and learn from one another. [5]

In Image Guided RT (To see what we treat): Imaging plays an important role in providing the precise guidance during the radiation treatment. The latest mode of MRI Guided Radiation Therapy combines two technologies of MRI scanner and a linear accelerator in a single system. This allowing radiotherapy to be adjusted in real time and delivered more accurately and effectively even to moving tumors than ever before. MRI solves both of the primary issues with CBCT — poor soft tissue contrast and difficulty capturing moving organs — while delivering no extra radiation dose to the patient.

In adaptive RT (ART): Once it is possible to "see what we treat", the next step is to perform ART. The huge impact has a graphics processing units (CPUs) which can run accurate Monte Carlo based VMAT dose calculations in less than 40 s – opening up the possibility of dose recalculation while the patient is on the table [6] and to create the adapt treatment plan according to the patient specific changes, that are unaccounted in the initial plan.

In dosimetry systems: The precise dosimetry systems and extensive QA programs are cornerstone of the safe and effective radiation cancer treatment. World's leading manufacturers providing a new generation dosimetry systems with several attractive features for radiation dosimetry including real-time display of dose & dose-rate, fully automated in vivo dose monitoring requiring no user interaction with high resolution, minimal perturbation, high dynamic range of dose measurements, reliability and robustness.

Most of the above mentioned technologies such as CT, PET/CT, MRI and Multimodality Linacs have been successfully put in our routine clinical practice and RT has improved considerably. The significant change has been achieved in radiotherapy of patients with gynecological cancer in terms of clinical outcome and improved radiation protection.

In Bulgaria cervical cancer is still a medical and social problem. It ranks second among gynecological tumors in the period 1993-2002, while in 2011 it is the fourth most common cancer in women and accounts for 7.2% of all cancer cases. The five year relative survival for cervical cancer in Bulgaria is 54.8%, comparing with European average – 65.4%. [7, 8] Cervical cancer management varies depending on the International Federation of Gynecology and Obstetrics (FIGO) stage. Modern radiotherapy is a highly effective and curative treatment for patients with invasive cervical cancer, and it is the standard of care for locally advanced disease. [9] All patients with cervical cancer were treated using a 4-field box technique (See Fig.1. Left) only five years ago. Currently, we are using multiple modern imaging modalities - CT, MRI, PET/CT for delineation of target volume and adjacent normal organs-at-risk (OAR). All patients were CT-scanned supine with both full and empty bladder to take into account the internal organ variation with bladder filling status. Clinical Target Volume (CTV) was contoured in accordance with Lim et al. [10]. OARs were defined as the rectum, bladder, bowel and femoral heads. All patients for cervical cancer are treated with two 360º coplanar 6MV VMAT arcs (Varian RapidArc®), following manufacturer instructions (See Fig.1. Right).

FIG. 1. Left – 4-field box technique; Right – VMAT technique

3. Results

The newest treatment technique has offered precise dose confirmation to this very complicated in geometrical terms target volume. In this way the radiation dose distributions are shaped to the target with a steep fall in the dose to the neighboring normal tissues (See Fig.1. Right), while the conventional 4FB technique resulted

in a bath of high-dose radiation to a large volume (See Fig.1.Left). High precision in delivery is achieved by image guided radiotherapy (IGRT), where the target is imaged immediately before treatment with the patient in the treatment position. The dosimetric advantages in organ sparing has maintained excellent long term cure rates and reducing GI, GU and hematologic toxicity, especially in patients treated with concurrent chemotherapy [11]. In terms of radiation protection it means that we are ensuring, that exposures to target volumes are individually planned taking into account that doses to non-target volumes and tisues will be as low as reasonably achievable (ALARA) and cosistent with the intended radiotherapeutic purpose.

4. Discussion

The need of effective modern radiotherapy treatment is growing as the global cancer epidemic continues to spread. It saves lives, prolongs lives and improves the quality of life. Currently, radiotherapy is widely recognized to be one of the safest areas of modern medicine and errors in radiotherapy are very rare. [12] Patient safety is of the utmost concern to radiation oncologists and safety considerations are woven into all aspects of clinical practice. Technological advances and clinical research over the past few decades have given radiation oncologists the capability to personalize treatments for accurate delivery of radiation dose based on clinical parameters and anatomical information. Two major strategies, acting synergistically, will enable further widening of the therapeutic window of radiation oncology in the era of precision medicine: technology-driven improvement of treatment conformity, including advanced image guidance and particle therapy, and novel biological concepts for personalized treatment, including biomarker-guided prescription, combined treatment modalities and adaptation of treatment during its course. [13]
The following challenges are facing radiation professional community: The imaging doses in modern radiotherapy and secondary cancers should be observed in future. IGRT is a rapidly growing field and imaging is increasingly used in modern radiation therapy. The imaging devices are using ionizing radiation and justification and optimization of protection and safety must be observed. The concomitant doses connected with diagnostic and theraupetic imaging increase. They are becoming nonnegligeblae and must be managed. Innovations in radiotherapy have contributed considerably to increasing the survival rates for several cancer diseases. New radiotherapy techniques deliver higher low dose radiation to large volume of normal tissues and are in debating as more secondary cancer inducers. A secondary cancer after radiotherapy is in important issue that reduces treatment efficiency and should be decreased. [14] The development of new techniques and methods for predicting long term effects from radiation treatment becomes vital in order to confidently introduce new approaches. [15]

5. Conclusion

Modern radiotherapy requires advanced equipment and a reasonable treatment strategy to gain the best clinical outcome moreover, when the vision of European Society for Radiotherapy & Oncology for 2020 is: "Every cancer patient in Europe will have access to state of the art radiation therapy, as part of a multidisciplinary approach where treatment is individualized for the specific patient's cancer, taking account of the patient's personal circumstances".[16] We are doing our best to provide safe and effective radiotherapy, but we know, that we can do better. Times have changed, mostly for the better. Few would be argue with the fact, that the tools with which we operate today are vastly superior and enormously more complex than a few years ago. Advances in technology provide more sophisticated, promising and accurate techniques for targeting malignancies while minimizing normal tissue damage are crucial for patients who treated with radiation therapy. In terms of radiation protection it means that we are doing much more good than harm – overarching justification of medical exposure and we are ensuring that for each patient the exposure of volumes other than the planning target volume is kept as low as reasonably achievable consistent with delivery of the prescribed dose to the planning target volume within the required tolerances (ALARA). [17] The newest technologies undoubtedly lead to constant trends in the enhancing of the basic principles of radiation protection - justification and optimization, allowing us to treat more cancer patients efficiently, effectively and safely.
Finally, authors highly appreciate the long-term efforts and activities of IAEA to improve radiation protection of patients, providing standards, training and guidance, direct technical assistance and building capacity, and awareness.

REFERENCES

[1] Ola Holmberg, Renate Czarwinski, et al. The importance and unique aspects of radiation protection in medicine. European Journal of Radiology 76 (2010) 6 - 10.
[2] Available on: http://www.irpa.net/members/P07.16fp.pdf
[3] Accuracy Requirements and Uncertainties in Radiotherapy. IAEA Human Health Series №31. INTERNATIONAL ATOMIC ENERGY AGENCY, VIENNA, 2016.
[4] Available on: https://www.itnonline.com/content/ct-dose-management
[5] Available on: https://www.itnonline.com/issue/julyaugust-2016
[6] Available on: http://medicalphysicsweb.org/cws/article/opinion/65540

[7] Petya Kostova,Victor Zlatkov, S Danon. Five-year overall survival and prognostic factors in patients with cervical cancer in Bulgaria. Journal of B.U.ON.: official journal of the Balkan Union of Oncology 13 (2008) 363 - 8.

[8] Bulgarian National Cancer Registry, Том XXII, Volume XXII, 2013.

[9] Danielle Rodin, Timothy P. Hanna, Emily Burger, et al. GLOBAL ACCESS TO RADIOTHERAPY FOR CERVICAL CANCER: THE COST OF INACTION, IJRBP 96 (2),2016, S14 - S15.

[10] Karen Lim, M.B.B.S., William Small Jr., M.D., Lorraine Portelance, M.D., et al. Consensus Guidelines for Delineation of Clinical Target Volume for Intensity-Modulated Pelvic Radiotherapy for the Definitive Treatment of Cervix Cancer. IJRBP, 79(2), 2011, 348 - 355.

[11] Ana Fernandez-Ots, Juanita Crook. The role of intensity modulated radiotherapy in gynecological radiotherapy: Present and future. RPOR 18 (2013) 363 - 370.

[12] General guidelines on risk management in external beam radiotherapy, EU, RADIATION PROTECTION N° 181, 2015.

[13] Michael Baumann, Mechthild Krause, Jens Overgaard, et al. Radiation oncology in the era of precision medicine. Nature Reviews Cancer 16, 2016, 234 - 249.

[14] Abdollahi et al.: Radiation protection and secondary cancer prevention. IJCTO 3 (3), 2015, 1 - 9.

[15] Workshop: Risk of secondary cancer following radiotherapy. 8-9 September 2016, Stockholm.
Available on: www.crpr-su.se/smn/Workshop%20Book.pdf

[16] Available on: http://www.estro.org/about/mission-values/vision

[17] Radiation Protection and Safety of Radiation Sources: International Basic Safety Standards, IAEA Safety Standards Series No. GSR Part 3, INTERNATIONAL ATOMIC ENERGY AGENCY, VIENNA, 2014.

REPORT ON THE STATUS OF
QUALITY ASSURANCE OF RADIOTHERAPY
AND RELATED REGULATORY ACTIVITIES IN KOREA

H.I. KIM
Korea Institute of Nuclear Safety
Daejeon, Korea
hikim@kins.re.kr

M.K. KIM
Korea Institute of Nuclear Safety
Daejeon, Korea

M.C. SONG
Korea Institute of Nuclear Safety
Daejeon, Korea

Abstract

Systematic QA of radiotherapy is important to ensure the accuracy of radiotherapy. Therefore, The comprehensive QA program is needed, including the organization as well as treatment machine to maintain a certain level of precision. The paper aims to share the issues related to the quality assurance of medical radiation set out in the Korean law.

1.   INTRODUCTION

Radiotherapy using the high energy radiation in megavolt (MV) units is currently one of the major treatment methods for curing cancer. The goal of radiotherapy is to maximize the probability of controlling the tumor while minimizing the effect on normal tissue near the tumor, because of the property of radiation transmits the dose to the target tumor as passing through the normal tissue. In this regard, radiotherapy technology is rapidly advancing in sophisticated form to deliver the dose to the target locally.

In the mid-1990s, 3D CRT(Three-dimensional Conformal Radiation Therapy) was introduced, IMRT(Intensity Modulated Radiation Therapy) was been started to use in radiotherapy as the imaging and treatment equipment had been developed[1]. In this kind of high-precision radiotherapy, as the treatment planning is more complex than the 2D or 3D CRT while it can be delivered the high dose locally to the tumor volume. Because of this, the errors that can be occurred is increased. Therefore, The comprehensive quality assurance program is needed, including the organization (QA Team) as well as treatment machine to maintain a certain level of precision in radiotherapy[2]. Also, Unexpected accidents in radiotherapy can be occurred by various factors such as lack of education and training of treatment team, inadequacy of quality assurance procedures, scarcity of independent verification by qualified experts, insufficiency of comprehensive management. This is why the establishment of the systematic QA program is important in radiotherapy.

In this regard, the paper aims to share the issues related to the quality assurance of medical radiation statutory in the Korea Nuclear Safety law and activities implemented by regulatory body.

2.   THE KOREA NUCLEAR SAFETY LAW OF QUALITY ASSURANCE IN RADIOTHERAPY

Regarding the use of radiation in the medical field, the current law system in Korea is divided into Medical law of the Ministry of Health and Welfare and the Nuclear Safety law of the Nuclear Safety and Security Commission (NSSC). Relevant facts about using the X-ray generator for the purpose of patient diagnosis is regulated by the Medical law, and the safety regulations related to radiation generators and radioactive isotopes used for other purposes such as research, treatment are covered by Nuclear Safety law. This involves the regulations related radiation treatment machine used in cancer treatment. The contents of procedures and personnel requirements to carry out proper quality assurance are provided in the law: 'The regulations on technical standards about the radiation safety management of the NSSC'. The important thing here is that the "Patient" is an important aspect of the object in the Medical law, but In Nuclear Safety law, "Employee and Environment" is the most important subject. In relation to radiotherapy, the focus of this law is on the process related to deliver the dose prescribed by medical doctor correctly, not on what the prescribed dose of patients is.

The domestic legislation associated with the quality assurance of radiation treatment machine   was enacted as the 'Technical Standard for Radiation Safety Management in Medical Fields' in 2001 by Ministry of Science and Technology No.2001-18. Thereafter, It made amendments on April 1, 2015. It reflected the frequency of use in machine and diversification of radiation treatment machine used in Korea. To put it concretely, Quality assurance requirements such as procedures for each radiation treatment machine, frequency and tolerance was suggested. According to this prescript(The quality management experts in the medical radiation (Article 9)), it is required to report the person performing quality assurance.

There are now five types of radiation treatment machine used in 91 medical centers in Korea. It shows the status of permission for use of each machine in Fig.1.
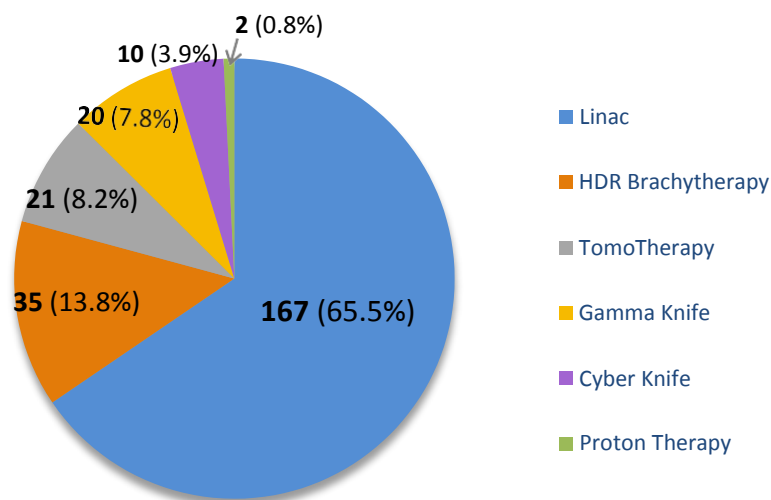
FIG. 1. Number of licensed treatment machine in radiotherapy of Korea. (2017.07)

A linear accelerator, which accounts for about 65.5% of the total of 255 radiation treatment machine, is the majority of those in Korea at present. In case of High- DoseRate(HDR) Brachytherapy, the rate of which is 13.8% (35 machine) and HDR Brachytherapy machine using Ir-192 source takes up most of them. There are only 3 HDR Brachytherapy machine using the Co-60 source. Currently, proton therapy machine are recently introduced to Korea, and that are used in only two medical centers. As it is expected to be increased the use of the proton therapy and heavy ion accelerator in the near future, the importance of quality assurance of those will be emphasized. The recent domestic laws related to the quality assurance of radiation treatment machine, to prevent the accidental exposure in radiotherapy, is divided into the following three categories according to the implementation aspect of the quality assurance program.

2.1.   The responsible for the management of the QA: Qualified expert for QA

The QA of radiotherapy can cause direct radiation accident due to minor error in procedure of QA and operator mistakes. Most of the accidents that occurred in radiotherapy are attributed to human error[2]. Therefore, it is one of the important factors in QA to obtain qualified expert with the capacity to manage the QA in medical center[3]. In Nuclear Safety law in Korea, the center which uses the X-ray generator to the human body for the purpose of treatment has the obligation to maintain and manage the radiation treatment machine in order to deliver the dose of the patient as prescribed dose by the medical doctor. To do this, It states that the expert for QA should be set up as the main body for managing the QA program. The term 'expert for QA' refers to a person who performs the duties under the supervision of a radiologist(medical doctor), has the responsible for the handling of radiation treatment machine, dosimetry, establishment and confirmation of the patient treatment planning. According to the domestic laws and regulations, medical centers designate their own expert for QA and report them to regulatory bodies.

The number of total experts for QA reported from 91 medical centers are 232 person by July 2017. Figure 2 shows the ratio of management experts per radiation treatment machine.
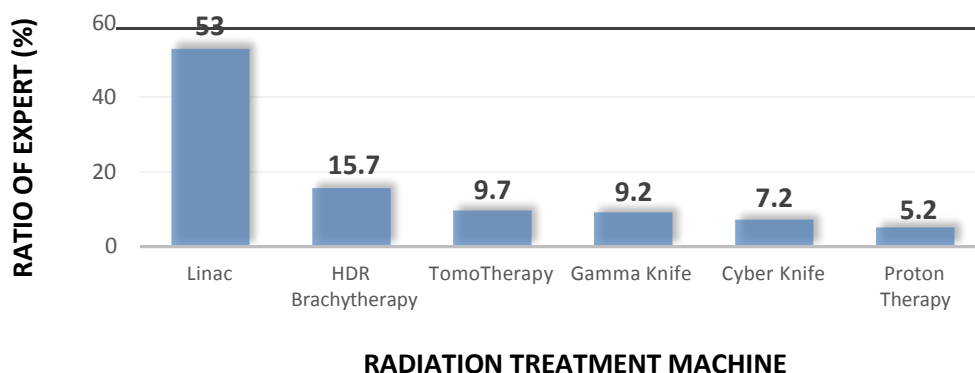
FIG. 2. Status of management experts according to radiation treatment machine. (2017.07)

The linear accelerators is the dominant radiation treatment machine in Korea with more than half the rate, due to the fact that the majority of linear accelerators are used for radiotherapy. Even if only two proton therapy machine are used in Korea but the ratio is 5.2%. It can be seen that a relatively large number of experts perform QA of proton therapy compared to other treatment machine.

2.2. The Systematic QA programme: Quality assurance manual, establishment of procedures

It is important to establish the systematic QA procedures in order to increase the accuracy of doses delivery in radiotherapy[4]. This kind of QA programme can reduce the size and frequency of system errors and random errors that can be occurred in radiotherapy. In the Nuclear Safety law in Korea, The following factors are required to perform the QA, and the medical centers establish its own QA manual based on it.

TABLE 1.   Factors of quality assurance manual mandated by domestic law in Korea.

(a)   Quality assurance management organization and duties
(b) Equipment for QA
(c) QA procedures, frequency, tolerance and the set of action level
(d) Output calibration and evaluation of radiation treatment machine
(e)   Method of radiation treatment planning verification
(f)   Training and education of experts for QA
(g) External Audits by independent organization (every three years)

According to the domestic law based on the TG-40 and TG-142 guidelines issued by AAPM, It includes the QA procedures, frequency, and tolerance in using the radiation treatment machine. The factors of QA proposed in the relevant law and regulations in Korea are intended to maintain a certain level of QA among medical centers using at least the same radiation treatment machine.

3. REGULATORY BODY ACTIVITIES OF IMPLEMENTAION OF THE LAW REGARD TO QA

In QA, It is not only important that the medical centers perform properly according to their own QA manual, but also important to objectively verify the procedures and results[5]. In situation of continuously being increased the number of radiotherapy in Korea, In addition to the independent external audit, it is important to verify and confirm the actual implementation situation of QA in the objective position. However, in Korea, there is no organization that can independently verify these kinds of QA management activities. Therefore, the regulatory body is in the process of establishing the plan at the national level and carrying out the verifying output of radiation treatment machine considering the domestic situation.

3.1. On-site Audit

From 2015, The NSSC and regulatory body(KINS; Korea Institute of Nuclear Safety) have organized the external audit team consisting of six qualified experts from other group to confirm the status of the QA of radiation treatment units. They visit the site and carry out the external audit by field measurement through independent method. With reviewing the appropriateness of the QA manual, external audit team check the basic requirements for performing the minimum 3D CRT which includes mechanical/radiation rotation isocenter check, light/radiation field coincidence, beam profile constancy, output constancy, physical wedge transmission factor constancy. After starting to implement since 2015, the team have conducted on-site audits of a total of 19 medical centers as of July 2017. This year, QA team they check the additional procedure including the photon beam quality.

3.2. Postal Audit

There is a limitation to verify the status of QA of all the radiation treatment machine used in 91 medical centers through current on-site audit. Therefore, It is needed to build an infrastructure that can be used to perform independent verification of QA of treatment units from a long-term perspective. To secure standards and maintain the uniform standard among the different medical centers, it is desirable to establish the institution to conduct external audit at the national level[6], [7]. In Korea, to form the external environment, the regulatory body have started to establish the system for postal audit from this year. To operate the postal audit system in the form of verification of the output and mechanical isocenter check using the glass dosimeter and film, in the first half of the year, It is being established that development of technical accuracy in film dosimetry and standard procedure for postal audit. Based on the established system, regulatory body will conduct safety evaluation of radiation treatment machine for about 45 medical centers in the second half of the year.

On-site audit and postal audit are expected to improve the reliability of radiotherapy and reduce the error among the facilities through continuous and accurate QA monitoring system.

REFERENCES

[1] Ezzell GA., Galvin JM., Low D., et al., "Guidance document on delivery, treatment planning, and clinical implementation of IMRT: report of the IMRT Subcommittee of the AAPM Radiation Therapy Committee.", Medical physics 30.8 (2003) 2089-2115.

[2] ICRP, "Prevention of Accidents to Patients Undergoing Radiation Therapy", ICRP Publication 86., Ann. ICRP 30.3, (2000).

[3] International Atomic Energy Agency Annual Report for 2014, Vienna (2015).

[4] ICRP, "Preventing Accidental Exposures from New External Beam Radiation Therapy Technologies", ICRP Publication 11., 2Ann.ICRP 39.4, (2009).

[5] Scalliet,P. "Comprehensive a Audits of Radiotherapy Practices: a Tool for Quality Improvement: Quality Assurance Team for Radiation Oncology(QUATRO)." International Atomic Energy Agency, Vienna (2007).

[6] Clark, Catharine H., et al. "Radiotherapy dosimetry audit: three decades of improving standards and accuracy in UK clinical practice and trials." The British journal of radiology 88.1055, (2015).

[7] AAPM Task Group No.40, "Comprehensive QA for radiation oncology", American Association of Physicists in Medicine, (1994).

SECONDARY RADIATION DOSE MEASUREMENTS IN SCANNING PROTON RADIOTHERAPY
Overview of the activity within EURADOS WG9 (SG2)

Ž. KNEŽEVIĆ
RBI, Zagreb, Croatia
Email: zknez@irb.hr

I. AMBROZOVA
NPI, Řež, Czech Republic

C. DOMINGO
UAB, Barcelona, Spain

M. DE SAINT-HUBERT
SCK-CEN, Mol, Belgium

M. MAJER
RBI, Zagreb, Croatia

I. MARTÍNEZ-ROVIRA
UAB, Barcelona, Spain

S. MILJANIĆ
RBI, Zagreb, Croatia

N. MOJŻESZEK
CCB IFJPAN, Krakow, Poland

O. PLOC
FNSPE, Prague, Czech Republic

M. ROMERO-EXPÓSITO
UAB, Barcelona, Spain

L. STOLARCZYK
CCB IFJPAN, Krakow, Poland

S. TRINKL
HZM, Neuherberg, Germany and TUM, Garching bei München, Germany

P. OLKO
CCB IFJPAN, Krakow, Poland

R.M HARRISON
Newcastle University, Newcastle upon Tyne, United Kingdom

Abstract

Proton therapy is used increasingly in cancer treatment because of the possibility of sparing healthy tissue close to the target volume. However, the interactions of protons with matter result in the production of secondary radiation comprised mostly of neutrons and gamma radiation. Unwanted doses, deposited distantly from the target volume may lead to an increasing probability of late effects of radiotherapy including the generation of secondary cancers which is of especial importance for children. The hadron therapy sub-group of EURADOS Working Group 9 (Radiation protection in medicine) is engaged in a measurement campaign designed to investigate the secondary radiation generated by a scanning proton beam. Experiments were carried out in the IBA (230 MeV) active-scanning proton beam therapy facility in Trento, Italy and in Krakow, Poland. The first part of the work included the characterization of the neutron and gamma radiation field inside the water tank phantom using different passive dosimetry systems. Depth dose distributions along the beam axis and profiles at various depths were measured. The second part of the measurement campaign was designed to measure out-of-field organ doses using 5 and 10 year-old anthropomorphic phantoms also with different types of passive dosimeters.

1.   INTRODUCTION

The aim of European Radiation Dosimetry Group, EURADOS (wwww.eurados.org), is to promote research and development and European cooperation in the different field of dosimetry of ionizing radiation.

Due to constant development and improvement of radiotherapy techniques (IMRT, IGRT, IART) survival rates in radiotherapy are increasing, but secondary cancers (and other long term conditions) might also increase in the future. Also patients especially young patients have good prognosisare cured and have long life-expectancies, which increase their chances of developing secondary malignancies. WG9 Radiation dosimetry in Radiotherapy is dealing with different aspects of dosimetry in radiotherapy. The aims are to assess and develop existing and potential dosimetric techniques in radiotherapy. At present the main topics were to assess out of field patient doses and the related risks of secondary malignancy, with the emphasis on a detailed evaluation of dosimetry methods for the measurement of doses remote from the target volume in different phantom experiments. One of the goals is to determine complete dose specification for patients undergoing radiotherapy, i.e the total dose to all organs from all sources of radiation, including the imaging procedures necessary for planning and treatment verification. The complete dose specification is of special importance for input into epidemiological studies as well as providing robust dosimetric data for the long term studies of radiation effects. Within WG9 the hadron therapy sub-group (SG2) has been formed. The hadron therapy sub-group is engaged in measurement campaigns designed to investigate the secondary radiation generated in proton radiotherapy.

Proton therapy is used increasingly in cancer treatment because of the possibility of sparing healthy tissue close to the target volume. Proton beams show an increase in energy deposition with penetration depth up to a sharp maximum at the end of their range and almost no dose is deposited in the normal tissue beyond the Bragg peak. Thus cancer cells may be destroyed whilst surrounding normal tissue is spared more than in conventional radiotherapy with x-rays. However, the interactions of protons with matter result in the production of secondary radiation comprised mostly of neutrons and gamma radiation. Unwanted doses, deposited distantly from the target volume (out-of-field doses), may lead to an increasing probability of late effects of radiotherapy including the generation of secondary cancers. A hadron radiation dosimetry sub-Group has been formed to address dosimetric aspects this field. The SG2 subgroup main tasks are: studying, developing and harmonising dosimetric techniques for proton and neutron dosimetry in proton therapy facilities including experimental and computational studies of phantom and ambient mixed radiation fields. The Group also promotes the development of dosimetric techniques for mailed dosimetry audits of proton therapy beams.

2.   TOPICS AND TASKS OF THE SUBGROUP

The topics addressed by hadron radiotherapy subgroup are:
1. Characterization of the neutron and gamma radiation field inside the water tank phantom and inside the treatment room from a proton pencil beam scanning system
2. Measurements of out-of-field organ doses using child anthropomorphic phantoms in active-scanning proton beam therapy facility
3. Mailed Dosimetry Auditing in Proton Therapy

3.   CURRENT ACTIVITIES

3.1.   Characterization of the neutron and gamma radiation field inside the water tank phantom and inside the treatment room from a proton pencil beam scanning system

The experiments were carried out in the IBA (230 MeV) active-scanning proton beam therapy facility in Trento, Italy. The characterization of the neutron and gamma radiation field were performed inside the water tank phantom using different passive dosimetry systems. A volume of 10 x 10 x 10 cm^3 inside the water phantom (60 x 30 x 30 cm^3) was irradiated uniformly to a dose of 100 Gy. In the phantom, the dosimeters were mounted in pipes. Five frames were laid out at depth increments of 5 cm along the beam axis. Each frame contained 5 pipes mounted in a vertical plane. Therefore, depth doses along the beam axis and profile at various

depths were measured. The following dosimeters were used: thermoluminescent (TLD-700, MTS-7, MTS-6 and MTS-N), radiophotoluminescent (GD-352M and GD302-M) optically stimulated (OSL) and poly-allyl-diglycol carbonate (PADC) track detectors. The details about dosimetry methods used were described in the paper previously published by EURADOS WG9 [1-2].

Figure 1 Water phantom (60 x 30 x 30 cm^3), and pipes filled with RPL dosimeters

Main sources of secondary radiation inside and around the treatment room were evaluated by direct measurements using a wide array of neutron monitors (HAWK (Far West Technology) WENDI II, Berthold (IFJ, PAN, Krakow), (NPI, Prague), (IRSN, Paris), (SCK-CEN, Mol))
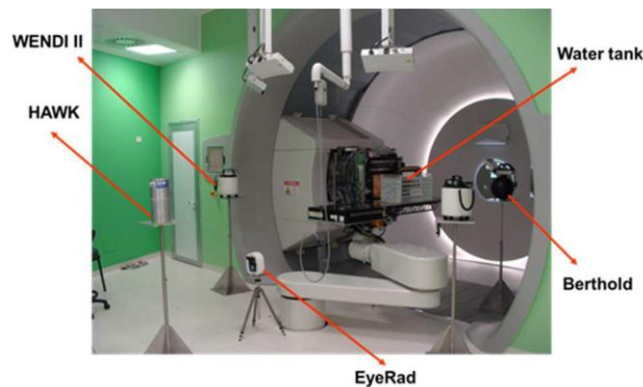
Figure 2 Active detector environmental measurements of radiation field generated around the water phantom during the treatment

Measurements were also accompanied by Monte Carlo transport calculations using MCNPX, FLUKA and GEANT 4 codes. Preliminary results showed that doses measured inside the phantoms far from the field edge are by up to four orders of magnitude lower than those inside the target volume. Significantly higher neutron and gamma doses were measured in the forward direction, due to angular characteristics of (p,n) reactions within the patient's body. RPL- measured gamma doses outside the target volume are lower by 25-40% than those measured by MTS-7 detectors due to lower efficiency of RPL dosimeters in comparison to MTS-7. The in-phantom doses and environmental doses strongly depend on the treatment volume and on the proton beam energy. Neutron ambient dose equivalent, $H^*(10)$, inside the gantry room was correlated with the treatment volume and depth of exposure. The highest $H^*(10)$ value was of 60 µSv/Gy for a 10 cm^3 volume in the water phantom and below 2 µSv/Gy for a 25 cm^3 treatment volume located in the child's head [2].

3.2. Measurements of out-of-field organ doses using child anthropomorphic phantoms in active-scanning proton beam therapy facility

The measurement campaign was designed to measure out-of-field organ doses using anthropomorphic phantoms produced by ATOM, Computerized Imaging Reference Systems (CIRS), Inc, Norfolk, VA), which represent 5 and 10 year old children. These phantoms are referred to in this paper as 5 y or 10 y phantoms. The measurements were carried out in the Bronowice Cyclotron Center in Krakow, Poland in IBA Proton Therapy System- Proteus 235. Doses were measured in different organs with thermoluminescent (MTS-7, MTS-6 and MCP), radiophotoluminescent (GD-352M and GD302-M), optically stimulated (OSL), bubble and poly-allyl-

diglycol carbonate (PADC) track detectors. The isocenter (at the centre of a sphere 6 cm diameter, representing the tumour) was located in the head of the phantom and the applied target dose was 100Gy. The planned energy layers were in the range from 70 MeV to 140 MeV. For both experiments the detectors were calibrated with ^{60}Co source in terms of kerma "free in air", K_{air} (K_{air} was then converted to absorbed dose to water, D_w) or directly in terms of D_w as described in the paper previously published by EURADOS WG9[6].
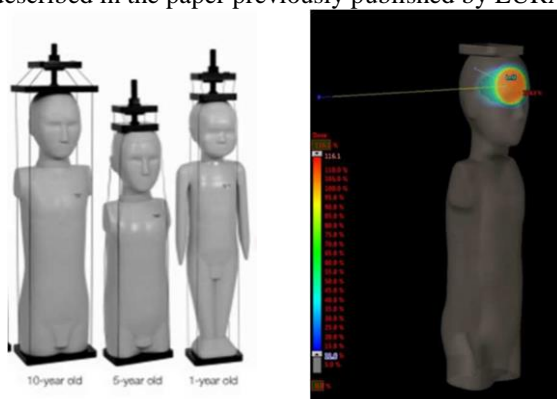
Figure 3. Anthropomorphic phantoms representing 1, 5 and 10 year old children. Position of the irradiated simulated tumor in 10y old phantom

Preliminary results showed that the contribution of neutron doses outside the treatment volume during the proton therapy is strongly related to the primary beam direction. All the detectors were in good agreement and suitable for out of field measurements. Doses measured with different passive dosimetry systems for intensity modulated proton therapy (IMPT) outside the treatment field produced by scattered radiation are lower than the target dose by 4-5 orders of magnitude. First results showed that the estimated mean organ out-of-field doses in 5 y phantom in IMPT are by two orders of magnitude lower than in IMRT.

To determine the fast neutron contribution, measurement with other type of detectors and Monte Carlo simulations are performed and under analysis.

3.3. Mailed Dosimetry Auditing in Proton Therapy

Dosimetry auditing of proton therapy is still not available in Europe. At present approximately 60 proton therapy facilities all over the world are in operation, more than 30 are under construction and more than 15 are in the planning stage. In order to control proper dose delivery to patients as well as part of a comprehensive approach to quality assurance (QA) in radiotherapy, independent external dosimetric audits are an important and necessary component to ensure adequate quality of practice and delivery of treatment in radiation oncology. Auditing procedures would contribute to dosimetry harmonisation among proton therapy centres.

The hadrontherapy sub-group started activities in this field and one of the objectives is to build and test a system for auditing proton therapy centres allowing assistance, quality control and harmonization of proton therapy centres in Europe. The first step was to perform an intecomparison and full characterization of different solid state detectors in proton fields. Four institutes, IFJ-PAN from Poland, SCK•CEN from Belgium, RBI from Croatia and ISS from Italy participated in the measurement campaign with different dosimetry systems. The following dosimeters were tested thermoluminescent (LiF:Mg,Cu,P;MCP-n), radiophotoluminescent (GD-352M and GD302-M) optically stimulated (Al_2O_3:C Luxel) and alanine. The measurements were carried out in the Bronowice Cyclotron Center in Krakow, Poland using an IBA Proton Therapy System- Proteus 235. The PTW 41023 water phantom was irradiated with 8 different Spread Out Bragg peaks (SOBPs) with 10x10cm^2 fields varying in modulation (R20M5, R20M10, R20M15, R20M20) and in range (R5M5, R10M5, R15M5, R20M5, R25M5). For each configuration 6 dosimeters were placed in the centre of the SOBP and received a dose of 10 Gy (alanine) or 2 Gy (MCP-N and Luxel). The tested dosimeters were also irradiated in a Theratron 780E unit (according to TRS-398 protocol) to measure the relative efficiency of the dosimeters to Co-60. Dosimeter repeatability and reproducibility were tested in the different participating institutes by irradiations in Co-60.

Figure 4 PTW water phantom and holders for alanine, TLDs, RPLs and OSLs alanine dosimeters

All the measurements were supported by MC simulations (MCNPx 2.7.0) of the proton energy spectrum at the dosimeter locations. Preliminary results show that the relative efficiency is lowest for MCP-N ranging from 0.70 to 0.79 and show LET dependence; increased response for increasing modulation. For alanine a relative efficiency of 0.95 was observed, while for RPL dosimeters it was 0.76 to 0.80 for type GD-302M and 0.80 to 0.85 for type GD-352M with only minimal rise in the response for increased modulation. The OSLD dosimeters demonstrate a relative response of about 0.9. The MCNPx energy spectra in the center of the SOBP demonstrated increasing proton energies for larger modulation width while for differing range (i.e. the same modulation) the average energy in the center of the SOBP was comparable.

4. CONCLUSIONS

The detailed analysis of results measured with different dosimetry systems combined with future Monte Carlo calculations will give valuable information about doses from scattered radiation distant from the target volume. This will add knowledge quantify out-of-field doses in active scanning proton therapy and help confirm the advantages of such a technique in sparing healthy organs, compared with conventional or intensity modulated x-ray techniques, despite the involved stray neutrons. Also the results gatherd in the database can be used as input into the selected theoretical models for secondary malignancy risk estimates.

REFERENCES

[1] Knežević Ž, Stolarczyk L, Bessieres I, Bordy J.M, Miljanić S, and Olko P. Photon dosimetry methods outside the target volume in radiation therapy: Optically stimulated luminescence (OSL), thermoluminescence (TL) and radiophotoluminescence (RPL) dosimetry. Radiat. Meas. 57, 9–18 (2013).

[2] Romero-Expósito M, Domingo C, Sánchez-Doblado F, Ortega-Gelabert O, Gallego S. Experimental evaluation of neutron dose in radiotherapy patients: Which dose? Med. Phys. 43:360-367 (2016).

[3] Farah J, Mares V, Domingo C, Dufek V, Frojdh E, George S, Harrison R, Klodowska M, Kubancak J, Knežević Ž, Liszka M, Majer M, Miljanić S, Ploc O, Romero-Expósito M, Schinner K, Stolarczyk L, Trinkl S, Trompier F, Wielunski M, and Olko P. Measurement of stray radiation within an active scanning proton therapy facility: EURADOS WG9 intercomparision exercise of active dosimetry systems. Med Phys. 42(5):2572-84. (2015).

DEVELOPMENT OF A RADIOPROTECTOR FOR RADIATION-INDUCED PNEUMONITIS IN MICE MODEL

A. Kunwar[1], V. K. Jain[2], K. Indira Priyadarsini[2]
[1]Radiation & Photochemistry Division, [2]Chemistry Division,
Bhabha Atomic Research Centre,
Trombay, Mumbai-400085, India
Email: kamit@barc.gov.in

V. Gota[3], J. Goda[4]
[3]Department of Clinical Pharmacology, [4]Department of Radiation Oncology,
Advanced Centre for Treatment, Research and Education in Cancer (ACTREC),
Tata Memorial Centre, Navi Mumbai -410210, India

Abstract

Late lung tissue responses of pneumonitis are the most serious dose-limiting side effects of thoracic radiotherapy, which has a considerable impact on patient morbidity and mortality. Oral corticosteroids have been the mainstay of therapy for radiation pneumonitis in clinics. However, corticosteroids are associated with numerous side effects including osteoporosis, adrenal suppression, and increased susceptibility to infection warranting the need to develop new drugs. In order to address this, we developed a mice model for thoracic radiation-induced pneumonitis and evaluated an in house synthesized organoselenium (DSePA) for radioprotection. The results indicated that oral supplementation (2.5 mg/kg body weight for three days a week following radiation exposure) with DSePA significantly ($P<0.05$) delayed the onset of radiation-induced pneumonitis and improves the asymptomatic survival. Thus organoselenium has potential to be developed as an oral supplement for the treatment of radiation induced pneumonitis.

1. INTRODUCTION

Radiation treatment of the thorax, which is frequently used as a therapy in breast, lung and oesophageal cancer and in Hodgkin's disease, produces pneumonitis and fibrosis in the lungs of up to 30% of treated patients [1]. Pneumonitis is an acute inflammatory response that occurs two to four months following irradiation, whereas fibrosis develops four to six months post-irradiation and is characterized by progressive scarring of the lung, with vascular cell damage and collagen deposition [2]. These pathologies of pneumonitis and/or fibrosis can result in impaired lung function and, ultimately, respiratory failure and therefore have a considerable impact on patient morbidity and mortality [1,2]. Oral corticosteroids have been the mainstay of therapy for radiation pneumonitis in clinics. However, corticosteroids are associated with numerous side effects including osteoporosis, adrenal suppression, and increased susceptibility to infection warranting the need to develop new drugs.

Selenium a micronutrient in different chemical forms for both humans and animals has gained a lot of attention as a new class of radioprotector. Selenium is the constituent of major redox active antioxidant enzymes such as glutathione peroxidase (GPx), and thioredoxinreductase (TRxR), which play a vital role in combating oxidative stress [3]. Some of the selenium compounds that have been tested for radioprotection in cells and *in vivo* models include sodium selenite, selenomethionine, selenocysteine, and ebselen [4]. On similar hypothesis, our group previously reported the radioprotective activity of a synthetic organoselenium (DSePA) at an intraperitoneal (IP) dosage of (2 mg/kg body weight) following whole body irradiation and thoracic irradiation [5-7]. All these reports together prompted us to presume that DSePA has potential to be developed as a clinical radioprotector. One of the criterion for a compound to be developed as a drug is that it should be administrable orally. Therefore in present investigation we performed a proof of concept study on the radio protective activity of DSePA in mice through oral administration against thoracic irradiation.

2.   METHODS

The study was approved by the Institutional Animal Ethics Committee of Advanced Centre for Treatment, Research and Education in Cancer (ACTREC), India. DSePA was synthesized and characterized as described in our previous reports [5]. For pharmacokinetic studies, mice of C3H/HeJ (pneumonitis responding) strain were administered DSePA (2 mg/kg, IP) and following this animals were sacrificed at different time points and lung tissue samples were collected for determination of selenium concentration by graphite furnace atomic absorption spectrometry (GFAAS) method. For radioprotection, mice received a single 18 Gy (^{60}Co, 0.6 Gy/min), whole thorax irradiation and a subset of these were treated with DSePA orally (2.5 & 10 mg/kg), three times per week beginning at 2 hours after radiation exposure and continued in the post irradiation period until euthanasia due to respiratory distress symptoms. The progression of pneumonitis in the irradiated mice was monitored phenotypically as appearance of respiratory distress and by acquiring CT (thorax) scans on regular time intervals. The respiratory distress in mice was defined as the loss of body weight by >20%, and the visibly accelerated breathing.

3.   RESULTS

To evaluate the efficacy of DSePA as a lung radioprotector through oral administration, it was necessary to establish the oral dosage equivalent to that of an IP (efficacious) dosage of 2 mg/kg. In order to achieve this, bio-equivalence analysis was performed by administering DSePA through IP (2 mg/kg body weight) and monitoring the level of selenium by atomic absorption spectroscopy in the lung homogenates prepared at various time points starting from 5 min to 24 h post administration. The results were compared with that of the previously available pharmacokinetic data of oral administration (50 mg/kg body weight) [7]. This study revealed that IP vs. oral administration resulted similar pharmacokinetics pattern of DSePA in the lung. Normalizing lung concentration of DSePA with respect to the dosage administered to the mice through IP vs oral mode, it was found that the lung availability ($C_{max} = 0.32 \pm 0.05$ µg/g) was comparable irrespective of the mode of administration. This suggested that the probable efficacious oral dosage of DSePA could be in the similar range of IP dosage (2 mg/kg).
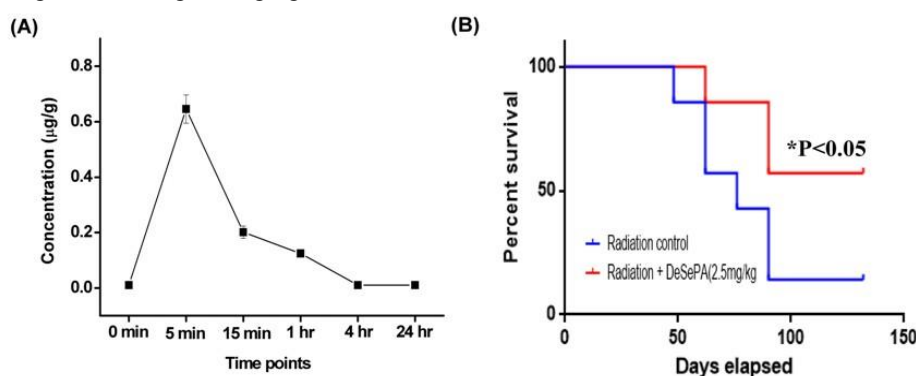
Fig. 1. (A) Concentration–time profile of selenium in lung following IP administration of DSePA (2 mg/Kg) in mice. Data shown as mean ± SEM for each time point (N = 3/time point). (B) Effect of DSePA administration (2.5 mg/Kg) on the progression of thoracic radiation-induced pneumonitis in C3H/HeJ mice as studied by Kaplan-Meier survival curve.

Accordingly lung radioprotection studies were carried out at the dosage of 2.5 and 10 mg/kg. The results of the CT scan analysis of lung performed on biweekly intervals indicated that the pathogenesis of pneumonitis started ~ 80 days post irradiation and within a week of onset got consolidated in the entire lung causing respiratory distress symptoms. The oral administration of DSePA at a dose of 2.5 mg/kg significantly (P<0.05) delayed the progression of pneumonitis and improved the asymptomatic survival compared to radiation control, whereas DSePA dose of 10 mg/kg was found to be toxic.

4. CONCUSION

The oral supplementation with DSePA (2.5 mg/kg body weight) prevented thoracic radiation-induced pneumonitis. Our future studies are focused on evaluating the effect of dose escalation of DSePA in context of lung radioprotection, toxicological changes and the *in vivo* lung tumor response.

REFERENCES

[1] Movsas, B., Raffin, T.A., Epstein, A.H., et al. Pulmonary radiation injury. Chest 111 (1997) 1061-1076.

[2] Marks, L.B., Yu, X., Vujaskovic, Z., et al. Radiation-induced lung injury. Semin. Radiat. Oncol. 13 (2003) 333-345.

[3] Papp, L.V., Lu, J., Holmgren, A., et al. From selenium to selenoproteins: synthesis, identity, and their role in human health. Antioxid. Redox Signal. 9 (2007) 775–806.

[4] Weiss, J.F., Landauer, M.R., History and development of radiation-protective agents, Int. J. Radiat. Biol. 85 (2009) 539–573.

[5] Kunwar, A., Bansal, P., Kumar, S.J., et al. In vivo radioprotection studies of 3,3'-diselenodipropionic acid, a selenocystine derivative, Free Radic. Biol. Med. 48 (2010) 399–410.

[6] Kunwar, A., Jain, V.K., Priyadarsini, K.I., et al. A selenocysteine derivative therapy affects radiation-induced pneumonitis in the mouse, Am. J. Respir. Cell Mol. Biol. 49 (2013) 654–661.

[7] Gota, V., Goda, J.S., Doshi, K., et al. Biodistribution and pharmacokinetic study of 3,3' diseleno dipropionic acid (DSePA), a synthetic radioprotector, in mice, Eur. J. Drug. Metab Pharmacokinet. 41 (2016) 839-844.

DOSIMETRIC COMPARISON OF SCATTERED RADIATION BETWEEN 3DRT AND VMAT IN CRANISPINAL IRRADIATION

LACHOS Alberto
Instituto Nacional de Enfermedades Neoplásicas
Lima, Perú
Email: alachosd1271@yahoo.com

ABSTRACT

The development of new technologies in radiotherapy offers us a large arsenal of tools to improve the coverage of PTV and the protection of organs at risk (OAR). In our institution we have begun to perform treatments with VMAT techniques to patients requiring crani-axial irradiation, however there is a great concern for the dispersed radiation and the increased risk of carcinogenesis, so we decided to compare the doses received by the different Organs in this group of patients.

The VMAT technique decreases the high doses in OAR near the PTV, such as thyroid, crystalline, esophagus and low dose to the skin, however when evaluating the most peripheral organs such as lungs, liver, kidneys, heart and breasts in women Total organ dose in VMAT may be 10 to 12 times greater than in conventional 3D. The average dose received for the entire circumference of the body is on average 10% of the prescribed dose.

These data must be taken into account du to possibility of development of secondary cancers induced by radiation, no only in the field of treatment but also by increase of low absorbed doses due to exposure to scattered radiation.

1. **INTRODUCTION**.

With the development of Intensity Modulated Radiation Therapy (IMRT). The scattered radiation was always a matter of concern.

Erick Hall et al, reported an increase in relative risk from 1% to 1.75% of secondary neoplasms in patients treated with radiotherapy a 10-year survival. This risk increases if the patient is younger and the longer the survival.

In patients treated with radiotherapy, an increase in secondary neoplasms is described not only in the treatment field. Sarcomas are the most common in the field of treatment and carcinomas outside the field of treatment. According to Saint Jude, there is a high rate of primary seconds in irradiated patients, from 12 to 20%.

In patients who have received total body irradiation the risk of second neoplasias is 20 to 25%.

In evaluations performed the relative risk of secondary cancer in patients receiving radiation therapy is 2%, patients receiving chemotherapy of 4.4% and patients receiving radiotherapy with chemotherapy for synergistic effect is up to 20%.

In a study, evaluating children who received irradiation for lymphomas the risk of breast cancer was up to 11%.

Relative risk for developing secondary neoplasms in Mantel field with dose 20 Gy was of 3 to 4. Greater risk if doses increase up to 30 Gy.

Technological advances in radiotherapy in their different techniques offer advantages in covering the white volume and protecting organs at risk. The IMRT technique offers greater conformity and greater protection of the organs at risk, a greater integral dose than the conventional 3D technique. Volumetric modulated arc radiotherapy (VMAT) offers better integral dose than others simpler techniques of IMRT and in a much shorter duration of treatment by changes in the dose rate during the administration of the radiation.

Proton therapy is a new technology that is spreading in the world due to the decrease in installation costs, it offers lower irradiation volume, lower integral dose, among its disadvantages neutron formation. Proton therapy reduces the incidence of secondary Neoplasms in pediatric patients, by lower radiation dispersed due to the physical properties of the protons. For example in Medulloblastoma is reduced by half.

Due to this background, we decided to evaluate the dispersed radiation to which our patients are exposed with the linear accelerators that have advanced technology such as VMAT. When irradiating with technique of arcs, greater dispersed radiation is absorbed by the organism. For that, patients with cranioaxial irradiation were selected.

2. METHODS

Seven patients were selected for this evaluation previously treated with radiotherapy in conventional 3D or with VMAT technique. A single radioncologist performed the delimitation of the PTV and the organs at risk. The organs of interest contoured for the evaluation included crystalline, thyroid, lung, heart, liver and kidneys, breasts for women. In all cases, the planning was done in conventional 3D in XIO and for VMAT with the MONACO planning system for its dosimetric comparison, as indicated in Table 1, where the planned dosimetry data in conventional 3D and VMAT are compared for the same patients.

3. RESULTS

Analysing the doses received by each organ at risk (OAR) planned with conventional 3D technique where the treatment beams are direct, compared to VMAT technique, where the treatment beam enters in a rotary form giving the low doses in the circumference of the patient. The dosimetric comparison indicates that the organs close to the PTV receive higher doses with conventional 3D technique, which must be taken into account in order not to exceed the tolerance doses of the OAR and decrease the likelihood of deterministic effects on OARs, however, it is necessary to take into account that when planning with VMAT technique where the doses received by the organs distant to the PTV are greater when compared to the schedules for the same patients with conventional 3D technique. These doses are subclinical doses, which will not produce deterministic effects on OAR, but must be taken into account the possibility of significantly increase secondary neoplasms.

The VMAT technique decreases high doses in OARs close to PTV, such as thyroid, crystalline, oesophagus, however when evaluating the most peripheral organs such as lungs, liver, kidneys, heart and breasts in women, doses can be 10 to 12 times higher than in conventional 3D.

The dose received by the circumference of the body is on average ten percent of the prescribed dose. Fig. N° 1.

5. CONCLUSIONS

Many times we disregard the low doses received by the rotation of the beam in the VMAT technique, which could be related to a probable increase in the secondary cancer induced by radiation. The choice of optimal treatment should be evaluated individually in each patient considering the risks of damage to normal tissues and the different risks for stochastic effects in the long term.

6. TABLES

VMAT(cGy)

	PULMONES		TIROIDES		CRISTALINOS		HIGADO		LARINGE		GO		RIÑONES	
D100	231.4	D100	854.5	D100	491	D100	0.0	D100	1049.9	D100	425.5	D100	504.5
D50	871.3	D50	1262	D50	558	D50	0.0	D50	1728.6	D50	1148.2	D50	1040.9
DMED	1037.6	DMED	1279.75	DMED	562	DMED	0.0	DMED	1775.4	DMED	1198.2	DMED	1091.7
D2%	2843.9	D2%	1668.75	D2%	652.2	D2%	0.0	D2%	2645.3	D2%	2176.3	D2%	1971.7

	CORAZON		BAZO		RECTO		PAROTIDAS		VEJIGA		ESOFAGO		ESTOMAGO	TESTICULO
D100	233.3	D100	277.3	D100	2.9	D100	138.2	D100	11	D100	979.5	D100	328	3
D50	686.0	D50	649.3	D50	37.9	D50	1092.4	D50	28	D50	1844	D50	947	
DMED	727.3	DMED	700.1	DMED	39.6	DMED	1075	DMED	30	DMED	1901.5	DMED	932	
D2%	1367.0	D2%	1495.7	D2%	74.9	D2%	2048.3	D2%	55	D2%	2915	D2%	1419	

3D(cGy)

	PULMONES		TIROIDES		CRISTALINOS		HIGADO		LARINGE		GO		RIÑONES		CORAZON
D100	22.5	D100	2402.5	D100	290	D100	15	D100	2133.3	D100	125.4	D100	40	D100	100
D50	203.8	D50	2847.5	D50	371.7	D50	145	D50	2840.0	D50	590.8	D50	203.75	D50	1690
DMED	457.4	DMED	2838	DMED	377.2	DMED	546.8	DMED	2791.3	DMED	845.5	DMED	322.6	DMED	1517.3
D2%	3031.3	D2%	3035	D2%	585	D2%	2742.5	D2%	3113.3	D2%	2417.9	D2%	1588.75	D2%	2950

	BAZO		RECTO		PAROTIDAS		VEJIGA		ESOFAGO		ESTOMAGO	TESTICULO
D100	16.7	D100	0	D100	45	D100	0	D100	1515	D100	70	15
D50	46.7	D50	10	D50	825	D50	70	D50	3115	D50	220	
DMED	103.7	DMED	16	DMED	1101.5	DMED	77	DMED	3066.5	DMED	208	
D2%	550.0	D2%	70	D2%	3450	D2%	150	D2%	3410	D2%	380	

Table No. 1. Dosimetric comparison of the absorbed dose of different organs between conventional VMAT and 3D techniques

7. FIGURES
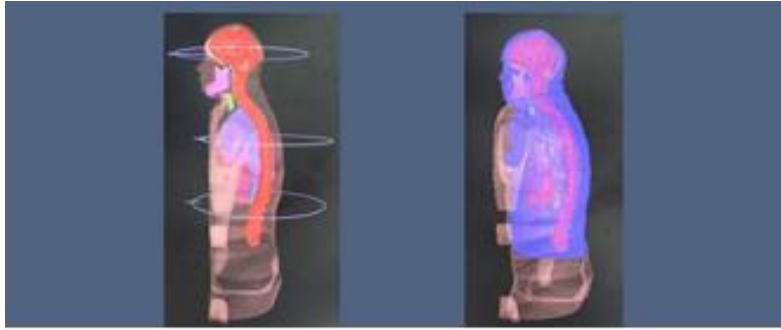
Figure 1. Distribution of dispersed dose in treatment with VMAT technique compared to conventional 3D.

REFERENCES

[1] Yasser Abo Madyan et al, Second cancer risk after 3D CRT, IMRT and VMAT for breast cancer. Radiation and Oncology 110 (2014) 471-476.

[2] E. J. Hall, IMRT - Increased risk of second cancer. International Journal of Radiation Oncology Biology Physics 65 (1) 1-7, 2006.

[3] Nguyen et al, Review of second malignancies. Red Journal, 2008.

OUT-OF-FIELD DOSE MEASUREMENTS FOR RADIOTHERAPY TREATMENTS OF PAEDIATRIC BRAIN TUMOUR USING DIFFERENT TECHNIQUES (3D CRT, IMRT AND GAMMA KNIFE)
Overview of the activity within EURADOS WG9

M. MAJER
RBI, Zagreb, Croatia
Email: mmajer@irb.hr

M. DE SAINT-HUBERT
SCK-CEN, Mol, Belgium

H. HRŠAK
UHC, Zagreb, Croatia

Ž. KNEŽEVIĆ
RBI, Zagreb, Croatia

S. MILJANIĆ
RBI, Zagreb, Croatia

N. MOJŻESZEK
CCB IFJPAN, Krakow, Poland

L. STOLARCZYK
CCB IFJPAN, Krakow, Poland

R.M. HARRISON
Newcastle University, Newcastle upon Tyne, United Kingdom

Abstract

The aim of the EURADOS Working Group 9 (WG 9) (Radiation Dosimetry in Radiotherapy) is to assess unwanted, non-target patient doses and the related risks of secondary cancer in different radiotherapy techniques. Paediatric patients are of particular concern due to their possible longer life expectancy and increased organ radiosensitivities compared to adult patients together with higher organ doses, if they are treated same as adults, because of their smaller body size. A vulnerable group of patients are children with brain tumours. Within the EURADOS WG 9, measurement campaigns were designed and carried out with the aim of measuring out-of-field doses in clinical conditions using anthropomorphic paediatric phantoms which received a simulated treatment of a brain tumour with three different techniques (intensity modulated radiotherapy (IMRT), 3D conformal radiotherapy (3D CRT) and Gamma Knife). Dosimetry was performed with 3 different techniques: thermoluminescence (TL), radiophotoluminescence (RPL) and optically stimulated (OSL) dosimetry. In addition to evaluation and comparison of out-of-field organ doses for two phantoms and three irradiation techniques, agreement of used dosimetry systems and underestimation of out-of-field doses by a treatment planning system for organs remote from the target volume were shown.

1. INTRODUCTION

The motivation of the Working Group 9 (WG 9) (Radiation Dosimetry in Radiotherapy) of the European Radiation Dosimetry Group (EURADOS) is to assess and develop existing and potential dosemeters and dosimetric techniques in radiotherapy and, in particular, to assess unwanted non-target patient doses and the related risks of secondary cancer, with the emphasis on a thorough evaluation of dosimetry methods for the measurement of doses remote from the target volume in phantom experiments.

Paediatric patients are of particular concern due to their possible longer life expectancy and increased organ radiosensitivities compared to adult patients together with higher organ doses, if they are treated same as adults, because of their smaller body size. A vulnerable group of patients are children with brain tumours. Brain and central nervous system-tumours are the second most common tumours in children and have a high survival rate. The out-of-field doses in these patients therefore raise an important radioprotection concern.

Within the EURADOS WG 9, measurement campaigns were designed and carried out in the radiotherapy facilities in Krakow, Poland and Zagreb, Croatia with the aim of evaluating and comparing the out-of-field

doses for the treatment of a brain tumour in two paediatric phantoms with different irradiation techniques, to gain information on the performance of used dosimetry systems in measuring out-of-field doses in radiotherapy and finally, to compare measured doses with the values given by the treatment planning system (TPS). Clinically relevant treatment plans for three different techniques (intensity modulated radiotherapy (IMRT), 3D conformal radiotherapy (3D CRT) and Gamma Knife) according to commonly used planning protocols were prepared for a simulated treatment of the same brain tumour in an anthropomorphic paediatric phantoms representing 5 and 10 year old children. Doses were measured with thermoluminescence (TL), radiophotoluminescence (RPL) and optically stimulated (OSL) dosimeters.

2. METHODS

2.1. Irradiation techniques

2.1.1. 3D CRT and IMRT

The experiments were carried out on a Varian Clinac 2300 linear accelerator in the Centre of Oncology, Krakow, Poland. Treatment of the brain tumour was simulated using two different radiotherapy techniques: 3D CRT and IMRT. In both cases, 6 MV photon beams were used. Treatment plans were generated by an Eclipse External Beam Planning System version 8.6 (Varian Medical Systems, Palo Alto, CA). For both techniques, optimal plans were produced according to the typical planning protocol used in paediatric radiotherapy and adopted by the Centre of Oncology, Krakow. For both phantoms the IMRT plan included 9 coplanar fields equally distributed in angle and with similar number of monitor units (MU). For 3D CRT, three non-coplanar fields were used for both phantoms, but plans were created using different beam orientations, beam weights and wedge angles. For the 10-year old phantom, only dynamic wedges were used, while for the 5 year old phantom for one beam a mechanical wedge was used for 3D CRT. The ratio of total MU for IMRT compared with the total MU for 3D CRT was 1.32 and 1.79 for 5 and 10 year old phantoms, respectively. All irradiations were performed for a target dose of 2 Gy and all results are, after normalization to target dose, presented as (mGy/Gy).

2.1.2. Gamma Knife (GK)

Radiosurgery treatments of an idealised brain tumour in an anthropomorphic phantoms were carried out at the University Hospital Centre Zagreb, Croatia using a Lexell Gamma Knife (GK) Model C (Elekta Instruments, Stockolm, Sweden). GK Model C uses 201 ^{60}Co sources arranged in a concave half-spherical surface. Narrow photon beams, shaped with circular collimators, intersect at the isocentre producing a nearly spherical dose distribution with 4 possible diameters (4, 8, 14 and 18 mm) defined by a changeable collimator. In order to achieve better conformity of the dose distribution to the tumour, clinical treatment plans usually employ more than one collimator, each using many isocentres. A change of isocentre position is enabled by automatically repositioning the patient's head into the required position and during repositioning a small dose is experienced. The dose calculation algorithm used in the treatment planning system (TPS) was a tissue-maximum ratio algorithm Leksell Gamma Plan 10.1.1. Due to large tumour volume, for both phantoms, only the largest collimator (18 mm) was used with 25 and 31 isocentres for 5 and 10 year-old phantoms respectively. Measured doses were normalized to the mean target dose (4.1 Gy for both phantoms) and results are presented as (mGy/Gy).

2.2. Child anthropomorphic phantoms

Anthropomorphic phantoms produced by ATOM, Computerized Imaging Reference Systems (CIRS), Inc, Norfolk, VA, which represent a 5 year old child (type 705D) and a 10 year old child (type 706D) were used for this study. The phantoms consist of 26 and 32 slices with 180 and 231 holes for dosimeters in 5 and 10 year old phantom, respectively. Slices of thickness 2.5 mm are made of tissue equivalent materials and dosimeters can be inserted into holes of diameter 5 mm located on positions of different organs/tissues and fixed with appropriate plugs. Using a computed tomography (CT) images of the phantoms, distance of the middle of each

hole to the selected point in the phantom (centre of the spherical tumour) was evaluated. For both phantoms treatment of the same spherical brain tumour was simulated: Planning target volume (PTV) was a sphere with a diameter of 6 cm located on the left anterior side of the head. Phantoms and top view of the slice in the head of each phantom, where the centre of idealized spherical tumour was located, are shown in FIG. 1.
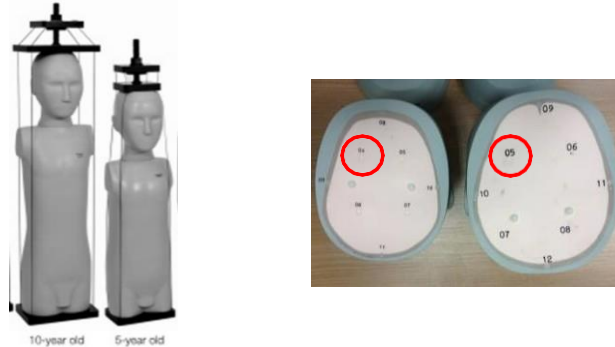
FIG. 1. Anthropomorphic phantoms representing 5 and 10 year old children and top view of slice in the head of both phantoms where the centre of the idealized spherical tumour was placed. Positions of the holes for dosimeters are marked with the numbers 04-11 and 05-12. The border of the PTV is marked with the circle.

2.3. Dosimetry systems

Dose measurements were performed using radiophotoluminescent (RPL) dosimeters type GD-352M, optically stimulated luminescent (OSL) dosimeters type Luxel and two types of thermoluminescent (TL) dosimeters: MCP-n and MTS-7. Detailed characteristics of the dosimetry systems used can be found in previously published papers [1-3] and a short summary is given in TABLE 1. Information which dosimetry system was used during each treatment irradiation can be found at the bottom of TABLE 1.

TABLE 1. Characteristics of the used RPL, TL and OSL dosimetry systems

Dosemeter	RPL GD-352M	TL MCP-n	TL MTS-7	OSL Luxel
Manufacturer	ATCG, Japan	IFJ PAN, Poland	IFJ PAN, Poland	Landauer Inc.
Material	Ag activated phosphate glass	^{nat}LiF:Mg,Cu,P	^{7}LiF:Mg,Ti	Al_2O_3:C
Dimensions (mm)	$\phi 1.5 \times 12$ (rod) $\phi 1.5 \times 14.5$ (holder)	$\phi 4.5 \times 0.9$	$\phi 4.5 \times 0.9$	$\phi 4.5 \times 0.13^a$
Reader	Dose Ace FGD-1000	Harshaw model 5500	Harshaw model 3500	TL/OSL-DA-20 reader system
Calibration/quantity	^{60}Co/K_{air}	^{60}Co/K_{air}	^{60}Co/D_w	^{60}Co/K_{air}
Conversion factor K_{air} to D_w	1.12^b	1.112^c	-	1.112^c
		IRRADIATION TECHNIQUES		
5 year old phantom	3D CRT, IMRT, GK	GK	3D CRT	GK
10 year old phantom	3D CRT, IMRT, GK	-	3D CRT, GK	-

[a] Thickness of the polyester foild: 0.05 mm (top) and 0.08 mm (bottom)
[b] Experimentally determined
[c] Determined using the ratio of mass energy absorption coefficient for water to air for the energy of ^{60}Co

The phantoms were filled with annealed dosimeters so that in each hole just one dosimeter was placed and it was fixed with plugs so that its active volume was in the middle of the hole. The measured doses for all dosimeters were expressed as absorbed dose to water, D_w (mGy), and normalized to the mean target dose (mGy/Gy). Relative standard uncertainty in the determined dose for RPL (GD 352-M), OSL (Luxel) and TL (MCP-n and MTS-7) were 2.1%, 4.5 %, 3.3% and 2.9%, respectively [1]. The mean organ doses in the

anthropomorphic phantoms, measured with selected type of dosimeters, were calculated as an average value of all dosimeters of that type placed in the particular organs. The number of dosimeters placed in a particular organ varies from 1 (for prostate in both phantoms) to 28 and 24 for lungs in 5 and 10 year old phantom, respectively.

3. RESULTS AND DISCUSSION

Comparison of RPL and TL MTS-7 dosimeters used for 3D CRT and IMRT and three dosimetry systems used for GK measurements showed good agreement. In particular, for RPL (GD-352M) and TL (MCP-n and MTS-7) dosimeters, no correction was needed while for OSL (Luxel) good agreement within 1-2% was achieved after energy correction using dual dosimetry analysis [5].

For 3D CRT and IMRT, measured values of each dosimeter were compared with the values given for the dosimeter's position in the phantom by TPS. For both techniques, for organs remote from the target volume (>12 cm from the isocentre in treatment plans) out-of-field doses were underestimated by the TPS used [4], indicating that estimation of second cancer risk using TPS values is not recommended unless the TPS algorithm has been independently validated by measurement. Observed underestimation tended to increase with distance from the treatment volume [4].

Out-of-field organ doses were on average 1.3 and 3.0 times higher for 5 year than for 10 year old phantom for IMRT and 3D CRT, respectively, and the different factors might be explained by differences in 3D CRT plans [4]. For GK, measured doses for out-of-field organs were comparable for both phantoms and that might be connected with the different number of isocentres [5]. The highest eye dose was measured for IMRT, followed by GK and 3D CRT, whilst for the thyroid, the highest dose was measured for GK, followed by IMRT and 3D CRT. For 3D CRT, eye doses were 3-6% and for IMRT 27-30% of the treatment dose, respectively [4]. For thyroid and more distant organs, doses were less than 1% of the treatment dose for all treatments. For the more appropriate comparison of irradiation techniques, different treatment regimens for GK, IMRT and 3D CRT treatment of the selected tumour have also to be taken into account.

4. CONCLUSIONS

Although the measured dose values are still quite specific for the investigated brain tumour case and the phantoms and treatment plans used, they provide useful information about out-of-field dose levels and emphasize the importance of out-of-field dose dosimetry.

REFERENCES

[1] Knežević, Ž., Stolarczyk, L., Bessieres, I., Bordy, J.M., Miljanić, S., Olko, P., Photon dosimetry methods outside the target volume in radiation therapy: Optically stimulated luminescence (OSL), thermoluminescence (TL) and radiophotoluminescence (RPL) dosimetry, Radiat. Meas. 57 (2013) 9–18.

[2] ATGC. Explanation Material of RPL Glass Dosemeter: Small Element System. Asahi Techno Glass Corporation, Tokyo, Japan (2007).

[3] Nascimento, L.F., Saldarriaga, C.V., Vanhavere, F., D'Agostino, E., Defraene, G., De Deene, Y., Characterization of OSL Al2O3:C droplets for medical dosimetry, Radiat. Meas. 56 (2013) 200-204.

[4] Majer, M., Stolarczyk, L., De Saint-Hubert, M., Kabat, D., Knežević, Ž., Miljanić, S., Mojzeszek, N., Harrison, R., Out-of-field dose measurements for 3D conformal and intensity modulated radiotherapy of a paediatric brain tumour, Rad. Prot. Dos. 27 (2017) 1-10.

[5] De Saint-Hubert, M., Majer, M., Hršak, H., Heinrich, Z., Knežević, Ž., Miljanić, S., Porwol, P., Vanhavere, F., Harrison R., Out-of-field doses in children treated for large arteriovenous malformations using hypofractionated gamma knife radiosurgery and intensity modulated radiotherapy, Submitted to Rad. Prot. Dos. (2017)

Radiation Protection Shielding Evaluation Report

Facility: American University of Beirut, New Medical Center, Cyberknife

Address:

Architect:

Equipment: **Date:**   May 18, 2017

Signature: Draft Shielding Design

Physicist:
Melissa C. Martin, M.S., DABR, FACR
Therapy Physics, Inc.
879 W 190th St., Ste. 400, Gardena, CA 90248
310-217-4114, FAX 310-217-4118
e-mail: melissa@therapyphysics.com

Max Field Size (cm)

7.5

Energy (MV)	Patients per day	Workload (Gy/pt)	SAD (cm)	Workload (Gy/wk)	MU/cGy Ratio	Leakage Workload (Gy/wk)
6	12	20	80	768	15	18000

Workload per patient is at the indicated SAD from the X-ray source.
Weekly workload is normalized to 1 m from the X-ray source.

Primary + Secondary Barrier Summary (Walls)

Protected Location	Inner Barrier Layer Thickness	Inner Barrier Layer Material	Outer Barrier Layer Thickness	Outer Barrier Layer Material	P (mSv/wk)	TADR (mSv/wk)	
A - Corridor (if primary) (T=0.2			1600 mm	Concrete	0.020	0.008	**
A2 - Control (if primary)			1600 mm	Concrete	0.020	0.018	
B - Vault 2 (T=0.5)			1600 mm	Concrete	0.020	0.017	**
C - Vault 2 (T=0.5)			2200 mm	Concrete	0.020	0.000	**
D - Vault 2 (T=0.5)			1600 mm	Concrete	0.020	0.003	**
E - ext (below ground) (T=0.05	600 mm	Concrete	2000 mm	Earth	0.020	0.000	**
F - Brachy room (T=0.5)			1600 mm	Concrete	0.020	0.008	**
G - Brachy control			1800 mm	Concrete	0.020	0.008	

** Occupancy < 1 included in TADR calculation.

Secondary Barrier Only Summary (Ceiling)

Protected Location	Inner Barrier Layer Thickness	Material	Outer Barrier Layer Thickness	Material	P (mSv/wk)	TADR (mSv/wk)
A - Corridor (T=0.2)			1300 mm	Concrete	0.020	0.005
A2 - Control			1300 mm	Concrete	0.020	0.010
P - Above isocenter			1400 mm	Concrete	0.020	0.010
S - Above isocenter			1200 mm	Concrete	0.020	0.016

Door Requirements Summary (if primary)   **Note: Additional shielding adjacent to door is also required**

P (mSv/wk): _____0.020_____   Shielded Dose (mSv/wk): _____0.008_____ Location I

Door Component	Thickness	Material
Door Inner Face	6 mm	Steel
Core Layer 1	229 mm	Lead
Core Layer 2		
Core Layer 3		
Door Outer Face	6 mm	Steel

**American University of Beirut
New Medical Center, Cyberknife
Beirut, Lebanon**

NORTH

Protected Locations

AI-1008 (5 May 2017)

Isocenter location is approximate. This assumes back wall of Cyberknife is to the west, with no pointing toward the west wall permitted (allows west wall to be secondary only).

1600 mm thickness recommended for the Vault 2 south secondary barriers to protect Vault 2 from the Cyberknife primary beam

CH 3 m²

CH 3 m²

CH 2 m²

CH 2 m²

RL FE

A2

A

C-KNIFE

4200

5200

8500

5700

4000

C-KNIFE EQ 20 m²

3000

1300

I

ALCV EQUIP 4 m²

1600

2200

7500

4000

11' 6"

3300

6500

9700

E

1800

1600

G

F

SUBWA

CNTRL BRACH

If west wall is secondary (no pointing to west) 1300 mm thickness is recommended.
If west wall is primary (no pointing constraints), 1600 mm thickness recommended

1800 mm recommended to protect control area (full occupancy immediately beyond wall)

Minimum 1600 mm recommended to protect brach room (1/2 occupancy)

American University of Beirut
New Medical Center. Cyberknife
Beirut, Lebanon

Section Looking North

A-3001 (5 May 2017)

P

S

9700

2000   2000

1200

1400

7500

5500

Ceiling is secondary barrier.

Does P correctly indicate the closest location directly above vault with occupancy?

Is there occupancy on Basement Level 4 directly beneath vault? If so, the floor would need to be a primary barrier.

**American University of Beirut
New Medical Center. Cyberknife
Beirut, Lebanon**

NORTH

Nearby Locations

AI-1008 (5 May 2017)

BOILED ELEV
8 m²

CNTRL LINAC
12 m²

ASSESS/CONS
13 m²

9 m²

9 m²

LINAC
#1
62 m²

1
AI-6006

CH
3 m²

CH
3 m²

SUBWAIT
11 m²

TLT PAT
5 m²

EQUIP
8 m²

NS / CNTRL
13 m²

LINAC
#2
70 m²

SUBWAIT
12 m²

CH
3 m²

CH
3 m²

CLEAN ELEV
9 m²

CH
2 m²

CH
2 m²

TLT PUB
M/F
6 m²

CNTRL
C-KNIFE
12 m²

C-KNIFE
62 m²

C-KNIFE EQ
20 m²

1
AI-6007

PREP/RECOV
15 m²

ALCV EQUIP
4 m²

SUBWAIT
8 m²

CNTRL
BRACH
10 m²

BRACH
36 m²

1
AI-6008

NS
16 m²

TLT PAT
6 m²

SCRUB
1 m²

TLT PAT
6 m²

PPE

TLT STF
6 m²

ALCV EQUIP
3 m²

FHC

4

NORTH

Construction Guidance

These calculations assume 147 lb per cubic ft concrete density, 490 lb per cubic ft steel density, 708 lb per cubic ft lead density, and 95 lb per cubic ft earth density (per NCRP 151). Borated polyethylene (BPE) is assumed to include 5% Boron by weight. Ensure that construction contracts specify the density of the materials that provide shielding. In the case of modifications to an existing facility, the additional material recommended here may not be adequate if the existing material does not conform to these standards.

In addition to providing the required density, cured concrete must contain no air bubbles, voids, cracks or other defects that can affect the shielding. There must be no hollow structural support columns in the concrete shielding walls. This is particularly important for primary barriers. Ensuring there are no voids in the concrete during the pour may require measures such as vibration of concrete.

If recesses are made in the walls for the image guidance system (e.g., laser, etc.), the recesses must be backed by steel or lead plates of a thickness to retain the recommended shielding value.

Continuous pours are preferred for the concrete walls and ceiling. For non-continuous concrete pours, avoid having a cold joint within approximately 3 feet of isocenter. Specifically avoid stopping a pour between 1 feet and 7 feet above the finished floor. If portions of the walls are poured at different times, the cold joint between pours must not be within 3 feet of isocenter (i.e., a corner is the preferred location for a cold joint).

Any lead brick used in construction must be interlocking. Shielding joints between any concrete blocks or steel plates must be staggered, both horizontally and vertically. Shielding joints must not be aligned with isocenter.

Junction Boxes: Provide 1.5 inches (38 mm) thick steel shielding with 1" (25 mm) margin behind all new junction boxes recessed in secondary shielding walls. No junction boxes should be located in primary barriers.

There shall be no penetrations that are directly aligned with either isocenter or a target location (i.e., the vault exterior must not be visible through the penetration from a target location).

Physics Port: This penetration shall be approximately 4" in diameter and shall be angled both vertically and horizontally 15° or more (in both cases with the port opening outside the vault closer to isocenter than the port opening inside the vault). The penetration opening inside the vault shall be located as desired by the linear accelerator manufacturer, typically 12" to 15" above the floor and located inside a cabinet. Because of the small cross-section and angle of this penetration, no specialized shielding is required for the physics port.

Pipe and Conduit Penetrations: All pipes and conduit penetrations must be located in secondary barriers (i.e., they shall not be located in a primary barrier). Conduits or pipes can be routed through the floor with no special shielding required if the vault is slab on grade with no occupancy beneath the vault. At elevations below 8' above the finished floor (AFF) penetrations up to 3" diameter for pipes or conduits are acceptable in secondary walls provided the penetration is made at an angle (not straight through the wall). There shall be no penetrations that point directly to the linear accelerator isocenter or target location. The separation between penetrations must be at least as large as the greater of the two adjacent penetration diameters, with a minimum of 4" separation preferred. Above 8' AFF penetrations up to 4" diameter can be made straight through the secondary barrier wall without requiring any special shielding. As with penetrations below 8' AFF, the separation between penetrations must be at least as large as the greater of the two adjacent penetration diameters, with a minimum of 4" separation preferred. Penetrations larger than 4" diameter may require lead shielding lining the penetration to make up for the missing concrete, depending on the penetration location and whether or not the penetration is made at an angle. Penetrations larger than 4" diameter should be coordinated with me.

5/18/2017
AUBNMC - Cyberknife.xlsm

Page 7
Construction Guidance

Therapy Physics, Inc.
310-217-4114

Construction Guidance (Continued)

Duct Penetrations for Ventilation: The HVAC penetration for a vault with a maze is typically above the door. A shelf is required beneath the duct (and above the door) constructed of either concrete or the same material as the door, with the shelf extending from the exterior wall at least 3 times the width of the penetration. Alternatively, the duct can be wrapped with the same shielding material as the door, with the wrapping extending at least 3 times the width of the penetration. If the same material as the door is used for the duct shielding, approximately 1/3 as much material required as the door, with a minimum of 0.25 inches lead (and 1" borated poly if > 6 MV) recommended for a long maze.

An HVAC penetration for vaults with direct-shielded doors shall be located as close to the ceiling as possible in a lateral barrier as far from isocenter as practical. The exterior of the vault must not be visible from isocenter through this penetration, and no more than 10% of the area of the penetration exterior opening must be visible from the target at any gantry position. The ducting bottom and sides shall be shielded with a baffle containing 2" lead and 4" borated polyethylene (BPE). The baffle must include at least one 90° bend, with the BPE outside the lead (toward isocenter) in the shielding baffle. The baffle length must be sufficient to ensure direct leakage from any target position must pass through the baffle to reach the penetration entrance (this generally requires the baffle length to be at least twice the larger penetration dimension).

There must be sufficient ventilation to provide at least three room air changes per hour to prevent build-up of ozone in the treatment room.

Emergency power or battery back-up is required for the door.

The linac vault shall be equipped with one red beam-on warning signal light inside the vault and one visible at the control console.

The linac vault shall be posted with "CAUTION X-RAY" signs.

The door at the vault entrance shall be interlocked to prevent beam-on if the door is open.

The linac vault shall be equipped with emergency off buttons.

The vault shall be equipped with two independent video systems for remote viewing of the patient.

The vault shall be equipped with an intercom system to maintain audio contact with the patient during treatment.

A last person out switch should be located inside the room and near the door.

An interior radiation monitor mounted in the treatment room so that it is visible from the room shall be provided. There should also be a remote radiation monitor located outside the treatment room.

Comments

Radiation exposures are calculated not to exceed 0.1 mSv per week for all occupational radiation workers and 0.02 mSv per week for both the public and general employees of the facility, as recommended by current California Radiation Control Regulations and by reference 10 CFR 20 for public and occupational occupancy.

The state radiological protection agency requires that a representative of the facility submit this report and facility drawings for review and approval before construction begins. This review and approval process may require as long as two months. A copy of this report must remain on file in the Department of Radiation Oncology.

The workload assumed in this report is a conservatively-high estimate of the planned machine usage that has been reviewed by the organization that will be operating the linear accelerator. The access designation of locations (public, controlled, or restricted), along with the associated occupancy, have been reviewed by the organization that will be operating the linear accelerator.

The energy rating of the particle accelerators assumes the BJR #11 megavoltage (MV) definition. X-ray leakage is assumed to be a maximum of 0.1% of the useful beam at isocenter. Neutron leakage is negligible at 6 MV.

The calculations are per NCRP 151 and are based on the supplied architectural drawings. Deviation in the construction from these drawings will require further review.

Wall shielding distances are calculated from isocenter to a position at one foot beyond the exterior surface of the wall for which the calculation applies.

The floor is slab on grade, with zero occupancy beneath the vault.

The total patient workload per day (8) is equivalent to 40 patient treatments per week. Assuming a maximum of 2 patient treatments per hour, any uncontrolled access location with occupancy greater than

$$T_{min} = 2/40 = 0.05 \quad \text{(or equivalently } P/T_{max} = 0.02 \times 40/2 = 0.400 \text{ mSv/wk)}$$

will be constrained by the average weekly workload, not the maximum workload in any hour requirement. All locations in this report have an assumed occupancy of at least 0.05, and are therefore constrained by the average weekly workload, not the maximum workload in any hour.

A preliminary radiation survey shall be performed by a qualified radiological physicist immediately after the accelerator has been made operational to ensure there are no radiation hazards to the installation engineer and other personnel working in the vicinity of the facility.

A complete radiation survey must be performed by a qualified radiological physicist after the linear accelerator output is fully operational.

5/18/2017
AUBNMC - Cyberknife.xlsm

Page 9
Comments

Therapy Physics, Inc.
310-217-4114

Recommendations

All walls of a Cyberknife vault are potentially considered primary barriers. However physical constraints of the robotic arm make it essentially incapable of pointing toward the wall behind the robotic arm. If there are no pre-configured treatment nodes in the direction of the wall behind the robotic arm, it can be considered a secondary-only barrier. If the robotic arm is located so the back wall is toward the entrance, the door will require significantly less shielding. Since the control area is typically beyond the entrance wall, this may also decrease staff exposure.

The isocenter location is tentatively assumed to be located at approximately the location indicated on Page 3, with the entrance wall behind the robotic arm. If the entrance wall is assumed to be a secondary barrier (i.e., not pre-configured treatment nodes toward the west wall) 1300 mm concrete thickness is recommended for the west wall. If the west wall is considered to be a primary barrier (no pointing constraints), 1600 mm thickness recommended. Similarly the door requires 9" lead if the west wall is a primary barrier vs. 7" as a secondary barrier. Note that groundshine may result in an unacceptably high dose rate if there is a pre-configured treatment node directed toward the bottom of the door.

The Vault 2 secondary barriers should be increased to 1600 mm thick to protect Vault 2 from the Cyberknife. The south wall of the Cyberknife vault should be increased to 1800 thick to protect the Control area to the south to full occupancy. The portion of the the south wall protecting the Brachy room can be 1600 mm instead of 1800 mm if desired.

If there is occupancy below the Cyberknife vault, a primary barrier will be required for the floor.

The ceiling is a secondary-only barrier. The thickness required will depend on the distance to the nearest high occupany location above the vault, but is tentatively recommended to be 1400 to 1200 mm thick, as illustrated on Page 4.

CyberKnife Calculations

The CyberKnife system combines a small 6 MV linear particle accelerator with a robotic arm that allows the energy to be directed at any part of the body from any direction. The field size ranges from 5 mm to 60 mm at 80 cm from the target, with 60 mm assumed for shielding calculations. The relatively small field size compared to a conventional linear accelerator results in a relatively low use factor in any particular direction, with U = 0.05 recommended by NCRP 151 for shielding calculations. Any wall can be considered to be a primary barrier.

The CyberKnife system invariably uses IMRT, with an IMRT ratio of 15 MU per cGy considered typical. Because of the high leakage dose rate and the relatively low primary use factor, both primary and secondary barrier calculation are performed for each wall, with the results added to yield the total dose rate. Scatter is negligible for walls, and is not included in the wall calculations.

The Cyberknife beam will not point higher than 22° above horizontal. The beams will also pass within 12 cm of the room isocenter. Thus, the highest intersection with a wall would be a beam with an angle 22 degrees above horizontal, traveling through a point 12 cm above the room isocenter and striking the closest wall to the isocenter. The room isocenter is 3' 1/4" above the floor. This implies only a secondary calculation is appropriate for the ceiling in most cases.

The Cyberknife has a variable target to isocenter distance (or source-axis-distance (SAD)) that varies between 65 cm to 120 cm. The shielding calculations assume an 80 cm SAD (considered to be the nominal value of SAD). A typical workload per session (e.g., 20 Gy per treatment) is considered to be delivered at 80 cm from the target, with the workload normalized to 1 meter for shielding calculations. The typical patient workload cited by NCRP 151 is 8 patients per day. A maximum of 2 treatment sessions per hour is assumed for compliance with the NRC dose rate per hour requirement.

The Cyberknife system is programmed by Accuray to point only in specific pre-configured treatment nodes. In some cases a facility may restrict the treatment nodes available to avoid pointing in a particular direction (e.g., the back wall or toward the entrance). If such a pointing constraint is imposed, only a secondary barrier calculation is required in the direction not having any treatment nodes.

Workload and Maximum Shielded Dose Rate
The dose rate reaching a protected location is directly proportional to the linear accelerator workload. The *workload* (**W**), specified in Gy/wk, is the absorbed-dose rate at the depth of maximum dose, 1 meter from the target. It is calculated by multiplying the patient workload (*patients per day* as indicated on the summary page of this report) times the workload per patient treatment (*Workload Gy/pt*, also on the summary page) times 5 days per work week. The default workload per patient treatment is 8 Gy per patient treatment normalized to 1 meter SAD.

The *shielding design goal* (**P**) is a practical reference limit (or dose constraint) on the dose rate calculated beyond a protective barrier. A *controlled area* is a limited-access area in which the occupational exposure of personnel to radiation or radioactive material is under the supervision of an individual in charge of radiation protection. NCRP 151 recommends a 0.1 mSv/wk shielding design goal for controlled areas. NCRP 151 recommends a 0.02 mSv/wk shielding design goal for uncontrolled areas.

A *protected location* is a location outside the therapy vault that may be occupied. For walls, this is customarily considered to be no closer to isocenter than 1 foot (0.3 m) beyond the barrier. For ceilings, this is considered to be no closer to isocenter than 1.5 feet (0.5 m) above the floor of the room above. For floors, it is considered to be no closer to isocenter than 5.5 feet (1.7 m) above the floor of the room below.

Occupancy factor reflects the fraction of time a particular location may be occupied. The maximum permissible value of shielded dose rate at a location with occupancy T is given by P/T. It is traditional to refer to the maximum shielded dose rate simply as **P/T**.

The NRC requires that shielded dose rate at any unrestricted location must not exceed 0.02 mSv in any hour. Based on NCRP 151 Equation 3.14, the maximum dose rate in any hour (R_h) is given by Equation 1, where N_{max} is the maximum number of patient treatments per hour, N_w is the average number of patient treatments per week, and R_w is the shielded dose rate per week.

$$R_h = (N_{max} / N_w) \, R_w \leq 0.02 \text{ mSv/hr} \qquad (1)$$

The 0.02 mSv in any hour requirement effectively places an upper limit on the weekly P/T limit, as given by Equation 2.

$$R_w \leq 0.02 \text{ mSv/hr} \, (N_w / N_{max}) = (P/T)_{max} \qquad (2)$$

The maximum value of P/T in turn implies a limit on the minimum occupancy permitted for an uncontrolled area, given by Equation 3.

$$T_{min} = N_{max} / N_w \qquad (3)$$

Primary Barrier Calculations

The primary barrier calculations use the geometry illustrated in Figure 1.
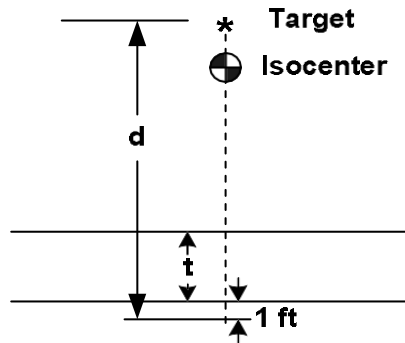
Figure 1. Primary Barrier Distances

The *unshielded dose rate* (**H_{ux}**) in Sv/wk is given by Equation 1.

$$H_{ux} \quad = \quad \frac{W\,U}{d^2} \tag{1}$$

In Equation 1, **W** is the *workload* (measured 1 meter from the target) in Gy/wk, **U** is the *use factor*, and **d** (the *target to protected point distance*) is the distance from the target to the protected point in meters.

The *shielded X-ray dose rate* (**H_{tr}**) (i.e., the calculated transmitted x-ray dose equivalent rate) is given by Equation 2.

$$H_{tr} \quad = \quad H_{ux}\,B \tag{2}$$

In Equation 2, B is the x-ray transmission factor for the barrier. The transmission factor is calculated separately for each layer of material in the barrier, with B the calculated by multiplying the transmission factor for these layers together. The transmission factor for layer i is given by:

$$B_i \quad = \quad 10^\wedge[-t_{i1}/TVL_1] \times 10^\wedge[-t_{ie}/TVL_e] \tag{3}$$

where TVL_1 is the first tenth-value layer thickness, TVL_e is the thickness for each subsequent tenth-value layer, t_i is the thickness of layer i of the barrier, t_{i1} is the amount of t_i (if any) that falls within the first TVL of the barrier, and t_{ie} is t_i - t_{i1}. Following the guidance in Example 7.2 of NCRP 151, the hardened 6 MV primary TVLs are used for both TVL_e and TVL_1 for a Cyberknife.

If the distance traveled through the protected point is at a slant angle (θ), then the distance t is increased by the slant factor $1/\cos(\theta)$, with the resulting thickness termed the slant thickness. As θ increases, scatter can cause the shielded dose to be underestimated if calculated using slant thickness alone. To compensate for this, the slant thickness is divided by an obliquity factor (Table 1), with the result termed the oblique thickness. Note that both the oblique thicknesses and TVLs are included at the bottom of the page, with both given in millimeters. The obliquity factors are based on Biggs (1996), with Biggs values at 45° modified to comply with the NCRP 151 recommendation to add 2 HVL at low MV and 1 HVL at high MV for angles above 45 degrees. Interpolation is used at MVs between the values given in Table 1.

Experience indicates margin for H_{tr} should be recommended for all primary barriers to compensate for variation in the density of the barrier material. It is recommended that the product of H_{tr} and the recommended margin be no greater than P/T. Note that the *minimum outside barrier layer* does not include recommended margin.

Table 1. Obliquity Factor

Angle	Lead			Concrete			Steel		
	4 MV	10 MV	18 MV	4 MV	10 MV	18 MV	4 MV	10 MV	18 MV
0	1.00	1.00	1.00	1.00	1.00	1.00	1.00	1.00	1.00
30	1.03	1.02	1.03	1.02	1.00	1.00	1.02	1.02	1.04
45	1.12	1.12	1.10	1.12	1.12	1.06	1.12	1.12	1.08
60	1.21	1.21	1.22	1.20	1.14	1.08	1.20	1.17	1.20
70	1.44	1.47	1.52	1.47	1.28	1.22	1.48	1.42	1.45

The *minimum outside barrier layer* is the minimum thickness of the outside layer of material in the barrier required to make H_{tr} no greater than P/T. The *recommended outside layer* is the actual thickness of the outside layer used to calculate the shielded dose rate.

Experience indicates margin for H_{tr} should be recommended for all primary barriers to compensate for variation in the density of the barrier material. It is recommended that the product of H_{tr} and the recommended margin be no greater than P/T. Note that the *minimum outside barrier layer* does not include recommended margin.

Secondary Barrier Calculations

Typically, secondary radiation comes from two sources: leakage from the shielding around the target and scattered radiation from the patient. However, because of the Cyberknife small field size, scatter is negligible and it is not included in the calculations. Since the accelerator energy is less than 10 MV, neutron leakage is also not applicable. The secondary barrier unshielded dose rate for lateral secondary barriers is calculated using the geometry in Figure 1.
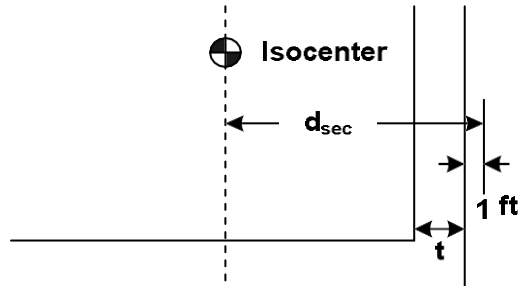
Figure 1. Secondary Barrier Distance

The *x-ray leakage unshielded dose rate* due to leakage from the target (H_{UL}) in Sv/wk is given by Equation 1.

$$H_{UL} = \frac{W_L \, 10^{-3}}{d_{sec}^2} \tag{1}$$

The 10^{-3} factor (the *x-ray leakage fraction*) reflects the standard manufacturer's requirement that the average x-ray leakage outside the beam must be less than 0.1% of the dose rate at isocenter. Note that x-ray leakage is typically on the order of a factor of 4 to 5 lower than the requirement. The *x-ray leakage workload* (W_L) is equal to the conventional workload (W) if IMRT is not used.

Intensity Modulated Radiation Therapy (IMRT) requires an increase in monitor units (MU) compared to conventional radiation therapy. The *IMRT ratio* (the ratio of MU to cGy at isocenter when IMRT is used) is given on the summary page of this report, with a value of unity indicating no IMRT. The *IMRT factor* is the average IMRT ratio, given by:

$$\text{X-Ray IMRT Factor} = \text{IMRT Ratio} \times \% \text{ IMRT} + (1 - \% \text{IMRT}) \tag{2}$$

The *x-ray leakage workload* (W_L) is then given by:

$$W_L = W \times \text{X-Ray IMRT Factor} \tag{3}$$

The *x-ray leakage shielded dose rate* (H_L) is given by Equation 4.

$$H_L = H_{UL} \, B_L \tag{4}$$

Here B_L is the leakage transmission calculated from the x-ray leakage TVL_1 and TVL_2 given at the bottom of the each page of calculations using the same procedure used to calculate the primary barrier transmission. The lead leakage TVLs come from the Accuray White Paper *Tenth-Value Layer Measurements of Leakage Radiation and Secondary Barrier Shielding Calculations fort the CyberKnife® Robotic Radiosurgery System*. Note that these concrete TVLs are somewhat larger than the values recommended in NCRP 151 Table B.7.

Protected Location: **A - Corridor (if primary)**

Distance from Isocenter to Location (d): 5.5 m	X-ray Energy (MV): 6	
Workload (W) (Gy/wk): 768	Occupancy Factor (T): 0.2	
X-Ray Leakage Workload (Gy / wk): 18000	**Dose Constraint (P) (mSv / wk): 0.020**	
	X-Ray Leakage Fraction: 1.00E-03	

Slant (deg)

Inside Barrier Layer:	_____ mm	0	Material:	_____
Barrier Layer #2:	_____ mm		Material:	_____
Barrier Layer #3:	_____ mm		Material:	_____
Barrier Layer #4:	_____ mm		Material:	_____
Min Recommend Outside Barrier Layer:	1468 mm	0	Material:	Concrete
Outside Barrier Layer:	1600 mm	0	Material:	Concrete

Shielded Primary Dose Rate (mSv/wk): 0.014	Shielded Sec Dose Rate (mSv / wk): 0.002
Recommended Primary Margin: 2.7	**Shielded Dose Rate (mSv/wk): 0.039**

Shielded TADR including occupancy (mSv/wk): 0.008

Additional values used in shielded dose rate calculation

	Primary	*Leakage*
Use Factor:	0.05	1
Unshielded Dose Rate (mSv/wk):	969.81	595.04
Slant (mm)	Transmission	Transmission
Inside Barrier Layer: 0	1.00E+00	1.00E+00
Barrier Layer #2: 0	1.00E+00	1.00E+00
Barrier Layer #3: 0	1.00E+00	1.00E+00
Barrier Layer #4: 0	1.00E+00	1.00E+00
Outside Barrier Layer: 1600	1.42E-05	3.93E-06
Total:	1.42E-05	3.93E-06

	Oblique Thickness (mm)	Primary TVL (mm) TVL1	TVLe	Leakage TVL (mm) TVL1	TVLe
Inside Barrier Layer:	0				
Barrier Layer #2:	0				
Barrier Layer #3:	0				
Barrier Layer #4:	0				
Outside Barrier Layer:	1600	330	330	296	296

Protected Location: **A2 - Control (if primary)**

Distance from Isocenter to Location (d): _____8.5_____ m   X-ray Energy (MV): _____6_____

Workload (W) (Gy/wk): _____768_____   Occupancy Factor (T): _____1_____

X-Ray Leakage Workload (Gy / wk): _____18000_____   **Dose Constraint (P) (mSv / wk):   0.020**

X-Ray Leakage Fraction: 1.00E-03

Slant (deg)

Inside Barrier Layer:	_____ mm	0	Material:	_____
Barrier Layer #2:	_____ mm		Material:	_____
Barrier Layer #3:	_____ mm		Material:	_____
Barrier Layer #4:	_____ mm		Material:	_____
Min Recommend Outside Barrier Layer:	1585 mm	0	Material:	Concrete
Outside Barrier Layer:	1600 mm	0	Material:	Concrete

Shielded Primary Dose Rate (mSv/wk): _____0.006_____   Shielded Sec Dose Rate (mSv / wk): _____0.001_____

Recommended Primary Margin: _____2.7_____   **Shielded Dose Rate (mSv/wk):   0.018**

Shielded TADR including occupancy (mSv/wk):   0.018

Additional values used in shielded dose rate calculation

	Primary	*Leakage*
Use Factor:	0.05	1
Unshielded Dose Rate (mSv/wk):	444.70	249.13

	Slant (mm)	Transmission	Transmission
Inside Barrier Layer:	0	1.00E+00	1.00E+00
Barrier Layer #2:	0	1.00E+00	1.00E+00
Barrier Layer #3:	0	1.00E+00	1.00E+00
Barrier Layer #4:	0	1.00E+00	1.00E+00
Outside Barrier Layer:	1600	1.42E-05	3.93E-06
Total:		1.42E-05	3.93E-06

	Oblique Thickness (mm)	Primary TVL (mm) TVL1	TVLe	Leakage TVL (mm) TVL1	TVLe
Inside Barrier Layer:	0				
Barrier Layer #2:	0				
Barrier Layer #3:	0				
Barrier Layer #4:	0				
Outside Barrier Layer:	1600	330	330	296	296

Protected Location: **B - Vault 2**

Distance from Isocenter to Location (d): 5.9 m	X-ray Energy (MV): 6	
Workload (W) (Gy/wk): 768	Occupancy Factor (T): 0.5	
X-Ray Leakage Workload (Gy / wk): 18000	**Dose Constraint (P) (mSv / wk): 0.020**	
	X-Ray Leakage Fraction: 1.00E-03	

Slant (deg)

Inside Barrier Layer: _____ mm	0	Material: _____		
Barrier Layer #2: _____ mm		Material: _____		
Barrier Layer #3: _____ mm		Material: _____		
Barrier Layer #4: _____ mm		Material: _____		
Min Recommend Outside Barrier Layer: 1581 mm	0	Material: Concrete		
Outside Barrier Layer: 1600 mm	0	Material: Concrete		

Shielded Primary Dose Rate (mSv/wk): 0.012	Shielded Sec Dose Rate (mSv / wk): 0.002
Recommended Primary Margin: 2.7	**Shielded Dose Rate (mSv/wk): 0.035**
	Shielded TADR including occupancy (mSv/wk): 0.017

Additional values used in shielded dose rate calculation

	Primary	*Leakage*
Use Factor:	0.05	1
Unshielded Dose Rate (mSv/wk):	857.35	517.09
Slant (mm)	Transmission	Transmission
Inside Barrier Layer: 0	1.00E+00	1.00E+00
Barrier Layer #2: 0	1.00E+00	1.00E+00
Barrier Layer #3: 0	1.00E+00	1.00E+00
Barrier Layer #4: 0	1.00E+00	1.00E+00
Outside Barrier Layer: 1600	1.42E-05	3.93E-06
Total:	1.42E-05	3.93E-06

	Oblique Thickness (mm)	Primary TVL (mm)		Leakage TVL (mm)	
		TVL1	TVLe	TVL1	TVLe
Inside Barrier Layer:	0				
Barrier Layer #2:	0				
Barrier Layer #3:	0				
Barrier Layer #4:	0				
Outside Barrier Layer:	1600	330	330	296	296

Protected Location: **C - Vault 2**

Distance from Isocenter to Location (d):	6.5 m		X-ray Energy (MV):	6
Workload (W) (Gy/wk):	768		Occupancy Factor (T):	0.5
X-Ray Leakage Workload (Gy / wk):	18000		**Dose Constraint (P) (mSv / wk):**	**0.020**
			X-Ray Leakage Fraction:	1.00E-03

Slant (deg)

Inside Barrier Layer:		mm	0	Material:	
Barrier Layer #2:		mm		Material:	
Barrier Layer #3:		mm		Material:	
Barrier Layer #4:		mm		Material:	
Min Recommend Outside Barrier Layer:	1556	mm	0	Material:	Concrete
Outside Barrier Layer:	2200	mm	0	Material:	Concrete

Shielded Primary Dose Rate (mSv/wk):	0.000	Shielded Sec Dose Rate (mSv / wk):	0.000
Recommended Primary Margin:	2.7	**Shielded Dose Rate (mSv/wk):**	**0.000**
		Shielded TADR including occupancy (mSv/wk):	**0.000**

Additional values used in shielded dose rate calculation

		Primary	***Leakage***
Use Factor:		0.05	1
Unshielded Dose Rate (mSv/wk):		722.07	426.04
	Slant (mm)	Transmission	Transmission
Inside Barrier Layer:	0	1.00E+00	1.00E+00
Barrier Layer #2:	0	1.00E+00	1.00E+00
Barrier Layer #3:	0	1.00E+00	1.00E+00
Barrier Layer #4:	0	1.00E+00	1.00E+00
Outside Barrier Layer:	2200	2.15E-07	3.69E-08
Total:		2.15E-07	3.69E-08

	Oblique Thickness (mm)	Primary TVL (mm) TVL1	TVLe	Leakage TVL (mm) TVL1	TVLe
Inside Barrier Layer:	0				
Barrier Layer #2:	0				
Barrier Layer #3:	0				
Barrier Layer #4:	0				
Outside Barrier Layer:	2200	330	330	296	296

Protected Location: **D - Vault 2**

Distance from Isocenter to Location (d): ___6.8___ m   X-ray Energy (MV): ___6___

Workload (W) (Gy/wk): ___768___   Occupancy Factor (T): ___0.5___

X-Ray Leakage Workload (Gy / wk): ___18000___   **Dose Constraint (P) (mSv / wk):** ___**0.020**___

X-Ray Leakage Fraction: ___1.00E-03___

Slant (deg)

Inside Barrier Layer:	_____ mm	30	Material:	_____
Barrier Layer #2:	_____ mm		Material:	_____
Barrier Layer #3:	_____ mm		Material:	_____
Barrier Layer #4:	_____ mm		Material:	_____
Min Recommend Outside Barrier Layer:	1354 mm	30	Material:	Concrete
Outside Barrier Layer:	1600 mm	30	Material:	Concrete

Shielded Primary Dose Rate (mSv/wk): ___0.002___   Shielded Sec Dose Rate (mSv / wk): ___0.000___

Recommended Primary Margin: ___2.7___   **Shielded Dose Rate (mSv/wk):** ___**0.006**___

Shielded TADR including occupancy (mSv/wk): ___**0.003**___

Additional values used in shielded dose rate calculation

		Primary	*Leakage*
Use Factor:		0.05	1
Unshielded Dose Rate (mSv/wk):		663.91	387.82
	Slant (mm)	Transmission	Transmission
Inside Barrier Layer:	0	1.00E+00	1.00E+00
Barrier Layer #2:	0	1.00E+00	1.00E+00
Barrier Layer #3:	0	1.00E+00	1.00E+00
Barrier Layer #4:	0	1.00E+00	1.00E+00
Outside Barrier Layer:	1848	2.99E-06	5.73E-07
Total:		2.99E-06	5.73E-07

	Oblique Thickness (mm)	Primary TVL (mm)		Leakage TVL (mm)	
		TVL1	TVLe	TVL1	TVLe
Inside Barrier Layer:	0				
Barrier Layer #2:	0				
Barrier Layer #3:	0				
Barrier Layer #4:	0				
Outside Barrier Layer:	1823	330	330	296	296

Protected Location: **E - Exterior (below ground)**

Distance from Isocenter to Location (d):	8.0	m		X-ray Energy (MV):	6
Workload (W) (Gy/wk):	768			Occupancy Factor (T):	0.05
X-Ray Leakage Workload (Gy / wk):	18000			**Dose Constraint (P) (mSv / wk):**	**0.020**
				X-Ray Leakage Fraction:	1.00E-03

Slant (deg)

Inside Barrier Layer:	600	mm	0	Material:	Concrete
Barrier Layer #2:		mm		Material:	
Barrier Layer #3:		mm		Material:	
Barrier Layer #4:		mm		Material:	
Min Recommend Outside Barrier Layer:	901	mm	0	Material:	Earth
Outside Barrier Layer:	2000	mm	0	Material:	Earth
Shielded Primary Dose Rate (mSv/wk):	0.001		Shielded Sec Dose Rate (mSv / wk):		0.000
Recommended Primary Margin:	2.7		**Shielded Dose Rate (mSv/wk):**		**0.003**
			Shielded TADR including occupancy (mSv/wk):		**0.000**

Additional values used in shielded dose rate calculation

	Primary	*Leakage*
Use Factor:	0.05	1
Unshielded Dose Rate (mSv/wk):	496.72	281.25

	Slant (mm)	Transmission	Transmission
Inside Barrier Layer:	600	1.52E-02	9.40E-03
Barrier Layer #2:	0	1.00E+00	1.00E+00
Barrier Layer #3:	0	1.00E+00	1.00E+00
Barrier Layer #4:	0	1.00E+00	1.00E+00
Outside Barrier Layer:	2000	1.35E-04	4.89E-05
Total:		2.06E-06	4.60E-07

	Oblique Thickness (mm)	Primary TVL (mm)		Leakage TVL (mm)	
		TVL1	TVLe	TVL1	TVLe
Inside Barrier Layer:	600	330	330	296	296
Barrier Layer #2:	0				
Barrier Layer #3:	0				
Barrier Layer #4:	0				
Outside Barrier Layer:	2000	517	517	464	464

Protected Location: **F - Brachy room**

Distance from Isocenter to Location (d):	6.4 m		X-ray Energy (MV):	6
Workload (W) (Gy/wk):	768		Occupancy Factor (T):	0.5
X-Ray Leakage Workload (Gy / wk):	18000		**Dose Constraint (P) (mSv / wk):**	**0.020**
			X-Ray Leakage Fraction:	1.00E-03

Slant (deg)

Inside Barrier Layer:	_____ mm	20	Material:	_____
Barrier Layer #2:	_____ mm		Material:	_____
Barrier Layer #3:	_____ mm		Material:	_____
Barrier Layer #4:	_____ mm		Material:	_____
Min Recommend Outside Barrier Layer:	1479 mm	20	Material:	Concrete
Outside Barrier Layer:	1600 mm	20	Material:	Concrete
Shielded Primary Dose Rate (mSv/wk):	0.006	Shielded Sec Dose Rate (mSv / wk):		0.001
Recommended Primary Margin:	2.7	**Shielded Dose Rate (mSv/wk):**		**0.016**
		Shielded TADR including occupancy (mSv/wk):		**0.008**

Additional values used in shielded dose rate calculation

		Primary	*Leakage*
Use Factor:		0.05	1
Unshielded Dose Rate (mSv/wk):		745.38	441.51
	Slant (mm)	Transmission	Transmission
Inside Barrier Layer:	0	1.00E+00	1.00E+00
Barrier Layer #2:	0	1.00E+00	1.00E+00
Barrier Layer #3:	0	1.00E+00	1.00E+00
Barrier Layer #4:	0	1.00E+00	1.00E+00
Outside Barrier Layer:	1703	7.69E-06	1.77E-06
Total:		7.69E-06	1.77E-06

	Oblique Thickness (mm)	Primary TVL (mm)		Leakage TVL (mm)	
		TVL1	TVLe	TVL1	TVLe
Inside Barrier Layer:	0				
Barrier Layer #2:	0				
Barrier Layer #3:	0				
Barrier Layer #4:	0				
Outside Barrier Layer:	1688	330	330	296	296

Protected Location: **G - Brachy control**

Distance from Isocenter to Location (d):	6.0 m		X-ray Energy (MV):	6
Workload (W) (Gy/wk):	768		Occupancy Factor (T):	1
X-Ray Leakage Workload (Gy / wk):	18000		**Dose Constraint (P) (mSv / wk):**	**0.020**
			X-Ray Leakage Fraction:	1.00E-03

Slant (deg)

Inside Barrier Layer:		mm	0	Material:	
Barrier Layer #2:		mm		Material:	
Barrier Layer #3:		mm		Material:	
Barrier Layer #4:		mm		Material:	
Min Recommend Outside Barrier Layer:	1675	mm	0	Material:	Concrete
Outside Barrier Layer:	1800	mm	0	Material:	Concrete

Shielded Primary Dose Rate (mSv/wk):	0.003	Shielded Sec Dose Rate (mSv / wk):	0.000
Recommended Primary Margin:	2.7	**Shielded Dose Rate (mSv/wk):**	**0.008**
		Shielded TADR including occupancy (mSv/wk):	**0.008**

Additional values used in shielded dose rate calculation

		Primary	*Leakage*
Use Factor:		0.05	1
Unshielded Dose Rate (mSv/wk):		832.29	500.00
	Slant (mm)	Transmission	Transmission
Inside Barrier Layer:	0	1.00E+00	1.00E+00
Barrier Layer #2:	0	1.00E+00	1.00E+00
Barrier Layer #3:	0	1.00E+00	1.00E+00
Barrier Layer #4:	0	1.00E+00	1.00E+00
Outside Barrier Layer:	1800	3.51E-06	8.30E-07
Total:		3.51E-06	8.30E-07

	Oblique Thickness (mm)	Primary TVL (mm)		Leakage TVL (mm)	
		TVL1	TVLe	TVL1	TVLe
Inside Barrier Layer:	0				
Barrier Layer #2:	0				
Barrier Layer #3:	0				
Barrier Layer #4:	0				
Outside Barrier Layer:	1800	330	330	296	296

Secondary Barrier Protected Location: **A - Corridor**

Secondary Distance (d):	5.5 m	X-ray Energy (MV):	6
Workload (W) (Gy / wk):	768	Occupancy Factor (T):	0.2
X-Ray Leakage Workload (Gy / wk):	18000	**Dose Constraint (P) (mSv / wk):**	**0.020**
		X-Ray Leakage Fraction:	1.00E-03

Slant (deg)

Inside Barrier Layer:	____ mm	0	Material:	____
Barrier Layer #2:	____ mm		Material:	____
Barrier Layer #3:	____ mm		Material:	____
Barrier Layer #4:	____ mm		Material:	____
Minimum Outside Barrier Layer:	1118 mm	0	Material:	Concrete
Outside Barrier Layer:	1300 mm	0	Material:	Concrete

Shielded Dose Rate (mSv / wk): **0.024**

Shielded TADR including occupancy (mSv / wk): **0.005**

Additional values used in shielded dose rate calculation

Leakage

Use Factor:	1
Unshielded Dose Rate (mSv/wk):	595.04

	Slant (mm)	Transmission
Inside Barrier Layer:	0	1.00E+00
Barrier Layer #2:	0	1.00E+00
Barrier Layer #3:	0	1.00E+00
Barrier Layer #4:	0	1.00E+00
Outside Barrier Layer:	1300	4.06E-05
Total:		4.06E-05

0.0241

	TVL1 (mm)	TVLe (mm)
Inside Barrier Layer:		
Barrier Layer #2:		
Barrier Layer #3:		
Barrier Layer #4:		
Outside Barrier Layer:	296	296

Secondary Barrier Protected Location: **A2 - Control**

Secondary Distance (d):	8.5	m	X-ray Energy (MV):	6
Workload (W) (Gy / wk):	768		Occupancy Factor (T):	1
X-Ray Leakage Workload (Gy / wk):	18000		**Dose Constraint (P) (mSv / wk):**	**0.020**
			X-Ray Leakage Fraction:	1.00E-03

Slant (deg)

Inside Barrier Layer:		mm	0	Material:	
Barrier Layer #2:		mm		Material:	
Barrier Layer #3:		mm		Material:	
Barrier Layer #4:		mm		Material:	
Minimum Outside Barrier Layer:	1213	mm	0	Material:	Concrete
Outside Barrier Layer:	1300	mm	0	Material:	Concrete

Shielded Dose Rate (mSv / wk): **0.010**

Shielded TADR including occupancy (mSv / wk): **0.010**

Additional values used in shielded dose rate calculation

Leakage

Use Factor:	1
Unshielded Dose Rate (mSv/wk):	249.13

	Slant (mm)	Transmission
Inside Barrier Layer:	0	1.00E+00
Barrier Layer #2:	0	1.00E+00
Barrier Layer #3:	0	1.00E+00
Barrier Layer #4:	0	1.00E+00
Outside Barrier Layer:	1300	4.06E-05
Total:		4.06E-05

0.0101

	TVL1 (mm)	TVLe (mm)
Inside Barrier Layer:		
Barrier Layer #2:		
Barrier Layer #3:		
Barrier Layer #4:		
Outside Barrier Layer:	296	296

Secondary Barrier Protected Location: **P - Above isocenter**

Secondary Distance (d):	5.8 m	X-ray Energy (MV):	6
Workload (W) (Gy / wk):	768	Occupancy Factor (T):	1
X-Ray Leakage Workload (Gy / wk):	18000	**Dose Constraint (P) (mSv / wk):**	**0.020**
		X-Ray Leakage Fraction:	1.00E-03

Slant (deg)

Inside Barrier Layer:	_____ mm	0	Material:	_____
Barrier Layer #2:	_____ mm		Material:	_____
Barrier Layer #3:	_____ mm		Material:	_____
Barrier Layer #4:	_____ mm		Material:	_____
Minimum Outside Barrier Layer:	1311 mm	0	Material:	Concrete
Outside Barrier Layer:	1400 mm	0	Material:	Concrete

Shielded Dose Rate (mSv / wk): **0.010**

Shielded TADR including occupancy (mSv / wk): **0.010**

Additional values used in shielded dose rate calculation

Leakage

Use Factor:	1
Unshielded Dose Rate (mSv/wk):	535.08

	Slant (mm)	Transmission
Inside Barrier Layer:	0	1.00E+00
Barrier Layer #2:	0	1.00E+00
Barrier Layer #3:	0	1.00E+00
Barrier Layer #4:	0	1.00E+00
Outside Barrier Layer:	1400	1.86E-05
Total:		1.86E-05

0.0100

	TVL1 (mm)	TVLe (mm)
Inside Barrier Layer:		
Barrier Layer #2:		
Barrier Layer #3:		
Barrier Layer #4:		
Outside Barrier Layer:	296	296

Secondary Barrier Protected Location: **S - Above isocenter**

Secondary Distance (d):	5.3	m		X-ray Energy (MV):	6
Workload (W) (Gy / wk):	768			Occupancy Factor (T):	1
X-Ray Leakage Workload (Gy / wk):	18000			**Dose Constraint (P) (mSv / wk):**	**0.020**
				X-Ray Leakage Fraction:	1.00E-03

Slant (deg)

Inside Barrier Layer:		mm	28	Material:	
Barrier Layer #2:		mm		Material:	
Barrier Layer #3:		mm		Material:	
Barrier Layer #4:		mm		Material:	
Minimum Outside Barrier Layer:	1178	mm	28	Material:	Concrete
Outside Barrier Layer:	1200	mm	28	Material:	Concrete

Shielded Dose Rate (mSv / wk): 0.016

Shielded TADR including occupancy (mSv / wk): 0.016

Additional values used in shielded dose rate calculation

Leakage

Use Factor:	1
Unshielded Dose Rate (mSv/wk):	640.80

	Slant (mm)	Transmission
Inside Barrier Layer:	0	1.00E+00
Barrier Layer #2:	0	1.00E+00
Barrier Layer #3:	0	1.00E+00
Barrier Layer #4:	0	1.00E+00
Outside Barrier Layer:	1359	2.56E-05
Total:		2.56E-05

0.0164

	TVL1 (mm)	TVLe (mm)
Inside Barrier Layer:		
Barrier Layer #2:		
Barrier Layer #3:		
Barrier Layer #4:		
Outside Barrier Layer:	296	296

Direct-Shielded Door Calculations

If the vault has no maze, the adequacy of the entrance door is assessed with a secondary barrier calculation. The door will invariably include lead to attenuate the x-rays with steel covers. Unless the door is designed to potentially accommodate a future high energy linear accelerator (> 6 MV), borated polyethylene is not required since neutron shielding is not required for a Cyberknife. In some cases, a stub wall (also sometimes referred to as a nib wall) may extend out from the wall next to the entrance, which decreases the required door thickness.

A direct-shielded door will typically be adjusted to leave 1/4" gap at the vertical location on the wall having least clearance. A maximum gap of 1/2" between wall and door is expected after allowing for fit-and-finish in the wall construction. A maximum gap of 3/4" is permissible based on the NCRP 151 recommendation of a 10-to-1 ratio of door overlap to maximum gap.

The limited overlap of the door with the entrance to the accelerator room requires additional specialized shielding. As illustrated in Figure 1, a direct leakage path occurs at the far lateral edge of the door. To compensate for the short slant thickness at corner of the entrance, additional material is typically added in two different locations, as shown in Figure 2.
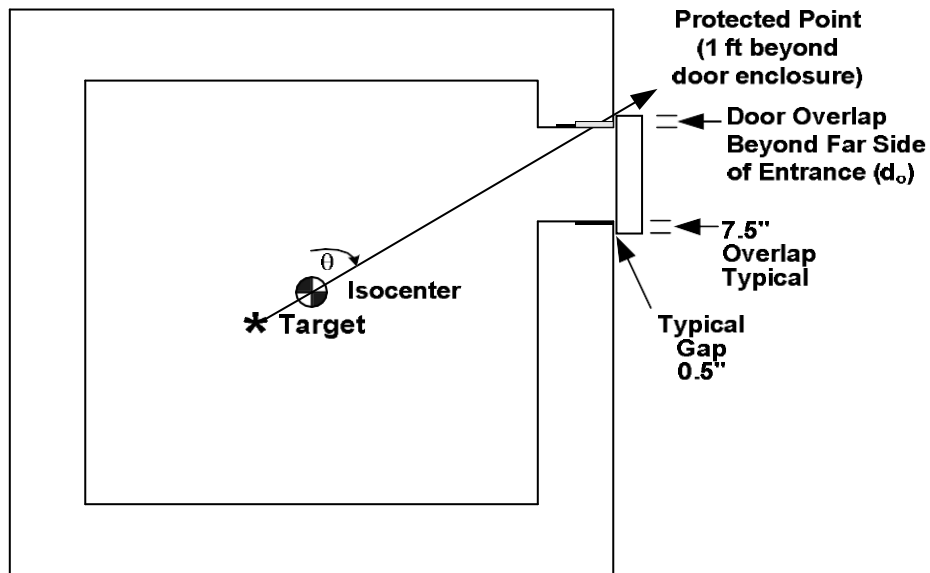
Figure 1. Distance to Protected Location at Far Side of Entrance

Lead added to the entrance wall attenuates x-ray leakage. The location and length of the additional material must be sufficient length to ensure the secondary barrier slant thickness is sufficient for any path through the wall next to the door.
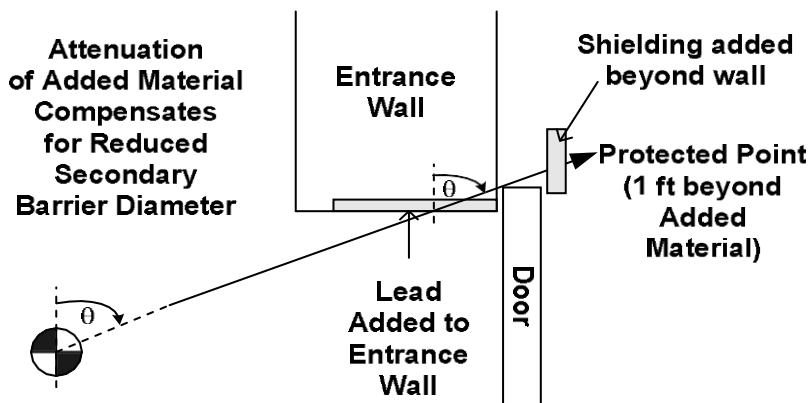
Figure 2. Additional Material at Far Side of Direct-Shielded Door

Scatter at Near Side of Entrance

The geometry at the near side of the entrance is similar to that of a maze, with primary wall scatter and leakage scatter radiation present. Patient scatter is implicitly included in the leakage scatter calculation. Scatter is combined with the direct primary and leakage radiation through the wall to determine the total shielded dose rate at this location.

Primary Wall Scatter

The primary beam wall scatter unshielded dose rate at the near side of the entrance is calculated using the geometry in Figure 3. The unshielded dose rate due to wall scatter (H_{UWS}) in Sv/wk is given by Equation 1.

$$H_{UWS} = \frac{W \; U \; \alpha_0 \; A_0}{d_0^2 \; d_Z^2} \tag{1}$$

As shown in Figure 3, d_0 (meters) is the target to scatter location (far wall of entrance) distance, d_Z (meters) is the distance from the scatter location to the protected location, W is the workload in Gy/wk, U is the use factor,

    α_0 =   Reflection coefficient at linac MV with 45º incidence 30º reflection (NCRP 151 Table B.8a)

and

    A_0 =   beam area at first reflection = $(F \, d_0)^2$ where F is the field size in m normalized to 1 m from the X-ray source.

Because the wall scatter undergoes only a single bounce, the tenth value layer is calculated using primary TVL at 0.5 MV. A slant thickness of 45 degrees to normal is assumed at the corner.

Leakage Scatter

The unshielded dose rate at the near side of the door due to leakage scatter is calculated using the geometry in Figure 3. The *leakage scatter unshielded dose rate* (**H_{ULS}**) in Sv/wk is given by Equation 2.

$$H_{ULS} = \frac{10^{-3} \; W_L \; U \; \alpha_1 \; A_1}{d_{\text{sec}}^2 \; d_z^2} \tag{2}$$

As shown in Figure 3, **d_{sec}** (meters) is the distance from isocenter to the scatter location (far wall of entrance), **d_z** (meters) is the distance from the scatter location to the protected location, W_L is the leakage workload in Gy/wk (i.e., W times the IMRT factor), U is use factor,

    α_1 =   reflection coefficient at 1.4 MV with 45º incidence and 30º reflection (NCRP 151 Table B.8b)

    A_1 = $w_1 \, h$ = area (m^2) of the entrance wall, where w_1 is the width of the entrance wall and h is the height of the room.

The 10^{-3} factor (the *x-ray leakage fraction*) reflects the standard manufacturer requirement that the average x-ray leakage outside the beam must be less than 0.1% of the dose rate at isocenter.

The single-bounce leakage scatter tenth value layer is based on the primary TVL at 0.3 MV. A slant thickness of 45 degrees to normal is assumed at the corner.
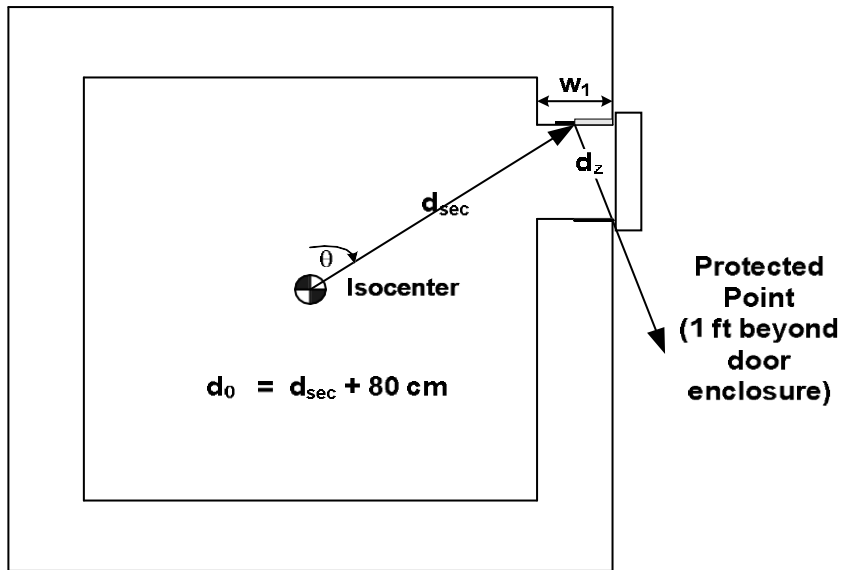
Figure 3. Scatter at Near Side of Direct-Shielded Door

5/18/2017
AUBNMC - Cyberknife.xlsm

Page 30
Direct-Shielded Door Calculations

Therapy Physics, Inc.
310-217-4114

Protected Location: **I - Corridor beyond door (if primary)**

Distance from Isocenter to Location (d):	6.6	m		X-ray Energy (MV):	6
Workload (W) (Gy/wk):	768			Occupancy Factor (T):	0.2
X-Ray Leakage Workload (Gy / wk):	18000			**Dose Constraint (P) (mSv / wk):**	**0.020**
				X-Ray Leakage Fraction:	1.00E-03

Slant (deg)

Inside Face:	6	mm	33	Material:	Steel
Core Layer 1:	229	mm	33	Material:	Lead
Core Layer 2:		mm		Material:	
Core Layer 3:		mm		Material:	
Outside Face:	6	mm	33	Material:	Steel

Shielded Primary Dose Rate (mSv/wk):	0.014	Shielded Sec Dose Rate (mSv / wk):	0.003
Recommended Primary Margin:	2.7	**Shielded Dose Rate (mSv/wk):**	**0.041**
		Shielded TADR including occupancy (mSv/wk):	**0.008**

Additional values used in shielded dose rate calculation

		Primary	*Leakage*
Use Factor:		0.05	1
Unshielded Dose Rate (mSv/wk):		710.72	418.53
	Slant (mm)	Transmission	Transmission
Inside Face:	7	8.54E-01	8.48E-01
Core Layer 1:	273	2.66E-05	1.11E-05
Core Layer 2:	0	1.00E+00	1.00E+00
Core Layer 3:	0	1.00E+00	1.00E+00
Outside Face:	7	8.54E-01	8.48E-01
Total:		1.94E-05	7.96E-06

	Oblique Thickness (mm)	Primary TVL (mm)		Leakage TVL (mm)	
		TVL1	TVLe	TVL1	TVLe
Inside Face:	7	100	100	100	100
Core Layer 1:	261	57	57	55	55
Core Layer 2:	0				
Core Layer 3:	0				
Outside Face:	7	100	100	100	100

Protected Location: **I2 - Prep / Recovery beyond door (if primary)**

Distance from Isocenter to Location (d):	10.1 m	X-ray Energy (MV):	6
Workload (W) (Gy/wk):	768	Occupancy Factor (T):	1
X-Ray Leakage Workload (Gy / wk):	18000	**Dose Constraint (P) (mSv / wk):**	**0.020**
		X-Ray Leakage Fraction:	1.00E-03

Slant (deg)

Inside Face:	6	mm	33	Material:	Steel
Core Layer 1:	229	mm	33	Material:	Lead
Core Layer 2:		mm		Material:	
Core Layer 3:		mm		Material:	
Outside Face:	6	mm	33	Material:	Steel

Shielded Primary Dose Rate (mSv/wk):	0.006	Shielded Sec Dose Rate (mSv / wk):	0.001
Recommended Primary Margin:	2.7	**Shielded Dose Rate (mSv/wk):**	**0.018**
		Shielded TADR including occupancy (mSv/wk):	**0.018**

Additional values used in shielded dose rate calculation

		Primary	*Leakage*
Use Factor:		0.05	1
Unshielded Dose Rate (mSv/wk):		321.58	175.23
	Slant (mm)	Transmission	Transmission
Inside Face:	7	8.54E-01	8.48E-01
Core Layer 1:	273	2.66E-05	1.11E-05
Core Layer 2:	0	1.00E+00	1.00E+00
Core Layer 3:	0	1.00E+00	1.00E+00
Outside Face:	7	8.54E-01	8.48E-01
Total:		1.94E-05	7.96E-06

	Oblique Thickness (mm)	Primary TVL (mm) TVL1	TVLe	Leakage TVL (mm) TVL1	TVLe
Inside Face:	7	100	100	100	100
Core Layer 1:	261	57	57	55	55
Core Layer 2:	0				
Core Layer 3:	0				
Outside Face:	7	100	100	100	100

Secondary Barrier Protected Location: **I - Corridor beyond door (if seondary)**

Secondary Distance (d):	6.6	m	X-ray Energy (MV):	6
Workload (W) (Gy / wk):	512		Occupancy Factor (T):	0.2
X-Ray Leakage Workload (Gy / wk):	9600		**Dose Constraint (P) (mSv / wk):**	**0.020**
			X-Ray Leakage Fraction:	1.00E-03

Slant (deg)

Inside Barrier Layer:	6	mm	33	Material: Steel
Barrier Layer #2:	178	mm	33	Material: Lead
Barrier Layer #3:		mm		Material: Borated Polyethylene
Barrier Layer #4:		mm		Material: Lead
Outside Barrier Layer:	6	mm	33	Material: Steel

Shielded Dose Rate (mSv / wk): **0.022**

Shielded TADR including occupancy (mSv / wk): **0.004**

Additional values used in shielded dose rate calculation

Leakage

Use Factor:	1
Unshielded Dose Rate (mSv/wk):	223.22

	Slant (mm)	Transmission
Inside Barrier Layer:	7	8.48E-01
Barrier Layer #2:	212	1.40E-04
Barrier Layer #3:	0	1.00E+00
Barrier Layer #4:	0	1.00E+00
Outside Barrier Layer:	7	8.48E-01
Total:		1.01E-04

0.0224

	TVL1 (mm)	TVLe (mm)
Inside Barrier Layer:	100	100
Barrier Layer #2:	55	55
Barrier Layer #3:	733	733
Barrier Layer #4:	55	55
Outside Barrier Layer:	100	100

5/18/2017
AUBNMC - Cyberknife.xlsm

Page 33
Direct Door Sec I

Therapy Physics, Inc.
310-217-4114

Secondary Barrier Protected Location: **I - Corridor beyond door (if secondary)**

Secondary Distance (d):	10.1	m		X-ray Energy (MV):	6
Workload (W) (Gy / wk):	512			Occupancy Factor (T):	1
X-Ray Leakage Workload (Gy / wk):	9600			**Dose Constraint (P) (mSv / wk):**	**0.020**
				X-Ray Leakage Fraction:	1.00E-03

Slant (deg)

Inside Barrier Layer:	6	mm	33	Material:	Steel
Barrier Layer #2:	178	mm	33	Material:	Lead
Barrier Layer #3:		mm		Material:	Borated Polyethylene
Barrier Layer #4:		mm		Material:	Lead
Outside Barrier Layer:	6	mm	33	Material:	Steel

Shielded Dose Rate (mSv / wk):   **0.009**

Shielded TADR including occupancy (mSv / wk):   **0.009**

Additional values used in shielded dose rate calculation

Leakage

Use Factor:	1
Unshielded Dose Rate (mSv/wk):	93.46

	Slant (mm)	Transmission
Inside Barrier Layer:	7	8.48E-01
Barrier Layer #2:	212	1.40E-04
Barrier Layer #3:	0	1.00E+00
Barrier Layer #4:	0	1.00E+00
Outside Barrier Layer:	7	8.48E-01
Total:		1.01E-04

0.0094

	TVL1 (mm)	TVLe (mm)
Inside Barrier Layer:	100	100
Barrier Layer #2:	55	55
Barrier Layer #3:	733	733
Barrier Layer #4:	55	55
Outside Barrier Layer:	100	100

Retrospective analysis of dose, fororgans at risk in 3D image-based treatment planning in cervix cancer for HDR Brachytherapy, in Hospital Regionalde Alta Especialidad de Ixtapaluca(HRAEI) patients.

Mayer González A.*, Valle González M., Chagoya González A.

Departamento de Oncología, Hospital Regional de Alta Especialidad de Ixtapaluca, Carretera Federal México-Puebla km. 34.5, Pueblo Zoquiapan, Municipio de Ixtapaluca, Estado de México CP. 56530

Abstract.

Since obtaining the Operating Licence, of the HDRBrachytherapy, in HRAEI, it was established, by matterof Radiological Protection to Patients, the criteriaof Simulate these by means of Computer Tomography (CT), and carry out the treatment plan by volumetricoptimization, with the objective of limiting abetterway the Organs at Risk (OAR) and evaluate the accumulation of the dose that receive.

The present work consists of the retrospective analysis, by means of the dose volume histograms (DVH), of the accumulated dose in the OAR, rectum and bladder, of patients with gynecological cancer (endometrium and cervix) of the HRAEI, treated by HDR brachytherapy, with f letcher and vaginal cylinder, considering, as recommended in GEC-ESTRO, the minimum dose in the most irradiated tissue volume adjacent to the applicator($D_{0.1cc}$, D_{1cc}, D_{2cc} and D_{5cc} for 0.1, 1, 2 and 5 cm^3), and comparing with the dose constraints.

Introduction:

The advancement of technology, allows us to use othertools in everyday clinical practice, for the planning of treatment of cervical cancer, through brachytherapy of high rate of dose, in Mexico, traditionally used images radiographic, which does not have a representation of the target of treatment orcritical organs beyond what can be estimated based on the bone anatomy, surgical or markers clips inserted into the patient [1]. Using the computerized Axial Tomography, reconstructions in 3D, can be made which determines the anatomical description of the target volume and risk organs, the dose to the target volume, the dose may be documented to the risk organs and statistics of the volumetric doses [2]. In the case of the Regional Hospital of high specialty of Ixtapaluca (HRAEI), it boasts a computed Axial Tomography (CT) and a Gammamed equipment of high dose rate brachytherapy for Ir-192, BrachyVision system for planning of treatments, which began to operate from 2 years ago and where currently are treated, only patients with cervical cancerand endometrial, using fletcherand vaginal cylinders applicators.

During this time, radiation therapy team determined that; but he is also having a system of acquisition of images in 2-D(C-arm), all the planning of treatment, would be carried out using the HDR-3D, aiming to quantify, to control and record the distribution of dose in the white and, as i s recommended by the Working Group GEC-ESTRO, at 0.1 cm^3, 1 cm^3 and 2 cm^3 of the volume of the bladderand the rectum ($D_{0.1cc}$, D_{1cc}, D_{2cc}) [3].

The objective of the present study is to compare, under the quadratic linear model, the total effectivedose (EQD_2) who receive the organ at risk treatments Braquiterapia HDR-3D, under the parameters reported by the GEC ESTRO Working Group.

Method:

In order to perform retrospective analysis, patients who were treated with external beam radio therapy (EBRT) undera prescription of 50Gy in 25 fractions, then these patients were considered, were divided into two groups according to the type of applicator and the prescription of the complementary treatment with high rate dose brachytherapy (HDR); the first group was formed by those whose used applicatorwas the fletcherand patients were prescribed them 24Gy into 4 fractions; While the second group was composed by those patients whose applicatorwas Vaginal cylinderand that they had a prescription of 18Gy in 3 fractions.

Once these patients have concluded theirtreatments is proceeded to calculate the EQD_2 at 0.1, 1, 2 and 5cc volume of risk organs (bladder and rectum), due to the sum of both treatments (EBRT+HDR), assuming that, in accordance with the recommendations of the GEC ESTRUS, both bladder and rectum received 100% of the dose prescribed to total organ in the EBRT.

Once obtained the previous data, determined the EQD_2 average who received the organ at risk patients of these two groups under the previously mentioned parameters and were compared with those reported by the GEC ESTRO Working Group.

Results:

Graph 1, shows the average of the EQD_2 in the organ at risk in the case of patients who make up the group 2, while the graph 2 shows the EQD_2 average in the organ at risk in the case of patients who satisfice group 1.
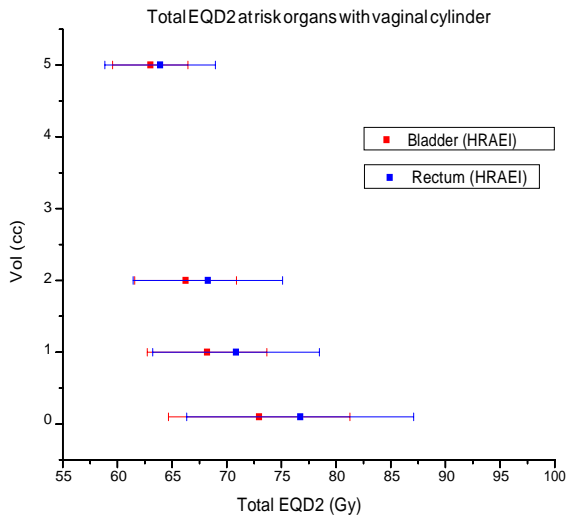
Graph 1. Total EQD2, EBRT+HDR, at risk organs with vaginal cylinder.
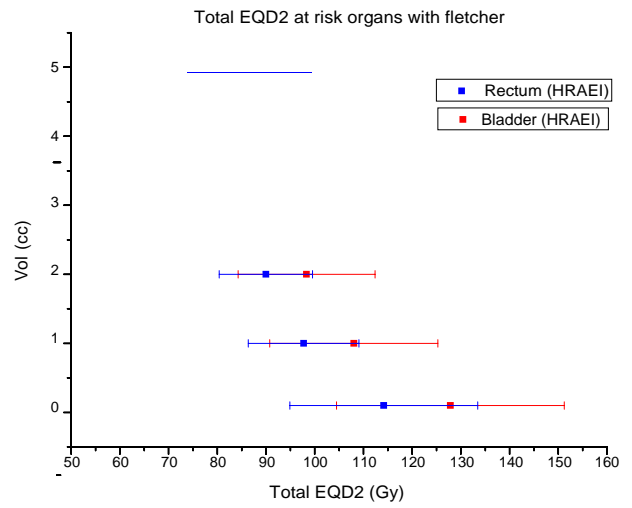
Graph 2. Total EQD2, EBRT+HDR, at risk organs with fletcher.

Discussions:

Graph 3, shows the comparison of the EQD_2 risk organs of group 2, using the Vaginal cylinder between the results obtained in the HRAEI and those reported in the GEC-ESTRO.
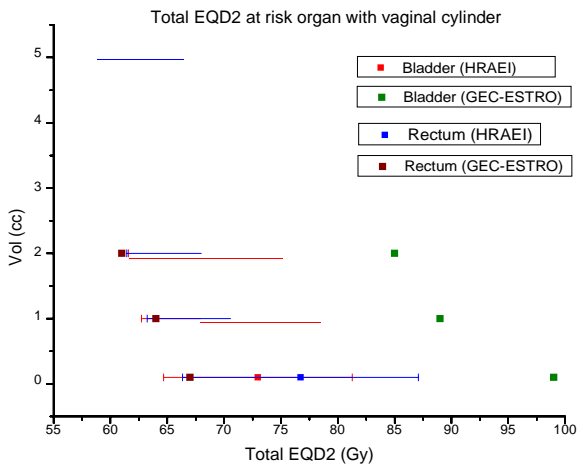
Graph 3. Total EQD2, EBRT+HDR, at risk organs with vaginal cylinder.
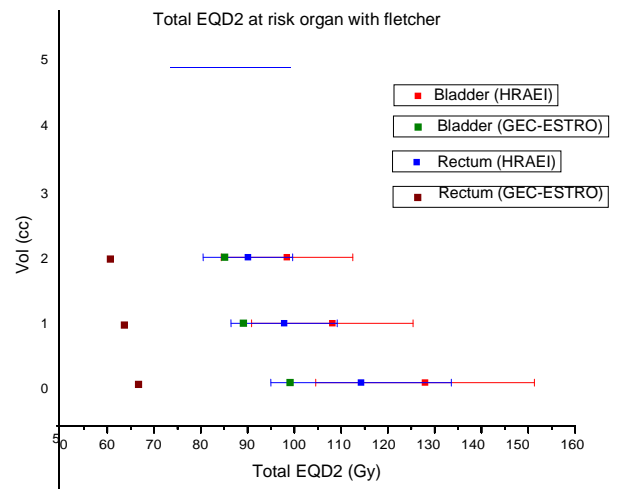
Graph 4. Total EQD2, EBRT+HDR, at risk organs with fletcher.

Graph 4, shows the comparison of the EQD_2 of the organ at risk, group 1, using the Fletcher, between the results obtained in the HRAEI and those reported in the GEC-ESTRO.

Conclusions:

We can observer that, only in the case where he used the vaginal cylinder as applicator, the average of the EQD_2 bladder, below that reported in the GEC-ESTRO, so the Group of medical physics and medical radiation oncologist of the radiotherapy unit must be agreater emphasis o n the restrictions of the organs of risk as well as a clinical follow-up on the patients of these two groups.

Noteworthy is the importance that has the use of the planning of treatments using tomographic images since it is possible to quantify the dose using the DVHand thus calculate the EDQ_2 for the organ at risk.

[1] QA Review of Brachytherapy Treatment Plans, Zuofeng Li, D.Sc. Department of Radiation Oncology, Mallinckrodt Institute of Radiology, Washington University School of Medicine, St. Louis, Missouri.

[2] ACR-AAPMTechnical Standard forthe performance of High-Dose-Rate Brachytherapy Physics, Revised 2015 (Resolution 50).

[3] Pötter R, Haie-Meder C, Van Limbergen E, et al. GEC ESTRO Working Group. Recommendations from gynaecological (GYN) GEC ESTRO working group (II): concepts and terms in 3D image-based treatment planning in cervix cancerbrachytherapy-3Ddose volumeparameters and aspects of 3D image-based anatomy, radiation physics, radiobiology. RadiotherOncol. 2006; 78: 67-77.

THE APPLICATION OF DOSE CALCULATION ALGORITHMS MODEL: CONVOLUTION, SUPERPOSITION, AND FAST SUPERPOSITION IN 3-DIMENSIONAL CONFORMAL RADIOTHERAPY (3D-CRT)

H. Murat
National Cancer Institute
Putrajaya, Malaysia
Email: fzhusain@nci.gov.my

M.K.A Karim
National Cancer Institute
Putrajaya, Malaysia

Abstract

Application of dose calculation algorithm model in a computerized radiotherapy treatment planning system (TPS) is important to ensure that the predicted radiation dose to the patient through a TPS is accurate and optimized. Therefore, the aim of this study is to compare the implementations of several available dose calculation algorithms: convolution, superposition, and fast superposition dose calculation algorithm in TPS, (CMS) XiO (USA) in the National Cancer Institute, Malaysia. The study was conducted by using four typical treatment techniques (a single beam technique, multi-beam technique, wedge beam technique, and multi-leaf collimated (MLC) beam technique). The study shows that the percentage of deviation of measured dose in two linear accelerators (LINACS) with the tolerance of ±3% were 1.4% and 2.5% for 6 megavoltage (MV) and 10 MV, respectively. It is indicated that the superposition algorithm satisfies predetermined criteria (±3%) which passed 100% of all reference points, whilst the convolution algorithm and fast superposition of presented reference point were 82% and 91%, respectively. In conclusion, the assessment of radiotherapy treatment plan shall take into account the type of dose calculation algorithm model in order to optimize radiotherapy treatment and ensure the radiation safety to the patient.

1. INTRODUCTION

Computerized radiotherapy treatment planning system (TPS) is used to plan and calculate complex dose distribution to the tumour for final treatment [1]. However, the effectiveness and the performance of TPS are depending on the type of dose calculation algorithms used in the system. [2] This algorithm evolved rapidly since the 50s, mainly caused by the rapid development in the fields of nuclear physics and computer science which aid to describe the physical processes involved in the radiation interaction [3]. Generally, dose calculation algorithms are divided into three groups which are correction-based, model-based; and principle-based [3]. Of these three models, principle based Monte-Carlo (MC), deliver the most accurate dose calculation by simulating the real physical processes of beam particles during transportation [4][5]. Hence, the principle based overcomes other model that still using a basic measurement as a reference.

Several researchers have published their works on how to evaluate the performance and the accuracy of dose calculation algorithms. The simple way for this process is to perform measurements and then compare the measured results with the calculated dose. Noting that, there are still little works on model-based method algorithm that focusing on its accuracy. According to Muralidhar et. al [2], the implementation of convolution, superposition, and fast superposition should be compared in term of their performance and accuracy. However since no dose calculations can be performed perfectly, each has to account uncertainty which can affect the dose delivery in final treatment. The International Commission on Radiation Units (ICRU) stated that dose calculation accuracy must be within 2-3%.[6] Therefore, it is important to understand the general principles of the algorithm and its implementation details since each algorithm suffers from limitations to deal with a complex system such as in radiotherapy treatment.

2. METHODS AND MATERIALS

2.1 Beam arrangement

This study adopted protocols as described in IAEA-TECDOC 1583.[7] The reference points were arranged from 1-5 on Computerized Imaging Reference System (CIRS) thorax phantom as shown in Figure 1. The reference points were standardized for all measurement and calculated absorbed dose in this study. In order to make this study more reliable in clinical situation, four typical treatment planning techniques were configured in terms of single beam, multi beam, wedge beam, and MLC beam as illustrated in Figure 2. The details of techniques, beams, and reference point location were summarized in Table 1.

(A)   (B)
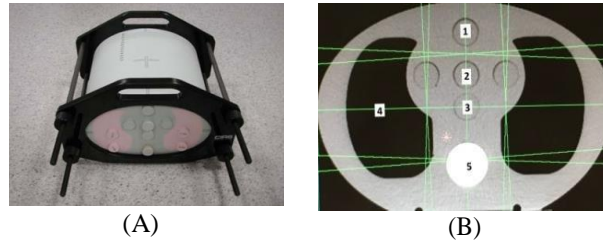
Figure 1: (A) CIRS thorax phantom and (B) arrangement of the corresponding plug
for the reference point 1-5.

(1)   (2)

(3)   (4)
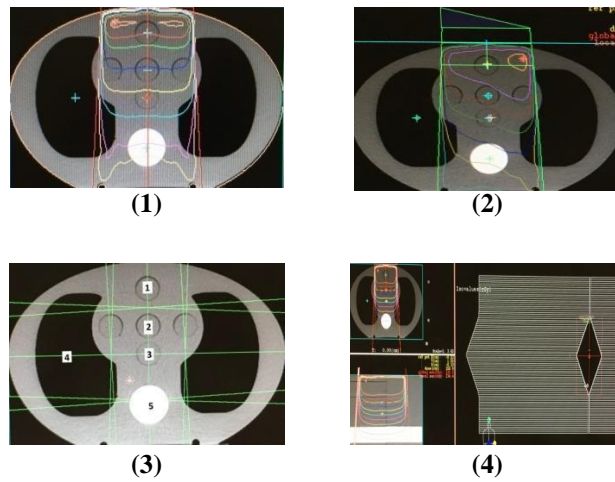
Figure 2 : Four techniques involved in this study (1) single beam, (2)multi beam,
(3)wedge beam, and (4)MLC beam

Table 1 : DETAILS OF TECHNIQUES, BEAMS, AND REFERENCE POINT LOCATION USED IN THIS
EXPERIMENTAL SET-UP

Technique (6MV,10MV)	Description of beams (field size/wedge/MLC)	Reference point location
Single beam	FS:5x5,10 x 10,20x20,30x30,40x40	1,2,3,4,5
Multi beam	FS:15x8(AP/AP) FS:15x10(Lateral)	2,3,4,5
Wedge beam	FS:10x10 Wedge $15^0,30^0,45^0,60^0$	1
MLC beam	FS:10x10 MLC closed each corner	1,2,3,4,5

2.2 Measurement, dose calculation,and analysis

By using different algorithm in a TPS (XiO, USA), the calculated doses were obtained from each technique. Small volume of Ionisation Chamber (CC01 IBA, USA) was placed in the dedicated phantom to verify with the measured dose. The results obtained were analysed to evaluate the deviation related to measured dose values. The relative error from measured and calculated values was formulated as in Equation 1.

$$D(\%) = 100\% \times \frac{(D_{cal} - D_{meas})}{D_{meas}}$$

where D_{cal} is calculated dose from TPS and D_{meas} is measured dose from the IC.

4. RESULTS

The calculated doses from all of the algorithms were obtained to compare with the measured dose. The summary of the results is presented in Table 2. It is observed that superposition algorithm has produced relative error less than ±3% for all reference points. Whilst convolution and fast superposition produced relative error more than ±3% for some of the failed reference points.

TABLE 2 : PERCENTAGE OF PASSED REFERENCE POINTS

Technique	Energy	Number of reference points (POI) passed agreement criteria, deviation ±3%		
		Convolution	Superposition	F.Superposition
Single beam Technique	6MV	120(96%)	125(100%)	119(95%)
	10MV	120(96%)	125(100%)	124(99%)
Multi beam Technique	6MV	11 (58%)	16 (100%)	13 (81%)
	10MV	13 (81%)	16 (100%)	14 (88%)
Wedge beam Technique	6MV	8 (100%)	8 (100%)	7 (88%)
	10MV	8 (100%)	8 (100%)	8 (100%)
MLC beam Technique	6MV	15 (100%)	15(100%)	14 (93%)
	10MV	11 (73%)	15(100%)	15 (100%)

5. DISCUSSIONS

The aim of this study is to compare the implementation of dose calculation algorithm model, convolution, superposition, and fast superposition in typical radiotherapy treatment planning. Each dose calculation algorithm showed differences in the dose prediction which contributed to the relative error [3][8][2][9]. This is due to difference in modelling approach in each dose calculation algorithms. In this experimental set-up, CIRS thorax phantom contains high density material will cause the beam attenuation where photon beam were hardened as it passes through the phantom. Dose difference between the algorithms and failed reference point could be due to inaccurate estimation and assumption of the physical processes of the beam attenuation as a result of high density material.[10] However, calculations at reference point with low density region, dose calculation algorithm may have insufficient tissue build-up in order to achieve electronic equilibrium.[10] Therefore, the amount of low density area in calculation region will reduce the accuracy of the dose calculations. The failed reference points of convolution and fast superposition in this study were no clear dependency on the field size, technique, and energy.

The accuracy of the superposition algorithms to predict dose for a variety of clinical situations was proved and accepted. However, convolution and fast superposition algorithms were slightly better under certain conditions, but no algorithm clearly perfect for all situations.[8] This finding is in agreement with the study by Muralidhar et. al.[2] In this study also showed that the failed reference points which relative error more than ±3% were no clear dependency on the field size, technique, and energy used. However, S. Oyewale reported that convolution algorithms may produce errors in present of heterogeneous media in complex system, whilst reliable in simple situation in homogenous media. Muralidhar et. al. also has proved that fast superposition produced predicted dose within agreement with lower calculation time compared to other algorithms. The results presented in this study reveal that each dose calculation algorithms have limitations in predicting accurate dose. However this study has only several limitations including small sample size and only focus on 3D CRT technique.

6. CONCLUSIONS

As conclusions, the accuracy of dose calculation algorithms is important for tumour control and inaccurate dose prediction may result to tumour recurrence or higher normal tissue toxicities. Hence, this study has proved that, appropriate algorithm must be used in clinical situation in order to optimize the predicted dose to the tumor.

REFERENCES

[1]   L. Korhonen and L. Korhonen, *Methods For Dose Calculation And Beam Characterization In External Photon Beam Doctoral Dissertation*. 2009.

[2]   K. R. Muralidhar, N. P. Murthy, A. Krishnam Raju, N. Sresty, and K. Raja Muralidhar, "Comparative study of convolution, superposition, and fast superposition algorithms in conventional radiotherapy, three•dimensional conformal radiotherapy, and intensity modulated radiotherapy techniques for various sites, done on CMS XIO planning system," *J Med Phys Jan-Mar;*, vol. 34, no. 1, pp. 12–22, 2009.

[3]   L. Lu, "Dose calculation algorithms in external beam photon radiation therapy," *Int. J. Cancer Ther. Oncol.*, vol. 1, no. 2, pp. 1–4, 2013.

[4]   M. J. Holt JG, Laughlin JS, "The extension of the concept of tissue-air ratios (TAR) to high-energy x-ray beams," *Radiology*, pp. 437–46, 1970.

[5]   L. R. Karzmark CJ, Deubert A, "Tissue-phantom ratios — an aid to treatment planning," *Br J Radiol*, pp. 38–158, 1965.

[6]   T. Dorje, "Limitation of pencil beam convolution (PBC) algorithm for photon dose calculations in inhomogeneous medium," *J. Cancer Treat. Res.*, vol. 2, no. 1, pp. 1–4, 2014.

[7]   IAEA, "Commissioning of Radiotherapy Treatment Planning Systems : Testing for Typical External Beam Treatment Techniques Commissioning of Radiotherapy Treatment Planning Systems : Testing for Typical External Beam Treatment Techniques. TECDOC 1583," *Iaea Tecdoc*, no. January, 2008.

[8]   S. J. Kim, D. H. Kim, and S. K. Kim, "Comparison of Pencil beam, Collapsed cone and Monte-Carlo algorithm in radiotherapy treatment planning for 6 MV photon," 2015.

[9]   A. K. Hauer, "Department of Radiation Physics the Impact of Different Dose Calculation Algorithms and Grid Sizes on Aperture-Based Complexity Metrics," 2015.

[10]   S. Rana and S. Pokharel, "Verification of dose calculation algorithms in a multi-layer heterogeneous phantom using films.," *Gulf J. Oncolog.*, vol. 1, no. 14, pp. 63–9, 2013.

COMPARATIVE ASSESSMENT OF DOSE AND TIME PARAMETERS IN 2D BRACHYTHERAPY INVOLVING TWO RADIOACTIVE SOURCES

E.O. OYEKUNLE
Department of Radiation Oncology, University College Hospital,
Ibadan, Nigeria
Email:
emmanuel.oyekunle@uch-ibadan.org.ng emmanueloyekunle.eo@gmail.com

I.B. UWADIAE
Department of Radiation Oncology, University College Hospital,
Ibadan, Nigeria

Abstract

The study which considered applications of Cobalt-60 and Iridium-192 in high-dose-rate (HDR) brachytherapy, is in a bid to enhance quality assurance and radiation protection. Four treatment plans with Co-60 were created on the planning system at University College Hospital, Nigeria. The plans were specifically for a 4 cm tandem – 3 cm ring applicator with prescription of 5, 6, 7 and 8 Gy at point 'A'. Total Dwell Times (TDT) were evaluated and corrected for radioactive decay. Total Time Index (TTI) was calculated by: $TTI = (TDT \ldots a \ldots \ldots \ldots)/(\ldots 'A' \ldots \ldots \ldots)$. The doses to point 'B', bladder and rectum reference points were deduced using international guidelines. At the Medical University Hospital, Austria, using Ir-192, same evaluation protocols were followed. Using Co-60, TDT and TTI were greater by a factor of about 1.70 and 1.20 respectively. Also, the mean bladder-dose was higher (4.54 vs. 4.20 Gy). However, corresponding rectal and point 'B' doses were higher with Ir-192 (5.06 vs. 3.79 and 1.58 vs. 1.36 Gy). Cobalt-60 offers a relatively longer treatment time and a higher bladder-dose. However, it engendered lower doses to the rectum and the point 'B'. Air-kerma-strength and the number of dwell positions contributed to these differences.

1. INTRODUCTION

Brachytherapy (BT) is a type of radiotherapy where higher radiation doses are used for the treatment of a smaller body (cancerous) area in a shorter time than is possible with external beam radiotherapy [1]. Cervical cancer is the third-most common cancer among women worldwide, with an annual incidence of 530,000 cases and 250,000 deaths. In the developing world, it is the second leading cause of cancer death among women [2]. High-dose-rate (HDR) BT is a decisive radiotherapy technique for cancer management particularly gynaecological malignancies. Many centres worldwide have moved from the initial technique of Low Dose Rate (LDR) BT to the present HDR approach using Iridium-192 and Cobalt-60 as radioactive sources. Preference for use of any of these radionuclides depends on the peculiar status and demands of an individual hospital. Intracavitary brachytherapy (ICBT) is often carried out using a variety of applicators such as vaginal cylinders, tandem-ovoid and more importantly tandem-ring applicators. The dimensions of the ring applicators differ according to the manufacturers. The Bebig (Germany) company is known to produce rings of diameters 25, 30 and 35 mm while Nucletron (Netherlands) offers 26, 30 and 34 mm rings. Potential radiation doses to the bladder and the rectum is of prime concern in cervical cancer BT. This study is aimed at evaluating certain dose and time parameters in ICBT involving Co-60 and Ir-192 in a bid to promote quality assurance (QA) and radiation protection in HDR brachytherapy.

2. MATERIALS AND METHODS

The first HDR brachytherapy equipment in West Africa was procured in 2007 at University College Hospital (UCH), Ibadan, Nigeria with the support of the International Atomic Energy Agency (IAEA). The main components of the equipment are brachytherapy planning system, treatment applicators and an afterloader (Gynesource, Bebig) of five channels containing Cobalt-60 of an initial activity of 74.74 GBq (22870.44 U). The afterloader has been predominantly applied for treatment of gynecological cancer due to the limited number of applicator channels available. Tandem-ring applicators (Bebig, Germany) have been primarily used at the Department of Radiation Oncology, UCH, Ibadan, Nigeria for this purpose because of its constant geometry and the pattern of cervical cancer common at the center.

Four standard (2D) BT plans were created with the HDR-Basic treatment planning system (TPS) using a Co-60 source of 0.5 cm step size. Each treatment plan was specifically designed for the combination of a 4 cm long intrauterine tandem and a 3 cm wide ring applicator. The tandem-ring components in each case are of 45^0 defined relative to the ring and

the axis of the applicator, and assigned varying prescription doses of 5, 6, 7 and 8 Gy at the reference point A. Total dwell times for the plans were corrected for radioactive decay. Total time index (TTI) was calculated by:

$$TTI = \text{...} ai \text{...} h(\text{...} A' \text{...})$$

as proposed in literature [3], while the doses to point 'B', bladder and rectum reference points were deduced on the plans according to the International Commission on Radiation Units and Measurements (ICRU).

The rectal and bladder reference points were determined according to the International guidelines [4]. For dose assessment, the positional coordinates of the bladder and rectal reference points (corrected for magnification or otherwise on the radiographs) for four related patients were used. At the Medical University Hospital (MUH), Vienna, Austria, same protocol was followed in carrying out a similar study on another set of four standard plans created with the Flexiplan TPS. In this case, Nucletron's tandem-ring applicator of same dimensions and angle as Bebig's, and Ir-192 of an initial activity of 370 GBq (40700.00 U) in 0.5 cm step size. The positional coordinates used at UCH were also applied to the new plans generated on Flexiplan TPS. The dose and time parameters evaluated at the two hospitals were then statistically compared.

3.   RESULTS

Comparisons of total dwell time, total time index, doses to Point B, ICRU bladder point and rectal point between Cobalt-60 and Iridium-192 for varying prescription doses are presented in Table 1. In Table 2, the dose and time parameters expressed as ratios of ^{60}Co values to that of ^{192}Ir are given.

Figure 1 shows the relative percentage differences of treatment parameters between Cobalt-60 vs. Iridium-192. Total dwell times ranging from 453.0 s to 746.4 s and 262.8s to 435.6 s were required to deliver point A doses of 5 – 8 Gy for Cobalt-60 and Iridium-192 respectively. Therefore, the total treatment time with Co-60 is only slightly longer than with Ir-192. The average TTI were 0.173±0.003 and 0.144±0.003 (Gy m2 s)/(h Gy) for Co-60 and Ir-192 sources respective

TABLE 1: COMPARISONS OF TOTAL DWELL TIME, TOTAL TIME INDEX, DOSES TO POINT B, ICRU BLADDER POINT AND RECTAL POINT BETWEEN COBALT-60 AND IRIDIUM-192 FOR VARYING PRESCRIPTION DOSE

Prescribed Dose at Point 'A' (Gy)	HDR brachytherapy source	Point 'B' dose (Gy)	ICRU Bladder Point dose (Gy)	ICRU Rectal Point dose (Gy)	Total dwell Time (sec.)	Dwell Points	Total Time Index, TTI (Gy m^2 s)/ (h Gy)
5	Co-60	1.04 (20.8 %)	3.49 (69.8%)	3.17 (63.3%)	453.0	12	0.173
	Ir-192	1.22 (24.4 %)	3.18 (63.6%)	4.28 (85.6%)	262.8	15	0.143
6	Co-60	1.26 (21.0%)	3.70 (61.7%)	4.17 (69.5%)	535.8	12	0.170
	Ir-192	1.46 (24.3 %)	3.59 (59.8%)	5.29 (88.2%)	315.0	15	0.142
7	Co-60	1.47 (21.0 %)	5.46 (78.0 %)	3.13 (44.7 %)	632.4	12	0.172
	Ir-192	1.70 (24.3%)	4.80 (68.6%)	4.70 (67.14 %)	367.8	15	0.143
8	Co-60	1.67 (20.9%)	5.52 (69.0%)	4.69 (58.6 %)	746.4	12	0.178
	Ir-192	1.95 (24.4%)	5.21 (65.1%)	5.97 (74.6%)	435.6	15	0.148
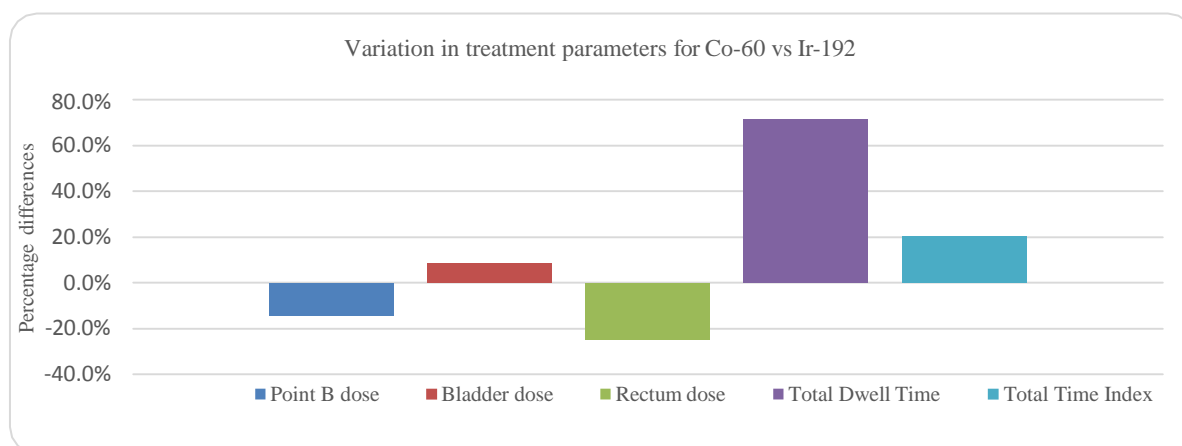
FIG. 1. Graph showing relative percentage differences of treatment parameters between Cobalt-60 vs. Iridium-192.

TABLE 2: DOSE AND TIME PARAMETERS EXPRESSED AS RATIOS OF COBALT-60 VALUES TO IRIDIUM-192

Point 'A' dose (5 Gy)	Point 'B' dose	ICRU Bladder Point dose	ICRU Rectal Point dose	Total dwell Time, TDT	Total Time Index, TTI $(Gy\ m^2\ s)/(h\ Gy)$
5	0.85:1	1.10:1	0.74:1	1.72:1	1.21:1
6	0.86:1	1.03:1	0.79:1	1.70:1	1.20:1
7	0.86:1	1.14:1	0.67:1	1.72:1	1.20:1
8	0.86:1	1.06:1	0.79:1	1.71:1	1.20:1

4. DISCUSSION

The dose distribution of an intracavitary application depends on a number of parameters. The type, size and geometry of the applicators, patient position, positioning and loading of the sources and the prescription of reference points are the most important parameters. In the present work, source loading and variation in air kerma strength (AKS) only are considered. This study shows that Cobalt-60 engendered lower doses to the reference point B which is in proximity to the bony pelvis (mean 20.93 vs. 24.35%) and the rectum (mean 59.03 vs. 78.89%) as compared to Iridium-192. The reverse is however the case for the urinary bladder (mean 69.63 vs. 64.28%) as further depicted in Table 2 above. Ideally, Cobalt-60 which has a higher average photon energy of 1.25 MeV will produce less scatter which is attributable to its slightly smaller values of radial dose function than Ir-192 with 0.35 MeV. High dose rate BT with ^{60}Co would therefore lead to fewer doses to organs at risk (OAR) or healthy tissue within approximately 20 cm from the source as compared with Ir-192. The lower doses obtained at the point B and rectal point are therefore justified by this phenomenon. On the other hand, the slightly higher doses recorded at the ICRU bladder point with the applications of Cobalt-60 at UCH could be attributed to source loading of 8 dwell positions on the intrauterine tandem. This was not the case for treatments with Iridium-192 at MUH where 7 dwell positions were activated on the IUT. Ideally, the uterine sources would give more contribution to bladder dose than the ring sources. However, as regards the rectal dose, the reverse is the case. In a retrospective study of 1992 patients who received HDR ICBT at the Division of Radiation Oncology, Chiangmai University, Thailand, the percentage of point B dose was approximately 20% point A dose [5]. This published data is comparable to the outcomes of the present study where doses at point B ranged from 20.8 – 24.4 % of the prescription doses. It could be observed that the point B doses are consistent for both cases of the radionuclides (21 % and 24 %) across the different prescription doses.

In HDR BT practice, the typical activity of 74.74 GBq for Co-60 is significantly lower than that (370 GBq) for Ir-192. Also, the Co-60 dose rate is normally slightly lower (than Iridium's) due to the higher air kerma rate constant (306 vs. 110 μGy · m2 · GBq-1 · h-1). Theoretically, it is therefore logical that the total

treatment time with Co-60 would be slightly longer than with Ir-192 as documented in literature by a source manufacturer [6]. The outcome of the present study has shown the same trend. Specifically, the results indicated that the treatment times for varying prescription doses (5 – 8 Gy) with Co-60 were higher than with Ir-192 by 41.2 – 42.0 %. This represents an increase by an average factor of 1.7 as indicated in Table 2 above. Another parameter assessed in this study is the total time index (TTI) which is closely related to the TDT of the source in the applicator. The index gives the average reference air kerma over all dwell positions per unit dose and it relates to the integral dose to the patient. The resulting values of TTI given in Table 2 therefore imply that brachytherapy applications using a Cobalt-60 would engender higher (by a factor of 1.2) overall absorbed dose to the patients as compared with Ir-192. Based on half-lives, approximately 20 source exchanges of Ir-192 would have to be performed during the working life of a single ^{60}Co source. The significant time saved in performing QA checks after each source exchange makes the use of Co-60 particularly attractive for high volume clinics. It is important to note however that the use of Co-60 (with average photon energy of 1.25 MeV) in ICBT would require a more intensive structural shielding as compared to Iridium-192. The longer treatment duration for a fractional dose delivery with the application of ^{60}Co also justifies the need to ensure adequacy in facility shielding. Figure 1 shows the results of the evaluated treatment parameters for both BT sources expressed in percentage differences. The individual parameters are presented as means of measured values across the four prescription doses (5, 6, 7, and 8 Gy) for both sources. It could be observed that with Cobalt-60, the point doses to the bladder, TDT and TTI were 8.28%, 71.42%, and 20.41% higher respectively than with ^{192}Ir. The doses to 'point B' and the rectum were however lower with Cobalt-60 with percentage differences of 14.06% and 25.10% respectively. The lowest difference between the sources was seen in the bladder point doses (8.28%) while the significantly highest difference was seen in the TDT (71.42%). Every institution has the prerogative to use any BT source, based on the prevailing social-economic situations. But due attention must be paid to QA vis-à-vis patient and personnel dosimetry. Although, ^{60}Co normally may result in reduced doses to the OAR in ICBT, a close attention should be paid to the number and positions of dwell points in the applicator.

5 CONCLUSIONS

A comparative assessment of certain dosimetric parameters for two BT sources was made. Cobalt-60 offers a relatively longer treatment time and a higher bladder point dose. It however, resulted in lower doses to the rectal point and point 'B' as compared to ^{192}Ir. The source AKS and the number of dwell positions are key factors that could be attributed to the observed differences. This study is relevant to QA as it shows the possible trend in dose and time parameters with the clinical applications of the two available HDR BT sources.

REFERENCES

[1] JOSLIN, C., Smith, C., Mallik, A. The treatment of cervix cancer using high activity cobalt-60 sources. Brit. J.Radio 45 (1972) 257-270

[2] KAMANGAR F, DORES G., ANDERSON W. Patterns of cancer incidence, mortality,and prevalence across five continents: Defining priorities to reduce cancer disparities in different geographic regions of the world. J Clin Oncol 24 14 (2005) 2137–2150

[3] WILLIAMSON J., NATH R. Clinical implementation of AAPM Task Group 32 recommendations on brachytherapy source strength specification. Med Phys 18 (1991) 439-448.

[4] International commission on radiation units and measurements (1985) Dose and volume specification for reporting intracavitary therapy in gynecology. ICRU report 38, ICRU, Bethesda, MD

[5] LORVIDHAYA V, TONUSIN A, CHANGWIWIT W et al (2000) High-dose-rate afterloading brachytherapy in carcinoma of the cervix: an experience of 1992 patients. Int. J. Radiation Oncology Biol. Phys 46(5):1185–1191

[6] Cobalt-60 in HDR brachytherapy: http://www.bebig.com/international/products/hdr_brachytherapy/cobalt_60/

STUDY OF CYTOPATHOLOGICAL ACTINIC EFFECTS IN PATIENTS SUBMITTED TO RADIOTHERAPY OF CANCER OF THE UTERINE CERVIX AT THE NATIONAL INSTITUTE OF CANCER / INCA, RIO DE JANEIRO, BRAZIL

PADILHA, C.M.L.
Universidade Federal do Rio de Janeiro/UFRJ - Instituto Nacional de Câncer/INCA
Rio de Janeiro/RJ, Brazil.
E-mail: cmpadilha@inca.gov.br

BERGMANN, A.
Instituto Nacional de Câncer/INCA
Rio de Janeiro/RJ, Brazil.

CHAVES, C.B.P.
Instituto Nacional de Câncer/INCA
Rio de Janeiro/RJ, Brazil.

PADILHA FILHO, L.G.
Universidade Federal do Rio de Janeiro/UFRJ
Rio de Janeiro/RJ, Brazil.

THULER, L.C.S.
Instituto Nacional de Câncer/INCA
Rio de Janeiro/RJ, Brazil.

ARAÚJO JUNIOR, M.L.C.
Instituto Nacional de Câncer/INCA
Rio de Janeiro/RJ, Brazil.

SOUZA, S.A.L.
Universidade Federal do Rio de Janeiro/UFRJ
Rio de Janeiro/RJ, Brazil.

ABSTRACT

The aim of the present study was to evaluate the evolution of the cervical-vaginal smear cell changes in cervical cancer patients who underwent radiotherapy. This is a cohort study, with a descriptive analytical approach of the cytopathological exams (Papanicolaou smears) performed at Hospital do Câncer II - RJ / INCA, of patients who underwent radiotherapy for cervical cancer. In the years 2009 and 2010, 875 patients underwent radiation therapy for cervical cancer at the Hospital do Câncer II / INCA, however 407 patients were included in the study because they had two or more cytopathological exams after radiotherapy. The total number of smears performed was 2168, with an average of 5 smears per patient (ranging from 2 to 11 smears), until the first semester of 2017. More than half of the cytopathological examinations (1327) presented cytopathic actinic (radiotherapeutic) effects. Follow-up by means of cytopathological analysis of tumor persistence or post-radiotherapy recurrence has shown a satisfactory result with regard to the number of negative cases (1725), however, it is always a great challenge for the professional, even experienced, to differentiate the radiotherapy effects of neoplastic cell atypia.

Keywords: Radiotherapy, Actinic Effects, Cytopathology, Cervical Cancer.

1. INTRODUCTION

In the world, cervical cancer represents the fourth most common type of cancer among women, except for cases of non-melanoma skin. It is responsible for approximately 265.000 deaths per year [8].

In Brazil, it is considered a public health problem, in 2016, 16.340 new cases were registered, with an estimated risk of 15.85 cases per 100.000 women The most common treatments for cervical cancer are surgery and radiation therapy. The type of treatment will depend on disease staging, tumor size and personal factors, such as age and desire to maintain fertility [7].

Very often patients with malignant uterine cervix tumors are referred to radiotherapy when the disease is in advanced stages and this fact determines high rates of relapse [6,7].

Radiation therapy consists of the use of ionizing radiation to destroy tumor cells; it is divided into Teletherapy (external) and Brachytherapy (internal). Teletherapy is performed by administering radiation from a source placed away from the patient [18]. The distances most used today are 80 cm for the ancient linear accelerators and the cobalt equipment or 100 cm for the modern linear accelerators. Cobalt therapy equipment is falling into disuse. Linear accelerators can be presented in two main versions: with or without electron beams [12,13]. Each patient can be treated with one or more radiation fields. The sum of the contribution of each field will produce a scheduled dose distribution in a Planning System [12].

When the source of radiation is placed inside the patient or very close to the patient's skin, the treatment is called brachytherapy. The dose rate which the treatment is given defines the type of brachytherapy: low rate (LDR), medium rate (MDR) or high dose rate (HDR). Few radioisotopes are currently used for this purpose. The most used is the Iridium-192, followed by Iodine-125, Cesium-137 and Cobalt-60 [12].

Radiation treatment causes actinic morphological changes, not only in neoplastic epithelial cells, but also in normal cells. These changes induced by radiation often hamper the differential diagnosis of residual lesions, resulting in great difficulties in differentiating neoplastic cells from those with actinic (radiotherapeutic) effects [14,15].

There are intracellular mechanisms capable, in many cases, of leading the cell back to its initial state. However, if the injury is very serious, or the repair mechanisms are compromised or overwhelmed by excessive radiation, the cell will transform [2].

Therefore, the objective of the present study was to evaluate the evolution of cervical-vaginal smear cell changes in patients with uterine cervix cancer who underwent radiotherapy.

2. METHODOLOGY

This is a cohort study, with a descriptive analytical approach of the cytopathological exams (Papanicolaou smears) performed at Hospital do Câncer II (HC2) - RJ / National Cancer Institute (INCA), of patients who underwent radiation therapy for cervical cancer. The work was approved by the INCA Ethics Committee (CAAE: 57701616.6.0000.5274).

Patients with uterine cervix cancer submitted to radiotherapy in the period between January 2009 and December 2010 were included, and patients without reference to radiotherapy, without information on the clinical staging of the lesions, patients who did not perform at least two Cytological exams after radiotherapy and that did not have at least two smears with satisfactory cellularity for analysis were excluded from the study.

Patients were identified through the HC2 / INCA Hospital Registry of Cancer (RHC). The clinical-epidemiological data were cataloged through the medical records available in the HC2 / INCA files. A reevaluation of cytopathological smears was performed to evaluate the evolution of actinic cytopathic effects. This information was complemented by the cytopathological report of the smears available in the archives of the Division of Pathology (DIPAT) - INCA. The data were collected in instruments developed for this purpose.

3. RESULTS

In the 2009-2010 period 875 patients underwent radiation therapy for cervical cancer at the Hospital do Câncer II / INCA. However, only 407 patients reached the inclusion criteria of two or more cytopathological exams (Papanicolaou smears) after radiotherapy to enter the study.

The mean age of the patients included was 51.4 years (ranging from 24-87 years). The total number of smears performed was 2168, with a mean of 5 smears per patient (ranging from 2 to 11 smears), until the first semester of 2017, where 79.6% (n = 1725) of cytopathological results were negative for neoplasia.

More than half of the cytopathological exams, 61.2% (n = 1327), presented cytopathic actinic / radiotherapeutic effects. **(Graph 1)**

GRAPHIC 1. Cytopathologic exams performed after radiotherapy in patients with cervical cancer

TOTAL CYTOPATHOLOGICAL EXAMS = 2168
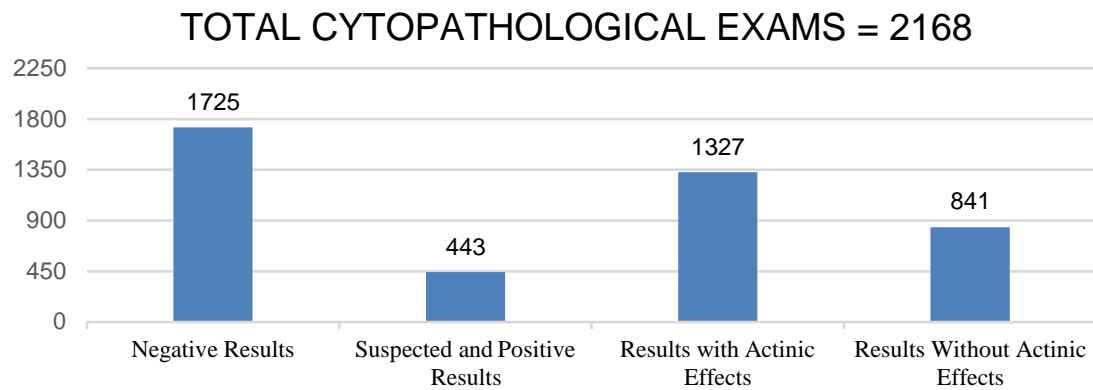
The most frequent actinic effects observed were: binucleation **(Fig.1A)**, dyskeratosis **(Fig.1B)**, prominent nucleoli **(Fig.1C)**, intracytoplasmic vacuoles **(Fig.1D)**, as well as amphophilia, macrocytosis, nuclear activation, Cellular atrophy, pleomorphism, multimucleation, and nuclear picnosis. Another finding found in most smears was the intense exsudate leukocyte and necrotic and hemorrhagic areas.

A. Binucleated epithelial cell
 (optical microscopy increased - 40x)
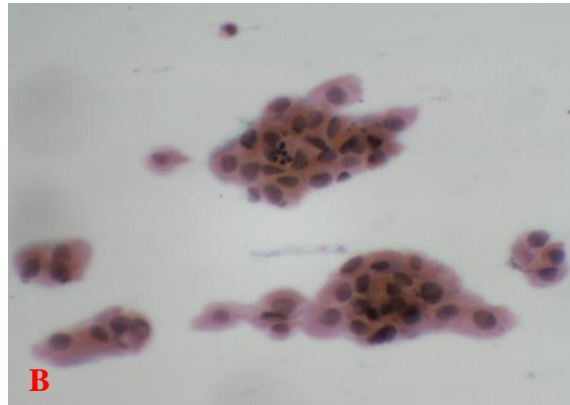
B. Dyskeratosis cell clusters
(optical microscopy increased - 40x)
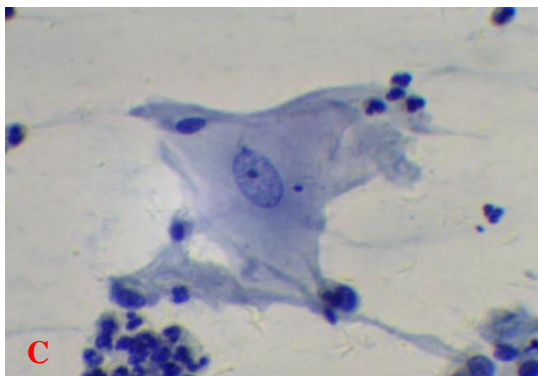
C. Epithelial cell with prominent nucleolus
(optical microscopy increased 40x)
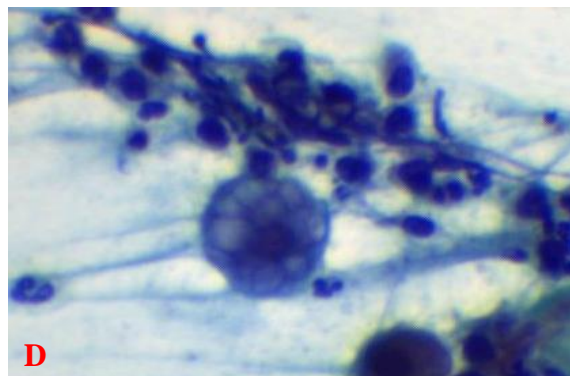
D. Cell with intracytoplasmic vacuoles (optical microscopy increased 40x)

FIGURE. 1. Epithelial cells showing actinic effects (study cases: patients undergoing radiation therapy for cervical cancer).

4. DISCUSSION AND CONCLUSION

There are many factors that determine the biological response to radiation exposure that include variables associated with the radiation source and the system being irradiated. Among them are radiation dose, type and energy, radiation rate and conditions under which the dose is administered [11].

According to Murad and August (1995), almost all cells undergo radiation-induced changes. The cellular alterations, even presenting a pattern already described in the literature, can evidence a wide and complex series of morphological modifications, with the appearance of bizarre cytological formations difficult to interpret [10].

To date, it has not been possible to establish a protocol that can accurately differentiate the morphological characteristics between benign cells with actinic effects of recurrent malignant cells on post-radiotherapy smears. [14,15].

In our results, we observed through cytopathologic analysis of tumor persistence or post-radiotherapy recurrence, a satisfactory result with regard to the number of negative cases (79.6%), but more than half of the cases had actinic effects (61.2%).

It is always a great challenge for the professional, even experienced, to differentiate the radiotherapy effects from neoplastic cell atypia. Further studies on the subject are important to contribute to the quality of the diagnostic evaluation for the follow-up of post-radiotherapy patients.

5. BIBLIOGRAPHY

1. BRASIL. MINISTÉRIO DA SAÚDE. INSTITUTO NACIONAL DE CÂNCER JOSÉ ALENCAR GOMES DA SILVA / INCA. Estimativa 2015: Incidência de Câncer no Brasil. Disponível em : http://www.inca.gov.br/estimativa/2016/ Acesso em: 10 março 2017.

2. BUSHBERG JT; SEIBERT JA; LEIDHOLDT EM; BOONE JM. The essential physics of medical imaging. 2nd ed. Philadelphia: Lippincott Williams & Wilkins; 2002.

3. COSTA MOLP, HERÁCLIO AS, COELHO AVC, ACIOLY VL, , SOUZA PRE, CORREIA MTS. Comparison of conventional Papanicolaou cytology samples with liquid-based cervical cytology samples from women in Pernambuco, Brazil. Braz J Med Biol Res, Ribeirão Preto, v.48, n.9, p.831-838, set. 2015.

4. GRAHAM JB, GRAHAM RM, LUI W. Prognosis in cancer of the uterine cervix based on the vaginal smear before tratament. SR: the sensitization response. Surg. Gynec. Obstet. 99:11, 1954.

5. GUPTA S, MUKHERJEE K, GUPTA YN, KUMAR M. Sequential radiation changes in cytology of vaginal smears in carcinoma of cervix uteri during radiotherapy. Int J Gynaecol Obstet. 1987; 25: 303-308.

6. Instituto Nacional do Câncer. INCA. Programa Nacional de Controle de Câncer de Colo do Útero. 2013. Disponível em: http://www.inca.gov.br/. Acesso em: 08 abril 2016.

7. INSTITUTO NACIONAL DE CÂNCER JOSÉ ALENCAR GOMES DA SILVA / INCA. Estimativa 2014: Incidência de Câncer no Brasil / Instituto Nacional de Câncer José Alencar Gomes da Silva. Coordenação de Prevenção e Vigilância. Rio de Janeiro: INCA, 2014. 124p.

8. JEMAL, A, BRAY F, MELISSA M, FERLAY J, WARD E, FORMAN D. Global cancer statistics. CA: A Cancer Journal for Clinicians. Volume 61, Issue 2. March/April 2011. Pages 69–90.

9. LU CH, CHANG CC, HO ESC, CHEN SJ, LIN SJ, FU TF, CHANG MC. Should adequacy criteria in cervicovaginal cytology be modified after radiotherapy, chemotherapy, or hysterectomy? Cancer Cytopathology, 118: 474–481. 2010 doi: 10.1002/cncy.20110

10. MASUBUCHI K, KUBO H, TENJIN Y, ONO M, YMAZAKI M. Follow-up studies by cytology on cancer of the cervix uterine after tratament. Acta. Cytol. 13:313-326, 1969.

11. MURAD TM, AUGUST C. Radiation-induced atypia. A rewiew. Diagn. Cytopathol. 1:135-152, 1985.

12. NOUAILHETAS Y; ALMEIDA CEB; PESTANA S. Comissão Nacional de Energia Nuclear / CNEN. Radiações Ionizantes e a vida. Acesso maio 2016. Disponível em www.cnen.gov.br

13. OLIVEIRA ACZ de; et al. Braquiterapia intersticial para recidivas de câncer de colo uterino pós-radioterapia. Radiol Bras. 2005; 38(2) 170-120.

14. PADILHA, C.M.L; ARAÚJO JUNIOR, M.L.C.; de SOUZA, S.A.L. Cytopathologic evaluation of patients submitted to radiotherapy for uterine cervix cancer Rev Assoc Med Bras 2017; 63(4):379-385.

15. PADILHA, C.M.L.; FELICIANO, G.D.; PADILHA FILHO, L.G. Analysis of Actinic Effect after Radiotherapy in the Uterine Cervix Carcinomas. The Journal of American Science, 1(1), 2005:17-22.

16. PANOBIANCO, M.S. et al. Women Diagnosed with Advanced Cancer of the Cervix: Coping with the Disease and Treatment. Revista Brasileira de Cancerologia 2012; 58(3): 517-523.

RADIATION MONITORING SYSTEM DESIGN FOR THE STEREOTACTIC LINEAR ELECTRON ACCELERATOR TRUEBEAM STX IN THE N.N. ALEXANDROV NATIONAL CANCER CENTER OF BELARUS

M. PIATKEVICH
N.N. Alexandrov National Cancer Centre of Belarus
Minsk, Belarus
Email: MaxPetkevichN@gmail.com

E. TITOVICH
N.N. Alexandrov National Cancer Centre of Belarus
Minsk, Belarus

V.A. HERTSYK
N.N. Alexandrov National Cancer Centre of Belarus
Minsk, Belarus

Abstract

This article describes the structure of radiation monitoring, which is used on a linear accelerator (energy > 10 MV) in N.N. Alexandrov National Cancer Centre of Belarus.

1. INTRODUCTION

The main source of radiation hazard when the medical linear accelerator is operating is generated the wide energy spectrum bremsstrahlung. In addition when photon energy is above the reaction threshold ($\geq$ 10 MV), a photonuclear reaction occurs and secondary neutrons are formed [1]. To ensure radiation safety and security for both personnel and patients, the accelerator must be equipped with a radiation monitoring system with dosimetric devices installed in the treatment room, labyrinth and console room.

2. METHODS

During the radiation monitoring system for the Stereotaxic Medical Accelerator Truebeam STx, design the following technical requirements were met: the ambient dose rate of gamma radiation and the ambient dose of neutrons in the procedural room, labyrinth and console room automatic measurement; collection of information from detectors (at least 3 channels) and live display of information on the operator control panel.

Taking into account the technical requirements for radiation monitoring, the measuring instrument-detector SRK-AT2327 was used. The use of this dosimeter has made it possible to create a flexible and reliable multi-channel stationary radiation protection system for monitoring the radiation situation in the treatment room, labyrinth and console room.

The meter-detector is built on the basis of intelligent gamma-ray detection units: BDKG-02, BDKG-04, BDKG-11/1, BDKG-17, BDKG-27, BDKG-204. beta radiation of BDPB-01 and neutron radiation BDKN-02, BDKN-04.

These detecting units are completely independent devices which measure the dose rate of gamma and neutron radiation and beta particles and neutrons flux density at a two-second interval [2]. Also, they manage the sound and light signaling which intended to alert personnel about the occurrence of radiation hazard. Information from the detection units is transmitted to the control panel or computer (RS485 interface).

3. RESULTS

Currently, to ensure radiation safety of personnel and patients when working on the Truebeam STx linear accelerator the system of the following detection units is used: BDKG-04 (3 pcs.), BDKN-04 (3 pcs.), emergency dosimetry indicator DRG-AT2331 (3 pcs.). Figure 1 depicts the scheme of arrangement of all blocks in the rooms of the linear accelerator. Figure 2 depicts the composition of each block
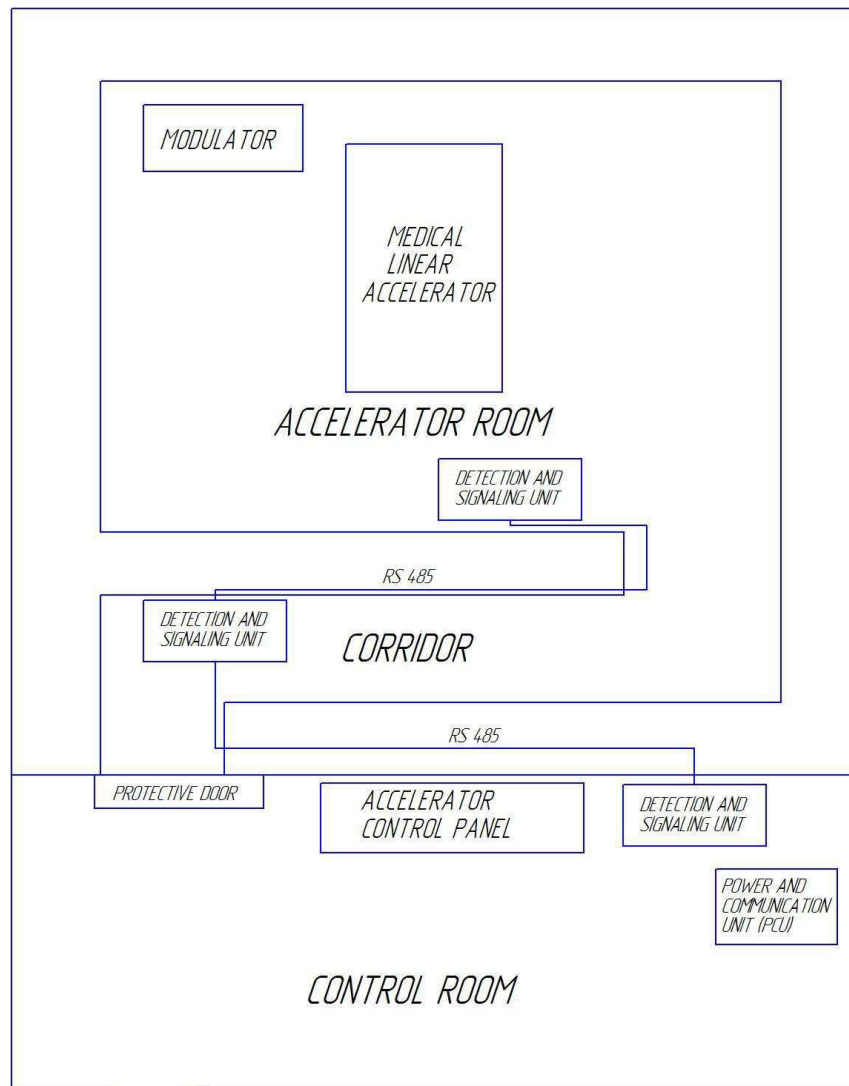
Figure 1 – Radiation monitoring system
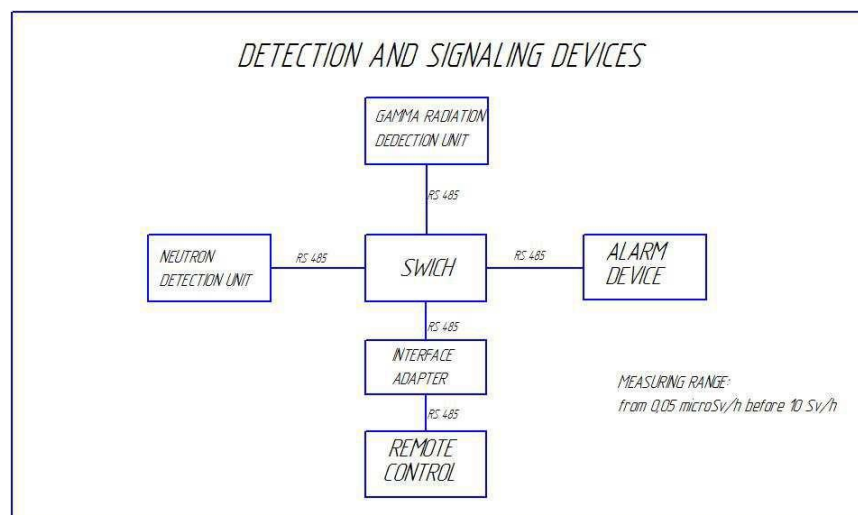
Figure 2 - Structure of the detecting unit

4. CONCLUSIONS

The radiation monitoring system based on the measuring instrument-detector SRK-AT2327 allows to ensure the level of control over the radiation situation in linear electron accelerators required by the legislation of the Republic of Belarus and international recommendations.

REFERENCES

[1] TARUTIN, I., TITOVICH E., HATSKEVICH G., Radiation protection in Radiotherapy, Bel. Nauka, Minsk (2015).

[2] ATOMTEX, Instruments and technologies for nuclear measurement and radiation monitoring, Minsk, 2017.

RADIATION HAZARD DUE TO THE ACTIVATION OF IONIZATION CHAMBERS

K. Polaczek-Grelik
Medical Physics Department, Institute of Physics, University of Silesia
Katowice, Poland
Email: kinga.polaczek-grelik@us.edu.pl

Nu-Med Cancer Diagnosis and Treatment Centre Katowice
Katowice, Poland
Email: kinga.polaczek-grelik@nu-med.pl

Abstract

Induction of radioactivity as a consequence of (X/γ,n) interaction of high-energy photon beam generated by linear accelerator used in radiotherapy as well as (n,γ) reactions of secondary particles produced therein, is generally known regarding elements of linac head, due to high intensity of beam hitting collimation system. However, any other irradiated objects could be activated at measurable level provided the time of exposition is long enough. During long-time linac beam emission needed e.g. in quality assurance tests, such conditions are fulfilled in relation to the dosimeters used. These equipment could therefore be a source of radiation hazard for medical physicists who perform the QA tests. Irradiation of four types of ionization chambers was carried out in a water phantom during emission of 10 000 monitor units of 15 MV photon beam (Elekta Synergy). Induced radioactivity has been investigated using HPGe spectrometry system. The main radionuclides: Mn-56, Cu-66, Al-28 and Cl-38 were activated in (n,γ) process, however some of long-lived radioisotopes: Cu-64, Al-26 and Mn-54 were generated via (X,n) reaction of primary beam. Moreover, the intensive process of positron annihilation (511 keV) was observed. The estimated equivalent dose rates to the eye lens and the skin were in the range of 1.4 – 2.0 μSv/min. These were calculated on the base of net count rates in photopeaks from registered spectra using fluence-to-dose conversion coefficients adopted from ICRP report 74. The effective half-life of the apparent radioactivity of about 10 minutes has been estimated regardless the ionization chamber model.

1. INTRODUCTION

Induced radioactivity as a consequence of high-energy beam (above ~8 MeV) interactions is a well known phenomenon in any kind of particle accelerator operation. In case of medical linear accelerators (linacs) used in external beam radiotherapy this issue has been studied either by Monte Carlo simulation, e.g. [1,2], or experimental measurements. These investigations are qualitative, aiming at identifying activated nuclides, e.g. [3-5], as well as quantitative, assessing the absorbed/equivalent dose connected with decay gamma rays, e.g. [4-8]. However, neutron flux, generated via nuclear photo effect (X/γ,n), is more commonly studied since neutron binding energy in heavy materials constituting the accelerator head is quite easy to exceed by beams (having a continuous spectrum) generated by linac operating at nominal potential of 10 MV and above. Photonuclear reaction cross section of various materials commonly used in accelerator production technology often reach the global or at least local maximum in the energy range of linac beam spectrum, what is exemplary shown in Fig.1. It should be noted that, the heavier element the lower energy of maximum cross section of photoactivation. Therefore the problem of activation is mainly focused on linac head. However, some studies point out the activation of the air and tissue during accelerator operation [9-12].

Nuclei could become unstable/radioactive as neutron-defficient or neutron-excess one, generated during photonuclear reaction (X/γ,n) of therapeutic beam or via the process of capturing the secondary neutrons (n,γ), respectively. The lower neutron energy the higher probability of neutron capture, therefore it could be expected that in moderating media such as water or solid phantoms, the neutron-induced activation will be increased.

The longer time of beam emission, the more radionuclides could approach or gain the saturation activity in the activation process and thus – raise at measurable/hazard–important level. Many situations in medical linac operation require long-time beam emission. Some of them are routinely repeated, like beam quality assurance (QA) tests or total body irradiation procedures, and some are conducted rarely, like commissioning of linac or treatment planning system (TPS). Medical physicists/dosimetrists usually are equipped with personal whole-body dosimeters estimating $H_p(10)$, but it appears that the main exposition connected with hand-holding

activated dosimeters will be on skin and eye lens during in-phantom mounting and positioning of this equipment.

The aim of the study was therefore to estimate the skin and eye doses connected with the activation of dosimetric equipment and time scale of this phenomenon as well as to identify the radionuclides responsible for this generated radiation hazard. The recognition of induced radionuclides and their contribution to the apparent activity enables the prediction of the risk connected with the secondary effect of linac beam usage. Additionally, the assessment of the time scale of dose decay allows for formulating the caution recommendations.
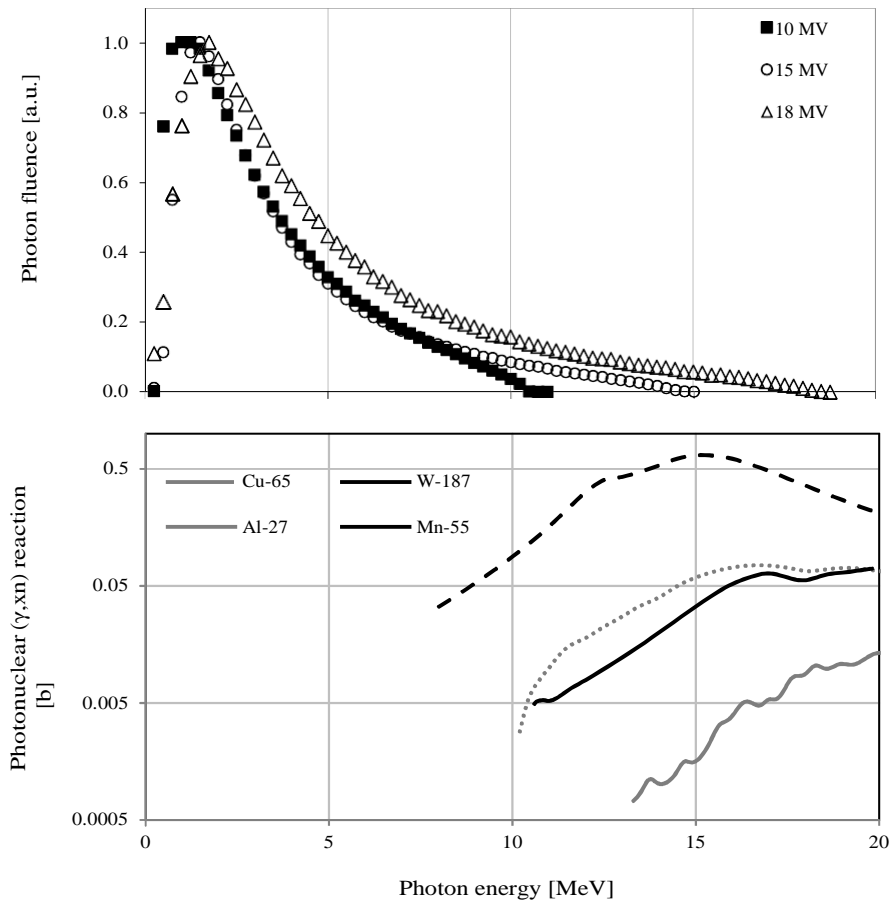
FIG.1. Therapeutic beam spectra, plotted on the base of data given by Sheikh-Bagheri and Rogers [13], in comparison with photonuclear reaction cross sections of elements commonly used in linac constructions, plotted on the base of data included in library JENDL-3.3 [14].

2. MATERIAL AND METHODS

Four models of ionization chambers (see: Table 1) were included in the study, of both − cylindrical and plane-parallel geometry. These types of dosimeters are commonly used for determination of absolute dose, output/wedge factors, beam quality on the base of percentage depth dose (PDD) measurements or beam profiles. Such dosimeters are mostly made of non-metallic components (H, C, O, N, F), however in some cases metallic (Al, steel) inner electrodes are still in use. Moreover, signal transmitting wires made of copper, are in most cases inside the irradiation field.

TABLE 1.   GENERAL INFORMATION REGARDING STUDIED IONIZATION CHAMBERS (IBA DOSIMETRY)

Dosimeter	Electrode	Wall material	Active volume [cm³]
FC65-G	Al	Graphite	0.65
CC13	C552[1]	C552	0.13
CC01	Steel	C552	0.01
PPC05	PEEK[2]	C552	0.05

Each ionization chamber for irradiation with 10 000 monitor units (MU) using 15 MV photon beam generated by Elekta Synergy linac was placed in water phantom (Blue Phantom 2, IBA Dosimetry), at the depth of 10 cm, in central beam axis (CAX) of the 30×30 cm³ field. Source-surface distance (SSD) of 90 cm was applied, placing the dosimeter in accelerator isocentric point. Applied beam emission rate of 600 MU/min corresponds to the beam-on time of approximately 17 min, which is not unusual during QA test performance.

2.1.   Spectrometric analysis of induced radioactivity

Radioactivity induced in ionization chambers was investigated with the use of portable spectrometric system, which contains coaxial high-purity germanium detector with reverse electrodes (REGe, Canberra Inc.) of 40% efficiency, multichannel analyser (MCA, 8194 channels) InSpector 2000 and Genie2000 software v.3.2.1. Measuring energy range was 6 – 3150 keV, due to applied spectrometric gain of 5.0 and the carbon-composite entrance window. For each of studied ionization chamber the spectrum was measured twice: before the irradiation, to estimate the background radiation containing intrinsic radiation signal of the dosimeter as well as the natural radiation at the place of measurement (outside the linac room), and immediately after (~2min) the end of beam emission, to investigate induced radioactivity. The measurements were carried out for 1 hour. Additionally, to trace the evolution of annihilation peak built at the spectrum by potentially generated pure positron-emitters, spectrum of activated ionization chamber has been recorded in 5-minute-intervals.

Energy as well as efficiency calibrations were preformed with the use of point-like 0.1 μCi sources (^{22}Na, ^{54}Mn, ^{57}Co, ^{60}Co, ^{65}Zn, ^{109}Cd, ^{133}Ba, ^{137}Cs). Thus, the identification of activated radionuclides was based on photopeak energy on registered spectra and the photopeak area was used for dose determination.

2.2.   Dose assessment

The area under each peak assigned to a monoenergetic photons emitted by particular radionuclides was used to estimate the fluence of photons at the distance of spectrum registration (10 cm in all cases), adopting the spectrometer efficiency curve. Subsequently, using fluence-to-dose conversion factors obtained from the Lagrange interpolation formula of 3rd degree (4-point) based on discreet values taken from ICRP report 74 [15], skin and eye lens equivalent doses were calculated. Since each spectrum of activated ionization chamber was registered for 1h, the correction of peaks' area based on nuclides half-lives for decay during measurement has been applied.

The total uncertainty of such method of dose assessment contains several components: peak area counting uncertainty (here: up to 15%), conversion coefficient values discrepancies stated in ICRP 74 publication (10%) and efficiency curve accuracy.

---

[1]C552 – air-equivalent plastic, 1.76 g/cm³ density, elemental composition: H – 2.5%, C – 50.2%,
    O – 0.5%, F – 46.2%, Si – 0.4%.

[2]PEEK – Polyether Ether Ketone (thermoplastic reisin), 1.32 g/cm³ density, elemental composition: C, H, O.

3. RESULTS

The analysis of gamma-energy spectra of activated ionization chambers, presented exemplary for CC01 dosimeter in Fig.1, has shown that among the activated radioisotopes, characterized in Table 2, prevail metals constituting the inner electrodes: aluminium in FC65-G chamber, manganese and iron of stainless steel in CC01 chamber, as well as copper wires in all studied dosimeters. Nevertheless, in applied experimental conditions (15MV beam, water phantom) activation concerns also chlorine in a plastic materials. Neutron capture is the dominant mechanism of inducing radioactivity in studied case, however photoactivation was also observed.

TABLE 2.   RADIONUCLIDES IDENTIFIED ON REGISTERED SPECTRA OF ACTIVATED IONIZATION CHAMBERS

Activation mechanism	Energy of γ-rays [keV]	Half-life, $T_{1/2}$	Dosimeter
$^{19}F(X/\gamma,n)^{18}F$	511	109.8 min	CC01, CC13, PPC05
$^{27}Al(n,\gamma)^{28}Al$	1779.0	2.2 min	FC65-G, PPC05
$^{37}Cl(n,\gamma)^{38}Cl$	1642.7, 2167.4	37.2 min	CC01, CC13, FC65-G, PPC05
$^{55}Mn(n,\gamma)^{56}Mn$	846.8, 1810.8, 2113.1	2.6 h	CC01, CC13, FC65-G
$^{55}Mn(X/\gamma,n)^{54}Mn$	834.9	312.1 d	CC01
$^{58}Fe(n,\gamma)^{59}Fe$	1291.6	44.5 d	CC01
$^{63}Cu(X/\gamma,n)^{62}Cu$	511	9.7 min	CC01, FC65-G
$^{65}Cu(X/\gamma,n)^{64}Cu$	511, 1345.8	12.7 h	CC01, FC65-G
$^{65}Cu(n,\gamma)^{66}Cu$	1039.3	5.1 min	CC01, CC13, FC65-G, PPC05

Among the positron emitters ^{18}F (C552) and ^{62}Cu (wires) do not emit deexcitation gamma rays, therefore have been recognized indirectly on the base of the analysis of annihilation peak decay at registered spectra.

Calculated equivalent doses for skin and eye lens, presented in Table 3, have shown that the main source of radiation hazard due to ionization chambers activation are positron emitters responsible for annihilation photons 511 keV, metallic electrodes and chlorine in plastic materials. Estimated effective half-life is of the order of 10 minutes regardless the type of studied dosimeter.

TABLE 3.   EQUIVALENT DOSE RATES TO A SKIN AND EYE LENS CONNECTED WITH ACTIVATED DOSIMETERS, ESTIMATED AT A DISTANCE OF 10 CM FROM ACTIVATED IONIZATION CHAMBERS

Dosimeter	Equivalent dose rate [µSv/min]		Main source	Effective half-life [min]
	Skin	Eye lens		
FC65-G	$1,38 \pm 0,22$	$1,41 \pm 0,28$	Annihilation, ^{28}Al	11 ± 2
CC13	$1,52 \pm 0,35$	$1,54 \pm 0,32$	Annihilation, ^{38}Cl	9 ± 2
CC01	$1,96 \pm 0,49$	$1,92 \pm 0,48$	Annihilation, ^{56}Mn	11 ± 2
PPC05	$1,59 \pm 0,33$	$1,60 \pm 0,32$	Annihilation, ^{38}Cl	12 ± 3
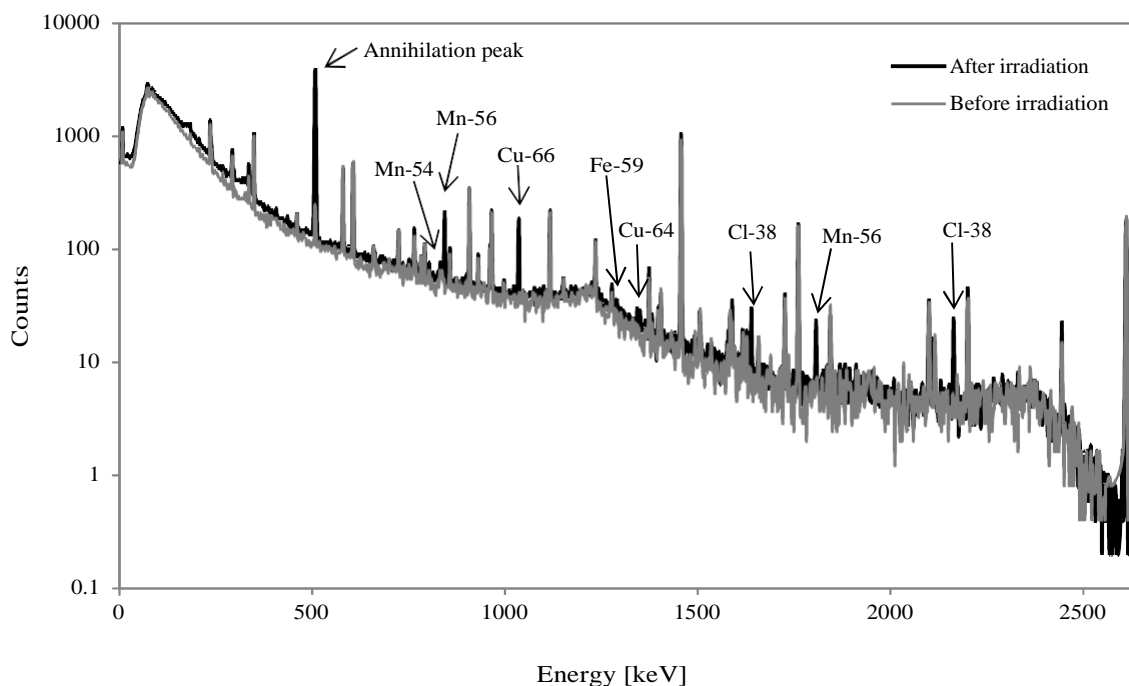
FIG.2. HPGe spectra of CC01 ionization chamber registered before and after emission of 10 000 MU using 15MV photon beam in a water phantom.

4. DISCUSSION AND CONSLUCIONS

Presented study has shown that the process of radionuclides activation takes place in materials of ionization chambers commonly used in radiotherapeutic beam commissioning and QA tests and could be quantify with the accuracy of about 25% using HPGe spectrometry.

The analysis of gamma-energy spectra of activated dosimeters has demonstrated, that for in-water-phantom irradiation conditions neutron capture (n,γ) process is the main mechanism of activation of γ-emitting radionuclides and photoactivation generates pure β+-emitters responsible for annihilation quanta, even in radiologically water-equivalent materials. Radionuclides originated these ways are rather short-lived, what has been pointed out by the assessment of effective half-lives of apparent radioactivity induced in each dosimeter under study, being of the order of 10 minutes. Furthermore, since intensity of neutron production depends on therapeutic beam end-point energy and linac construction (manufacturer), the studied phenomenon should be beam-quality dependent.

Skin of hands and eye lens – organs which are the most likely to be exposed to radiation during the operation and in-phantom positioning of dosimeters, are able to receive equivalent doses of the order of μSv/min, in which the activation of fluoride (β+), chlorine and inner electrode metals contribute the most. It is worth noticing that such an exposition is usually not detected by the personal dosimeters worn by the staff, which are calibrated in personal dose equivalent $H_p(10)$.

ACKNOWLEDGEMENTS

REFERENCES

[1] JUSTE, B., MIRO, R., VERDU, G., DIEZ, S., CAMPAYO, J., M., "Neutron activation processes simulation in an Elekta medical linear accelerator head", 36th Annual International Conference of the IEEE (Proc. Int. Conf. Chicago, IL, USA, 2014), IEEE Xplore (2014).

[2] BEGIN, F., SELLAM, A., NOURREDDINE, A-M., "Monte Carlo simulation of photoneutron activation in a medical LINAC", 4th International Conference on Advancements in Nuclear Instrumentation Measurement Methods and their Applications (ANIMMA, Lisbon, Portugal, 2015), IEEE Xplore (2016).

[3] FISCHER, H., W., TABOT, B., E., POPPE, B., Activation process in a medical linear accelerator and spatial distribution of activation products, Phys Med Biol 51 24 (2006).

[4] THOMADSEN, B., NATH, R., BATEMAN, F., B., FARR, J., GLISSON, C., ISLAM, M., LaFRANCE, T., MOORE, M., XU, G., YUDELEV, M., Potential hazard due to induced radioactivity secondary to radiotherapy: the report of task group 136 of the American Association on Physicists in Medicine, Health Phys 107 5 (2014) 442–460.

[5] POLACZEK-GRELIK, K., KARACZYN, B., KONEFAL, A., Nuclear reactions In linear medical accelerators and their exposure consequences, Appl Radiat Isot 70 (2012) 2332–2339.

[6] Rawlinson, J., A., Islam, M., K., Galbraith, D., M., Dose to radiation therapists from activation at high-energy accelerators used for conventional and intensity-modulated radiation therapy, Med Phys 29 4 (2002) 598–608.

[7] GURJAR, O., P., JHA, V., K., SHARMA, S., D., Radiation dose to radiotherapy technologists due to induced activity in high energy medical electron linear accelerators, Radiat Prot Environ 37 1 (2014) 25–29.

[8] JANISZEWSKA, M., POLACZEK-GRELIK, K., RACZKOWSKI, M., SZAFRON, B., KONEFAL, A., ZIPPER, W., Secondary radiation dose Turing high-energy Total body irradiation, Strahlenther Onkol 190 5 (2014) 459–466.

[9] HORST, F., FEHRENBACHER, G., ZINK, K., On the neutron radiation field and air activation around a medical electron linac, Radiat Prot Dosim 174 2 (2017) 147–158.

[10] TANA, L., CIOLINI, R., CIUFFARDI, E., ROMEI, C., D'ERRICO, F., Evaluation of air photoactivation at linear accelerators for radiotherapy, J Radiat Prot 35 2 (2015) 239–248.

[11] SAEED, M., K., POPPE, B., FISCHER, H., W., Direct air activation measurements at a 15–MV medical linear accelerator, Radiat Prot Dosim 163 2 (2015) 233–237.

[12] POLACZEK-GRELIK, K., ORLEF, A., DYBEK, M., KONEFAL, A., ZIPPER, W., Linear accelerator therapeutic dose – induced radioactivity dependence, Appl Radiat Isot 68 4-5 (2010) 763–766.

[13] SHEIKH-BAGHERI, D., ROGERS, D., W., O., Monte Carlo calculations of nine megavoltage photon beam spectra using the BEAM code, Med Phys 29 (2002) 391–402.

[14] JENDL-3.3 data base, Japan (2002), available on: www.nndc.bnl.gov/sigma/search.jsp

[15] SMITH, H. (ed.), Conversion coefficients for use in radiological protection against external radiation, ICRP Publication 74, Pergamon Press, Oxford, United Kingdom, 1996.

DOSES ASSESMENTS IN MAZELESS RADIOTHERAPY ROOMS

C. SALATA
Comissão Nacional de Energia Nuclear
Rio de Janeiro, Brazil
Email: camila.salata@cnen.gov.br

A. FACURE
Comissão Nacional de Energia Nuclear
Rio de Janeiro, Brazil

Abstract

Radiation protection has become an important field of study, as the use of ionizing radiation for diagnosis and therapy increased along the years. According to the ALARA principles, shielding is one of the most efficient ways to minimize radiation exposure. Linear accelerators for radiotherapy treatment can lead to a considerable risk due to radiation for public and workers if proper shielding is not calculated. Mazeless rooms for LINACS are becoming more usual, as they need less space to be constructed, but, on the other hand they are more expensive. The doors of those kinds of rooms are an important point, as they will have to be thicker in mazelles room to proper shield the radiation. The NCRP 151 lays out the general considerations for the shielding calculation of standard rooms, with mazes, but there are no specific recommendations for mazeless rooms on literature. The work herein presented evaluated the absorbed dose in a room model without maze, which will be constructed soon in Brazil. The applicant calculated the thickness of the door as if it was a room with maze, and the authors used computational simulation wit MCNP code to simulate the same room, and calculated the door thickness as if it was a secondary barrier. The dose limit considered was for public occupation, 1 mSv/sem, and the energy beam was of 6 MeV. The simulated results showed that the applicant calculation thickness for the door was underestimated in 88%. The obtained results are important to establish a better methodology for shielding calculation of mazeless radiotherapy rooms that are becoming more common in Brazil.

1. INTRODUCTION

The use of ionizing radiation in radiotherapy treatment has increased in recent years with a concomitant increase in exposure of patients and health workers to radiation hazards. According to the "ALARA" principle, acronym used for As Low As Reasonably Achievable, there is actually no safe dose of ionizing radiation. For the occurrence of stochastic effects, such as cancer, there is no threshold point and risk increases in a linear-quadratic fashion with dose. The three major principles to assist with maintaining doses "As Low As Reasonably Achievable" are time, distance and shielding[1,2].

Linear Accelerators for Radiotherapy can cause a considerable risk due to radiation to the occupationally exposed individuals (OEIs) and the public, if proper safety measures are not taken. A shielding design suitable for rooms with accelerators is an important security measure for the protection of OEIs and members of the general public [3]. The NCRP 151 lays out the general considerations for the calculation of shielding in standard radiotherapy rooms, although it is noted that many shield designs differ from this standard room, such as designs for rooms without mazes [4].

The mazes are concrete walls built between the accelerator and the entrance of the radiotherapy room, with the function of minimizing the dose of radiation at the door of the room. Rooms without mazes have been more used, as they require a smaller space to be built. In Brazil there are currently 2 radiation facilities without labyrinth, and another under construction. The doors of these types of room should have greater thickness, turning them extremely heavy and expensive. Because they are recent constructions, there is little literature about the doses in the doors at these types of rooms, and there is no international regulation or recommendation for rooms without mazes. Therefore, the objective of the study is to evaluate the absorbed dose in a room model without maze, which will be constructed soon in Brazil, and to verify if these doses are within the limits established by the Brazilian National Nuclear Energy Commission (CNEN).

2. METHODS

The simulated radiotherapy room was the exactly room, described in the shielding project, that an applicant sent to the CNEN for our evaluation. The main interest is about the door, which is the sensitive point in mazeless rooms. The applicant describes the door as being an area with occasional occupation of technicians

and patients. This region was considered a public area (in terms of shielding calculation) with U (use factor)= 1 and T (occupational factor) = 1/8. The applicant considered the following contributions to radiation in the door: patient scattering; Scattering of the primary beam on the walls of the room; Scattering of leakage radiation by the head on the walls of the room; Leakage radiation transmitted through the maze; And also the contribution of gamma capture and neutrons However this methodology is not suitable for this case because the room is not a standard model, there is no maze. The authors calculated the doses at the door as if the door was a secondary barrier, using a computer simulation.

To evaluate the absorbed doses at the door of this room, it was used a computer simulation with the code MCNPX (version 2.7.0). The head shielding of the accelerators were simulated in details. However, in order to simulate linacs with different energies, the energies of the electron hitting the target were changed (pencil beam). For the calculations a divergent beam of radiotherapy was simulated, with the collimator open to the maximum, generating a field of 40 x 40 cm^2 in the isocenter. The room was simulated without labyrinth with real dimensions, according to a shielding project of a radiotherapy facility in Brazil. Three detectors were positioned at different positions at the door, to estimate the equivalent dose of neutrons. The accelerator was first simulated with energy of 6 MeV, considering a working load of 1000 Gy/week. The simulated photon spectra was validated according to data published in the literature.

3. RESULTS

The simulated photon spectra presented agreement with those presented in the literature, with uncertainty less than 1% between them [5]. The simulated radiotherapy room is showed in Figure 1, all the lateral barriers will be constructed in concrete and the door will be constructed in lead, according to the applicant, and they were simulated with the same material and thickness as presented in the shielding project. The height of the door is 2,10 m and the width is 1,20 m; the distance from the door to the isocenter is 5,39 m.
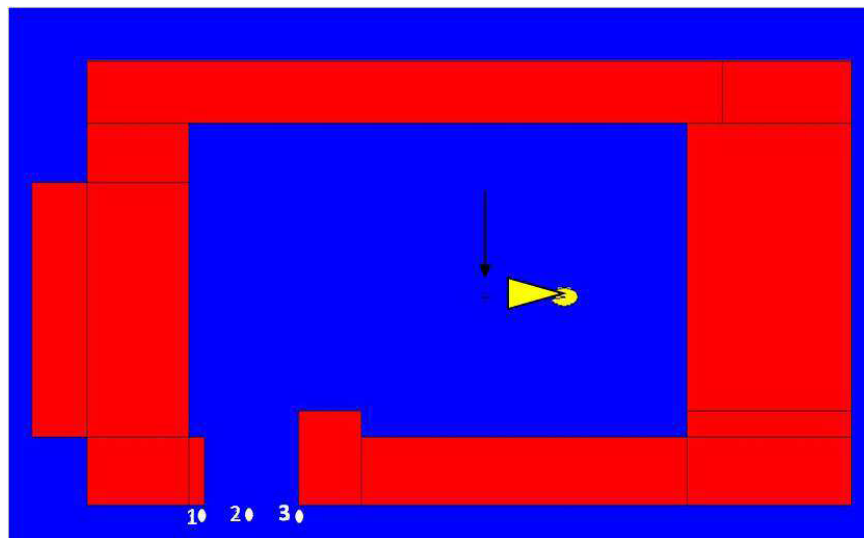
FIG. 1. Simulated mazeless room. 1, 2 and 3 are the detectors at the entrance door; Arrow points the isocenter; and in yellow, the LINAC.

The first simulation was for the 6 MeV energy beam. The final doses found in the detectors were: 13 mSv/week, at detector 1; 34 mSv/week, at detector 2; and 41 mSv/week at detector 3. It is important to note that there's a difference of more than 200% of the dose among detectors 1 and 3, highlighting the influence of the position along the door to measure the doses of radiation.

The necessary shielding for this room was considered for the highest dose, at detector 2, and the factor T= 1/8. It will be necessary 16,94 cm of lead to shield radiation, considering the Brazilian limits for public areas, which is 0,02 mSv/week. In the applicant's shielding project the calculated shielding was 9 cm of lead, as

he didn't consider the door as secondary barrier, he did the door calculation according the NCRP 151, considering the room a standard room with maze.

4. CONCLUSION

The computational simulation of a mazeless room showed that it is important to distinguish the calculation method of the door, from a room with maze. In this present work a shielding project submitted to the Brazilian National Nuclear Energy Commission for analysis was reproved. In this project the applicant calculated the door of a mazeless room as if it was a standard room. The calculated thickness of the door was underestimated in 88%, considering the Brazilian limits for public exposure of 1 mSv/week. This simulated room was for an energy beam of 6 MeV. As a future work the authors will calculate the same parameters, but with energies of 10 MeV and 15 MeV beans to study the neutron and gamma capture contributions in mazeless radiotherapy rooms. This will be important to evaluate the public and occupational doses in those kinds of bunkers, which are becoming more common in Brazil.

5. REFERENCES

[1] Healy; B.J., van der Merw,e D., Christaki, K.E., Meghzifene, A., Cobalt-60 Machines and Medical Linear Accelerators: Competing Technologies for External Beam Radiotherapy. Clin Oncol (R Coll Radiol). (2017) 29(2):110-115.

[2] Basran P.S., Baxter P., Beckham W.A.. Reducing radiation risks to staff for patients with permanently implanted radioactive sources requiring unrelated surgery. J Appl Clin Med Phys. (2015) 8;16(5):5372.

[3] Awosan K.J., Ibrahim M., Saidu S.A., Ma'aji S.M., Danfulani M., Yunusa E.U., Ikhuenbor D.B., Ige T.A., Knowledge of Radiation Hazards, Radiation Protection Practices and Clinical Profile of Health Workers in a Teaching Hospital in Northern Nigeria. J Clin Diagn Res. (2016) 10(8):LC07-12.

[4] Report No. 151 - Structural Shielding Design and Evaluation for Megavoltage X- and Gamma-Ray Radiotherapy Facilities (2005)

[5] Rezende G.F., Da Rosa L.A., Facure A., Production of neutrons in laminated barriers of radiotherapy rooms: comparison between the analytical methodology and Monte Carlo simulations. J Appl Clin Med Phys. (2014) 8;15(6):5035.

Trends in radiation protection of patients in modern radiotherapy

Katia Sergieva[1], Petya Kostova[2], Victor Zlatkov[3]
[1]Queen Giovanna University Hospital, Sofia, Bulgaria
[2]University Oncology Hospital, Sofia, Bulgaria
[3]University Obstetrics and Gynecology Hospital "Maichin Dom", Sofia, Bulgaria

E-mail address: sergievakm@abv.bg

Abstract.

Modern radiotherapy reached a very high degree of complexity and sophistication in the recent years and expected to represent an added value for the cancer patients in terms of clinical outcomes and radiation protection. New equipment in imaging and radiotherapy has been successfully put in our clinical practice and radiation therapy has improved considerably. The significant change has been achieved in treatment of patients with gynecological cancer in terms of clinical outcome and improved radiation protection. In Bulgaria cervical cancer is still a medical and social problem. The treatment of cervical cancer is complex and requires a multidisciplinary approach. In our hospital the patients for cervical cancer are treated with two 360° coplanar 6MV VMAT arcs, following manufacturer instructions. The treatment technique has offered precise dose confirmation to this very complicated in geometrical terms target volume. In this way the radiation dose distributions are shaped to the target with a steep fall in the dose to the neighboring normal tissues. The newest technologies undoubtedly lead to constant trends in the enhancing of the basic principles of radiation protection - justification and optimization, allowing us to treat more cancer patients efficiently, effectively and safely.

1. Introduction

Five years after the Bonn Conference is the time to present the progress in our daily clinical practice triggered by the joint statement of IAEA and WHO entitled: "**Bonn Call for Action to improve radiation protection in medicine in the next decade".** It identifies the main action which should be considered to be essential for the strengthen of radiation protection since the increasing use of ionizing radiation and to improve the balance between the benefits and risks for the human health.

The purpose is to present the authors' perspective on strengthened manufacturers' contribution leading to enhancement of basic principles of radiation protection: justification and optimization in modern radiotherapy, since it is the technologically and computer based medical specialty and our achieved change in clinical practice for radiation therapy (RT) of patients with gynecological cancer.

Radiation protection in medicine has unique aspects and is an essential element of medical practice. [1] Radiotherapy has been driven by constant technological advances since the discovery of X-rays in 1895. Advanced radiotherapy technologies have been continuously improved and refined with the principal aim of improving treatment outcome by means of dose distributions which conform more strictly to clinical target volumes. A highly conformal dose distribution allows for dose escalation in the target volume without increasing the radiation dose to neighboring normal tissues, and for a reduction in radiation dose to normal tissues without decreasing the dose to the target. [2] Modern radiotherapy reached a very high degree of complexity and sophistication in the recent years and expected to represent an added value for the cancer patients in terms of clinical outcomes and improved radiation protection.

2. Material and methods

Modern radiotherapy is a very complex process of treatment planning and treatment delivery. Steps in the process include patient identification, preparation of a treatment directive, patient positioning and immobilization for planning and treatment, volume delineation from patient images, treatment planning and review, and treatment delivery. [3] It based on different technologies in imaging, in dose delivering, in dose measurements and in treatment assessment. The cutting-edge technologies are in the base of observed enhance trends in improved radiation protection of cancer patients receiving modern radiotherapy. The following achievements are supported the effective and safety management of cancer patients.

In imaging: High quality imaging has a huge contribution in cancer screening and radiotherapy. Technology improvements in current generation computer tomography systems (CT) are realized in reducing the dose, improved image quality and speed of investigation. The latest iterative reconstruction software in combination with the latest scanner detector technology allowing to perform CT with doses of less than 1 mSv. In the last 12 months, several CT vendors have introduced new systems with the latest in dose reduction hardware and software. [4] Several manufacturers released software updates to integrate of positron emission/computed tomography (PET/CT) images into radiation therapy planning. PET/MRI Scanners align the features of MR imaging — such as soft tissue contrast, diffusion-weighted imaging and dynamic contrast-enhanced imaging with the PET provided quantitative physiologic and metabolic data. Currently, radiation oncology is an application gained major value from double

modality synergetic images for more precisely delineation of location of tumors and therefore to individualize treatment for each cancer patient.

In Treatment Planning Systems (TPSs): TPSs are at the heart of modern radiotherapy and the key to improved patient outcomes and safety. Technological advances in TPS provides: Significant speed enhancements (calculation speeds up to four times faster than in previous versions); Increasing Automation – giving capabilities such as auto-segmentation, dose optimization and auto planning help healthcare professionals to focus on the critical aspects of care; Robust optimization based on 4-D computed tomography (CT) images. Unlimited patient data storage (Knowledge-sharing Platforms) helps clinicians to share and learn from one another. [5]

In Image Guided RT (To see what we treat): Imaging plays an important role in providing the precise guidance during the radiation treatment. The latest mode of MRI Guided Radiation Therapy combines two technologies of MRI scanner and a linear accelerator in a single system. This allowing radiotherapy to be adjusted in real time and delivered more accurately and effectively even to moving tumors than ever before. MRI solves both of the primary issues with CBCT — poor soft tissue contrast and difficulty capturing moving organs — while delivering no extra radiation dose to the patient.

In adaptive RT (ART): Once it is possible to "see what we treat", the next step is to perform ART. The huge impact has a graphics processing units (CPUs) which can run accurate Monte Carlo based VMAT dose calculations in less than 40 s – opening up the possibility of dose recalculation while the patient is on the table [6] and to create the adapt treatment plan according to the patient specific changes, that are unaccounted in the initial plan.

In dosimetry systems: The precise dosimetry systems and extensive QA programs are cornerstone of the safe and effective radiation cancer treatment. World's leading manufacturers providing a new generation dosimetry systems with several attractive features for radiation dosimetry including real-time display of dose & dose-rate, fully automated in vivo dose monitoring requiring no user interaction with high resolution, minimal perturbation, high dynamic range of dose measurements, reliability and robustness.

Most of the above mentioned technologies such as CT, PET/CT, MRI and Multimodality Linacs have been successfully put in our routine clinical practice and RT has improved considerably. The significant change has been achieved in radiotherapy of patients with gynecological cancer in terms of clinical outcome and improved radiation protection.

In Bulgaria cervical cancer is still a medical and social problem. It ranks second among gynecological tumors in the period 1993-2002, while in 2011 it is the fourth most common cancer in women and accounts for 7.2% of all cancer cases. The five year relative survival for cervical cancer in Bulgaria is 54.8%, comparing with European average – 65.4%. [7, 8] Cervical cancer management varies depending on the International Federation of Gynecology and Obstetrics (FIGO) stage. Modern radiotherapy is a highly effective and curative treatment for patients with invasive cervical cancer, and it is the standard of care for locally advanced disease. [9] All patients with cervical cancer were treated using a 4-field box technique (See Fig.1. Left) only five years ago. Currently, we are using multiple modern imaging modalities - CT, MRI, PET/CT for delineation of target volume and adjacent normal organs-at-risk (OAR). All patients were CT-scanned supine with both full and empty bladder to take into account the internal organ variation with bladder filling status. Clinical Target Volume (CTV) was contoured in accordance with Lim et al. [10]. OARs were defined as the rectum, bladder, bowel and femoral heads. All patients for cervical cancer are treated with two 360° coplanar 6MV VMAT arcs (Varian RapidArc®), following manufacturer instructions (See Fig.1. Right).

FIG. 1. Left – 4-field box technique; Right – VMAT technique

3. Results

The newest treatment technique has offered precise dose confirmation to this very complicated in geometrical terms target volume. In this way the radiation dose distributions are shaped to the target with a steep fall in the dose to the neighboring normal tissues (See Fig.1. Right), while the conventional 4FB technique resulted

in a bath of high-dose radiation to a large volume (See Fig.1.Left). High precision in delivery is achieved by image guided radiotherapy (IGRT), where the target is imaged immediately before treatment with the patient in the treatment position. The dosimetric advantages in organ sparing has maintained excellent long term cure rates and reducing GI, GU and hematologic toxicity, especially in patients treated with concurrent chemotherapy [11]. In terms of radiation protection it means that we are ensuring, that exposures to target volumes are individually planned taking into account that doses to non-target volumes and tisues will be as low as reasonably achievable (ALARA) and cosistent with the intended radiotherapeutic purpose.

4. Discussion

The need of effective modern radiotherapy treatment is growing as the global cancer epidemic continues to spread. It saves lives, prolongs lives and improves the quality of life. Currently, radiotherapy is widely recognized to be one of the safest areas of modern medicine and errors in radiotherapy are very rare. [12] Patient safety is of the utmost concern to radiation oncologists and safety considerations are woven into all aspects of clinical practice. Technological advances and clinical research over the past few decades have given radiation oncologists the capability to personalize treatments for accurate delivery of radiation dose based on clinical parameters and anatomical information. Two major strategies, acting synergistically, will enable further widening of the therapeutic window of radiation oncology in the era of precision medicine: technology-driven improvement of treatment conformity, including advanced image guidance and particle therapy, and novel biological concepts for personalized treatment, including biomarker-guided prescription, combined treatment modalities and adaptation of treatment during its course. [13]

The following challenges are facing radiation professional community: The imaging doses in modern radiotherapy and secondary cancers should be observed in future. IGRT is a rapidly growing field and imaging is increasingly used in modern radiation therapy. The imaging devices are using ionizing radiation and justification and optimization of protection and safety must be observed. The concomitant doses connected with diagnostic and theraupetic imaging increase. They are becoming nonnegligeblae and must be managed. Innovations in radiotherapy have contributed considerably to increasing the survival rates for several cancer diseases. New radiotherapy techniques deliver higher low dose radiation to large volume of normal tissues and are in debating as more secondary cancer inducers. A secondary cancer after radiotherapy is in important issue that reduces treatment efficiency and should be decreased. [14] The development of new techniques and methods for predicting long term effects from radiation treatment becomes vital in order to confidently introduce new approaches. [15]

5. Conclusion

Modern radiotherapy requires advanced equipment and a reasonable treatment strategy to gain the best clinical outcome moreover, when the vision of European Society for Radiotherapy & Oncology for 2020 is: "Every cancer patient in Europe will have access to state of the art radiation therapy, as part of a multidisciplinary approach where treatment is individualized for the specific patient's cancer, taking account of the patient's personal circumstances".[16] We are doing our best to provide safe and effective radiotherapy, but we know, that we can do better. Times have changed, mostly for the better. Few would be argue with the fact, that the tools with which we operate today are vastly superior and enormously more complex than a few years ago. Advances in technology provide more sophisticated, promising and accurate techniques for targeting malignancies while minimizing normal tissue damage are crucial for patients who treated with radiation therapy. In terms of radiation protection it means that we are doing much more good than harm – overarching justification of medical exposure and we are ensuring that for each patient the exposure of volumes other than the planning target volume is kept as low as reasonably achievable consistent with delivery of the prescribed dose to the planning target volume within the required tolerances (ALARA). [17] The newest technologies undoubtedly lead to constant trends in the enhancing of the basic principles of radiation protection - justification and optimization, allowing us to treat more cancer patients efficiently, effectively and safely.

Finally, authors highly appreciate the long-term efforts and activities of IAEA to improve radiation protection of patients, providing standards, training and guidance, direct technical assistance and building capacity, and awareness.

REFERENCES

[1] Ola Holmberg, Renate Czarwinski, et al. The importance and unique aspects of radiation protection in medicine. European Journal of Radiology 76 (2010) 6 - 10.
[2] Available on: http://www.irpa.net/members/P07.16fp.pdf
[3] Accuracy Requirements and Uncertainties in Radiotherapy. IAEA Human Health Series №31. INTERNATIONAL ATOMIC ENERGY AGENCY, VIENNA, 2016.
[4] Available on: https://www.itnonline.com/content/ct-dose-management
[5] Available on: https://www.itnonline.com/issue/julyaugust-2016
[6] Available on: http://medicalphysicsweb.org/cws/article/opinion/65540

[7] Petya Kostova,Victor Zlatkov, S Danon. Five-year overall survival and prognostic factors in patients with cervical cancer in Bulgaria. Journal of B.U.ON.: official journal of the Balkan Union of Oncology 13 (2008) 363 - 8.

[8] Bulgarian National Cancer Registry, Том XXII, Volume XXII, 2013.

[9] Danielle Rodin, Timothy P. Hanna, Emily Burger, et al. GLOBAL ACCESS TO RADIOTHERAPY FOR CERVICAL CANCER: THE COST OF INACTION, IJRBP   96 (2),2016, S14 - S15.

[10] Karen Lim, M.B.B.S., William Small Jr., M.D., Lorraine Portelance, M.D., et al. Consensus Guidelines for Delineation of Clinical Target Volume for Intensity-Modulated Pelvic Radiotherapy for the Definitive Treatment of Cervix Cancer. IJRBP, 79(2), 2011, 348 - 355.

[11] Ana Fernandez-Ots, Juanita Crook. The role of intensity modulated radiotherapy in gynecological radiotherapy: Present and future. RPOR 18 (2013) 363 - 370.

[12] General guidelines on risk management in external beam radiotherapy, EU, RADIATION PROTECTION N° 181, 2015.

[13] Michael Baumann, Mechthild Krause, Jens Overgaard, et al. Radiation oncology in the era of precision medicine. Nature Reviews Cancer 16, 2016, 234 - 249.

[14] Abdollahi et al.: Radiation protection and secondary cancer prevention. IJCTO 3 (3), 2015, 1 - 9.

[15] Workshop: Risk of secondary cancer following radiotherapy. 8-9 September 2016, Stockholm.
Available on: www.crpr-su.se/smn/Workshop%20Book.pdf

[16] Available on: http://www.estro.org/about/mission-values/vision

[17] Radiation Protection and Safety of Radiation Sources: International Basic Safety Standards, IAEA Safety Standards Series No. GSR Part 3, INTERNATIONAL ATOMIC ENERGY AGENCY, VIENNA, 2014.

CURRENT STATE OF DOSIMETRY PROVIDING OF RADIOTHERAPY IN UKRAINE AND IAEA CONTRIBUTION TO ITS IMPROVEMENT:
The results of National survey and IAEA TLD-audit of dose calibration quality

L.L. STADNYK
Grigorev Institute for Medical Radiology
Kharkiv, Ukraine
Email: LStadnyk@ukr.net

O.Y. SHALOPA
Grigorev Institute for Medical Radiology
Kharkiv, Ukraine

Abstract

The efficiency of radiotherapy of oncology diseases directly depends on state of specialized treatment equipment, accuracy of delivery of the absorbed dose to the tumor (error should be less 5%), medical staff qualification. The important stage of radiotherapy is dosimetry providing which is including the dose planning and clinical dosimetry. The results of National survey of radiotherapy status and IAEA/WHO TLD postal audit of dose calibration quality for radiation beams in Ukraine are represented. Questionnaire included the detail questions concerning availability of equipment for simulation of radiotherapy, treatment planning systems, equipment for clinical dosimetry, used dosimetry protocols. The quality of clinical dosimetry of radiotherapy beams in Ukrainian Oncology Centers are estimated by IAEA/WHO TLD postal audit of dose calibration quality. During 1998-2016 there were checked 393 radiation beams (every radiotherapy unit participated in TLD-audit once per 2-3 years. Due to IAEA support in frame of National TCP (training of 65 medical physicists, delivery of 25 modern clinical dosimetry sets) the results of TLD-audit in 2014-2016 became significant better: the limit of acceptance error 5% was exceeded only for 8-12 % of teletherapy units in comparison with 25-35 % in 1998-2013. For every bad result the reasons of mistakes were analyzed.

1. INTRODUCTION

Radiation therapy is one of the main methods of cancer treatment. The effectiveness of radiotherapy is determined by such parameters as: the quality of the diagnosis and evaluation of the target tumor volume, the quality of treatment planning and clinical dosimetry, the accuracy of the dose delivery to tumor. In according with ICRU and IAEA requirements in radiotherapy the overall uncertainty of delivery of an absorbed dose to the tumor target volume should not exceed 5% [1, 2]. Such accuracy can be ensured by qualitatively conducted clinical dosimetry, the use of modern dosimetric protocols for determination of the absorbed dose in water.

In the paper the analysis of the current state of dosimetry providing in radiotherapy departments of Ukraine was carried out due to results of annually survey of Oncology Hospitals/Centers in framework of IAEA DIRAC programme (https://dirac.iaea.org) and the results of IAEA/WHO postal TLD-audit of dose calibration quality for external beams of radiotherapy units in 1998-2016. The significant influence of the IAEA technical support on improving the effectiveness of clinical dosimetry was shown due to training of medical physicists, using modern dosimetric protocol that led to a significant decrease in the number of observed errors in dosimetry calibration based on the results of the IAEA TLD postal audit.

2. MATERIALS AND METHODS

For organization of National survey of Ukrainian Oncology Hospitals/Centers on the status of radiation therapy, a detailed questionnaire was developed in according with information needed for IAEA DIRAC database. Concerning dosimetry providing in hospitals the questionnaire included the questions about the availability of equipment for the simulation of radiotherapy, treatment planning systems, equipment for clinical dosimetry.

A separate part of the questionnaire was concerned with clinical dosimetry: types of dosimeters in radiotherapy department, the frequency of dose calibration of radiation output by metrological organizations for certification of radiotherapy units and used dosimetric protocol, frequency and volume of the internal clinical

dosimetry in department and used dosimetric protocol, treatment planning systems, the system of absorbed dose verification on target volume and critical organs.

An analysis of the dose calibration quality of radiation beams of radiotherapy units in Oncology Hospitals was carried out based on the results of an independent IAEA/WHO TLD postal audit. Annually about 20-40 radiotherapy machines participate in the IAEA TLD-audit, usually each radiotherapy unit was monitored once every 2-3 years. During 1998-2016 there were 393 checking of radiation beams of radiotherapy units for 45 Radiotherapy Departments.

3.   RESULTS AND DISCUSSION

According to the results of the questionnaire within the framework of the DIRAC programme, it is established that in Ukraine currently there are 80 gamma-therapy machines (for external radiotherapy) and 24 linear accelerators. The 2D, 3D treatment planning systems (TPS) are available only in 70% radiotherapy departments of oncology institutions. In total, there are 57 TPSs for practice using with types: PLAN W 2000 (34%), Eclipse3D (15%), HDR plus and Brachyvision (15%), XiO 3D (9%), and others. Unfortunately in 13 (30%) oncology hospitals the method of manual planning and calculation of the absorbed doses is used.

Until 2012, the most of radiotherapy departments had been used only obsolete equipment for clinical dosimetry type 27012 or didn't have any clinical dosimeters and standard water phantoms for direct clinical dosimetry measurements. Within the framework of the National IAEA project - TCP UKR6010 "Developing and Implementing a National Quality Control System by Strengthening the Knowledge and Capacity of Medical Physics at Radiotherapy Departments" (2012-2013) Ukrainian Oncology Hospitals/Centers received 25 sets of dosimetry equipment, which included UNIDOS E dosimeters with two ionization chambers type PTW 30013 Farmer and standard water phantoms.

In Fig. 1 presents the data on the park of clinical dosimetry equipment in Ukraine before and after the IAEA technical support in frame of the IAEA National Technical Cooperation Project.
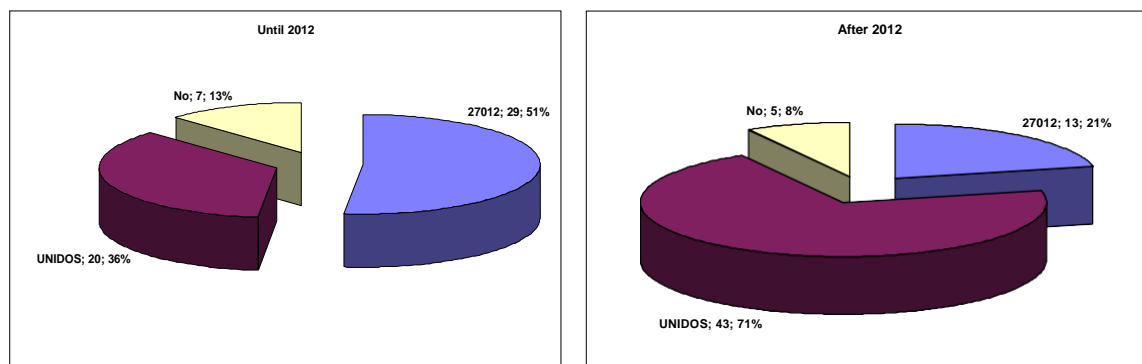
FIG. 1. Distribution of clinical dosimeters in Ukraine before and after IAEA TCP

As can be seen from Fig. 1 until 2012, dosimeters of type 27012 were the most used for clinical dosimetry in radiotherapy departments (51%), in 7 radiotherapy departments (13%) there was no dosimetric equipment. After IAEA technical support, the number of modern clinical dosimeters of the type UNIDOS increased to 43 units (71 %), while the number of obsolete dosimeters of type 27012 was reduced to 13 units (21 %). Unfortunately currently 5 oncology hospitals do not have clinical dosimeters at all and 3 oncology hospitals have only obsolete clinical dosimeters type 27012.

An important component of IAEA technical support in framework of the National TCP was the organization of four training courses on which 65 medical physicists from 39 Ukrainian Oncology Hospitals were trained as on clinical dosimetry and quality assurance of radiation therapy as on the quality assurance of automated planning systems for radiotherapy.

Beginning in 1969, the IAEA, together with WHO, conducts a regular postal audit of the dose calibration quality of external radiation beam of radiotherapy units (gamma-therapy machines and linear accelerators) in different countries using TLD-method [3]. The main goal of this programme is the estimation of level of radiation therapy quality and existing dosimetric practice in medical oncology institutions of the country, to improve the quality of clinical dosimetry by introducing the modern methodological documents for calculating absorbed doses. Ukraine participates in IAEA/WHO TLD postal audit program since 1998.

Results of IAEA/WHO TLD postal dose quality audit for radiotherapy units of Ukrainian Oncology Hospitals in 1998-2016 are presented in Fig 2-3.
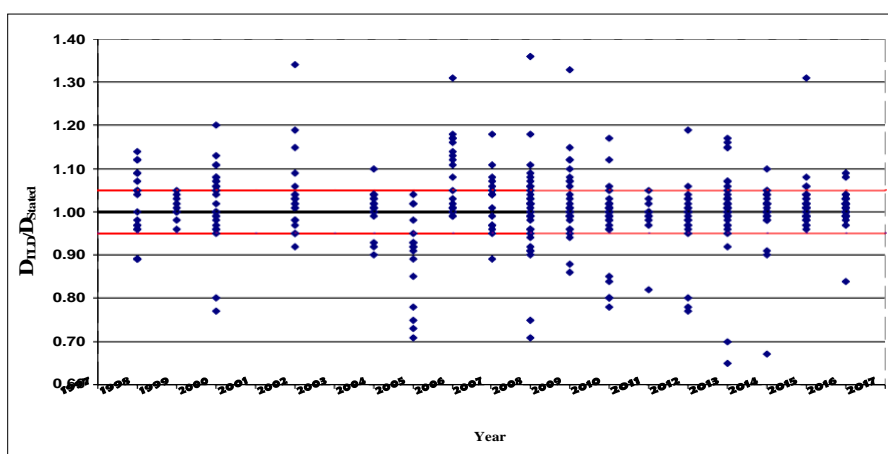
FIG. 2. Results of IAEA/WHO TLD postal audits in Ukraine: the 5% acceptable limit is indicated by red lines
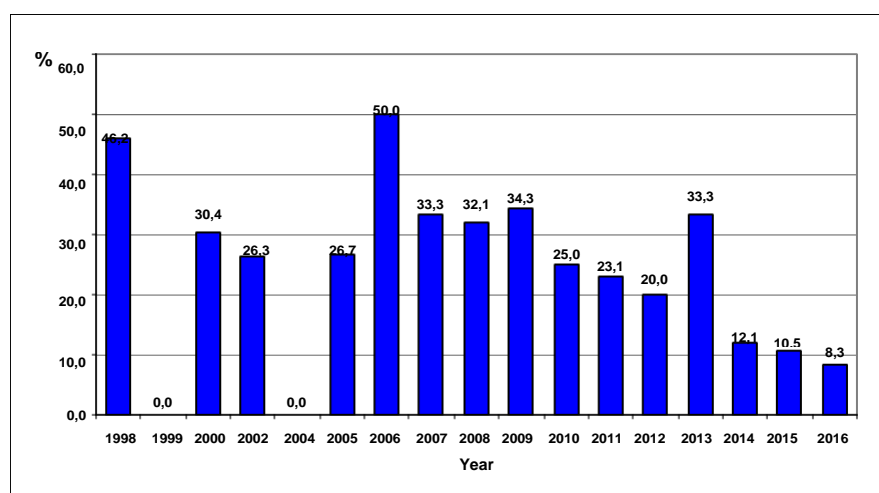
FIG. 3. Trend of number radiotherapy units (%) with error of more than 5%

As can be seen from Fig. 2 and 3, in 1998-2013, annually the results of IAEA TLD-audit for about 25-35% of radiotherapy units (twice – up to 50%) were unsatisfactory: the limit of acceptance error was exceeded 5%. For the most cases the errors were about 7-12 %, but for some radiotherapy units – up to 30-35 %. These radiotherapy units participated in the second stage of IAEA TLD-audit for determination whether the error was random or systematic.

Analysis of the errors showed that a significant number of them are associated with the calibration of radiation beam using obsolete equipment for clinical dosimetry and using of the old dosimetric protocol to determine the absorbed dose in water from the results of measurements of radiation output in air (in R/min).

In the process of IAEA training courses medical physicists from Ukrainian Oncology Hospitals studied the modern dosimetry protocol for determination of absorbed dose in water [4] and had the practical sessions of clinical dosimetry on gamma-therapy machine and linear accelerator using clinical dosimeter UNIDOS E and standard water phantom. Due to IAEA support in frame of National TCP (training of 65 medical physicists, delivery of 25 modern clinical dosimetry sets) the results of TLD-audit in 2014-2016 became significant better: the limit of acceptance error 5% was exceeded only for 8-12 % of teletherapy units in comparison with 25-35 % in 1998-2013 (Fig. 3).

In the work, an analysis of influence of used dosimetric protocols on IAEA TLD-audit results was made. These results have been showed in Fig.4: ratio of the number of radiotherapy units with good and unacceptable results in dependence of used dosimetry protocols: Protocol 1 – the calibration of the radiation beam in the exposition dose in air, Protocol 2 – the calibration in the absorbed dose in water. Red parts of histograms

indicate the number of radiotherapy units that showed unsatisfactory results (the error of dose delivery was more than 5%).
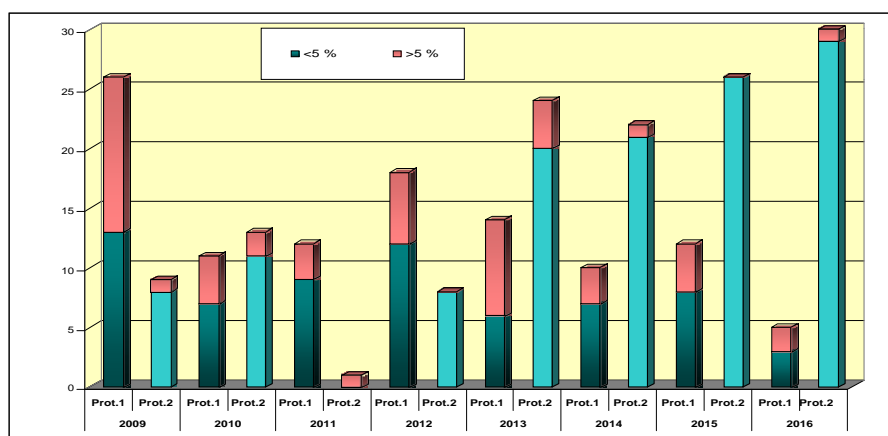
FIG. 4. Influence of used dosimetric protocol (Prot.1 or Prot.2) on TLD- audit results

As can be seen from Fig. 4, when for calibration of radiation beam it was used the protocol based on the measurements radiation exposure in air (R/min) the number of errors > 5% was about 30-50%, while using the dosimetry protocol based on standards of absorbed dose to water, the deviations more than 5% were 10-15% [4].

4. CONCLUSION

Due to the technical support of the IAEA the dosimetry providing of radiotherapy in Ukraine had been significant improved, which affected to the results of the IAEA/WHO TLD-audit of dose calibration quality of radiation beams for radiotherapy units. However, the situation in radiotherapy department is far from satisfactory. To improve the effectiveness of radiation treatment for cancer patients, Ukraine should give a large contribution: there are organization of national training and retraining of medical physicists, the re-equipment of radiotherapy departments with modern radiotherapy machines, treatment planning systems, modern dosimetry equipment.

REFERENCES

[1] INTERNATIONAL COMMISSION ON RADIOLOGICAL UNITS AND MEASUREMENTS, Determination of Dose in a Patient Irradiated by Beams of X or Gamma Rays in Radiotherapy Procedures, Rep. 24, ICRU, Bethesda, MD (1976).

[2] INTERNATIONAL ATOMIC ENERGY AGENCY, Quality Assurance in Radiotherapy, IAEA-TECDOC-1040, IAEA, Vienna (1997).

[3] IZEWSKA, J., ANDREO, P., VATNITSKY, S., SHORTT, K.R., The IAEA/WHO TLD postal dose quality audits for radiotherapy: A perspective of dosimetry practices at hospitals in developing countries, Radiother. Oncol. **69** (2003) 91–97.

[4] INTERNATIONAL ATOMIC ENERGY AGENCY, Absorbed Dose Determination in External Beam Radiotherapy: An International Code of Practice for Dosimetry Based on Standards of Absorbed Dose to Water, Technical Reports Series No. 398, IAEA, Vienna (2000).

STUDY : A YEAR EVALUATION OF RADIATION LEAKAGE AT LINAC ROOM USING RADIOCHROMIC FILM

W E WIBOWO[1], S ULYA[1,2], LAN FATIMAH[1,2], YS ASRIL[1,2], KARTUTIK[2], A FITRIANDINI[2], SA PAWIRO[2]

[1]Department of Radiotherapy, National General Hospital Dr.Cipto Mangunkusumo
Jakarta, Indonesia
[2]Department of Physics, Faculty of Mathematics and Natural Sciences, Universitas Indonesia
Depok, Indonesia

Email: wahyu.bovie@gmail.com

Abstract

Leakage room measurement was done for ensuring total exposure were not exceed the limit. The measurements mostly were done by using survey meter, film badge, and TLD. The Gafchromic EBT3 was one of radiochromic film type that has sensitivity dose range 0.1-10 Gy. Furthermore, the purpose of this study was measuring radiation leakage from high-energy LINAC room in a year. The measurement was done using Gafchromic EBT3 for Elekta Synergy S and Synergy Platform treatment room. Operator wall and door was chosen for measurement parameter. The Measurement was done by June 2016 until May 2017. The film that has been exposed until 30 days was scanning to get the pixel value converted to netOD. On the other side as a comparison using survey meter STEP OD-2 (PTW-Freiburg), data analyzing was done by netOD analysis with calibration curve taken from both linacs to get dose value. Then dose value was calculated into exposure value. The Synergy-S measurement result shows that highest value of exposure in operator and door exceed 2.893 µSv/h and 2.899 µSv/h for measurement in April and December 2016. Therefore, Synergy Platform measurement exceeds 3.851 µSv/h and 3.862 µSv/h for operator room and door respectively. In the range of reading differences with survey meters ranging from 0.04% to 4.58%, cumulative radiation leakages in the LINAC room of supervision area due to the high-energy photons can use the Gafchromic EBT3. As well as the consequences of patient care but also as a result of routine QA activities. Moreover, photoneutron effect due to activation of high energy photon (≥10 MV) to metal, also can be shown by using this film. Although more data is needed and other dosimeters can read well for cumulative dose or exposure and photoneutron effects.

1. INTRODUCTION

Radiation therapy was one of the modalities used for cancer therapy in addition to chemotherapy and surgery. According to best available practice, 52% of patients should receive radiotherapy at least once during the treatment of their cancer [1]. The aims of radiotherapy were to give the prescribed dose to the tumor and to protect as much as possible the organs at risk and surrounded tissue [2]. To achieve this, high energy radiation (in Mega-Voltage order) was commonly used Linear Accelerator (LINAC). Linear accelerator was commonly used for radiotherapy treatment. The high-energy radiation requires special treatment both in the planning of therapy as well as on the design of the room radiation therapy equipment.

The high-energy radiation therapy treatment room has a special design and shielding. The purpose of radiation shielding was to reduce the effective equivalent dose from a linear accelerator to a point outside the room to a sufficiently low level, one that is determined by individual states [3]. The states were commonly based on NCRP-151 [4]. Frequently, a higher level was chosen for areas restricted from public access (i.e., "controlled" areas) and occupied only by workers; this limit is 0.1 mSv/week. The purpose of radiation shielding is to limit radiation exposures to members of the public and employees to an acceptable level [4]. This goal it is expected that radiotherapy implementation reduces the risk of stochastic and deterministic effects for radiation worker and the public. Therefore, the situation did not exceed the exposure limit set by Nuclear Energy Regulatory Agency of Indonesia (BAPETEN). Radiation measuring instruments were needed to detect and quantity two type of exposure: external exposure to penetrating radiations emitted by sources outside the human body, and internal exposure which was associated with radioactive materials which were in a form capable of entering and interacting with the human body [5]. Based on that guideline, there was 4 type of radiation measuring instrument may be used in the work-place such as dose rate meters used to measure the external exposure, dosimeters which indicate the cumulative external exposure, surface contamination meters, airborne contamination meters and gas monitors which indicate the external exposure. On monitoring of exposure to

LINAC room, periodic checking was required by medical physicist and radiation protection officer using survey meter.

The type of survey meter used in monitoring LINAC room radiation exposure may use ionisation chamber, scintillation, and Geiger-Muller according to the energy range of the survey meter [5]. For monitoring of exposure received by officers using radiographic film badge and Thermoluminescent Dosimeter (TLD). TLDs and badge films was a great choice for knowing accumulated exposure over a period of time [6]. On the other hand, the radiochromic films in dose monitoring become one of the most commonly used options for radiotherapy. The radiochromic film has in the last ten years provided many advances and achievements in radiotherapy radiation dosimetry [7-12]. One of the major advances has been the continual increase in available dose sensitivity within the megavoltage as well as kilovoltage range. The radiochromic film consists of a single radiochromic film consists of a single or double layer of radiation-sensitive organic microcrystal monomers on an organic microcrystal monomers, on a thin polyester base with a transparent coating. Another reason was, the radiochromic film has the widest ranges of passive detectors between 0.01 until 1000 Gy [13-15]. And the Gafchromic EBT3 has dose range 0.1-10 Gy. For this reason, the author tries to make a study in evaluating exposure due to radiation leakage for LINAC room as a study as long as one year using Gafchromic EBT3.

2. METHODELOGY

2.1 LINAC Room

Two Room of Elekta LINAC (Elekta AB, Stockholm, Sweden) with maximum photon energy of 10 MV and 18 MeV electrons were evaluated for radiation leakage. Each linac having a maximum 40x40 cm^2 field size for Elekta Synergy Platform and 21x16 cm^2 for the Elekta Synergy S, there were has the same dose rate. Both rooms are designed using 10 MV photon energy with shielding goal of 20 mSv /year and 1 mSv /year for workers and public respectively, based on Nuclear Energy Regulatory Agency of Indonesia rules. The operating time for both LINAC is between 10-11 hours per day with 5 days per week and 50-65 patients per day. In addition, 1 hour for daily QA and 2 days for monthly QA and once time for yearly QA. The therapist worker was divided with 2-3 shift per day.

2.2 Film Calibration

The Gafhromic EBT3 by Ashland was used to evaluate the results of LINAC Elekta room exposure. The calibration was performed on the Elekta Synergy Platform and Elekta Synergy S with films placed at maximum depth on the range of doses 0-5 Gy as well as with 10x10 cm Field, 10 MV Energy, and 100 cm SSD. Moreover, the size of the film was cut into 3.2 x 2.5 cm^2. The calibration scheme could be seen at Figure 1 [16].

2.3 Film Data Evaluation

The radiation leakage measurements were performed monthly on the operator's room and maze doors using EBT3 films taped to the operator's wall and doors. This measurement was carried out from June 2016 to May 2017, each measuring duration of 30 days Performed a pixel value reading on the result of leakage measurement. Every month, the film revoked and re-paired a new film on both LINAC in the same position as the previous month. The film that have been exposed until 30 days was scanning to get the pixel value. On the other side as a comparison using survey meter STEP OD-2 (PTW-Freiburg), has been done yearly measurement of exposure to the operator's area and in front of the LINAC door for both LINAC. The position of the film data evaluation could be seen on figure 2.

2.4 Film Scanning

Films that have been exposed to calibration and data of exposure are scanned using EPSON scanner Expresio 11000 XL. ImageJ software was used to read the scanning results and plotted the calibration curve graph for both LINAC room calibration. Based on research conducted by Borca et al, 2013 [17], suggested the process of developing EBT3 film is 3×24 hours. Since the response of film reading will always change influenced by the length of developing process. After the process of developing, scanning the film using Epson Perfection V700 scanner with 48-bit mode, 16-bit each channel color consisting of RGB or grayscale and resolution 72 dpi and stored in the format (.TIFF) [17-20].
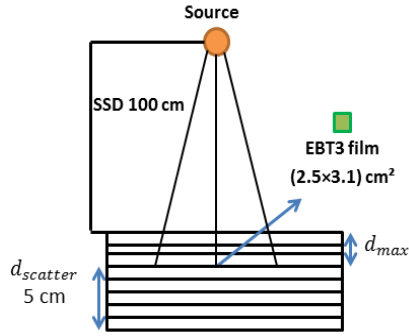
FIG.1. Scheme of film calibration
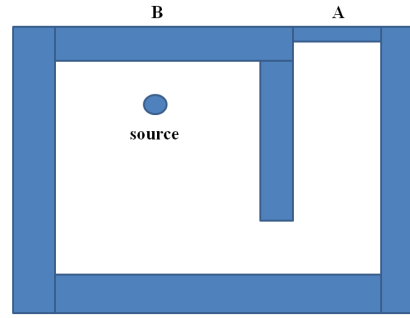
FIG.2. Position of film data evaluation at: A. door, B. Operator of LINAC room.

Furthermore, the readout of the film calibration was performed in the graph with the relation between dose and net Optical Density (netOD) to be calibration curve. The netOD value was calculated by subtraction the pre-scan OD value from the corresponding post-scan OD value [21]. The value of netOD which was used to analyse of the effect on radiation leakage room was given according to the equation (1):

$$net\theta = \log_{10}\left(\frac{PV_{un}}{PV_{ex}}\right) \tag{1}$$

where θV_{un} is an unexposed pixel value, and θV_{ex} is electron beam exposed pixel value [22].

3. RESULT AND DISCUSSION

The resulting dose or exposure result was obtained by inserting the netOD value for each film each month into Figure 3 and 4 as the calibration curve of the LINAC Elekta synergy S and synergy platform, respectively. In both calibration curve images obtained the relationship between netOD with a linear dose. This result is in line with the calibration curve in other studies [16][23]. Furthermore, the overall dose value is plotted in Table 1 and 2, which is the dose or exposure table received every month for both Elekta Synergy S and Synergy Platform.

In Table 1 the highest value for operator room and door was in April 2017 and December 2016, respectively with value 2.893 µSv/h and 2.899 µSv/h. In contrast to the lowest value of both the operator room and the door is in the same month ie in September 2016 with a value of 2.775 µSv/h and 2.738 µSv/h for operators and doors respectively. Furthermore, the value of exposure to the door except in September-October 2016 and March 2017 has a higher value compared to exposure to the operator. This result was possible because of the effect of photoneutron at 10 MV energy. Moreover, in December 2016, the value of door exposure is much higher than that of operators due to this month's annual QA which enables increased effects of photoneutron.
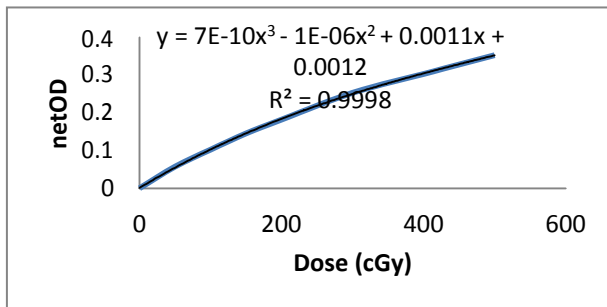
FIG.3. Calibration curve of LINAC Elekta Synergy S
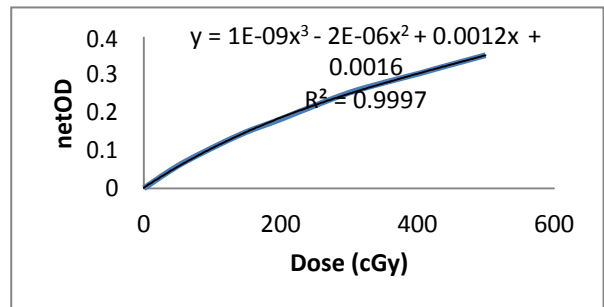
FIG.4. Calibration curve of LINAC Elekta Synergy Platform

TABLE 1. DOSE AND EXPOSURE MEASUREMENT FOR LINAC ELEKTA SYNERGY S ROOM

Month	netOD		Dose (Gy)/month		µSv/h	
	Operator room	Door	Operator room	Door	Operator room	Door

2016						
June	0.057	0.064	0.126	0.127	2.870	2.889
July	0.056	0.064	0.126	0.127	2.868	2.889
August	0.029	0.043	0.123	0.125	2.799	2.834
September	0.012	0.004	0.121	0.121	2.757	2.738
October	0.060	0.043	0.127	0.125	2.877	2.836
November	0.014	0.019	0.122	0.122	2.764	2.775
December	0.023	0.068	0.123	0.128	2.786	2.899
2017						
January	0.026	0.041	0.123	0.125	2.793	2.865
February	0.036	0.040	0.124	0.124	2.818	2.827
March	0.061	0.039	0.127	0.124	2.879	2.827
April	0.066	0.067	0.127	0.127	2.893	2.895
May	0.058	0.065	0.126	0.127	2.870	2.888

TABLE 2. DOSE AND EXPOSURE MEASUREMENT FOR LINAC ELEKTA SYNERGY PLATFORM

Month	netOD		Dose (Gy)/month		μSv/h	
	Operator room	Door	Operator room	Door	Operator room	Door
2016						
June	0.058	0.051	0.167	0.166	3.794	3.776
July	0.059	0.059	0.167	0.167	3.798	3.798
August	0.063	0.068	0.167	0.168	3.808	3.821
September	0.010	0.014	0.161	0.162	3.664	3.676
October	0.006	0.001	0.161	0.160	3.651	3.639
November	0.008	0.002	0.161	0.160	3.657	3.641
December	0.068	0.051	0.168	0.166	3.823	3.774
2017						
January	0.052	0.064	0.166	0.168	3.778	3.810
February	0.039	0.073	0.165	0.169	3.745	3.834
March	0.026	0.039	0.163	0.165	3.708	3.743
April	0.074	0.083	0.169	0.170	3.851	3.862
May	0.045	0.055	0.166	0.167	3.760	3.786
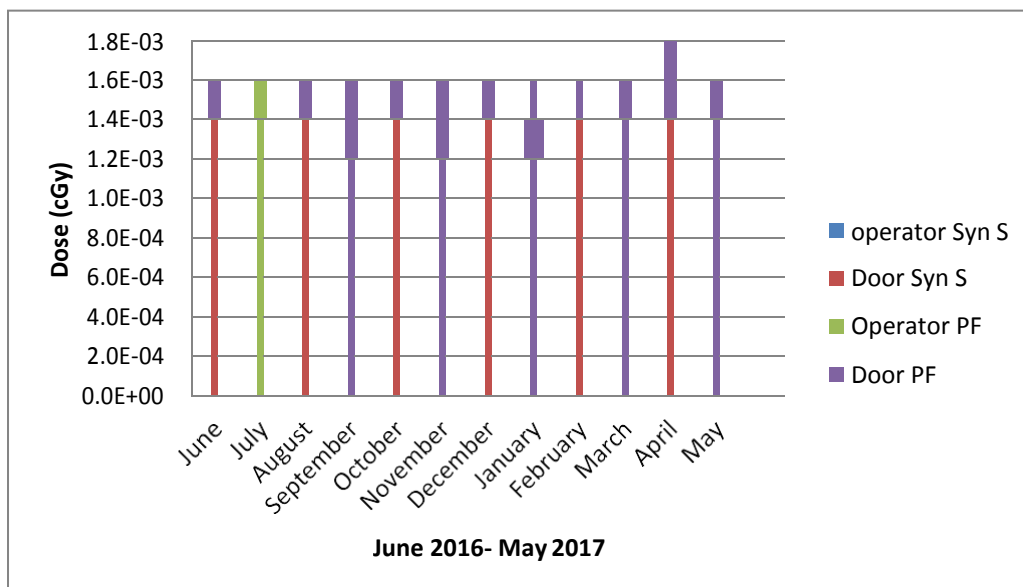
FIG.5. Comparison of dose mesurement in the Linac Synergy S and Synergy Platform

Table 2 were represented the dose or exposure values of the operator room and door for LINAC Elekta Sinergy platform. In this table the lowest values of operator room and door are in October with 3.651 μSv/h and 3.639 μSv/h respectively. In line with that, the highest value was within the same month with a value of 3.851 μSv/h and 3.862 μSv/h for operator room and door in April 2017. Overall of this table, the dose or exposure value at the door was higher than the operator room, but not for June, October, and December 2016 that have the opposite value. That is possible because of the same tendency in the results of Table 1, ie the effect of photoneutron.

Figure 5 is a comparison of dosage values on Synergy S and Synergy Platform every month for operator room and door. In this table, the value of all dose readings on the Synergy Platform was higher than that of Synergy S. Because, not only the number of patients but also the size of the field as well as the use of 10 MV energy on a larger Synergy Platform compared with Synergy S. The total dose or exposure value in a year for both LINAC either operated room or door not exceed the limit of shielding goal required by Nuclear Energy Regulatory Agency of Indonesia.

The highest difference of exposure in film reading for both LINAC and film positions compared with the results of annual exposure measurements using a survey meter is shown in Table 3. In this Table the overall value of the deviation is positive, which means that the reading value of the film was higher than that of the survey meter reading. The highest difference was in the LINAC Sinergy Platform operator room with a value of 4.58%, while the lowest value of 0.04% at the door Synergy S. The value is possible because the film reading was a cumulative dose every month. Where the dose due to daily, monthly, or annual QA activities would like add to the cumulative reading value in the film. Further to these two detectors, the possible photoneutron effect read in the door area exhibits less different results. Although the survey meter used was not a special neutron survey meter.

TABLE 3. DIFFERENCE OF EXPOSURE READING BETWEEN FILM AND SURVEYMETER

% Difference LINAC Synergy S		% Difference LINAC Synergy Platform	
Operator (B)	Door (A)	Operator (B)	Door (A)
3.32	0.04	4.58	0.39

4.   CONCLUSION

In the range of reading differences with survey meters ranging from 0.04% to 4.58%, cumulative radiation leakages in the LINAC room of supervision area due to the high-energy photons can use the Gafchromic EBT3 film dosimeter. As well as the consequences of patient care but also as a result of routine QA activities. Furthermore, photoneutron effect due to activation of high energy photon (≥10 MV) to metal, also can be shown by using this film. Although more data is needed and other dosimeters can read well for cumulative dose or exposure and photoneutron effects.

ACKNOWLEDGEMENTS

REFERENCES

[1] ACCIRAD., Patient safety in external beam radiotherapy Guidelines on risk assessment and analysis of adverse events and near misses, 2013.

[2] E. Bakiu, E. Telhaj, & E. Kozma., Comparison of 3D CRT and IMRT treatment plans ACTA INFORM MED, 2013; 21(3): 211-212 / professional paper.

[3] Biggs, Peter J., Radiation Shielding for Megavoltage Photon Therapy Machines. Boston: s.n., 2010.

[4] National Council on Radiation Protection and Measurements (NCRP)., Structural Shielding Design and Evaluation for Megavoltage X- and Gamma-Ray Radiotherapy Facilities, Bethesda MD, 2005.

[5] International Atomic Energy Agency (IAEA)., workplace monitoring for radiation and contamination. Vienna, 2004.

[6] European Radiation Dosimetry group (EURADOS)., Technical Recommendations for Monitoring Individuals Occupationally Exposed to External Radiation, Luxembourg, 2009.

[7] Klassen N V, van der Zwan L and Cygler J., 1997. GafChromic MD-55: investigated as a precision dosimeter Med. Phys. 24 1924–34.

[8] Butson M J, Cheung T and Yu P K 2002 Corresponding dose response of radiographic film with layered gafchromic film Phys. Med. Biol. 47 N285–N289.

[9]   Butson M J, Yu P K, Cheung T and Metcalfe P 2002 High sensitivity radiochromic film dose comparisons Phys. Med. Biol. 47 N291–N295.

[10] Butson M J, Yu K N, Cheung T and Metcalfe P E., 2003. Radiochromic film for medical radiation dosimetry Mater. Sci. Eng. R 41 61–120.

[11] Butson M, Yu P and Metcalfe P. 1998. Effects of readout light sources and ambient light on radiochromic film Phys. Med. Biol. 43 2407–12.

[12] Chiu-Tsao S T, Duckworth T, Zhang C, Patel N S, Hsiung C Y, Wang L, Shih J A and Harrison L B 2004 Dose response characteristics of new models of GAFCHROMIC films: dependence on densitometer light source and radiation energy *Med. Phys*. 31 2501–8.

[13] C. G. Soares, S. Trichter, and S. D. Davis, "Radiochromic film," in Clinical Dosimetry for Radiotherapy: AAPM Summer School, edited by D. W. O. Rogers and J. E. Cygler Medical Physics, Madison, WI, 2009, pp. 759–813.

[14] Ramani R, Lightstone A, Mason D and O'Brien P 1994 The use of radiochromic film in treatment verification of dynamic stereotactic radiosurgery. *Med. Phys*. 21 389–92.

[15] Meigooni A S, Sanders M, Ibott G and Szeglin S 1996 Dosimetric characteristics of an improved radiochromic film *Med. Phys*. 23 1883–8.

[16] S. Ulya, W. E. Wibowo, N. Nasution, S. A. Pawiro. Dosimetric characteristic of gafchromic EBT3 film on small field electron beam. *Journal of Physics*.: Conf. **851** 012023.

[17] Borca V C, Pasquino M, Russo G, Grosso P, Cante D, Sciacero P, Girelli G, Porta M R L and Tofani S, Dosimetric characterization and use of gafchromic EBT3 film for IMRT dose verification Journal Appl. Clin. *Med. Phys* 14 158, 2013

[18] Papaconstadopoulos P, Hegyi G, Seuntjens J and Devic S 2014 A protocol for EBT3 radiochromic film dosimetry using reflection scanning A protocol for EBT3 radiochromic film dosimetry using reflection scanning *Med. Phys* 41 122101–1

[19] Chełminski K, Bulski W, Georg D, Bodzak D, Maniakowski Z, Oborska D, Rostkowska J and Kania M 2010 Energy dependence of radiochromic dosimetry films for use Rep. Pract. Oncol. Radiother 5 40

[20] Villarreal-barajas J E and Khan R F H 2014 Energy response of EBT3 radiochromic films: implications for dosimetry in kilovoltage range J. Appl. Clin. *Med. Phys* 15 331

[21] Ning Wen, Siming Lu, Jinkoo Kim, Yujiao Qin, Yimei Huang, Bo Zhao, Chang Liu and Indrin J. Chetty 2016 Precise film dosimetry for stereotactic radiosurgery and stereotactic body radiotherapy quality assurance using Gafchromic™ EBT3 films Radiation Oncology 11 132

[22] C. Huet, S. Dagois, S. Derreumaux, Characterization and optimization of EBT2 radiochromic films dosimetry system for precise measurements of output factors in small fields used in radiotherapy. *Radiation Measurement* 47 (2012) 40-49.

IGRT DOSE MANAGEMENT

D. ZOLOTUHHIN
North Estonia Medical Centre
Tallinn, Estonia

E. GERSHKEVITSH
North Estonia Medical Centre
Tallinn, Estonia
Email: eduardger@yahoo.co.uk

Abstract

IGRT has become an indispensable tool in modern radiotherapy with kV imaging used in many departments due to superior image quality and lower radiation dose when compared to MV imaging. However, the manufacturer supplied protocols for imaging are not always optimized between image quality needed for anatomy matching and radiation dose. Dose management strategy would help to minimize the imaging dose without losing the accuracy of patient set-up verification. The paper reports the kV planar imaging doses from two different linac models and demonstrates the potential for imaging dose reduction.

1. INTRODUCTION

Image guided radiotherapy (IGRT) with in treatment room imaging is considered essential for modern radiotherapy in order to accurately position the patient and ensure that prescribed dose is delivered to the right place. Treatment units with on board kV X-ray capabilities became widely available and provide better image contrast at a lower radiation dose when compared to MV portal imaging. Since, the frequency of kV images continues to increase (intrafractional imaging, etc.) the reduction of additional dose assumes high priority. As with all medical uses of ionizing radiation, the general view is that this exposure should be carefully managed [1]. Many departments use manufacturer's supplied imaging protocols which are not always optimised between image quality and radiation dose and result in unnecessary dose (ALARA). The purpose of the study was also to investigate the ESDs difference between newer generation of linacs (Varian TrueBeam) and older generation linacs (Varian iX).

2. METHODS

In order to optimise the protocols anthropomorphic whole body phantom PBU-50 (Kyoto Kagaku ltd., Japan) designed for imaging studies in radiology has been used on Varian iX OBI 1.5 and TrueBeam 2.5 accelerators (Varian Medical Systems, USA). Manufacturer's default protocols were adapted by modifying kV and mAs values when imaging different anatomical regions of the phantom (head, thorax, abdomen, pelvis). Since the phantom represents a small size adult (weight 50 kg) for large pelvis protocols the slabs of bolus material (5cm to each side and 10 cm anterior) were added. Images with different settings were independently reviewed by two persons and their suitability for IGRT set-up correction protocols were evaluated. The suitable images with the lowest mAs were then selected. The entrance surface dose (ESD) for manufacturer's default protocols and modified protocols were measured with RTI Black Piranha device (RTI Group, Sweden) and compared. kV QC (Standard Imaging, USA) were used to measure Contrast to Noise Ratio (CNR).

3. RESULTS

ESD values for default and optimised protocols are given in Table 1. The default manufacturer's protocols on TrueBeam linac yielded on average 9.4 times lower ESD than on iX linac (range 2.5-24.8). The largest differences were for lateral images of thorax, abdomen and pelvis. For most cases it was possible to

reduce the ESD on average by a factor of 3 (range 0.9-8.5) on iX linac by optimising the imaging protocols. The protocol optimisation reduced CNR on average by 35%. The use of bow-tie filter reduced the ESD by 45%. ESD was reduced on average by a factor of 2 (range 1-4.7) also for TrueBeam linac. The new imaging protocols based on adjusted kV and mA values were created. Table 2 and 3 shows new settings for kV and mA for two linacs iX and TrueBeam, respectively.

TABLE 1.   MEASURED ESD (mGy) VALUES

Site	Varian iX OBI 1.5 default	Optimized kV, mA and bow-tie filter	Varian Truebeam default	Varian Truebeam optimised
Pelvis AP Large	0.89	0.67	0.36	0.08
Pelvis LAT Large	17.07	8.85	0.69	0.48
Head AP	0.74	0.20	0.12	0.06
Head LAT	0.23	0.06	0.07	0.05
Thorax AP	0.26	0.08	0.10	0.04
Thorax LAT	3.54	0.29	0.19	0.06
Abdomen AP	2.04	0.33	0.30	0.12
Abdomen LAT	2.89	0.97	0.49	0.48

TABLE 2.   OPTINISED ms AND kV SETTINGS FOR VARIAN iX LINAC

Site	Tube voltage (kV)	Explosure time (ms)
Pelvis AP Large	80	80
Pelvis LAT Large	125	400
Head AP	100	15.5
Head LAT	70	10
Thorax AP	75	12
Thorax LAT	95	25
Abdomen AP	80	40
Abdomen LAT	85	100

TABLE 3.   OPTINISED mAs AND kV SETTINGS FOR VARIAN TRUEBEAM LINAC

Site	Tube voltage (kV)	Explosure (mAs)
Pelvis AP Large	85	3.2
Pelvis LAT Large	110	10
Head AP	85	2.5
Head LAT	80	2.5
Thorax AP	80	2
Thorax LAT	100	1.6
Abdomen AP	100	3.2
Abdomen LAT	100	13

4. CONCLUSION

The imaging doses on new TrueBeam accelerator is substantially lower than on previous iX platform due to improved image receptor, software processing and X-ray source. Manufacturer's default IGRT protocols could be optimised to reduce the ESD to the patient without losing the required image quality to perform patient set-up corrections. For patient set-up with planar kV imaging the bony anatomy is mostly used and optimization should take into account this aspect and could allow slightly higher noise in soft tissue regions. The use of bow-tie filter on iX accelerator for planar kV images reduces the ESD further. One more strategy to reduce the unnecessary radiation dose is to collimate the X-ray beam only to the region of interest. TrueBeam linac stores the settings of the blades and applies it to consecutive fractions, so that radiation therapy technologist do not need to adjust them manually every fraction, like in iX linac.

.

REFERENCES

[1] MURPHY, M. J., et al., The management of imaging dose during image-guided radiotherapy: Report of the AAPM Task Group 75, Med Phys. 34 (1) (2007) 4041–4063.